Durham E-Theses

Some kinetic and equilibrium studies of the reactions of carbonyl compounds with amines and/or sulfite

Ian J. Smith

How to cite:

Smith, Ian J. (2003) *Some kinetic and equilibrium studies of the reactions of carbonyl compounds with amines and/or sulfite.* Doctoral thesis, Durham University.

Use policy

Some Kinetic and Equilibrium Studies of

the Reactions of Carbonyl Compounds with

Amines and/or Sulfite

Ian J. Smith B.Sc. M.Sc. (Hons.)

(Graduate Society)

Thesis submitted for the qualification Doctor of Philosophy

University Of Durham, Chemistry Department

October 2003

Thesis
2003/
Sm1

Abstract

Studies have been made of the reaction of several carbonyl compounds with sulfite in aqueous solution. ^{1}H NMR results indicate the formation of hydroxyalkanesulfonates, HXS, of general structure, RR'C(OH)(SO$_3$Na). Equilibrium and kinetic studies of the decomposition reactions have been made making use of the rapid reaction of iodine with liberated sulfite. The decomposition shows an acidity dependence; above pH 3 reaction mainly involves the dianion, RR'C(O$^-$)(SO$_3^-$), while below pH 3 the monoanion, RR'(OH)(SO$_3^-$) is involved. In the case of adducts from propanal values obtained for the rate constants for decomposition were 370 s^{-1} and 3.9x10^{-6} s^{-1} for the dianion and monoanion respectively. pK$_a$ values for acid dissociation of several HXS compounds were measured and found to be in the range 9 – 12.

The reactions of hydroxypropanesulfonate, HPS, with aniline and aniline derivatives have been studied. ^{1}H NMR spectra accord with formation of anilinopropanesulfonates, APS, kinetic and equilibrium measurements were made spectrophotometrically in the presence of added sulfite ions. The overall equilibrium constant for the reaction with aniline was found to be 84 dm^3 mol^{-1}. The mechanism of the reaction is thought to involve decomposition of HPS to yield propanal which reacts with the amine to yield a carbinolamine intermediate. This subsequently dehydrates giving an imine which reacts rapidly with free sulfite to give the product, APS. The results suggest a change in rate limiting step from the reaction of aniline with propanal at low pH to carbinolamine dehydration at high pH, the change occurring at pH 6 -7. the effects of ring substituents in the aniline on reactivity have been examined.

Reaction of propanal with aniline in acetonitrile yields the imine. Kinetic studies of its decomposition back to reactants in the presence of aqueous sulfite solutions confirm the conclusion reached from measurements on the forward reaction.

Reactions of hydroxymethanesulfonate, HMS, with benzylamine and some derivatives were observed by ^{1}H NMR spectroscopy. Equilibrium constants for the formation of 1:1 and 1:2 adducts were measured and the variation of values with pH were examined. Trimerisations of the imines formed from formaldehyde and benzylamine and its derivatives were successfully achieved.

Acknowledgements

To my parents, mum and dad, you're the best

Declaration

The work in this thesis was carried out in the Chemistry Department at the University of Durham between 1st October 2000 and 30th September 2003. It has not been submitted for any other degree and is the author's own work, except where acknowledged by reference.

Copyright

Definitions

RNH_2	primary amine
$R'CHO$	aldehyde
HZ	nucleophile with an acidic hydrogen
ε_m	extinction coefficient
D_2O	deuterium oxide
UV	ultraviolet
Vis	visible
K_d	equilibrium constant of dehydration
K_{hyd}	equilibrium constant of hydration
σ^*	Taft polar effects of a subsituent
E_s	Taft steric effects of a subsituent
α	Brønsted coefficient
β	Brønsted coefficient
Nuc^-	general nucleophile
HA	solvent or acid
$B:$	base
k	rate constant
K	equilibrium constant
HSO_3^-	bisulfite ion
SO_3^{2-}	sulfite ion
HMS	hydroxymethanesulfonate, $CH_2(OH)(SO_3Na)$
K_a	acid dissociation constant
pK_a	$-Log_{10}K_a$
pH	$-Log_{10}[H^+]$
H^+	hydrogen ion or proton
OH^-	hydroxide ion
K_w	Dissociation constant of water $= 1\times10^{-14}$ mol dm^{-3}
pD	$-Log_{10}[D^+]$
D^+	deuterium ion or deutron
HXS	general hydroxyalkanesulfonate
HPS	hydroxypropanesulfonate, $EtHC(OH)(SO_3^-)$

HIPS	hydroxyisopropanesulfonate, $(Et)_2C(OH)(SO_3Na)$
HCPS	hydroxyiso-1-chloropropanesulfonate, $(CH_2Cl)(Et)C(OH)(SO_3Na)$
AXP	aminoalkanesulfonate
APS	anilinopropanesulfonate
K_a^{HSO3-}	acid dissociation constant of bisulfite ions $= 1 \times 10^{-8}$ mol dm^{-3}
ISO_3^-	iodosulfate
KI	potassium iodide
aqueous iodine solution	$I_2 + I_3^- + I^-$ species
I_3^-	triiodide
I^-	iodide
$[I_2]_{stoich}$	$[I_2] + [I_3^-]$
S(IV)	sum contribution of bisulfite and sulfite ions
$[X]_{stoich}$	stoichiometric concentration of X
I	ionic strength
λ / nm	wavelength / nanometres
λ_{max}	wavelength of peak maximum
A	absorbance
ΔA	change in absorbance
A_∞ / A_{inf}	absorbance at reaction completion
σ	Hammett substituent parameter
ρ	Hammett reaction parameter
^1H NMR	proton nuclear magnetic resonance
^{13}C NMR	carbon 13 nuclear magnetic resonance
CD_3CN	d-$_3$ acetonitrile
d-$_6$ DMSO	d-$_6$ dimethyl sulfoxide
δ / ppm	chemical shift / parts per million
J / Hz	coupling constant / hertz
s	singlet
d	doublet
t	triplet
m	multiplet

Chapter one

1 Introduction

1.1 Background

Condensation reactions involving an aldehyde, an amine and a nucleophile (Scheme 1.1) are potentially useful in commercial synthetic processes.

Scheme 1.1: $RNH_2 + R'CHO + HZ \longrightarrow RNHCHR'Z + H_2O$

One example of importance is the Mannich reaction[1], where HZ is a compound with an acidic hydrogen. The products formed are known as Mannich bases and are of great significance to the pharmaceutical and polymer industries. Specifically using hydrogen cyanide as HZ, constitutes the first step of the Strecker reaction[2]. This reaction is of interest as it is widely used to synthesize α-hydroxy-carboxylic acids, α-amino acids and β-amino alcohols.

Reactions of carbonyl compounds are reasonably well documented, however there has been little quantitative study in relation to the kinetics and mechanisms of the reactions shown in scheme 1.1, especially when the HZ compound contains sulfite. There is industrial interest when HZ is sulfite since the azo-dye industry uses the reaction in the production of printing inks. The focus of work described here is reaction of carbonyl compounds with sulfite, including reactions in the presence of amines.

1.2 Reactions of carbonyl compounds with nucleophiles

Reversible carbonyl addition reactions as shown in scheme 1.2, result from the carbonyl group being strongly polarized due to the electronegative oxygen, leaving a partial positive charge on the carbon atom, thus facilitating nucleophilic attack.

2

Scheme 1.2:

$$R'\!\!\diagdown\!\!{C}\!\!=\!\!O \;+\; HZ \;\rightleftharpoons\; Z\!\cdots\!\overset{R'}{\underset{R''}{C}}\!\!-OH$$
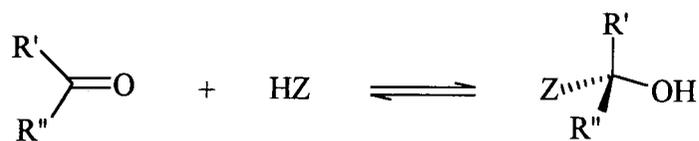
There is evidence that the nucleophile attacks the carbonyl carbon perpendicular to the plane of the carbonyl group. Addition produces a change from the planar sp^2 hybridisation with $120°$ bond angles to tetrahedral sp^3 hydridisation. The reversibility of these reactions depends on the stability of the anionic form of Z and the ability for elimination of the proton. The adduct is favoured when Z^- is unstable, as this would make the addition essentially irreversible; this occurs with anions such as hydride or carbanions. Steric, resonance and inductive effects determine the rate of reaction and equilibrium constants for the reaction shown in scheme 1.2, with most being subject to acid-base catalysis.

1.2.1 Hydration

Addition of water to ketones and aldehydes yields hydrates which are *gem*-diols (a diol that has both hydroxy groups on the same carbon). Carbonyl compounds with electronegative substituents can produce solid hydrates; a classic example is chloral hydrate, trichloroethanal hydrate[3]. At low enough temperatures even the hydrate of ethanal has been reported to crystallise, however no characterisation was completed[4]. Although the majority of carbonyl compounds do not give solid hydrates, there have been many studies producing evidence for the occurrence of the reaction in scheme 1.3.

Scheme 1.3:

$$R'\!\!\diagdown\!\!{C}\!\!=\!\!O \;+\; H_2O \;\rightleftharpoons\; HO\!\cdots\!\overset{R'}{\underset{R''}{C}}\!\!-OH$$
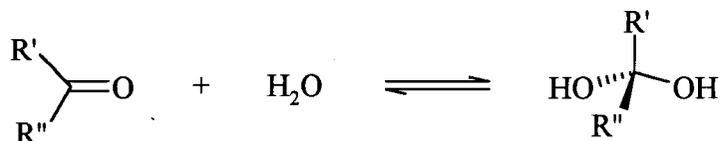
Early studies were conducted on the thermodynamics of the hydration of ethanal[5]. It was discovered that about 5 kcal mole[-1] of heat was evolved when ethanal was dissolved in water, providing evidence for hydration. Subsequent studies, using density as a method[6] were attempted, but were not sensitive enough to give quantitative results.

Little quantitative study of scheme 1.3 was therefore possible until the availability of UV methods. The carbonyl's broad n-π* absorption band at around 280nm was discovered to diminish on hydration. Early studies[7] showed many inconsistencies due to the uncertainty of the value for the true maximum extinction co-efficient (ε_m) of the unhydrated carbonyl. Problems arose from the solvent-dependency of this value on transfer from organic to hydroxylic solvents[8]. Assumptions were made that a series of aldehydes would have similar values to those of ketones of a similar structure where hydration is unimportant[9]. However this method only gave an outline as to what the correct ε_m value would be, so a method was devised giving an independent check on the value[10]. This involved comparison of equilibrium data obtained from calorimetric measurements and from spectrophotometric measurements. The results allowed an estimation for ε_m ethanal[9] of 17 at 278nm in water compared to a measured value for ε_m of 16.2 at 288nm for a hexane solution. It became possible with knowledge of the true ε_m for UV measurements, to be used to give compatible results for many other carbonyls which can be seen in table 1.1.

NMR studies using line broadening methods can be effectively used to measure rate constants for both forward and reverse reactions allowing an estimate of the equilibrium position. The first studies concentrated on ethanal[11]. The technique is more sensitive than UV and can detect even small amounts of hydration, as in the case of acetone, which is often regarded as unhydrated[12]. There is limited information for hydration in deuterium oxide, yet studies on five aliphatic aldehydes suggested that an isotope effect can make the dehydration constant up to 20% smaller in D_2O compared to studies in H_2O.[13]

The dissociation constant for the hydrates can be expressed as:

$$K_d = \frac{[R'R''CO]}{[R'R''C(OH)_2]} = \frac{1}{K_{hyd}}$$

(1.1)

Table 1.1: Equilibrium constants K_d and K_{hyd} for the addition of water to R'R''CO.

R'	R''	K_d (observed)	K_d (calculated)	K_{hyd} (observed)	Ref
H	H	5.3×10^{-4}	9×10^{-4}	2×10^{3}	3a, 14
H	CCl$_3$	3.6×10^{-5}	3.6×10^{-5}	2.8×10^{4}	3a, 13
H	CH$_3$	0.75	0.6	1.3	3a, 15
H	CH$_3$CH$_2$	1.4	1.6	0.71	3a, 13
H	C(CH$_3$)$_3$	4.1	-	0.24	16
H	CH$_2$Cl	0.027	0.002	37	3a, 17
H	Ph	$\sim 1.2 \times 10^{2}$	-	8.3×10^{-3}	18a, 18b, 18c
H	Ph (3-Cl)	~45	-	0.022	18a, 18d
H	Ph (3-NO$_2$)	~9	-	0.11	18a, 18b
H	Ph (4-NO$_2$)	~6	-	0.17	18a, 18d
CH$_3$	CH$_3$	5×10^{2}	5×10^{2}	2×10^{-3}	3a, 12
CH$_3$	CH$_2$Cl	1.6	2	~0.6	3a, 8b
CH$_3$	CHCl$_2$	0.35	0.5	2.9	3a, 8b
CH$_2$Cl	CH$_2$Cl	~0.1	-	10	3a, 19
CH$_3$	Ph	$\sim 1.5 \times 10^{5}$	-	6.6×10^{-6}	18c

Experimental values can be compared to values calculated from the Taft equation[20] (equation 1.2). Polar and steric effects are taken into account by using the substituent constants σ^* and E_s respectively, methyl groups being standard ($\sigma^* = 0$, $E_s = 0$). These values can be seen in table 1.1.

$$LogK_d = 2.7 - 2.6\sum \sigma^* - 1.3\sum E_s \qquad (1.2)$$

It is clear from the data that di-alkyl ketones and aryl aldehydes have equilibrium constants for hydration (K_{hyd}) less than unity, indicating the dominance of the unhydrated species. Conversely alkyl aldehydes with $K_{hyd} > 1$ are readily hydrated. Groups that donate electron

5

density to the electron deficient carbon stabilize the carbonyl form, hence decreasing K_{hyd}. Electron-attracting substituents increase the K_{hyd} due to polarisation of the carbonyl bond.

Since the bond angle decreases from *ca.* $120°$ to *ca.* $108°$ on going from sp^2 to sp^3 hybridisation, bulky groups tend to destabilize hydrates more than the parent molecule, hence decreasing K_{hyd}.

The equilibrium for the system seen in scheme 1.3 is generally believed to be reached rapidly but not instantaneously at standard temperatures. Several methods have been used[21], including; UV/Visible spectrometry, NMR, Raman spectroscopy and polarography, to obtain kinetic information for the hydration and dehydration pathways. These studies have concluded that the reaction is catalysed by acids and bases. Catalytic rate constants have been measured for acids and bases in carbonyl hydration-dehydration[22], and used to evaluate Brønsted α and β values.

Table 1.2: Brønsted coefficients for water addition[22]

	α	β
Formaldehyde	0.24	0.40
Ethanal	0.54	0.45
Dichloroacetone	0.27	0.50

The observation of general catalysis indicates that the reaction pathway for the addition/elimination of the water molecule must involve proton transfer either in the rate-determining step or proton transfer in a concerted rate-determining process if there is not one single step. A possible mechanism for the hydration reaction is written in scheme 1.4 (*Nuc⁻* represents a generalized nucleophile which may not be negatively charged, and HA can be solvent or acid)

6

Scheme 1.4:
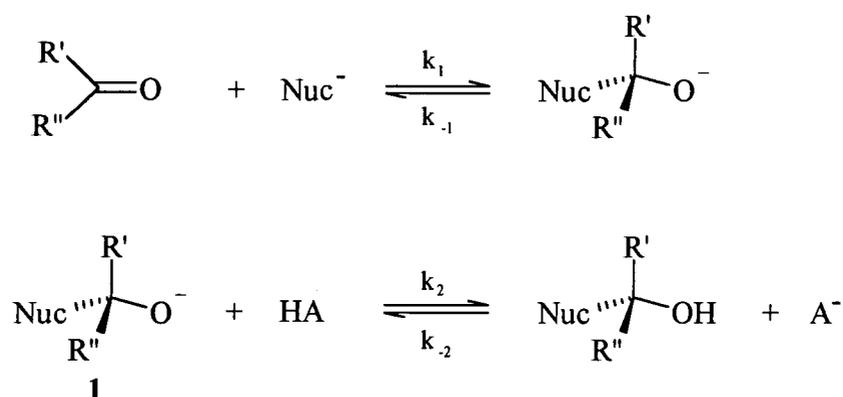
The detailed pathway depends heavily on the strength of the nucleophile, as this dictates the stability of the intermediate **1**. If the nucleophile is strong the intermediate should be relatively stable, predicting that the rate of protonation to the hydrate should be bigger than the rate of decomposition back to reactants. This therefore suggests that the first step is rate determining indicating no acid-base catalysis (if the pre-equilibrium formation of *Nuc⁻* from H-*Nuc* is included, specific base catalysis would occur). When the nucleophile is weaker as with water, the intermediate would be able to decompose much more easily, suggesting that reversion of **1** to reactants could compete with the protonation step. General catalysis would be observed as the proton transfer would become part of the overall kinetic expression. Jencks[23] described this process as enforced catalysis because the intermediate would revert back to reactants unless the protonation by HA traps it. However if k_{-1} were much larger than protonation the second step becomes rate limiting unlike the previous combined process. The intermediate wouldn't be able to exist if the nucleophile was even weaker still. This would predict that nucleophilic attack occurs simultaneously with proton transfer as shown in scheme 1.5. Thus, scheme 1.4 reduces to a single step, with a concerted proton transfer, where general acid catalysis is expected. This theory offers consistent explanations for the mechanism of hydration.

Scheme 1.5:
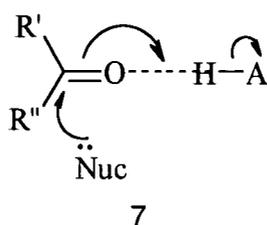
1.2.2: Addition of sulfite

The simple mechanism of scheme 1.4 may also apply to the addition of other nucleophiles to carbonyl compounds. Sulfite readily adds to aldehydes and unhindered ketones, with the equilibrium further to the right for the aldehydes than for the ketones. The addition requires the sulfite to be in its most basic form, its dianion (SO_3^{2-}). There is good evidence[24] that the bond to carbon involves the softer sulfur centre rather than the harder oxygen of the sulfite producing the acid and not the ester as shown in scheme 1.6. The sulfite ester would be unstable with respect to elimination of sulfur dioxide.

Scheme1.6:

Hydroxy sulfonic acid   Hydroxy sulfite ester
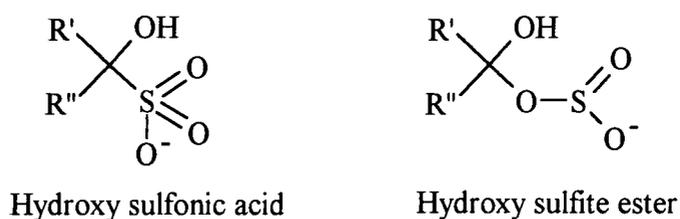
Some equilibrium studies for sulfite addition have been reported and values are given in table 1.3. The value of 6400 dm^3 mol^{-1} for benzaldehyde, obtained in acidic solution[25b] may be considered reliable. However, less confidence can be placed in the other values since the level of the acidity, and whether it was controlled, is not clear. The general trend is that increasing electron release and increasing steric size in the groups attached to the carbonyl function tend to reduce values of the equilibrium constant.

Scheme 1.7:

8
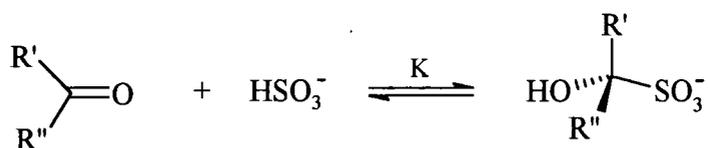
Table 1.3: Equilibrium constants for the addition of sulfite at 0°C [25]

R'	R''	K / dm^3 mol^{-1}
H	CH_3	800
H	C_6H_5	6400
CH_3	CH_3	200
CH_3	C_2H_5	40
CH_3	i-C_3H_7	8
CH_3	i-C_4H_9	1.6

Jencks and co-workers[27, 28] have investigated the catalysis by acids and bases of the reaction and have concentrated on the reverse process, i.e. sulfite elimination. Ring substituted benzaldehydes were studied where spectrophotometric detection of the parent aldehyde can be used. In acidic solutions, pH < 3, there was evidence for general acid catalysis. The mechanism proposed, scheme 1.8, involves slow acid assisted expulsion of hydrogen sulfite followed by rapid deprotonation. Above pH 3, general base catalysis was observed but with a Brønsted β value of 0.94. This is best interpreted as a rapid equilibrium proton transfer, followed by rate limiting expulsion of sulfite which is weakly assisted by the conjugate acid of the catalysing base. Since the rate-determining transition state contains the parent plus base, the observation of general base catalysis is explained. Weak catalysis of the decomposition by metal ions, particularly Zn^{2+} and Mg^{2+}, was interpreted in terms of association of the cation with the leaving sulfite group.

Scheme 1.8:

pH below 3

$$\text{HO}^{\prime\prime\prime}\!\!\underset{R^{\prime\prime}}{\overset{R^{\prime}}{\bigvee}}\!\!\text{SO}_3^- \quad + \quad HA \quad \xrightarrow{\text{slow}} \quad \underset{R^{\prime\prime}}{\overset{R^{\prime}}{\bigvee}}\!\!{=}\overset{+}{\text{OH}} \quad + \quad HSO_3^- \quad + \quad A^-$$

$$\underset{R^{\prime\prime}}{\overset{R^{\prime}}{\bigvee}}\!\!{=}\overset{+}{\text{OH}} \quad + \quad A^- \quad \underset{\text{fast}}{\rightleftharpoons} \quad \underset{R^{\prime\prime}}{\overset{R^{\prime}}{\bigvee}}\!\!{=}O \quad + \quad HA$$

pH above 3

$$\text{HO}^{\prime\prime\prime}\!\!\underset{R^{\prime\prime}}{\overset{R^{\prime}}{\bigvee}}\!\!\text{SO}_3^- \quad + \quad B\!: \quad \underset{\text{fast}}{\rightleftharpoons} \quad \overset{+}{HB}\cdots\overset{-}{O}^{\prime\prime\prime}\!\!\underset{R^{\prime\prime}}{\overset{R^{\prime}}{\bigvee}}\!\!\text{SO}_3^-$$

$$\overset{+}{HB}\cdots\overset{-}{O}^{\prime\prime\prime}\!\!\underset{R^{\prime\prime}}{\overset{R^{\prime}}{\bigvee}}\!\!\text{SO}_3^- \quad \xrightarrow{\text{slow}} \quad \underset{R^{\prime\prime}}{\overset{R^{\prime}}{\bigvee}}\!\!{=}O\cdots HB^+ \quad + \quad SO_3^{2-}$$
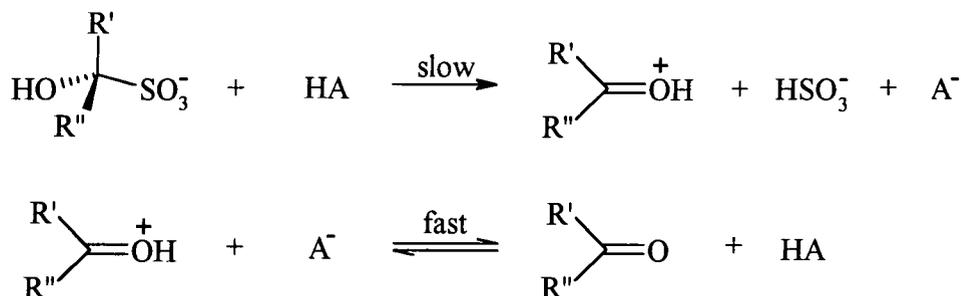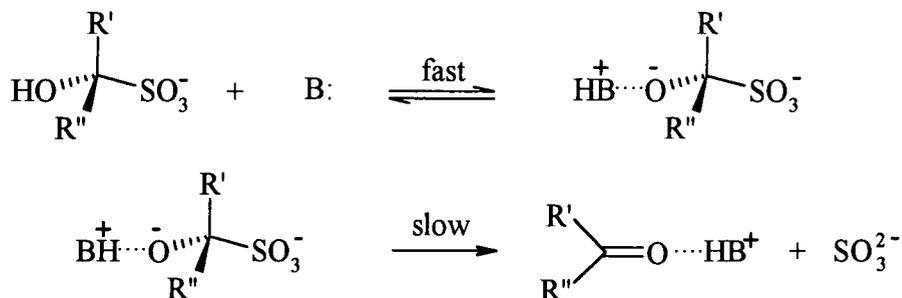
1.2.2.1: Hydroxymethanesulfonate, $CH_2(OH)(SO_3Na)$

In early studies[29], it was found that the addition of sulfite to carbonyl compounds produced hydroxyl sulfonic acids; 'the reaction between formaldehyde and sodium bisulfite', yielding hydroxymethanesulfonate, or HMS. HMS is a compound that is used to provide equimolar amounts of formaldehyde and sulfite '*in situ*', as it dissociates readily in aqueous solutions. Of the studies reviewed, several have focused on the decomposition of HMS, as shown in scheme 1.9. Stopped-flow techniques have been used to measure k_5 as 2.3×10^{-8} s^{-1} [30]; the method uses the rapid reaction with aqueous iodine to remove the liberated sulfite. A study by Sørensen and Andersen[31] examined the equilibria involved and obtained a value for K_a of $10^{-11.7}$ mol dm^{-3}, giving a pK_a for HMS as 11.7.

Scheme 1.9:
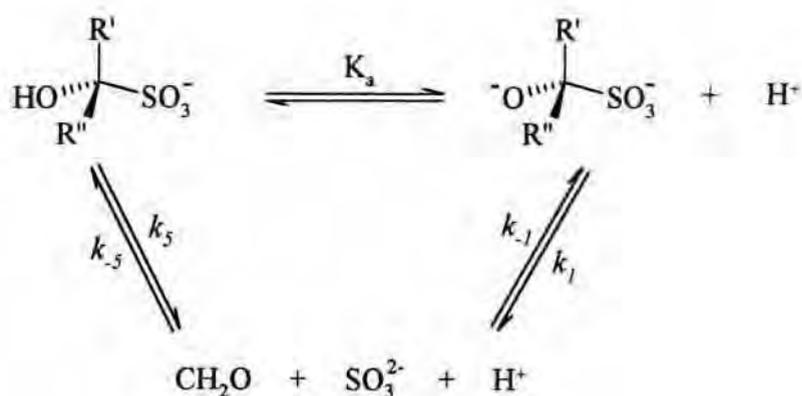
There have been few quantative studies on the reaction of HMS with amines, since the work carried out by Le Hénaff [32]. The reaction of HMS with ammonia was investigated, the products being the 1:1 and 1:2 ammonia: HMS adducts, $H_2NCH_2SO_3^-$ and $HN(CH_2 SO_3^-)_2$. Le Henaff postulated that the 1:3 adduct could be obtained if the free sulfite concentration was high enough.

However, more recently, studies by Crampton and Brown[31] have detailed reactions of HMS with amines. Kinetics were observed for the condensation reaction between HMS and aniline, as well as some aniline derivatives. Measurements for the overall reaction were made using aniline and 4-methylaniline, and the observed results were used to obtain the rate and equilibrium constants shown in table 1.4.

Table 1.4: Rate and equilibrium constants for the reactions between HMS and anilines[31]

	k_f / dm³ mol⁻¹ s⁻¹	k_r / s⁻¹	K / dm³ mol⁻¹
Aniline	$(7.8\pm0.2)\times10^{-3}$	$(1.0\pm0.2)\times10^{-5}$	780
4-Methylaniline	$(5.0\pm0.5)\times10^{-2}$	$(1.1\pm0.1)\times10^{-4}$	460

The results obtained indicated a mechanism for this process involving dissociation of HMS, to form free formaldehyde, which then undergoes an addition reaction with an amine, in this

case aniline. Via several further steps, sulfite as a nucleophile is introduced yielding an anilinomethanesulfonate. These processes will be discussed in greater depth later.

1.2.3: Addition of amines

The reactions of ketones and aldehydes with amines have been reviewed by a number of authors[33]. The amine addition to a carbonyl centre is similar to that of hydration and addition of sulfite, but the reaction products depend on whether the amine is primary, RNH_2, secondary, RR'NH, or tertiary, RR'R''N.

1.2.3.1: Primary amines

The reaction between primary amines and carbonyl groups produces an imine[34] of general formula RR'C=NR''. The mechanism of the reaction has two main steps. Firstly, there is the nucleophilic attack by the primary amine on the carbonyl group to yield a carbinolamine[35], $RNHCR_2OH$ (**2**, scheme 1.10). The second step involves dehydration of the carbinolamine to produce an imine, (**3**, scheme 1.10)

Scheme 1.10:
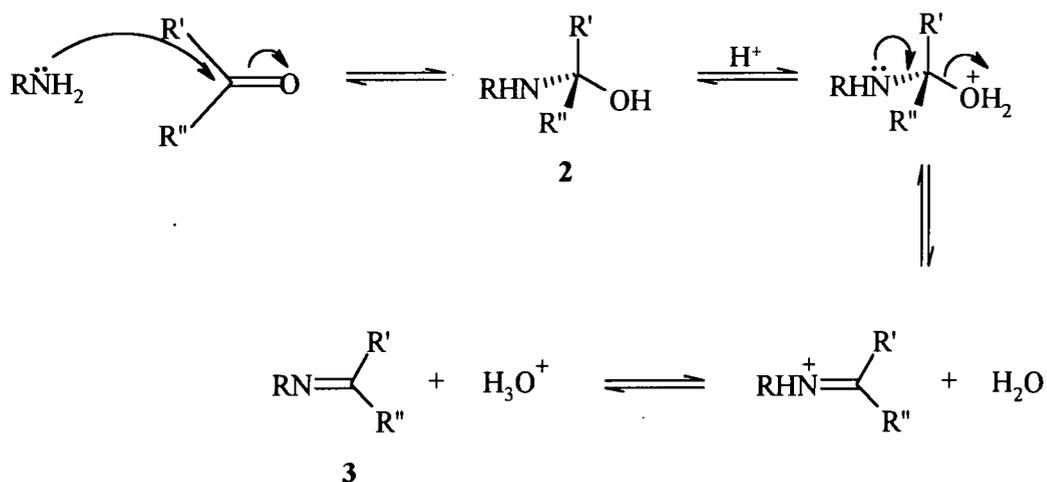
The first step of the mechanism, involves the thermodynamically favourable formation of the carbinolamine[33c]. The actual value of the equilibrium constant[36] for this step, is determined principally by the pKa value of the amine and by steric properties. For the reaction of aniline and formaldehyde, the equilibrium constant is 4.5×10^4 mol^{-1} dm^3 at 25°C, 1.0M ionic strength[35]. In comparison to the amine, the pK$_a$ of its respective carbinolamine is often 2 to 3 units lower[37]. This is primarily due to the decrease in solvation which is brought about by the exchange of one of the amines protons for a hydroxymethyl group.

The importance of imines can not be underestimated, as they have proven to be the focus of many industrial applications, both enzymatic and synthetic[38]. As in hydration and addition of sulfite to carbonyl groups, the reaction to produce the carbinolamine and then the dehydration yielding the imine may be subject to catalysis both from acids and bases. These issues, together with the mechanism itself, will be discussed in greater detail in section 1.3.

1.2.3.2: Secondary amines

The addition of a secondary amine to a carbonyl group, again produces a carbinolamine (**2a** scheme1.11), which then expels the hydroxyl group, yielding an iminium ion[39], RR'C=N$^+$R''R'''. As is shown in Scheme 1.11 elimination of a hydrogen on the α-carbon, can produce an enamine[40] (**4** scheme 1.11) which is an α,β-unsaturated tertiary amine, with a double bond in the α,β position relative to the nitrogen atom.

Scheme 1.11:

When R' = Methyl group
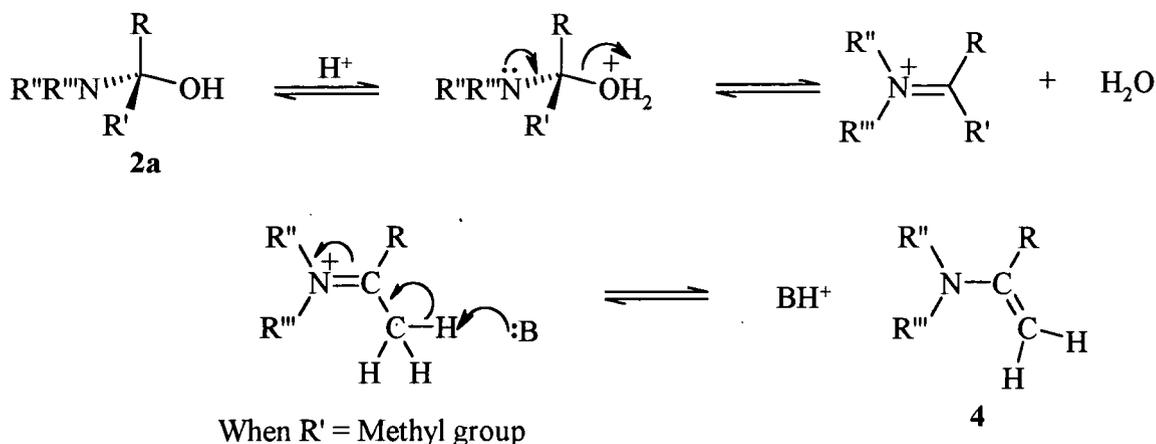
An enamine can also be produced from the reactions involving the addition of primary amines. The imine produced (when having α-hydrogens) can undergo imine – enamine tautomerism[41] (scheme 1.12). However, in this situation, the imine generally tends to be the more stable form.

Scheme 1.12:
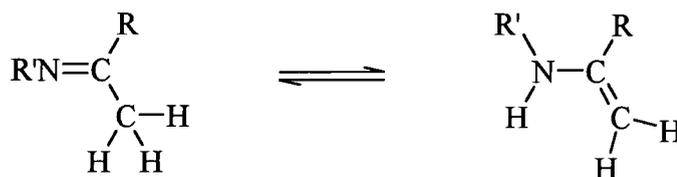
1.2.3.3: Tertiary amines

The addition of tertiary amines to carbonyl groups is often unfavourable, as it leads to the formation of unstable zwitterionic carbinolamines, which revert back to reactants. One example where this type of addition is possible, is when a ring system enhances the carbinolamine stability. For 3,3-dimethyl-4-dimethylaminobutanal[42], as shown in scheme 1.13.

Scheme 1.13:
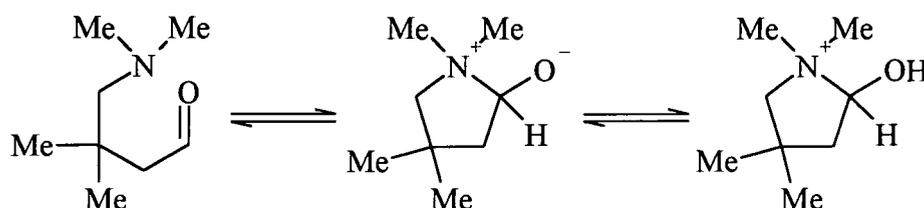
1.3: Imines

Imines or 'Schiff bases', so named because of their first discovery by Schiff[43] in 1864, contain a carbon – nitrogen double bond, C=N. However, throughout the literature, there is evidence that various other names have been used to refer to compounds containing this C=N grouping, with other groups attached around it. A summary of these variances can be seen in table 1.5.

Table 1.5: Nomenclature of RR'C=NR'' compounds

Term	R	R'	R''
Schiff base/imine	aryl	H	alkyl or aryl
Azomethine	aryl	H	Aryl
aldimine	alkyl or aryl	H	alkyl, aryl or H
ketimine	alkyl or aryl	alkyl or aryl	alkyl, aryl or H
anil	alkyl, aryl or H	alkyl, aryl or H	Ph
Semicarbazone	alkyl, aryl or H	alkyl, aryl or H	$-NHCONH_2$
oxime	alkyl, aryl or H	alkyl, aryl or H	-OH
Hydrazone	alkyl, aryl or H	alkyl, aryl or H	-NHR

It should be noted that here all compounds containing a C=N bond will be referred to as imines, unless stated. Also, the groups attached will have no special significance unless their identity is stated.

1.3.1: Formation of imines

Extensive studies of the reaction of amines with carbonyl compounds have been reported in the literature. However, most kinetic work has focused on the formation of semicarbazones, oximes and hydrazones, and few studies have been reported for the formation of imines from formaldehyde, $RN=CH_2$, or from the lower alkyl aldehydes. The reason for this lack of attention is that the imines produced are very unstable, and therefore, their formation can only be observed indirectly.

1.3.1.1: pH dependence

It is well documented[44] that many imine forming reactions show a bell-shaped profile when rate constant is plotted against pH. The maximum usually occurs in the region pH 4 – 6; for

15

example in the reaction of acetone with hydroxylamine to give the corresponding imine there us a rate maximum at pH 4.5, which is 1.5 units lower than the pK_a value for hydroxylamine. Dependences have been found between the pH maximum and the basicity of the imine; with weakly basic amines the maximum occurs at a slightly higher pH than for more strongly basic amines. Early works[45] recognised that the maximum was due to the opposing effects of amine protonation which decreases reactivity at low pH and acid catalysis which becomes important at higher pH values.

More detailed kinetic analysis has shown that the actual pH maximum can be attributed to the result of a change in the rate-determining step with pH[46]. Below the pH maximum, the rate-determining step is the attack of the amine on the carbonyl group, as the concentration of the free amine becomes lower due to a higher degree of protonation. Above the pH maximum, in neutral and basic solutions, the acid catalysed dehydration of the carbinolamine is rate limiting.

Formation of the carbinolamine can, in some types of reactions, become a stepwise process; the first step producing a zwitterionic form of the carbinolamine (shown in scheme 1.14), with the second step, being proton transfer. Taking this into account, studies have suggested that the bell shaped curve should show a break in the graph at very low pH (~1), which would correspond to a third, kinetically important step. At this pH, the rate-determining step is the uncatalysed formation of the zwitterions[47].

Scheme 1.14:

In the acidic region therefore, the reaction can be best illustrated as two concurrent pathways; **paths a** and **b**, as shown in scheme 1.15.

Scheme 1.15:

path a

$+H^+$

$RH_2\overset{+}{N}^{\prime\prime\prime}\overset{R'}{\underset{R''}{\rule{0pt}{1em}}}OH$

RNH_2 + $\overset{R'}{\underset{R''}{\rule{0pt}{1em}}}=O$

$+H^+$

$RH_2\overset{+}{N}^{\prime\prime\prime}\overset{R'}{\underset{R''}{\rule{0pt}{1em}}}O^-$

path b

$-H^+$

$RHN^{\prime\prime\prime}\overset{R'}{\underset{R''}{\rule{0pt}{1em}}}OH \longrightarrow RN=\overset{R'}{\underset{R''}{\rule{0pt}{1em}}} + H_2O$
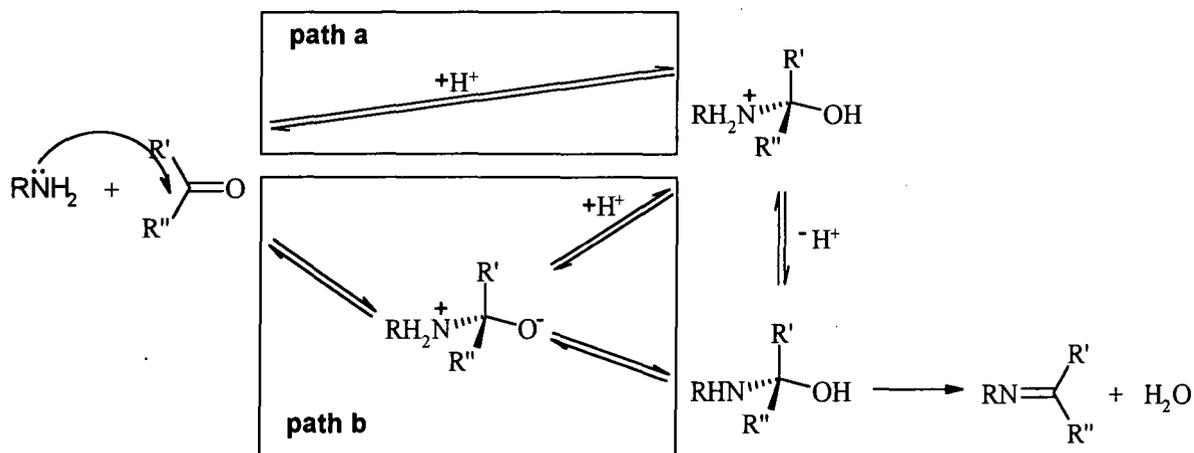
Path a involves both steps; the addition of amine to form the carbon nitrogen bond, and the protonation of the carbonyl group, which can be said to be concerted (scheme 1.16).

Scheme 1.16:

RNH_2 + $\overset{R'}{\underset{R''}{\rule{0pt}{1em}}}=O$ + $H-A$ $\rightleftharpoons$ $RH_2\overset{+}{N}^{\prime\prime\prime}\overset{R'}{\underset{R''}{\rule{0pt}{1em}}}OH$ + A^- $\rightleftharpoons$ $RHN^{\prime\prime\prime}\overset{R'}{\underset{R''}{\rule{0pt}{1em}}}OH$ + HA
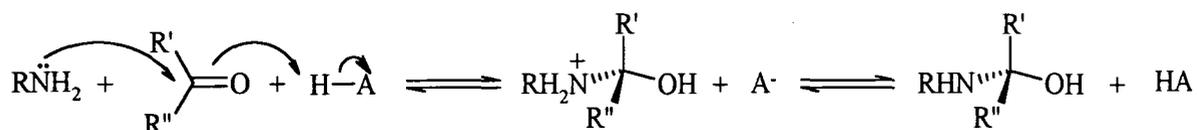
Path b follows a stepwise mechanism involving formation of the zwitterionic form of carbinolamine, which then undergoes proton transfer to produce the neutral carbinolamine (scheme 1.15). There have been several computational theoretical studies[48], producing evidence to suggest that this mechanism is not straightforward. It was proposed in the studies that conversion from the zwitterion to the neutral carbinolamine involved two water molecules, similar to the imidazole-catalysed hydration of carbonyls.

It is known that the pK$_a$ of the amine largely determines the pH maximum of the bell shape curve, and this together with the steric and electronic effects of the carbonyl compound dictate the contributions of each pathway[49]. The evidence suggests that for general purposes, two rules can be applied[47a]: -

1) For weakly basic amines, or carbonyl compounds where carbinolamine formation is unfavourable, the zwitterionic intermediate will be unstable and the reaction will proceed through the concerted process of path a.

2) For moderately basic amines, and carbonyl compounds that show favourable carbinolamine formation, the zwitterionic intermediate will be relatively stable and the reaction will follow path b.

Thus, if we were to equate the bell-shaped graph to rate determining steps, in the neutral and basic region, the dehydration of the carbinolamine, is generally the rate determining step. Whereas, in the acid region, attack of the amine on the carbonyl group is rate determining. However, as illustrated, the acidic region can be split into two. At very low pH values, the mechanism for formation of carbinolamine, proceeds stepwise, via the zwitterionic form of the carbinolamine. The other route conversely, is a concerted process, where addition of the amine and protonation of the carbonyl group occur simultaneously. Therefore, the factors stated can be attributed to the pK_a of the amine and the steric and electronic effects of the carbonyl compound.

Nonetheless, there are several reaction systems where these arguments fail to be supported, as the rate versus pH profile does not show the characteristic bell-shape. For some formations of semicarbazones, oximes and hydrazones, even at low pH values[50], the rate determining step is carbinolamine dehydration. This may be possible for reactions which can occur intramolecularly and involve the formation of a transition state with a cationic site on an aromatic ring. This cationic site can increase the rate of amine attack relative to carbinolamine dehydration. So that carbinolamine dehydration effectively becomes rate determining at all pH values.

1.3.1.2: General acid and base catalysis

The formation of imines by the addition of primary amines to carbonyl compounds is often subject to general acid and base catalysis[51]. It has been suggested that general acid catalysis, involves addition of the amine and transfer of a proton to the carbonyl group (scheme 1.17)

Scheme 1.17:

$$RNH_2 + \overset{R'}{\underset{R''}{\diagup}}C{=}O + H{-}A \rightleftharpoons \left[RH_2\overset{\delta+}{N}{-}{-}\overset{R'}{\underset{R''}{\diagup}}C{=}O{-}{-}H{-}{-}\overset{\delta-}{A} \right]$$

$$RHN{'''}\overset{R'}{\underset{R''}{\diagup}}C{-}OH + HA \xrightarrow{\text{fast}} RH_2\overset{+}{N}{'''}\overset{R'}{\underset{R''}{\diagup}}C{-}OH + A^-$$
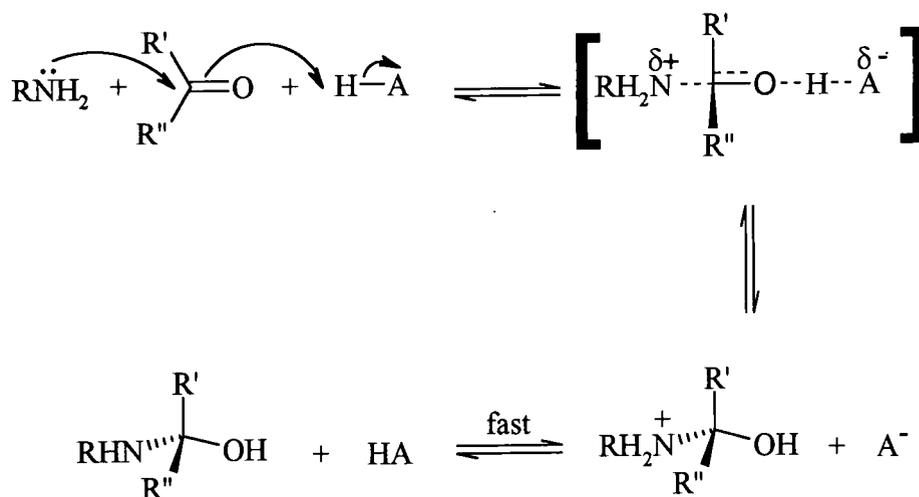
It is likely that general base catalysis involves concerted removal of the proton from the amine, to enable addition to the carbonyl group (scheme 1.18)

Scheme 1.18:

$$A^- + H{-}\ddot{N}HR + \overset{R'}{\underset{R''}{\diagup}}C{=}O \rightleftharpoons \left[\overset{\delta-}{A}{-}{-}H{-}{-}\underset{H}{\overset{R}{N}}{-}{-}\overset{R'}{\underset{R''}{\diagup}}C\overset{\delta-}{=}O \right]$$

$$RHN{'''}\overset{R'}{\underset{R''}{\diagup}}C{-}OH + A^- \xrightarrow{\text{fast}} RHN{'''}\overset{R'}{\underset{R''}{\diagup}}C{-}O^- + HA$$
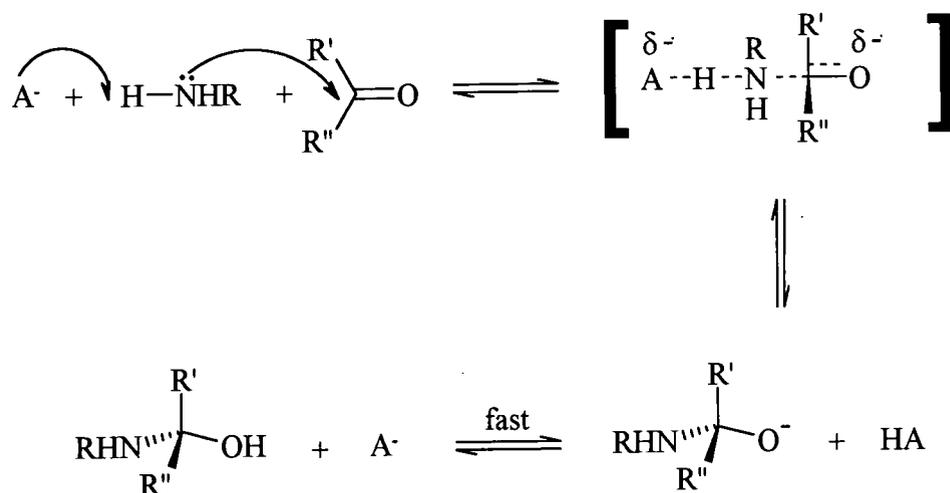
Dehydration of carbinolamines derived from strongly basic amines may involve direct expulsion of the hydroxide ion, facilitated by the driving force of the lone pair on the nitrogen atom (scheme 1.19).

Scheme 1.19:
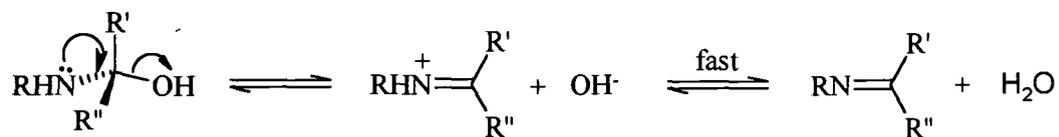
Acid catalysis of carbinolamine dehydration has also been reported. Kallen's work[52] yielded a value for the rate constant for the proton catalysed dehydration of the carbinolamine **5**, formed from formaldehyde and cysteine, of 1.4×10^8 dm^3 mol^{-1} s^{-1} at 25°C.
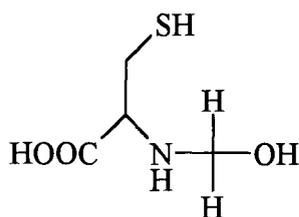
5

Jencks and co-workers[53] in studies of semicarbazone and oxime formation favoured that catalysis by anilinium ions is much more efficient than catalysis by other acids of comparable strength. The reaction pathway, as illustrated in scheme 1.20, demonstrates that aniline acts as a nucleophilic catalyst by reacting with the carbonyl in the rate-determining step to produce the imine. The fast step involves reaction of the imine with, for example, a semicarbazide to generate the product.

Scheme 1.20:

$$C_6H_5NH_2 + R_2CO \xrightarrow{\text{Slow}} C_6H_5N{=}CR_2 + H_2O$$

$$C_6H_5N{=}CR_2 + NH_2NHCONH_2 \xrightarrow{\text{Fast}} R_2C{=}NNHCONH_2 + C_6H_5NH_2$$
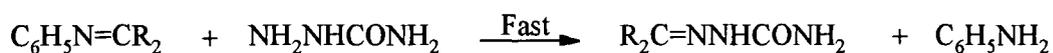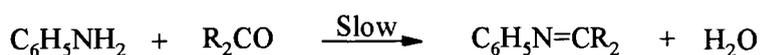
1.4: Reaction of imines

Many imines are very reactive and undergo further reaction, such as polymerization. They are generally only stable and easy to isolate when substituted with bulky groups, such as aryl groups, which sterically restrict reaction. Resonance effects can stabilise imines such as semicarbazones (**6**), oximes (**7**) and hydrazones (**8**), where the nitrogen in the C=N bond is attached to either a hydroxyl group or a second nitrogen atom.
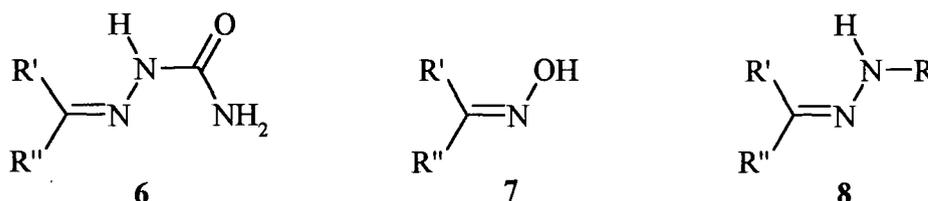
Imines derived from formaldehyde having the general formula $RN=CH_2$, are generally very unstable and can rarely be isolated. Methylene-aniline imine $C_6H_5N=CH_2$ exists only in the gas phase[54] as it is too unstable in solution. The only known stable imine of this type, is N-methylene-2,6-di-isopropylaniline (**9**), formed from formaldehyde and 2,6-di-isopropylaniline[55].
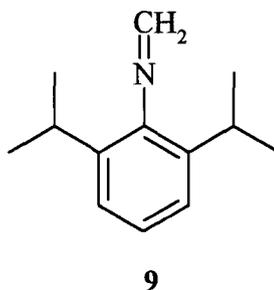
Many reactions of imines involve the intermediacy of iminium ions, $RR'C=N^+HR''$, which are very reactive and hence have short lifetimes in aqueous solution. Jencks and co-workers[56a] examined the kinetics of the decomposition reaction shown in Scheme 1.21.

Scheme 1.21:
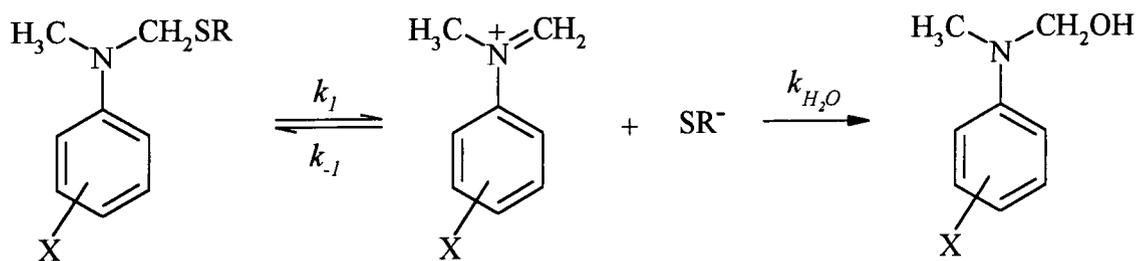
The overall rate constant for the reaction is given by equation 1.3, so that the decomposition is inhibited by added thiolate ion. Assuming that the reaction of iminium ions with thiolate ions is diffusion controlled, $k_{-1} = 5 \times 10^9$ dm^3 mol^{-1} s^{-1}, allowed the calculation, using equation 1.3, of values for k_{H2O}. These varied between 1.0×10^8 s^{-1} for X = 4 – NO$_2$ to 3.1×10^6 s^{-1} for X = 4 – Cl.

$$k_{obs} = k_1 \frac{k_{H_2O}}{k_{-1}[SR^-] + k_{H_2O}}$$

(1.3)

$$\frac{1}{k_{obs}} = \frac{1}{k_1} + \frac{k_{-1}[SR^-]}{k_1\,k_{H_2O}}$$

(1.4)

Very large rate constants for reactions of the iminium ions **10** and **11** with water have also been reported[56d, f].

(10)

(11)

22
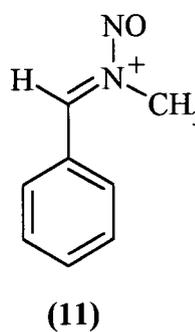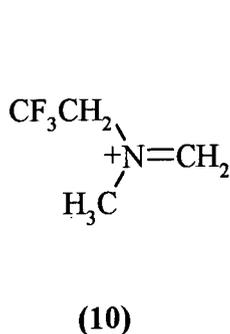
Due to the high reactivity of iminium ions with nucleophiles, imines have found wide use in synthetic work[57]. Some reactions of imines directly relevant to present work are detailed here.

1.4.1: Hydrolysis of imines

As previously discussed, the formation of imines involves reversible stepwise mechanisms and because of this, imines can readily revert back to starting materials. Hydrolysis normally involves reaction via the protonated derivative rather than the imine. The rate is dependent on steric factors and the electron withdrawing ability of the groups attached to the imine[56].

The principle of microscopic reversibility states that the forward and reverse reactions must occur by the same mechanism. A characteristic bell-shaped curve graph for hydrolysis against pH is observed[59]. This again, has been interpreted as corresponding to a change in rate determining step[60]. At basic pH, attack of hydroxide ion, on the iminium ion is rate determining[61] (scheme 1.22)

Scheme 1.22:
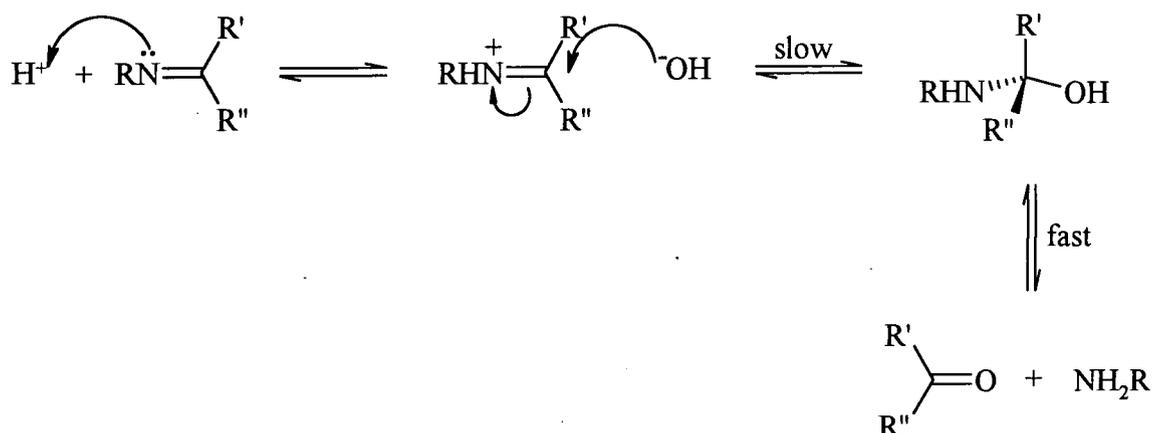
As the conditions become more acidic, attack of water, rather than hydroxide ion on the iminium ion, becomes the predominant pathway and rate determining (scheme 1.23)

Scheme 1.23:
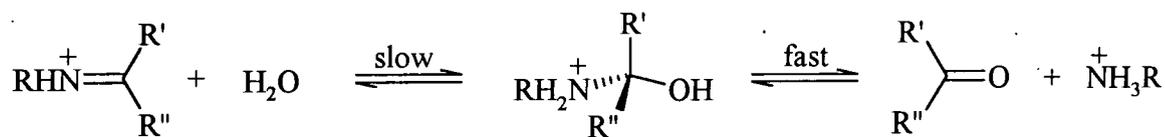
This reaction is general base catalysed: catalysis probably occurs as shown in scheme 1.24.

Scheme 1.24:
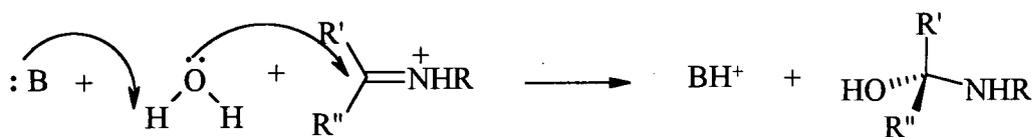
In still, more acidic conditions, the loss of amine from the carbinolamine, becomes rate determining (scheme 1.25).

Scheme 1.25:

24
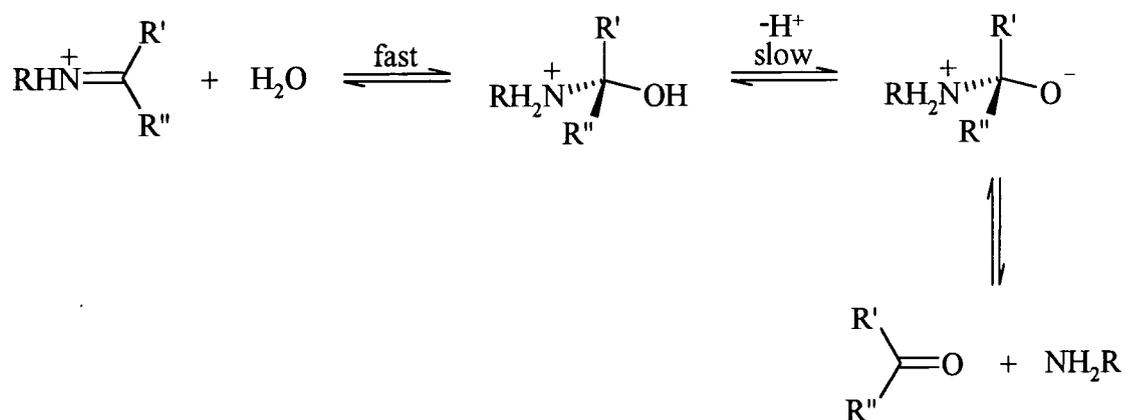
The reaction shown above is considerably slower at very low pH values, as a proton has to be removed from the oxygen atom of the carbinolamine, so that a sufficient driving force is obtained to expel the amine.

1.4.2: The Mannich reaction

The Mannich reaction results from the reaction between an aldehyde, usually formaldehyde, an amine and a compound with an easily removable acidic proton R'H (scheme 1.26). The latter is usually a ketone, an acid or an ester. The product R_2NCH_2R' is known as a Mannich base.

Scheme 1.26:

$$R_2NH \quad + \quad HCHO \quad + \quad R'H \quad \longrightarrow \quad R_2NCH_2R' \quad + \quad H_2O$$
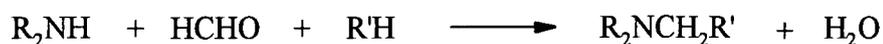
There have been several studies published on the synthesis and mechanism of this type of process, along with further reactions involving the Mannich bases[62]. The reaction mechanism has been discussed and kinetic studies have suggested two mechanisms that should be considered, 'acidic media' and 'basic media', depending on acidity[63].

Acidic media: Using cyclohexanones as an example[63d], the reaction involves electrophilic attack by an iminium ion on the enol form of the cyclohexanone, and is illustrated in scheme 1.27.

25
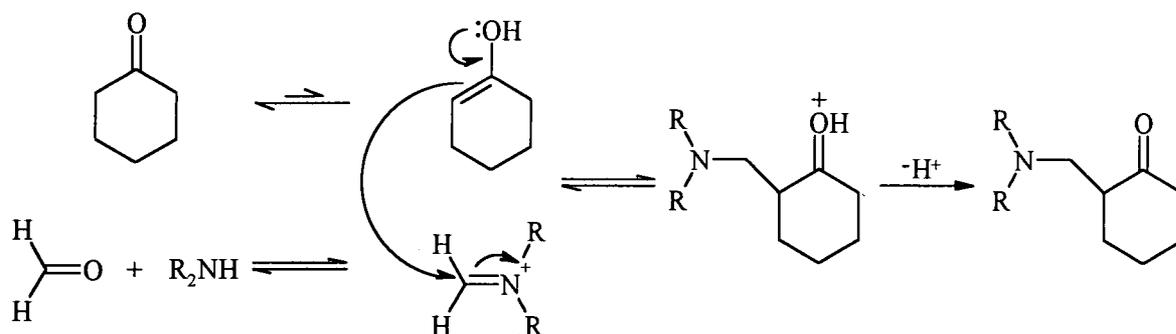
Scheme 1.27:

Basic media: Using the same system, the reaction involves electrophilic attack by an iminuim ion on the enolate form of cyclohexanone and can be seen in scheme 1.28.

Scheme 1.28:
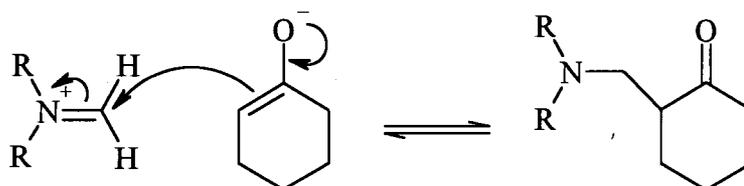
Mannich bases are useful intermediates in the synthesis of alkaloids[64], pharmaceuticals[65] and in the manufacture of paints[66]. Interest in the Mannich reaction is still significant, and there are numerous papers published where the reaction is an integral part of a new synthetic process[67].

1.4.3: The Strecker synthesis

The Strecker synthesis is an R'H specific Mannich reaction where R'H is hydrogen cyanide, HCN. The synthesis was developed[68] in 1850 and yields an α-aminonitrile as shown in scheme 1.29.

26

Scheme 1.31:

$$H_2NCR_2CN \xrightarrow{H^+, H_2O} H_2NCR_2COOH$$
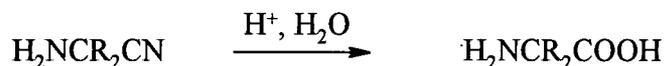
Another important application of α-aminonitriles is in the synthesis of sterically hindered amines[72].

1.4.4: Reaction with amines

Imines may react with amines in an exchange reaction. The aminolysis producing the exchange products, results in the replacement of the amine functionality on the imine with another amine. Reaction proceeds mainly through the cationic iminium ion[73] as shown in scheme 1.32.

Scheme 1.32:
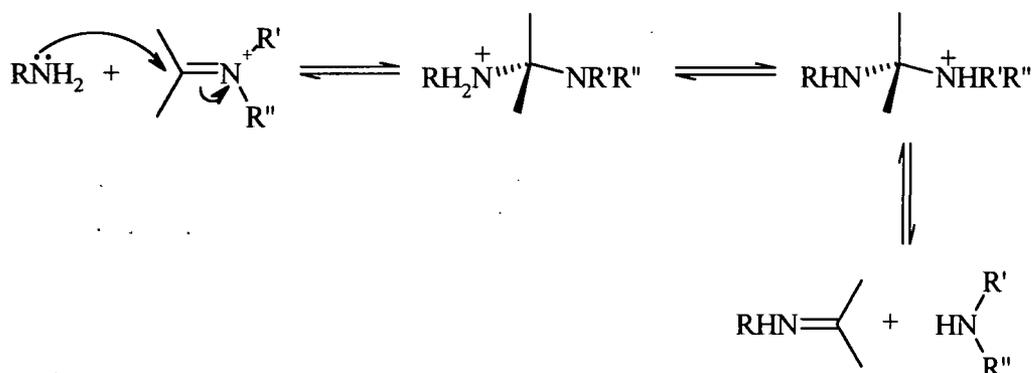
It has been suggested that the rate-determining step in the equilibration is the process that involves attack of the weaker amine on the imine containing the stronger amine[74]. The intermediate of this reaction is analogous to the carbinolamine intermediate in the imine formation.

28

1.4.5: 1,3,5-Hexahydrotriazines

It has been shown that reactions involving primary amine addition to carbonyl groups yield imines. However, due to stability problems they can polymerise. When formaldehyde reacts either in equimolar concentrations or in excess with amines in acidic media, spontaneous polymerization may occur, as shown below, forming a resinous chain polymer (**10**).

$$\left[CH_2NR \underset{}{\bigcirc} CH_2NR \underset{}{\bigcirc} \right]_n$$

10
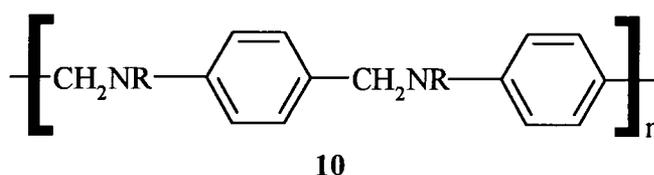
In neutral media, the imine rapidly polymerises to give a cyclic trimer, (scheme 1.33, **11**) 1,3,5-hexahydrotriazine, also known as a hexahydro-*s*-triazine.

Scheme 1.33:

$$3HCHO + 3RNH_2 \rightleftharpoons 3H_2O + 3[RN=CH_2] \rightleftharpoons$$

11
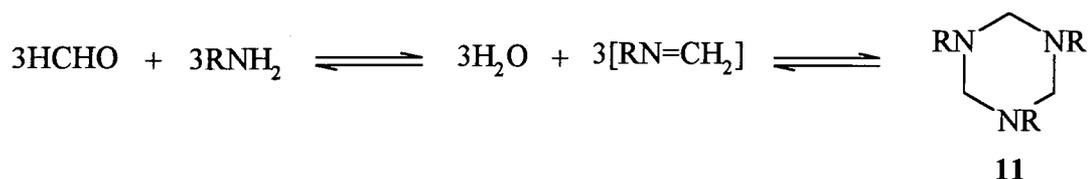
Some of these compounds have been isolated as crystalline solids[75] for both aliphatic and aromatic amines. Brown and Crampton[30] in their studies reacted formaldehyde with aniline and aniline derivatives, producing monomers, diazines, and triazines depending on the reactivity and steric properties of the derivatives. Amorphous higher polymers[76] are often observed as, by-products to the original triazine formation, and have been identified as cyclic tetramers[77]. An example of this, is the reaction of eqiumolar formaldehyde and ammonia, as it yields 1,3,5,7-tetraazatricyclo-(3.3.1.1$^{3.7}$)-decane,[78] or hexamine **12**.

29
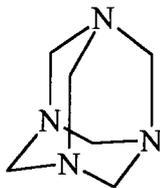
12

An important industrial use of triazines, 1,3,5-triphenyl-1,3,5-hexahydrotriazine in particular, is in the stabilization of plasticized synthetic rubbers[79].

1.5: Aims

The reactions of amine with carbonyl compounds in the presence of nucleophiles are synthetically important. However little detailed information is available regarding the kinetics and equilibrium associated with them. The major aim of the present work was to investigate in detail the processes involved in forming aminoalkanesulfonates from amines, carbonyl compounds and sulfite. There has been some previous work involving reaction of formaldehyde. This includes a brief report[32] of the reactions with ammonia in the presence of sulfite. A mechanistic study of the reactions of formaldehyde with aniline in the presence of sulfite was recently reported[30]. It was recognised that the imine formation was crucial to the overall process with the rate limiting step changing from carbinolamine formation to carbinolamine dehydration with increasing pH.

Of course, carbonyl compounds form addition compounds with sulfite in the absence of amine, and the equilibria involved in these processes are relevant to the overall formation of aminoalkanesulfonates. Here the kinetics and equilibria associated with the reactions of several carbonyl compounds with sulfite have been investigated.

The reaction of propanal with sulfite yields hydroxypropanesulfonate (HPS) and its reactions with aniline have been investigated in detail. The effects of pH on reaction rates, and the effects on reactivity of substituents in the aniline have been examined.

Initial studies of the reaction of benzylamine with hydroxymethanesulfonate have been reported[30]. It was thought to be of interest to make a more detailed study. Benzylamine, pK_a 9.33, is a considerably more basic amine than aniline, pK_a 4.6. Two consequences of this are: 1) the ready protonation of benzylamine which is likely to result in its deactivation and 2) the possibility of the formation of adducts **13** with 1:2 stoichiometry.

$$\underset{\text{CH}_2\text{SO}_3^-}{\underset{|}{\text{N}}} \text{--CH}_2\text{SO}_3^-$$
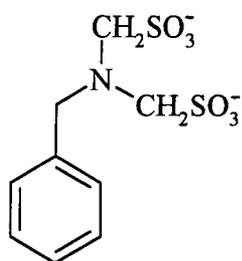
(13)

Comparisons with N-methylbenzylamine, where only formation of adducts with 1:1 stoichiometry is possible, were thought likely to be instructive.

A further aim was to investigate the possibility of stabilisation by metal cations of adducts formed from aniline and/or benzylamine with hydroxymethanesulfonate. It is feasible that cation complexing as shown in 14 and 15 might result in stabilisation of the adducts.
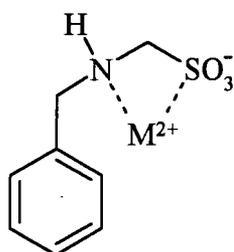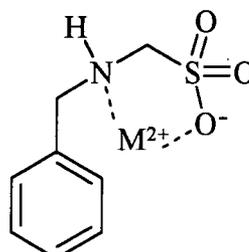
(14)   **(15)**

The reactions involving benzylamine and formaldehyde are likely to involve the imine **16**. the possibility of obtaining addition products, such as trimers, has been studied.

(16)

32
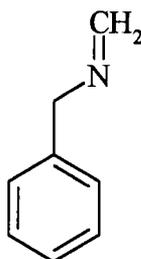
1.6: References

1. (a) M. Tramantini and L. Angiolini, *Tetrahedron*, 1990, **46**, 1971; (b) E. R. Alexander and E. J. Underhill, *J. Am. Chem. Soc.*, 1949, **71**, 4014

2. A. Strecker, *Liebigs Ann. Chem.*, 1850, **75**, 27

3. (a) R. P. Bell, 'Advances in Physical Organic Chemistry', Vol. 4 (Ed. V. Gold), Acad Press, London 1966; (b) Y. Ogata and A. Kawasaki, 'Equilibrium Additions to Carbonyl Compounds', 'The Chemistry of the Carbonyl Group Vol. 2', Ed. S. Patai and J. Zabicky, Interscience, London, 1970, pp. 1

4. I. F. Homfray, *J Chem. Soc.*, 1905, **87**, 1430

5. (a) W. Ramsay and S. Young, *Phil. Trans.*, 1886, **177**, 71; (b) W. H. Perkin, *J. Chem. Soc.*, 1887, **51**, 808

6. I. F. Homfray, *J Chem. Soc.*, 1905, **87**, 1435

7. (a) S. A. Schou, *Compt. Rend.*, 1926, **182**, 965; (b) S. A. Schou, *J. Chim. Phys.*,1929, **26**, 69; (c) W. Hérold and K. L. Wolf, *Z. Physik. Chem. B.*, 1929, **5**, 121; (d) W. Hérold and K. L. Wolf, *ibid.*, 1931, **12**, 165

8. (a) M. Dertooz and J. Nasielski, *Bull. Soc. Chim. Belges.*, 1961, **70**, 794; (b) R. P. Bell and A. O. McDongall, *Trans. Faraday Soc.*, 1960, **56**, 1281

9. P. Rumpf and C. Bloch, *Compt. Rend.*, 1951, **233**, 1364

10. R. P. Bell and J. C. Clunie, *Trans. Faraday Soc.*, 1952, **48**, 439

11. P. G. Evans, M. M. Kreevoy and G. R. Millar, *J. Phys. Chem.*, 1965, **69**, 4325

12. J. Hine and R. Redding, (1964), *Personal Communication* from Ref 3a

13. L. C. Gruen and P. T. McTigue, *J. Chem. Soc.*, 1963, 5217

14. (a) P. Valenta, *Coll. Czech. Chem. Comm.*, 1960, **25**, 853; (b) R. Bieber and G. Trümpler, *Helv. Chim. Acta.*, 1947, **30**, 1860

15. (a) J. O. Edwards, K. M. Ibne-Rasa, E. I. Choi and C. L. Rice, *J. Phys. Chem.*, 1962, **66**, 212; (b) E. Lombardi and P. B. Sogo, *ibid.*, 1960, **32**, 635; (c) Y. Fujiwara and S. Fujiwara, *Bull. Chem. Soc. Japan*, 1963, **6**, 574; (d) M. L. Ahrens and H. Strehlow, *Disc. Faraday Soc.*, 1965, **39**, 112; (e) R. P. Bell and P. G. Evans, *Proc. Roy. Soc. A*, 1966, **291**, 297 (f) Ref. 9 (g) Ref. 10 (h) Ref. 13 (i) Ref. 11

16. P. Greenzaid, Z. Luz and D. Samuel, *J Am. Chem. Soc.*, 1967, **89**, 749

17. P. Federlin, *Compt. Rend.*, 1952, **235**, 44

18. (a) R. A. McClelland and M. Coe, *J. Am. Chem. Soc.*, 1983, **105**, 2718; (b) P. Greenzaid, *J. Org. Chem.*, 1973, **38**, 3164; (c) G. M. Loudon, 'Organic Chemistry', 3rd Ed., 1995; (d) R. P. Bell and P. E. Sørensen, *J. Chem. Soc., Perkin Trans. 2*, 1976, 1594

19. T. H. Lowry and K. S. Richardson, Mechanism and Theory in Organic Chemistry, 2nd Ed., 1981

20. R. W. Taft, 'Steric Effects in Organic Chemistry', Ed. M. S. Newman, J. Wiley and Sons, New York, 1956, 556

21. (a) H. T. Brown and P. S. U. Pickering, *J. Chem. Soc.*, 1897, **71**, 774; (b) M. Cohn and h. C. Urey, *J. Am. Chem. Soc.*, 1938, **60**, 679; (c) J. B. M. Herbert and I. Lauder, *Trans. Faraday Soc.*, 1938, **34**, 432, 1219; (d) V. H. Booth and F. J. W. Roughton, *Biochem. J.*, 1938, **32**, 2049; (e) A. Vesely and R. Brdička, *Coll. Czech. Chem. Comm.*, 1947, **12**, 213; (f) R. P. Bell and W. C. E. Higginson, *Proc. Roy. Soc. A*, 1949, **197**, 141; (g) R. P. Bell and M. B. Jensen, *ibid*, 1961, **261**, 38; (h) R. P. Bell, M. H. Rand and K. M. A. Wynne-Jones, *Trans. Faraday Soc.*, 1956, **52**, 1093; (i) R. P. Bell and B. de B. Darwent, *ibid.*, 1950, **46**, 34; (j) W. P. Jencks, L. H. Funderburk and L. Aldwin, *J. Am. Chem.*

Soc., 1978, **100**, 5444; (k) Ref. 3a; (l) Ref. 5b; (m) Ref. 14b; (n) Ref. 15d; (o) Ref. 15e; (p) Ref. 16; (q) Ref. 19

22. Ref. 21 (g), (h), (j), (k)

23. W. P. Jencks, *Acc. Chem. Res.*, 1976, **9**, 425

24. (a) C. N. Caughlan and H. V. Tartar, *J. Am. Chem. Soc.*, 1941, **63**, 1265; (b) W. M. Lauer and C. M. Langkammerer, *ibid.*, 1935, **57**, 2360; (c) R. L. Shriner and A. L. Land, *J. Org. Chem.*, 1941, **6**, 888

25. (a) K. Arai, *Nippon Kagaku Zasshi*, 1961, **82**, 955; (b) F. C. Kokesh and R. E. Hall, *J. Org. Chem.*, 1975, **40**, 1632; (c) Ref. 19

26. G. E. K. Branch and M. Calvin, 'The Theory of Organic Chemistry', Prentice Hall, New York, 1941

27. (a) P. R. Young and W. P. Jencks, *J. Am. Chem. Soc.*, 1978, **100**, 1228; (b) *ibid*, 1979, **101**, 3288

28. R. Young and W. P. Jencks, *J. Am. Chem. Soc.*, 1977, **99**, 1206

29. J. Büchi, *Pharm. Acta Helv.*, 1931, **6**, 1

30. J. H. Atherton, K. H. Brown and M. R. Crampton, *J. Chem. Soc. Perkin Trans. 2*, 2000, 941

31. P. E. Sørensen and V. S. Andersen, *Acta Chem. Scand.*, 1970, **24**, 1301

32. P. Le Hénaff, *C. R. Acad. Sci.*, 1963, **256**, 3090

33. (a) B. Capon, *Org. React. Mech.*, 1975, 1; (b) M. M. Sprung, *Chem. Rev.*, 1940, **26**, 297; (c) W. P. Jencks, *Progr. Phys. Org. Chem.*, 1964, **2**, 63; (d) R. Bonnett, 'The Chemistry of the Carbon Nitrogen Double Bond', Ed. S. Patai, Interscience, London, 1970, pp. 64

34. R. W. Layer, *Chem. Rev.*, 1963, **63**, 489

35. (a) W. R. Abrams and R. G. Kallen, *J. Am. Chem. Soc.*, 1976, **98**, 7777; (b) *ibid.*, 7789

36. (a) R. G. Kallen, R. O. Viale and L. K. Smith, *J. Am. Chem. Soc.*, 1972, **94**, 576; (b) I. M. C. Brighente, L. R. Vottero, A. J. Terezani and R. A. Yunes, *J. Phys. Org. Chem.*, 1991, **4**, 107; (c) I. M. C. Brighente and R. A. Yunes, *J. Braz. Chem. Soc.*, 1997, **8**, 549; (d) R. Wolfenden and W. P. Jencks, , *J. Am. Chem. Soc.*, 1961, **83**, 2763

37. R. G. Kallen and W. P. Jencks, *J. Biol. Chem.*, 1966, **241**, 5864

38. (a) E. E. Snell and W. T. Jenkins, *J. Cell. Comp. Physiol.*, 1959, **54**, 161; (b) D. E. Metzler, M. Ikawa and E. E. Snell, , *J. Am. Chem. Soc.*, 1954, **76**, 648; (c) G. A. Hamilton and F. H. Westheimer, *ibid.*, 1959, **81**, 6332; (d) W. P. Jencks, 'Catalysis in Chemistry and Enzymology', Dover, New York, 1987; (e) A. E. Braunstein, 'The Enzymes', Vol. 2, Eds P. D. Boyer, H. Lardy and K. Myrback, Academic Press, Inc., New York, 1960, p. 113; (f) E. E. Snell, 'The Mechanism of Action of Water-soluble Vitamins', Little, Brown and Co., Boston, Mass., 1961, p. 18; (g) I. Fridovich and F. H. Westheimer, , *J. Am. Chem. Soc.*, 1962, **84**, 3208; (h) E. Grazi, T. Cheng and B. L. Horecker, *Biochem. Biophys. Res. Comm.*, 1962, **7**, 250; (i) E. Grazi, P. T. Rowley, T. Cheng, O. Tchola and B . L. Horecker, *ibid.*, **9**, 38; (j) R. A. Morton and G. A. J. Pitt, *Prog. Chem. Org. Nat. Prod.*, 1957, **14**, 244; (k) R. Hubbard, *Proc. Natl. Phys. Lab.*, London, *Symp. No. 8*, 1958, 151

39. (a) S. J. Benkovic, P. A. Benkovic and D. R. Comfort, , *J. Am. Chem. Soc.*, 1969, **91**, 1860; (b) J. W. Stanley, J. G. Beasley and I. W. Mathison, *J. Org. Chem.*, 1972, **37**, 3746

40. S. F. Dyke, 'The Chemistry of Enamines', Cambridge University Press, London, 1973

41. (a) D. Craig, L, Schaefgen and W. P. Tyler, , *J. Am. Chem. Soc.*, 1948, **70**, 1624; (b) G. O. Dudek and R. H. Holm, *ibid.*, 1961, **83**, 3914; (c) T. M. Patrick, Jr., *ibid.*, 1952, **74**, 2984; (d) M. Saunders and E. H. Gold, *J. Org. Chem.*, 1962, **27**, 1439

42. R. McGrindle and A. J. McAlees, *J. Chem.Soc., Chem. Comm.*, 1983, 61

43. H. Schiff, *Ann.*, 1864, **131**, 118

44. (a) E. Barrett and A. Lapworth *J. Chem. Soc.*, 1908, **93**, 85; (b) J. B. Conant and P. D. Bartlett, *J. Am. Chem. Soc.*, 1932, **54**, 2881; (c) F. H. Westheimer, *ibid.*, 1934, **56**, 1962; (d) A. Ölander, *Z. Physik. Chem.*, 1927, **129**, 1; (e) W. P. Jencks, *J. Am. Chem. Soc.*, 1959, **81**, 475; (f) E. H Cordes and W. P. Jencks, *ibid.*, 1962, **84**, 832; (g) J. E. Reimann and W. P. Jencks, *ibid.*, 1966, **88**, 3973; (h) L. do Amaral, W. A. Sandstrom and E. H. Cordes, *ibid.*, 2225; (i) B. M. Anderson and W. P. Jencks, *ibid.*, 1960, **82**, 1773; (j) A. V. Willi, *Helv. Chim. Acta*, 1956, **39**, 1193; (k) J. M. Sayer and W. P. Jencks, *J. Am. Chem. Soc.*, 1973, **95**, 5637; (l) A. Williams and L. Bender, *ibid.*, 1966, **88**, 2508; (m) W. P. Jencks, 'Mechanism and Catalysis of Simple Carbonyl Group Reactions', 'Progress in Physical Organic Chemistry', Vol 2, Eds S.G. Cohen, A. Streitwieser, Jr. and R. W. Taft, Interscience, London, 1964, p. 63

45. (a) L. P. Hammett, 'Physical Organic Chemistry', McGraw-Hill Book Co. Inc., New York, 1940, p. 333; (b) G. H. Stempel, Jr. and G. S. Schaffel, *J. Am. Chem. Soc.*, 1944, **66**, 1158; (c) Ref. 44b

46. (a) Ref. 44e – i; (b) A. S. Stachissini and L. do Amaral, *J. Org. Chem.*, 1991, **56**, 1419; (c) Ref. 33c

47. (a) J. M. Sayer, B. Pinsky, A. Schonbrunn and W. Washtein, *J. Am. Chem. Soc.*, 1974, **96**, 7998; (b) S. Rosenberg, S. M. Silver, J. M. Sayer and W. P. Jencks, *ibid.*, 7986; (c) J Hine, F. A. Via, J. K. Gotkis and J. C. Craig, Jr., *ibid.*, 1970, **92**, 5186; (d) J. M. Sayer and W. P.Jencks, *ibid.*, 1972, **94**, 3262; (e) H. Diebler and R. N. F. Thorneley, *ibid.*, 1973, **95**, 896

48. (a) N. E. Hall and B. J. Smith, *J. Phys. Chem.*, 1998, **102A**, 4930; (b) I. H. Williams, *J. Am. Chem. Soc.*, 1987, **109**, 6299; (c) M. Eigen, *Disc. Faraday Soc.*, 1965, **39**, 7; (d) Ref. 3b

49. (a) R. Fett, E. L. Simionatto and R. A. Yunes, *J. Phys. Org. Chem.*, 1990, **3**, 620; (b) I. M. C. Brighente, R. M. Budal and R. A. Yunes, *J. Chem. Soc., Perkin Trans 2*, 1991, 861; (c) Ref. 47a

50. (a) M. Calzadilla, A. Malpica and P. M. Diaz, *Int. J. Chem. Kinetics*, 1996, **28**, 687; (b) A. Malpica, M. Calzadilla, J. Baumrucker, J. Jiménez, L. López, G. Escobar and C. Montes, *J. Org. Chem.*, 1994, **59**, 3398; (c) P. Sojo, F. Viloria, L. Malave, R. Possamia, M. Calzadilla, J. Baumrucker, A. Malpica, R. Moscovici and L. do Amaral, *J. Am. Chem. Soc.*, 1976, **98**, 4519

51. (a) Ref. 44a, b, e, f, h, l; (b) E. H. Cordes and W. P. Jencks, *J. Am. Chem. Soc.*, 1962, **84**, 4319; (c) D. H. R. Barton, R. E. O'Brien and S. Sternhall, *J. Chem. Soc.*, 1962, 470

52. R. G. Kallen, *J. Am. Chem. Soc.*, 1971, **93**, 6236

53. E. H. Cordes and W. P. Jencks, *J. Am. Chem. Soc.*, 1962, **84**, 826

54. G. Distefano, A. G. Giumanini, A. Modelli and G. Poggi, *J. Chem. Soc., Perkin Trans. 2*, 1985, 1623

55. G. Verardo, S. Cauci and A. G. Giumanini, *J. Chem. Soc., Chem. Comm.*, 1985, **24**, 1787

56. (a) S. Eldin and W. P. Jencks, *J. Am. Chem. Soc.*, 1995, **117**, 4851; (b) *ibid.*, 9415; (c) W. P. Jencks, *J. Phys. Org. Chem.*, 1996, **9**, 337; (d) S Eldin, J. A. Digits, S.-T. Huang and W. P. Jencks, *J. Am. Chem. Soc.*, 1995, **117**, 6631; (e) C. K. Kim, I. Y. Lee, C. K. Kim and I. Lee, *J. Phys. Org. Chem.*, 1999, **12**, 479; (f) A. Vigroux, A. J. Kresge and J. C. Fishbein, *J. Am. Chem. Soc.*, 1995, **117**, 4433

57. R. Bonnett, 'The Chemistry of the Carbon Nitrogen Double Bond', Ed. S. Patai, Interscience, London, 1970, pp. 255

58. J. Hine, J. C. Craig, Jr., J. G. Underwood and F. A. Via, *J. Am. Chem. Soc.*, 1970, **92**, 5194

59. (a) K. Koehler, W. Sandstrom and E. H. Cordes, *J. Am. Chem. Soc.*, 1964, **86**, 2413; (b) Ref. 44f, k, m

60. (a) W. P. Jencks, 'Catalysis in Chemistry and Enzymology', Dover, New York, 1987, pp. 460-496; (b) M. A. E. D. El Taher, *J. Solution. Chem.*, 1996, **25**, 401; (c) M. Brault, R. M. Pollack and C. L. Bevins, *J. Org. Chem.*, 1976, **41**, 346; (d) E. H. Cordes and W. P. Jencks, *J. Am. Chem. Soc.*, 1963, **85**, 2846; (e) Ref. 44f; (f) Ref. 59a

61. (a) R. L. Reeves, *J. Am. Chem. Soc.*, 1962, **84**, 3332; (b) Ref. 44k

62. (a) F. F. Blicke, *Organic Reactions*, 1942, **1**, 303; (b) H. O. House, 'Modern Synthetic Reactions', 2nd Ed., W. A. Benjamin, Inc., Philippines, 1972, pp. 654-660; (c) Ref. 1a

63. (a) K. Bodendorf and G. Koralewski, *Arch. Pharm.*, 1933, **271**, 101; (b) S. V. Lieberman and E. C. Wagner, *J. Org.Chem.*, 1949, **14**, 1001; (c) E. R. Alexander and E. J. Underhill, *J. Am. Chem. Soc.*, 1949, **71**, 4014; (d) T. F. Cummings and J. R. Shelton, *J. Org.Chem.*, 1960, **25**, 419; (e) J. E. Fernandez and J. S. Fowler, *ibid.*, 1964, **29**, 402; (f) J. E. Fernandez, J. S. Fowler and S. J. Glaros, *ibid.*, 1965, **30**, 2787; (g) M. Masui, K. Fujita and H. Ohmori, *Chem. Comm.*, 1970, **13**, 182; (h) D. N. Kirk and V. Petrow, *J. Chem. Soc.*, 1962, 1091; (i) H. Volz and H. H. Kiltz, *Tetrahedron Letters*, 1970, **22**, 1917

64. R. Robinson, *J. Chem. Soc.*, 1917, **111**, 762

65. For example: (a) H. Bungard, *Methods in Enzymology*, 1985, **112**, 347; (b) J. R. Dimmock, S. K. Raghavan, B. M. Logan and G. E. Bigam, *Eur. J. Med. Chem.*, 1983, **18**, 249

66. M. Tramontini, L. Angiolini and N. Ghedini, *Polymer*, 1988, **29**, 771

67. Recent examples include: (a) K. Ishimaru and T Kojima, *J. Org. Chem.*, 2003, **68**, 4959; (b) S. Matsunaga, N. Kumagai, S. Harada and M Shibasaki, *J. Am. Chem. Soc.*, 2003, **125**, 4712; (c) A. Dieters, K. Chen, T. C. Eary and S. F. Martin, *ibid.*, 4541

68. A. Strecker, *Liebigs Ann. Chem.*, 1850, **75**, 27

69. (a) Y. Ogata and A. Kawasaki, *J. Chem. Soc., B*, 1971, 325; (b) T. D. Stewart and C. Li, *J. Am. Chem. Soc.*, 1938, **60**, 2782; (c) J. Taillades and A. Commeyras, *Tetrahedron*, 1974, **30**, 2493; (d) Ref. 39b

70. G. Moutou, J. Taillades, S. Bénefice-Malouet, A. Commeyras, G. Messina and R. Mansani, *J. Phys. Org. Chem.*, 1995, **8**, 721

71. (a) M. Béjaud, L. Mion, J. Taillades and A. Commeyras, *Tetrahedron*, 1975, **31**, 403; (b) R. M. Williams, 'Synthesis of Optically Active α-Amino Acids', Pergamon Press, New York, 1989, p. 208

72. (a) J. Sansoulet and C. Tackx, *C. R. Acad. Sci.*, 1960, **250**, 4370; (b) W. H. Taylor and C. R. Hauser, *J. Am. Chem. Soc.*, 1960, **82**, 1960

73. W. P. Jencks, 'Catalysis in Chemistry and Enzymology', Dover, New York, 1987, pp. 505-506

74. (a) B. A. Porai-Koshits and A. L. Remizov, *Prob. Mekhanizma Org. Reaktsii, Akad. Nauk Ukr. SSR, Otdel Fizmat. i Khim. Nauk*, 1953, 238; *Chem. Abstr.*, 1956, **50**, 16686; (b) Ref. 73; (c) Ref. 34

75. (a) J. Graymore, *J. Chem. Soc.*, 1932, 1353; (b) J. G. Miller and E. C. Wagner, *J. Am. Chem. Soc.*, 1932, **54**, 3698; (c) E. Zangrando, G. Poggi, A. G. Giumanini and G. Verardo, *J. f. prakt. Chem.*, 1987, **329**, 195

76. (a) H. Krassig and H. Ringsdorf, *Makromol. Chem.*, 1957, **22**, 163; (b) R. Carpignano, V. Bersano and A. Recorsio, *Ann. Chim., Rome*, 1959, **49**, 1593; (c) Ref. 75b

77. L. Randaccio, E. Zangrando, M. H. Gei and A. G. Giumanini, *J. f. prakt. Chem.*, 1987, **329**, 187

78. (a) J. F. Walker, 'Formaldehyde', American Chemical Society Monograph, Reinhold Publishing, New York, 1964, 3rd Ed., pp. 511-551; (b) E. M. Smolin and L. Rapoport, 'The Chemistry of Heterocyclic Compounds: *s*-Triazines and Derivatives', Interscience Publishers Ltd., London, 1959, pp. 545-596; (c) H. H. Richmond, G. S. Myers and G. F. Wright, *J. Am. Chem. Soc.*, 1948, **70**, 3659; (d) A. T. Nielsen, D. W. Moore, and M. D. Ogan and R. L. Atkins, *J. Org. Chem.*, 1979, **44**, 1678

79. E. Gartner and A. Kock, U.S. Patent 2365405, 1944

Chapter two

2 The reactions of carbonyl compounds with sodium sulfite

2.1: Introduction

2.1.1: Preparation and structure of hydoxyalkanesulfonates

It has been reported that many aldehydes and ketones form solid bisulfite addition products, which are commonly named hydroxyalkanesulfonates (HXS). This reaction is a known method for detection of carbonyl compounds as well as a purification method, due to regeneration of the C=O functionality on acidification of the solid[1].

Much of the early work on the addition compounds was concerned with distinguishing between the structures of hydroxysulfonic acids and esters of sulfurous acid. A useful summary of this work was reported by Raschig and Prahl[2], and by 1930 the hydroxysulfonic acid structure was established. Evidence from Raman spectroscopy[3] favoured this interpretation. More recently, equilibrium constants for the isotopic exchange reactions between the bisulfite ion and several sulfite addition compounds have been measured using ^{34}S (Scheme 2.1).

Scheme 2.1:

$$H^{34}SO_3^- + RR'C(OH)^{32}SO_3^- \rightleftharpoons H^{32}SO_3^- + RR'C(OH)^{34}SO_3^-$$
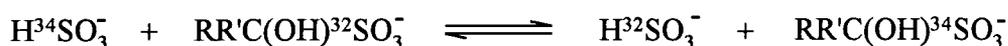
The isotope effects observed ranging from 1.021 for acetone to 1.010 for 4-methoxybenzaldehyde are small, but are much bigger than the value of 1.002 observed for the isotope exchange between diethyl sulphate and ethyl hydrogen sulphate (Scheme 2.2)

Scheme 2.2:
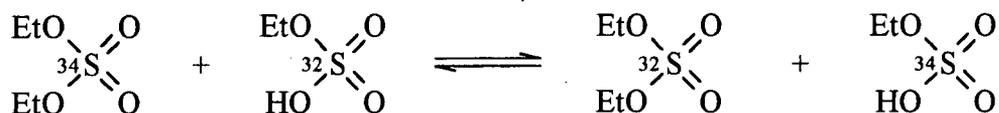
In the latter case the bonding of the sulphur is essentially the same in the two reacting species, leading to the low isotope effect. The larger value observed in the former cases signifies a change in bonding to sulphur, consistent with C-S bond formation[4].

There have been several reports[5] of the use of sulfite adducts as a stable source of the free aldehyde, or ketone. An example is the di-adduct (**2.1**) of glyoxal derivatives[6] used as a source for the 1,2-dicarbonyl compound in ring forming reactions with semicarbazide.
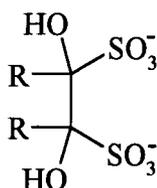
2.1

Hydroxyalkanesulfonates have also been used as a source of carbonyl compound in studies of cyanohydrin formation from methyl perfluoroheptyl ketone[7].

An early NMR study[8] showed that sodium alkane-1-sulfonate and sodium 1-hydroxyalkane-1-sulfonate could be distinguished on the basis of the ^1H signals of the β-group which were at δ *ca.* 2.85 and *ca.* 4.40 respectively. Slow H/D exchange of the signals from the 1-hydroxyalkane-1-sulfonates was rationalised as occurring through traces of the free aldehyde as shown in scheme 2.3.

Scheme 2.3:
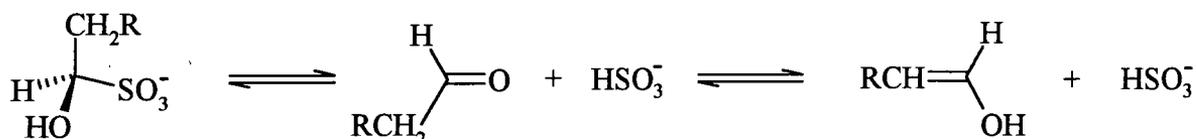
2.1.2: Rate and equilibrium studies for the hydroxyalkanesulfonate system

There have been relatively few quantitative studies involving the measurements of rate and equilibrium constants. Those which have been carried out, can be conveniently divided into two sections; 1) literature concerning the simplest form of these adducts, that of formaldehyde and bisulfite, giving hydroxymethanesulfonate, HMS; and 2) literature involving other generic forms of the adduct.

2.1.2.1: Hydroxymethanesulfonate, HMS

The reaction of formaldehyde with sulfite has been studied both because of its intrinsic interest, and also because of environmental issues. For example the oxidation of sulfur dioxide to sulfuric acid by peroxide is affected by presence of formaldehyde[9]. Several groups have reported kinetic and equilibrium studies for the overall process (scheme 2.4).

Scheme 2.4:

$$(HCHO)_{stoich} \quad + \quad S(IV) \quad \underset{k_b}{\overset{k_f}{\rightleftharpoons}} \quad HMS$$
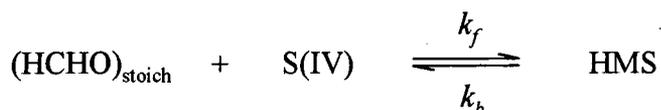
These have used the reaction of sulfite with iodine, or the UV absorbance of sulphur dioxide to monitor concentration changes. A summary of rate constants, k_f and k_b and equilibrium constant, K, (where $K = k_f / k_b$) is given in table 2.1.

Table 2.1: Literature values of the rate and equilibrium constants

k_f / mol^{-1} dm^3 s^{-1}	k_b / s^{-1}	K / mol^{-1} dm^3	Experimental conditions		Reference
			pH	T / °C	
-	-	8.5×10^6	4.0	20	12
1.94	4.8×10^{-7}	4.0×10^6	4.0	25	13
-	5.5×10^{-6}	-	5.0	20	14
12.6	3.5×10^{-6}	3.6×10^6	5.0	25	13
42	1.1×10^{-5}	3.8×10^6	5.6	25	15

The literature values are fairly self-consistent and show that values of k_f and k_b increase with increasing pH. 1. Over the pH range 4 – 6 the value of the equilibrium constant is invariant and indicates that the equilibrium favours the adduct. It is worth noting that in these studies, values were calculated using the total formaldehyde concentration. Since the hydration constant for formaldehyde is 2000, values of the equilibrium constant for the sulfite reaction would be considerably larger if written in terms of the free formaldehyde concentration.

More recently[10] rate constants have been reported for the decomposition reaction measured over a much wider pH range. These studies were made using the stopped-flow technique to observe the first order decomposition of HMS to sulfite and formaldehyde.

Table 2.2: Values obtained for the rate constant k_b at varying pH and 25 °C

pH	k_b / s^{-1}
1.2	$2.27 \times 10^{-8} \pm 1.2 \times 10^{-9}$
2.0	$2.25 \times 10^{-8} \pm 2.3 \times 10^{-9}$
3.1	$5.19 \times 10^{-8} \pm 3.4 \times 10^{-9}$
3.9	$2.98 \times 10^{-7} \pm 8.0 \times 10^{-9}$
5.0	$6.30 \times 10^{-6} \pm 8.3 \times 10^{-8}$
5.9	$4.14 \times 10^{-5} \pm 1.4 \times 10^{-6}$
7.0	$4.64 \times 10^{-4} \pm 5.0 \times 10^{-6}$
7.9	$3.94 \times 10^{-3} \pm 5.3 \times 10^{-5}$

These values are in reasonable agreement with the diverse literature values quoted in table 2.1. They show decreasing value with decreasing pH until a plateau is reached at low pH (<2.5).

A more complete kinetic picture is obtained by recognising that sodium hydroxymethanesulfonate itself is the salt of a strong acid and therefore exists over a large pH range as the monoanion (scheme 2.5, **2.2**). However due to the acidity of the hydroxyl group ionisation to give a dianion (**2.3**) will occur at sufficiently high pH. The overall equilibrium involves the decomposition products, bisulfite HSO_3^- or sulfite SO_3^{2-} and formaldehyde.

Scheme 2.5:
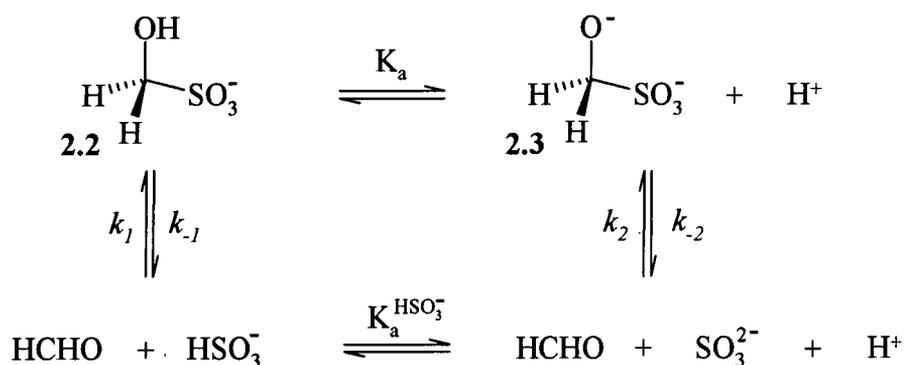
Sørensen and Andersen[11] made measurements over the pH range 9 – 12 and obtained a value for pK_a of 11.7. Their values together with those obtained by Boyce and Hoffmann (11) in acidic solutions, pH 0 – 3.5 and those obtained (Brown) in the pH range 1 – 8 are collected in table 2.3

Table 2.3: Literature values of rate and equilibrium constants at 25 °C

Constant	Value	pH	Reference
K_a	2.0×10^{-12} mol dm^{-3}	9 – 12	11
pK_a	11.7	9 – 12	11
k_1	7.90×10^2 mol^{-1} dm^3 s^{-1}	0 – 3.5	9
k_2	2.48×10^7 mol^{-1} dm^3 s^{-1}	0 – 3.5	9
k_2	9.5×10^6 mol^{-1} dm^3 s^{-1}	9 – 12	11
k_{-2}	43 s^{-1}	9 – 12	11
$K_2 = k_2 / k_{-2}$	2.2×10^5 mol^{-1} dm^3	9 – 12	11
k_2	6×10^6 mol^{-1} dm^3 s^{-1}	1 – 8	10
k_{-2}	25 s^{-1}	1 – 8	10
$K_2 = k_2 / k_{-2}$	2.4×10^5 mol^{-1} dm^3	1 – 8	10
k_{-1}	2.3×10^{-8} s^{-1}	1 – 8	10
$K_1 = k_1 / k_{-1}$	3.4×10^{10} mol^{-1} dm^3	1 – 8	10, 9

The values above show fair agreement with each other, even though varying techniques and experimental conditions were used. The value for k_{-2} is, as expected, considerably higher that that for k_{-1} corresponding to the easier expulsion of sulfite from the dianionic than the monoanionic species. Similarly the greater nucleophilicity of sulfite than of bisulfite is shown by the higher value for k_2 than for k_1. Mechanistically, bisulfite attack is likely to involve the kinetically indistinguishable process of sulfite attack on the protonated aldehyde (scheme 2.6). The equilibrium between the monoanion, **2.2**, and the dianion, **2.3**, will favour the monoanion when the pH is below 11.7. it should be noted that values of k_1 and k_2 given in table 2.2 represent the reaction of free formaldehyde rather than the hydrate.

Scheme 2.6:
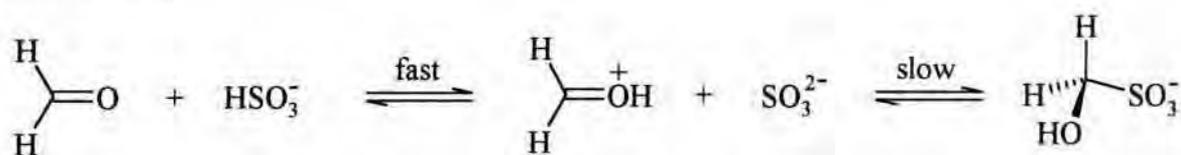
2.1.2.2: Other generic hydroxyalkanesulfonates

Values for the equilibrium constants for formation of bisulfite adducts from a number of aliphatic carbonyl compounds have been reported by Gubareva[12]. Values determined by iodometric titration are given in table 2.4.

Table 2.4: Equilibrium constants for the formation of bisulfite/carbonyl adducts at 20 °C

RR'CO	$K = \dfrac{[RR'C(OH)SO_3^-]}{[RR'CO][HSO_3^-]}$ / dm^3 mol^{-1}
Acetone	290.0
2-Butanone	54.6
Ethyl acetoacetate	91.3
Propanal	3000

The reaction conditions were not specified and the value obtained for the reaction of benzaldehyde was 660 dm^3 mol^{-1} which differs considerably from the more reliable value of 6400 dm^3 mol^{-1} reported by Kokesh and Hall[13]. Hence the values in table 2.4 are of uncertain validity.

Benzaldehyde shows a strong UV absorption at 249nm, while the sulfite adduct absorbs only weakly. Hence the reduction in absorbance has been used as a convenient method of measuring, both the equilibrium and kinetics of adduct formation. This method yields values[13], using the nomenclature of scheme 2.5 for K_1 = 6400 dm^3 mol^{-1}, K_2 = 0.9 dm^3 mol^{-1} and K_a = 2x10^{-11} mol dm^{-3}. Measurements in acidic media[14] pH 0 – 4 gave a similar value of 4800 dm^3 mol^{-1} for K_1.

Values of the rate constants for the dissociation process determined either spectrophotometrically or by titrating the liberated sulfite with iodine have been reported by several authors. Stewart and Donnally[15] reported a linear decrease with decreasing pH in the rate constant for dissociation of the benzaldehyde adduct. At pH 2 the values levelled off, and there was evidence for acid catalysed decomposition in more acidic solutions. Blackadder

and Hinshelwood[16] reported overall dissociation rate constants for reactions of a series of adducts at pH values of 3 and 5. Faster decomposition was observed at higher pH values.

Young and Jencks[17] have investigated the mechanism of the acid catalysed cleavage of the adduct, **2.4**, formed from acetophenone and bisulfite in solutions where pH < 2.

$$H_3C\cdots \underset{\underset{\bigcirc}{|}}{\overset{\overset{OH}{|}}{C}}\blacktriangleleft SO_3^-$$

2.4
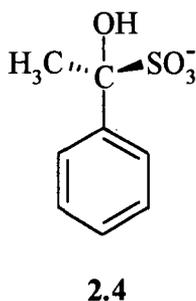
Their interpretation of the observed general acid catalysis was by a mechanism involving rate limiting proton donation to the leaving sulfite group. This is shown in scheme 2.7.

Scheme 2.7:

$$HO-\underset{R'}{\overset{R}{C}}-\underset{O}{\overset{O}{S}}-O^- + H-A \underset{}{\overset{Slow}{\rightleftharpoons}} \left(HO-\underset{R'}{\overset{R}{C}}-\underset{O}{\overset{O}{S}}-O^- \quad H-A \right)$$

$$O=\underset{R'}{\overset{R}{\diagup}} + HSO_3^- + H-A \underset{}{\overset{Fast}{\rightleftharpoons}} \cdot\overset{+}{HO}=\underset{R'}{\overset{R}{\diagup}} + HSO_3^- + A^-$$
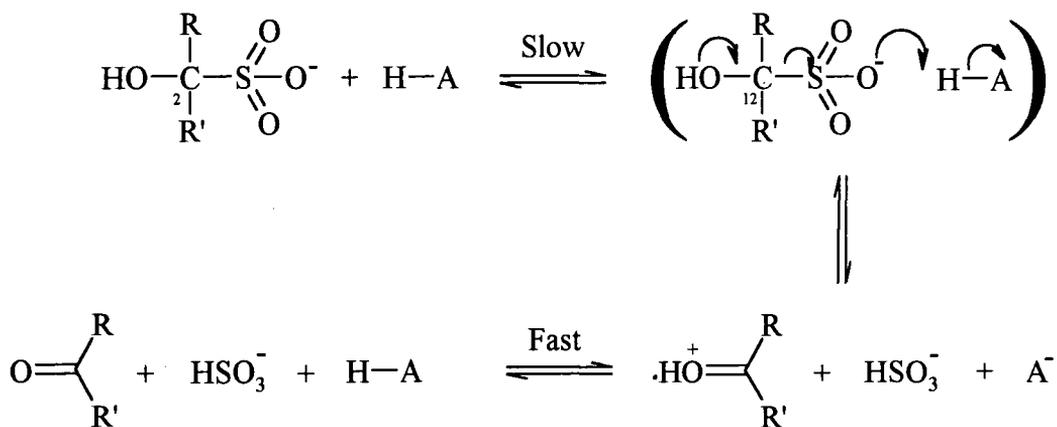
In the reverse, adduct forming direction, this corresponds to the rate limiting attack of bisulfite on the protonated carbonyl compound.

Hoffmann and co-workers[14] have made detailed kinetic studies of the reactions of benzaldehyde and methylglyoxal with sulfite in acidic solution. Values obtained, using the nomenclature of scheme 2.5, are reported in table 2.5

Table 2.5: Rate and equilibrium constants for carbonyl/sulfite, bisulfite systems. Experimental conditions 25 °C, I = 1.0M

R-CHO	k_1 / mol^{-1} dm^3 s^{-1}	k_2 / mol^{-1} dm^3 s^{-1}	K_1 / mol^{-1} dm^3	K_2 / mol^{-1} dm^3	K_a / mol dm^{-3}	pK$_a$	Ref
[a]H-	7.9×10^2	2.5×10^7	3.4×10^{10}	2.2×10^5	2×10^{-12}	11.7	9,14
[b]CH3CO-	3.5×10^3	3.7×10^8	8.2×10^8	5.4×10^4	2×10^{-11}	10.7	14
[c]C$_6$H$_5$-	0.71	2.2×10^4	4.8×10^3	*(1.2×10^2)**	*(6.3×10^{-8})**	*(7.2)**	14

Experimental pH ranges; a. pH 0 – 3.5, b. pH 0.7 – 7.0 and c. 2.5 – 4.4

* Values in italics are unreliable as measurements were obtained when pH < 4

Values of k_1 refer to addition of bisulfite while k_2 refers to sulfite addition. Values obtained with some substituted benzaldehydes, in table 2.6, show that p-NO$_2$ and p-Cl groups increase reactivity whilst p-Me, p-OMe and p-OH groups decrease reactivity.

Table 2.6: Rate constants for the addition reaction between substituted benzaldehydes and sulfite/bisulfite (14a).

Substituent	k_1 /mol^{-1} dm^3 s^{-1}	k_2 /mol^{-1} dm^3 s^{-1}
p-OH-	-	5.8×10^3
p-OCH$_3$-	-	7.8×10^3
p-CH$_3$-	0.68	1.6×10^4
p-Cl-	1.05	5.5×10^4
p-NO$_2$-	5.31	5.7×10^4

2.1.3: Rate and equilibrium studies with aqueous iodine

It can be seen from the literature values given in the previous tables, that work has been limited to relatively few carbonyl compounds, notably formaldehyde and benzaldehyde. Studies involving HMS have been predominant with work covering a wide pH range. The

studies investigated here, involve several ketones and aldehydes in the pH range of 1 to 12. The methods used to measure both rate and equilibrium constants involve determining sulfite concentration by their reactions with iodine.

Aqueous iodine solution with added iodide ions contains a number of species, primarily I_3^- with I_2 and I^-. The reported equilibrium constant[18, 9] for the formation of I_3^- from I_2 and I^- is approximately 720 mol^{-1} dm^3 at 25 °C. The reactions of these species with bisulfite and sulfite ions have been reported in literature, and are shown in scheme 2.8.

Scheme 2.8:

$$I_3^- + HSO_3^- \xrightarrow{k_1} ISO_3^- + 2I^- + H^+$$

$$I_2 + HSO_3^- \xrightarrow{k_2} ISO_3^- + I^- + H^+$$

$$I_3^- + SO_3^{2-} \xrightarrow{k_3} ISO_3^- + 2I^-$$

$$I_2 + SO_3^{2-} \xrightarrow{k_4} ISO_3^- + I^-$$
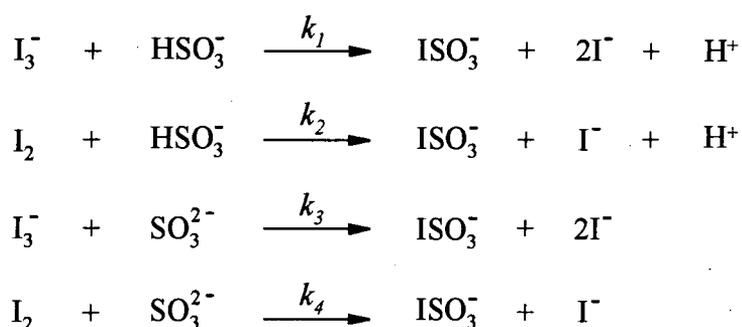
The second order rate constants are found to be $k_1 = 1.5 \times 10^7$, $k_2 = 1.7 \times 10^9$, $k_3 = 2.9 \times 10^8$ and $k_4 = 3.1 \times 10^9$ mol^{-1} dm^3 s^{-1}. When comparing the relative rate constants i.e; $k_2 > k_1$, $k_4 > k_3$, $k_3 > k_1$ and $k_4 > k_2$, it shows that the sulfite ion is a stronger nucleophile than bisulfite, whereas, I_2 is a stronger electrophile than I_3^-. Scheme 2.9 shows how the iodosulfate , ISO_3^-, formed, can rapidly hydrolyse, with the process having a reported first order rate constant of 298 s^{-1} at 25 °C[19].

Scheme 2.9: $$ISO_3^- + H_2O \longrightarrow I^- + SO_4^{2-} + 2H^+$$
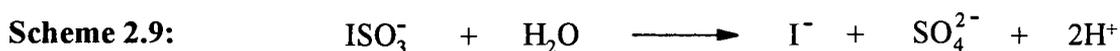
The reactions between the sulfite ions and bisulfite with iodine are essentially irreversible. The bisulfite / sulfite equilibrium[20] has a pKa of 7.0 – 7.2 depending on ionic strength therefore at pH values below 7 the bisulfite form predominates. Conversely, at pH values above 7 sulfite will be the major form. It can be seen from scheme 2.7 that protons are

generated in the reactions, and in order to maintain the correct pH, sufficiently high buffer capacities are needed and thus, were used.

The reaction of a general hydroxyalkanesulfonate, HXS (formed from a general carbonyl compound, RR'CO) with aqueous iodine solution can be written in terms of scheme 2.10[10b]. As a result, a rate expression for this system can be derived (equations 2.1 to 2.5), where terms S(IV), is the sum contribution of both sulfite and bisulfite ions, and $[I_2]_{stoich}$ is the sum of $[I_2]$ and $[I_3^-]$.

Scheme 2.10:
$$HXS \underset{k_f}{\overset{k_b}{\rightleftharpoons}} RR'CO + S(IV) \xrightarrow[k_4]{iodine_{(aq)}} products$$

$$- \frac{d[I_2]_{stoich}}{dt} = k_4[S(IV)][I_2]_{stoich} \tag{2.1}$$

$$\frac{d[S(IV)]}{dt} = k_b[HXS] - k_f[RR'CO][S(IV)] - k_4[I_2]_{stoich}[S(IV)] \tag{2.2}$$

Assuming S(IV) is a steady state intermediate:

$$\frac{d[S(IV)]}{dt} = 0 \tag{2.3}$$

$$\therefore [S(IV)] = \frac{k_b[HXS]}{k_f[RR'CO] + k_4[I_2]_{stoich}} \tag{2.4}$$

$$- \frac{d[I_2]_{stoich}}{dt} = \frac{k_4 k_b[HXS][I_2]_{stoich}}{k_f[RR'CO] + k_4[I_2]_{stoich}} \tag{2.5}$$

The above expression can be simplified to give equation 2.6, as it is expected that the rate of reaction of S(IV) with the aqueous iodine solution is likely to be much faster than that of S(IV) with the carbonyl compound, and therefore $k_4[I_2]_{stoich} \gg k_f[RR'CO]$. Hence the reaction should be zero order with respect to the total aqueous iodine concentration.

$$- \frac{d[I_2]_{stoich}}{dt} = k_b[HXS] = k_{obs} \tag{2.6}$$

To obtain k_{obs} / mol dm^{-3} s^{-1} from a zero order plot at the wavelength studied, its gradient must be divided by the extinction coefficient of the species involved, in this case, aqueous iodine. Thus the UV/Vis spectrum of a standardised aqueous iodine solution with added postassium iodide was taken. Two major peaks at 287 and 350nm were observed giving extinction coefficients of 19600 ± 300 and 13400 ± 300 mol^{-1} dm^3 cm^{-1} respectively. These values can be seen in chapter 7 and were recorded with [KI] at 1x10^{-3} M.

2.2: Results and Discussion

The reactions of propanal, propanone, chloropropanone and pentane-2,4-dione with sulfite were examined. The methods used are outlined below before the results are discussed in detail.

2.2.1: Methods used

2.2.1.1: UV/Vis spectroscopy

Carbonyl compounds show weak absorbance in the UV region due to the n–π* transition. For example propanal has a λ_{max} = 279nm and extinction coefficient, ε = 9 ± 0.1 mol^{-1} dm^3 cm^{-1}.

In the adducts with sulfite this absorption band diminishes. A complication is that bisufite absorbs at 257nm, $\varepsilon = 36 \pm 3$ mol^{-1} dm^3 cm^{-1}. The overall absorption of the bands means that it is difficult to make quantitative measurements using them.

2.2.1.2: NMR Spectrometry

The chemical shifts of groups attached to the carbonyl carbon often show large changes when sulfite addition occurs. These changes were used to determine quantitatively the values of equilibrium constants for adduct formation and their variation with pH. Measurements were necessarily made in deuterium oxide.

2.2.1.3: Equilibrium measurements

The overall equilibria between parent compounds and sulfite are dependent on pH as shown in scheme 2.11.

Scheme 2.11:

An additional factor is the possibility of hydration of the carbonyl compound to produce the diol (scheme 2.12)

Scheme 2.12:
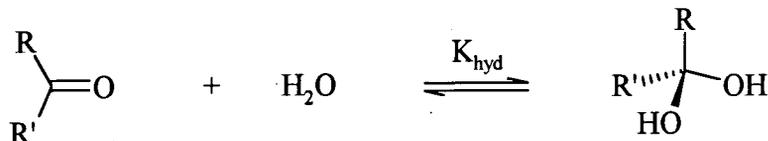
These schemes can be used to derive an expression for K_{obs} (equations 2.12 to 2.17), using the equilibria defined in equations 2.7 to 2.11.

$$K_a = \frac{[HXS^-][H^+]}{[HXS]}$$

(2.7)

$$K_a^{HSO_3^-} = \frac{[H^+][SO_3^{2-}]}{[HSO_3^-]}$$

(2.8)

$$K_1 = \frac{[HXS]}{[RR'CO][HSO_3^-]}$$

(2.9)

$$K_2 = \frac{[HXS^-]}{[RR'CO][SO_3^{2-}]}$$

(2.10)

$$K_{hyd} = \frac{[Hydrate]}{[RR'CO]}$$

(2.11)

K_{obs} is measured experimentally using;

$$K_{obs} = \frac{[HXS] + [HXS^-]}{([RR'CO] + [Hydrate])([SO_3^{2-}] + [HSO_3^-])}$$

(2.12)

$$K_{obs} = \frac{[HXS^-]\left(1 + \dfrac{[H^+]}{K_a}\right)}{[RR'CO](1 + K_{hyd})[SO_3^{2-}]\left(\dfrac{K_a^{HSO_3^-} + [H^+]}{K_a^{HSO_3^-}}\right)} \tag{2.13}$$

$$K_{obs} = \frac{[HXS^-]\left(\dfrac{K_a + [H^+]}{K_a}\right)}{[RR'CO][SO_3^{2-}](1 + K_{hyd})\left(\dfrac{K_a^{HSO_3^-} + [H^+]}{K_a^{HSO_3^-}}\right)} \tag{2.14}$$

$$K_{obs} = K_2\left(\frac{K_a + [H^+]}{K_a}\right)\left(\frac{K_a^{HSO_3^-}}{K_a^{HSO_3^-} + [H^+]}\right)\left(\frac{1}{1 + K_{hyd}}\right) \tag{2.15}$$

$$\text{Since} \quad K_1 = K_2\left(\frac{K_a^{HSO_3^-}}{K_a}\right) \tag{2.16}$$

$$K_{obs} = K_1\left(\frac{K_a + [H^+]}{K_a^{HSO_3^-} + [H^+]}\right)\left(\frac{1}{1 + K_{hyd}}\right) \tag{2.17}$$

The predicted plot of K_{obs} versus pH for this expression can be seen in figure 2.1.

Figure 2.1: Theoretical plot of log K_{obs} vs. pH for the equation 2.17
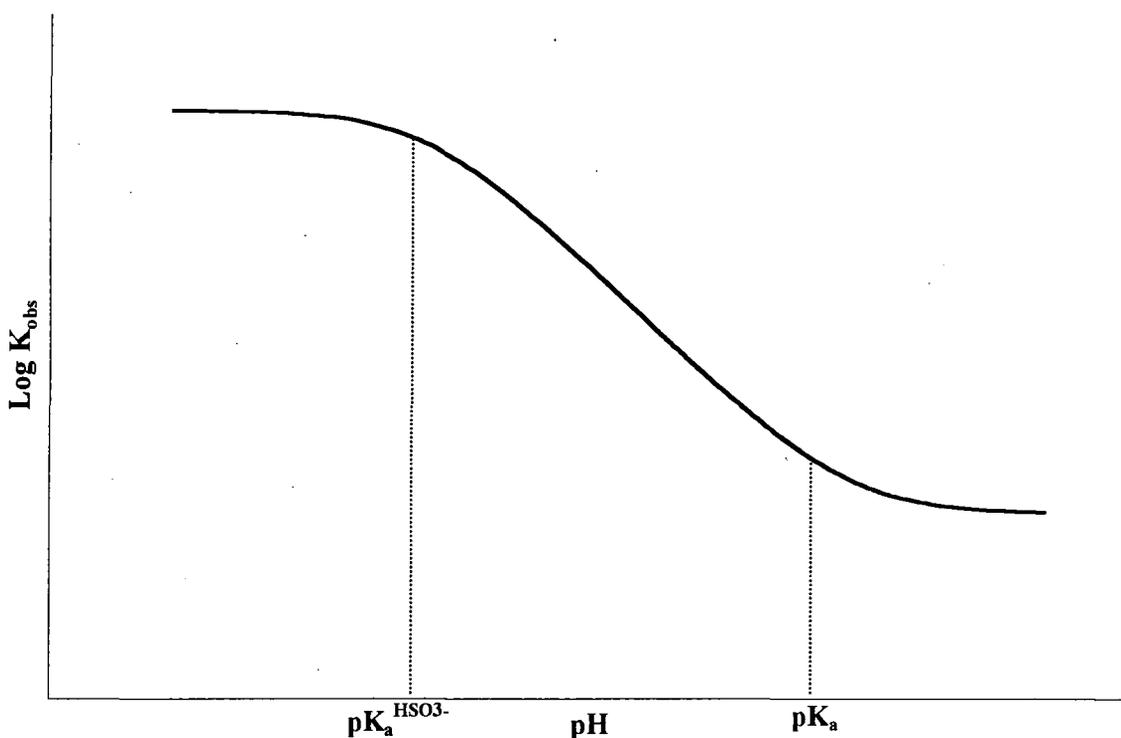
Sørensen and Andersen[11] developed a method for measuring the overall value K_{obs}. The methodology used, involved setting up an equilibrium between a carbonyl compound and sulfite at a given pH and then, rapidly quenching it with an aqueous acidic solution containing iodine and potassium iodide. This had the effect of freezing the equilibrium, while the free, but not bound, sulfite reacted rapidly with the aqueous iodine. Back-titration of the excess iodine allowed the calculation of the concentration of sulfite in the initial equilibrium mixture. Since the stoichmetric concentrations of sulfite and carbonyl compound are known there is sufficient information to calculate a value for K_{obs}. This method was used successfully in this way to determine values of K_{obs} at a series of pH values for the reaction of propanal, acetone and chloroacetone.

2.2.1.4: Kinetics of dissociation

Values of rate constants, k_{-1} and k_{-2}, for dissociation of the sulfite complexes were determined by measuring the rate of sulfite formation using the rapid reaction with aqueous iodine. Experimentally it was necessary to ensure that the initial concentration of sulfite in equilibrium with the carbonyl compound was small. Hence excess carbonyl compound was usually present. Experimentally k_{obs} is related directly to the rate constant for dissociation k_b, as seen equation 2.18.

$$k_b = \frac{k_{obs}}{[\text{HXS}]_{\text{stoich}}} = k_{-1} + \frac{k_{-2}\, K_a}{[\text{H}^+]} \tag{2.18}$$

Theoretically a plot for log k_b versus pH should exhibit two characteristic regions that would be accountable for by the dissociation of either the monoanion or the dianion. Dissociation of the monoanion via k_{-1}, would be independent of acidity and thus, show a plateau when plotted against pH. However the dissociation via the dianion, via k_{-2}, will show an inverse dependence on acidity gives a line of slope 1 when log k_b is plotted against pH.

These methods have been used to examine adducts with sulfite formed from propanal (**1**), acetone (**2**) and chloroacetone (**3**).

2.2.2: Propanal

2.2.2.1: Formation of hydroxypropanesulfonate, HPS

UV/Vis spectra for propanal in the presence of sulfite showed a decrease in absorbance at λ_{max} (279nm), but were not useful for quantitative study. However studies in D_2O using NMR yielded firm evidence showing HPS was formed. Initial NMR studies carried out solely on propanal, produced an equilibrium constant of hydration. Peaks for unhydrated propanal and hydrated diol were clearly observed, and can be seen in figure 2.2.

Figure 2.2: ^{1}H NMR spectrum of propanal 0.05M in D_2O
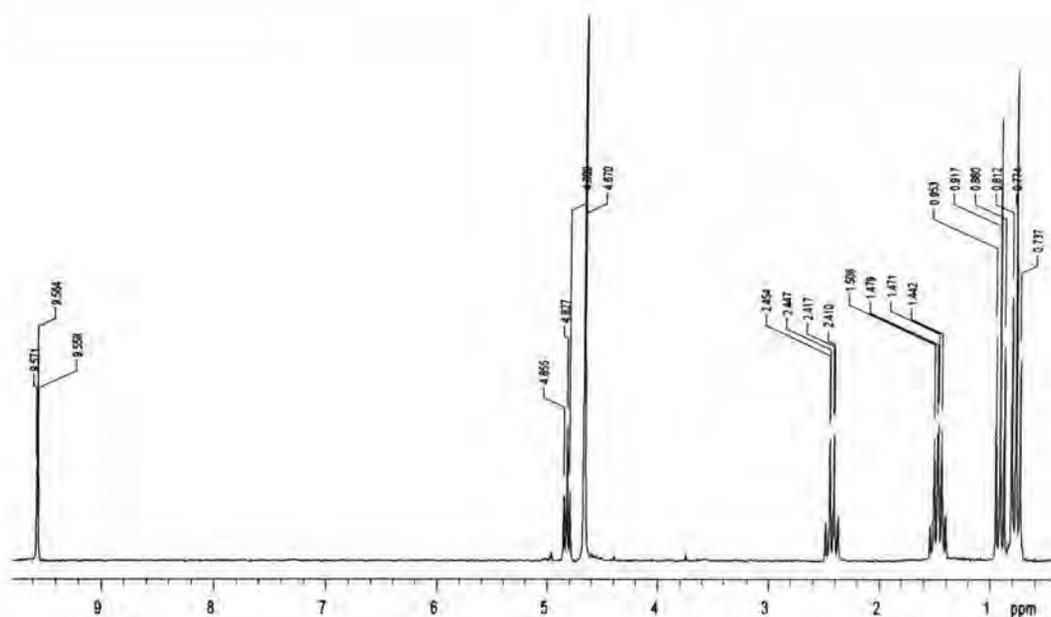
Table 2.7: ^{1}H NMR spectrum of propanal 0.05M in D_2O: peak assignment

δ / ppm	integral ratio	multiplicity	J / Hz	assignment
9.56	1	t	1.4	-CHO (unhyd)
4.82	1.4	t	5.4	-CH(OH)$_2$ (hyd)
4.67	-	-	-	H$_2$O
2.44	2	q	7.4	-CH$_2$- (unhyd)
1.47	3	q	7.6	-CH$_2$- (hyd)
0.92	3	t	7.4	-CH$_3$ (unhyd)
0.77	4.5	t	7.6	-CH$_3$ (hyd)

A value for the hydration constant, K_{hyd}, was calculated from relative intensities for each environment with respect to the number of protons responsible. The value obtained for the alkyl environments was 1.5, but for the carbonyl/diol proton, it was slightly smaller, at 1.4. This difference could either be accounted accountable for by the slight inaccuracy of the technique or by the possible proton/deuteron exchange on the carbonyl/diol system. Thus, the

value of 1.5 would be comparable to the value obtained by Herold[21] when a correction value for the solvent effect is taken into account. Gruen and McTigue[22] suggested from experiments with aliphatic aldehydes, that the solvent isotope effect would account for K_{hyd} being 10 – 20% larger with D_2O than for H_2O. Hence the NMR data give a value for K_{hyd} of 1.2±0.1 in water. This is close to Herold's value of 1.4, but larger that that, 0.7, obtained by Gruen and McTigue.

Reaction of equimolar propanal with sodium bisulfite, in an unbuffered D_2O solution produced an NMR spectrum consistent with the structure of HPS (figure 2.3). Absence of the free propanal and hydrate peaks, suggests that the adduct has a large value for the equilibrium constant of formation. Table 2.8 summarises the spectrum.

Figure 2.3: ^1H NMR spectrum of the reaction product of propanal and $NaHSO_3$ in D_2O
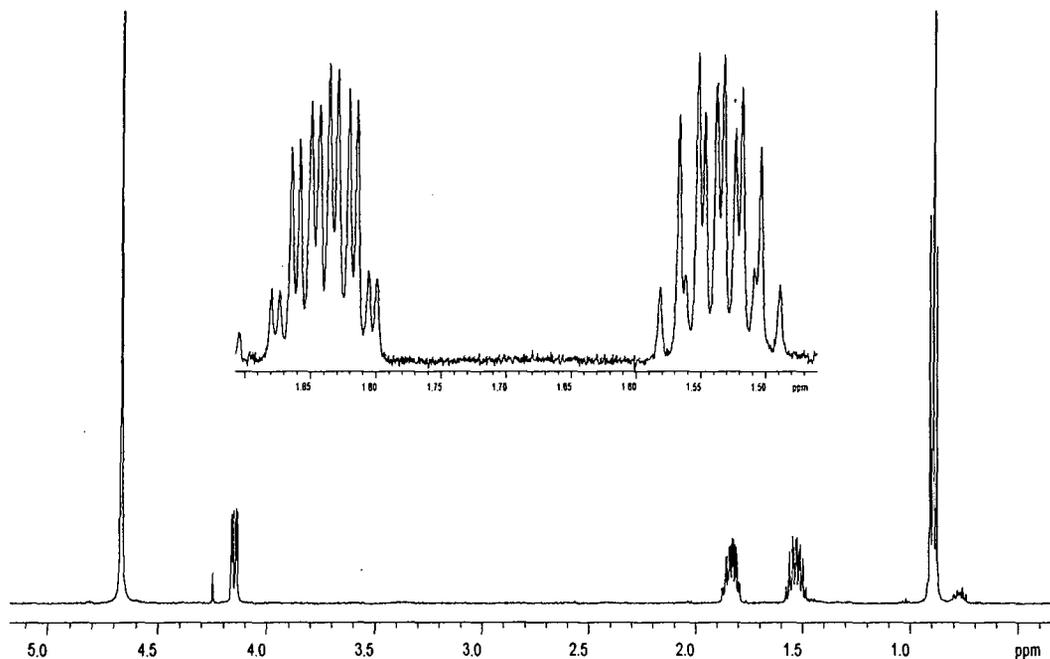
Table 2.8: ^{1}H NMR of the reaction product of propanal and NaHSO$_3$ (equimolar 0.1 mol dm^{-3}) in D$_2$O: peak assignment

δ / ppm	integral ratio	multiplicity	assignment
4.67	-	-	H$_2$O
4.15	1	dd	-CH(OH)(SO$_3$Na)
1.84	1	m	-CH$_A$H$_B$-
1.53	1	m	-CH$_A$H$_B$-
0.90	3	t	-CH$_3$

HPS shows chirality due to the three different groups and proton attached to the carbonyl carbon. This affects the α-carbon to the extent that it forces the two protons into different environments, as seen by the two distinct peaks at 1.84 and 1.53. For this reason, HPS is said to have a J$_{ABX}$ system for the coupled hydrogens, where A and B protons have close proximity, yet X, the methine proton, is too far away to be referred to as C, **2.5**
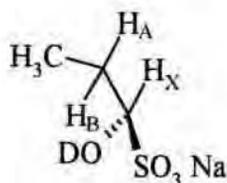
(2.5)

The system shows complex splitting (Figure 2.3) due not only to the three unequivalent protons but to the methyl group as well. Coupling constants can be seen in table 2.9, showing that each proton interacts separately with each other and the methyl group. H$_X$ produces a doublet of doublets showing that indeed, H$_A$ and H$_B$ are non-equivalent. H$_A$ and H$_B$ show complex multiplets. The methyl group interacts with both H$_A$ and H$_B$, with coupling constants which are equal t (7.5 Hz) within experimental error.

Table 2.9: Coupling constants for the HPS molecule

Proton environment	δ / ppm	Coupling interaction	J / Hz
CH$_3$	0.90	J$_{Methyl - Ha}$	7.5
		J$_{Methyl - Hb}$	7.5
H$_A$	1.53	J$_{Ha - Methyl}$	7.5
		J$_{Ha - Hb}$	15
		J$_{Ha - Hx}$	3.2
H$_B$	1.84	J$_{Hb - Methyl}$	7.5
		J$_{Hb - Ha}$	15
		J$_{Hb - Hx}$	10
H$_X$	4.15	J$_{Hx - Ha}$	3.2
		J$_{Hx - Hb}$	10

The unbuffered reaction of propanal 0.1 mol dm^{-3} and sodium sulfite 0.1 mol dm^{-3} was observed by ^{1}H NMR, to be unsuccessful in yielding much HPS. This can be explained by the low proton concentration within the system. The reaction will produce an equivalent of base, scheme 2.13, and independent measurements indicate that propanal is unstable in strongly alkaline media.

Scheme 2.13:

2.2.2.2: Decomposition of hydroxypropanesulfonate, HPS

2.2.2.2.1: Equilibrium studies of HPS

The dissociation of aqueous HPS, 5.0×10^{-3} mol dm^{-3}, was investigated by titration of the free sulfite with aqueous iodine, 0.01 mol dm^{-3}, containing potassium iodide 0.1 mol dm^{-3}. Measurements were made at 25 °C in the pH range of 8 to 12. The general procedure is outlined below and several specimen calculations are reported.

General procedure: A stock solution of the adduct was prepared with propanal 0.5 mol dm^{-3} and sodium bisulfite 0.5 mol dm^{-3}. A 1 cm^3 aliquot was added to a flask containing the appropriate buffer 90 cm^3, 0.1 mol dm^{-3} and sodium chloride 9 cm^3, 1 mol dm^{-3}. This resulted in a solution containing a stoichiometric concentration of 5×10^{-3} mol dm^{-3} of the adduct. After equilibration for ten minutes at 25 °C, the reaction was rapidly quenched by addition with stirring of a mixture containing hydrochloric acid, 1 mol dm^{-3}, iodine 0.01 mol dm^{-3}, and potassium iodide 0.1 mol dm^{-3}. The volume of the mixture added was varied, depending on the pH of the solution to be quenched. The excess iodine was back-titrated with sodium thiosulfate 0.01 mol dm^{-3}. This allowed the calculation of the concentration of the free, unbound, sulfite in the original mixture and hence, a value for K_{obs}. Reaction equilibria can be seen in scheme 2.14.

Scheme 2.14:

$$H_2O + (Sulfite)_{stoich} + I_2 \xrightarrow{\text{1:1 equivalence}} 2I^- + SO_4^{2-} + 2H^+$$

$$I_2 + 2Na_2S_2O_3 \xrightarrow{\text{1:2 equivalence}} 2NaI + Na_2S_4O_6$$
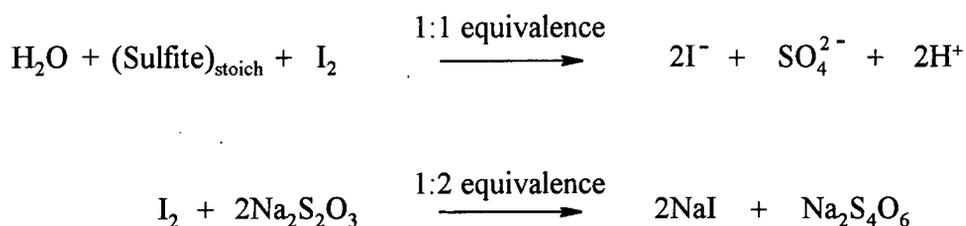
Specimen calculations: The total titration delivered, because of the 1:2 equivalence, gives half the concentration of unreacted iodine. Therefore, half the titration subtracted from the volume of iodine solution used to quench the adduct solution, gave the volume of 0.01 mol dm^{-3} iodine required to quench the free, unbound sulfite. Since the iodine was twice the

concentration of the original stoichiometric concentration of sulfite added to form the adduct, the value had to be doubled. This value divided by 100 (the volume of the original HPS solution) and then, multiplied by the initial sulfite concentration gave the concentration of the free, unbound sulfite. This value was used to calculate the concentrations of adduct and hence, free propanal, which were used to calculate a value of the equilibrium constant, K_{obs}. In table 2.10, the calculations used to obtain K_{obs} values are shown for several pH values. Experiments, for example B, where the initial propanal concentration was varied yielded concordant values for K_{obs}.

Table 2.10: Specimen calculations for the equilibrium dissociation reactions of HPS. All volumes are in cm^3

Exp. Cond	Total Titre	Vol. acidic I_2	Vol. I_2 used	Vol HSO_3^- (5×10^{-3} M)	$[HSO_3^-]$ / mol dm^{-3}	[adduct] / mol dm^{-3}	[EtCHO] / mol dm^{-3}	K_{obs} / dm^3 mol^{-1}
A	4.5	30	27.75	55.5	2.775×10^{-3}	2.225×10^{-3}	2.775×10^{-3}	288
B	5.0	30	27.5	55.0	2.75×10^{-3}	2.25×10^{-3}	3.25×10^{-3}	252
C	38.3	30	10.85	21.7	1.085×10^{-3}	3.915×10^{-3}	1.085×10^{-3}	3326
D	16.9	30	21.55	43.1	2.155×10^{-3}	2.845×10^{-3}	2.155×10^{-3}	613
E	16.2	50	41.9	83.8	4.19×10^{-3}	8.1×10^{-4}	4.19×10^{-3}	46

Experimental conditions A = Equimolar(0.5 mol dm^{-3}), pH 9.8; B = Propanal 0.55 mol dm^{-3} & Bisulfite 0.5mol dm^{-3}, pH 10.0; C = Equimolar (0.5 mol dm^{-3}), pH 8.5; D = Equimolar (0.5 mol dm^{-3}), pH 9.6; E = Equimolar (0.5 mol dm^{-3}), pH 11.8; concentrations are for the stock solutions before dilution.

Values obtained for K_{obs} for other pH values are summarised in Table 2.11

Table 2.11: Selected K_{obs} values calculated for the HPS formation reaction at 25 °C

pH	K_{obs} / dm^3 mol^{-1}
8.5	3300
8.8	2600
9.1	1500
9.3	1075
9.5	797
9.6	613
9.7	401
9.8	297
9.9	211
10.0	199
10.1	166
10.2	122
10.5	116
10.6	105
10.7	92
10.9	67
11.2	59
11.6	49
11.8	46
12.3	43

A plot of Log K_{obs} versus pH is shown in Figure 2.4. For propanal measurements were only possible, using this method, for pH values ≥ 8.5, since at higher acidities the values of K_{obs} were too large for accurate determination. In the measured range pH 8.5 – 12.3 the condition $K_a^{HSO3-} \gg [H^+]$ will apply hence equation 2.15 reduces to equation 2.19.

$$K_{obs} = K_2 \left(\frac{K_a + [H^+]}{K_a} \right) \left(\frac{1}{1 + K_{hyd}} \right)$$

(2.19)

The data at pH ≥ 8.5 give a good fit, as shown, with this equation with values of K_2 95 ± 5 dm^3 mol^{-1}, K_a $(2.3\pm0.3)\times10^{-11}$ mol dm^{-3} and using the known value for K_{hyd} of 1.2. The pK_a value for HPS is hence 10.64.

Since the dissociation constant, K_a^{HSO3-}, of the bisulfite ion is known[20] to have the value 8.0×10^{-8} mol dm^{-3} ($pK_a^{HSO3-} = 7.1$) equation 2.15 was used to construct the curve at higher acidities, pH <8.5.

Use of equation 2.16 yields a value for K_1 of $(3.3\pm0.2)\times10^{-5}$ dm^3 mol^{-1}.

Figure 2.4: Plot of Log K_{obs} versus pH for the HPS formation reaction with a superimposed fit of equation 2.17. $K_a^{HSO3-} = 8.0\times10^{-8}$ mol dm^{-3}, $K_{hyd} = 1.2$ mol dm^{-3}, $K_1 = 3.3\times10^5$ dm^3 mol^{-1}, $K_a = 2.3\times10^{-1}$ mol dm^{-3}
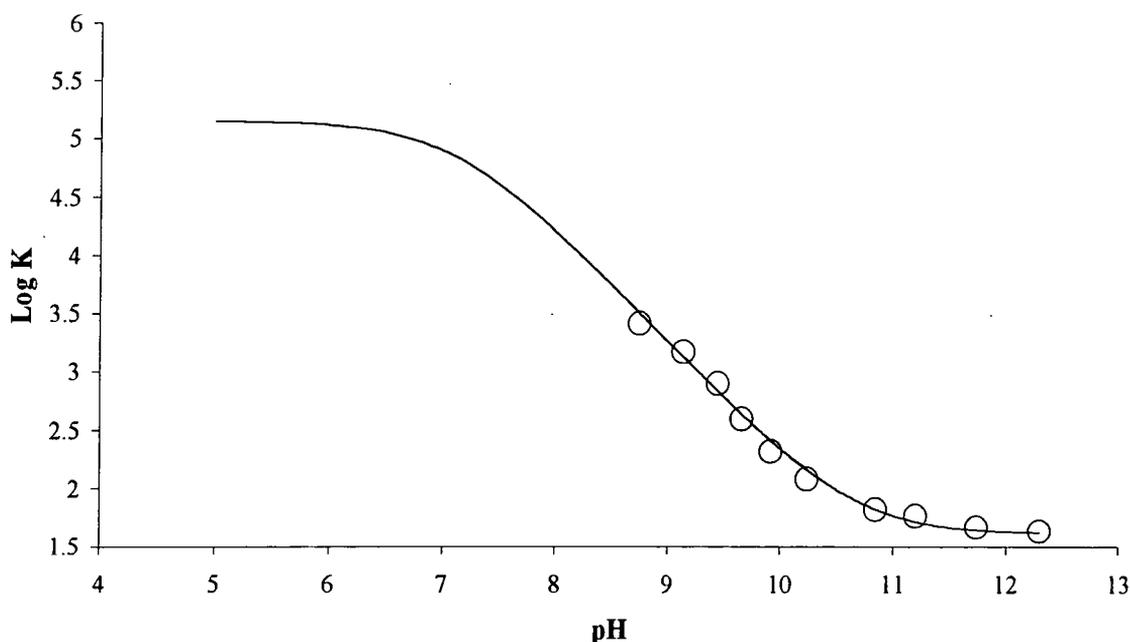
Søresen and Andersen[11] have shown how a linear plot can be obtained from the variation of the values of K_{obs} with hydroxide concentration. Their treatment, which for brevity is not reproduced here, uses the equilibria in scheme 2.15 to derive the relation shown in equation 2.20.

Scheme 2.15:

$$CHRO + H_2O \overset{K_{hyd}}{\rightleftharpoons} CHR(OH)_2$$

$$CHRO + SO_3^{2-} \overset{K_2}{\rightleftharpoons} CHR(O^-)SO_3^-$$

$$CHR(OH)SO_3^- + {}^-OH \overset{K_a/K_w}{\rightleftharpoons} CHR(O^-)SO_3^- + H_2O$$
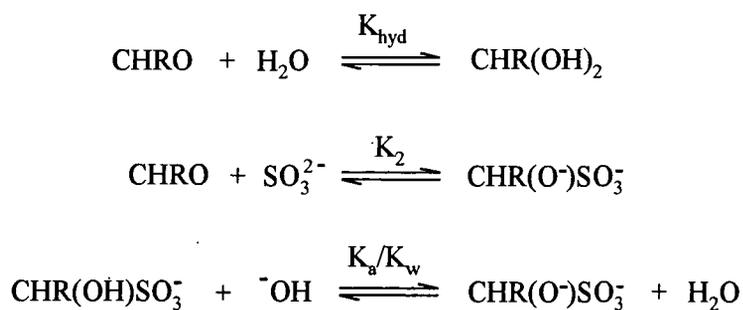
$$\frac{1}{[OH^-]} = K_{obs}\frac{(1 + K_{hyd})K_a}{K_2 K_w} - \frac{K_a}{K_w}$$

(2.20)

The plot shown in figure 2.5 is linear with an intercept on the y axis of -1870 dm^3 mol^{-1}. This allows the calculation of a value for K_a of $(2.0\pm0.2)\times10^{-11}$ mol dm^{-3}. The value of the slope is 51.7 leading to a value for K_2 of 85 ± 5 dm^3 mol^{-1}.

Hence the values obtained from directly fitting the experimental data and the linear plot are in good agreement.

Figure 2.5: K_{obs} versus $1 / [OH^-]$ for the HPS formation reaction
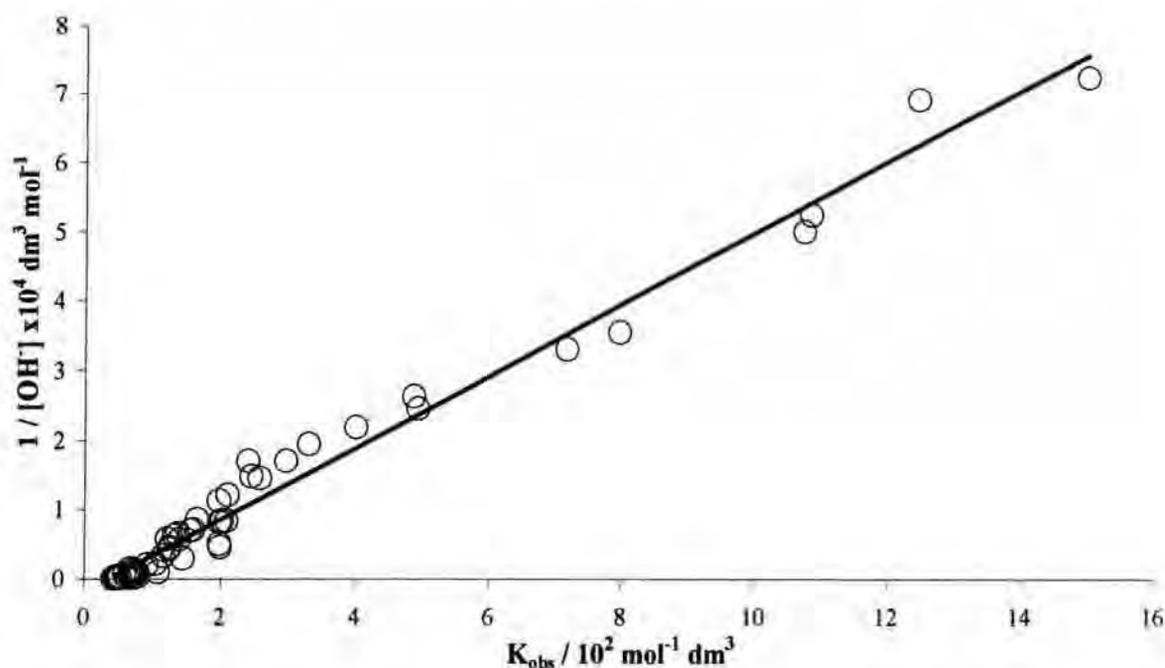
2.2.2.2.2: Kinetic studies of HPS

The reaction of aqueous HPS at concentrations of 1×10^{-3} to 0.1 mol dm^{-3} was measured with 1×10^{-4} mol dm^{-3} aqueous iodine solution ($KI = 1 \times 10^{-3}$ mol dm^{-3}) at 25 °C in the pH range of 1 to 7, using the stopped-flow method. HPS concentrations correspond to complete adduct formation, as propanal was twice as concentrated as bisulfite to ensure that the reaction observed, was that of the sulfite liberated from HPS. The disappearance of the iodine peak was observed at 350nm. Typical spectra of the reaction at pH 4.1 can be seen in figure 2.6. As predicted from equation 2.7, the reaction was found to be zero order with respect to the iodine concentration. Hence, plots for absorbance against time were linear, with the slope being dependent on the concentration of HPS; an example for pH 4.1 is shown in figure 2.7. Checks were made to ensure that negligible reactions occurred between propanal and iodine alone under the reaction conditions.

Figure 2.6: UV/Vis spectral plots for the reaction of 1×10^{-3} mol dm^{-3} HPS with 1×10^{-4} mol dm^{-3} aqueous iodine solution (KI = 1×10^{-3} mol dm^{-3}) at pH 4.1, 25 °C over time.
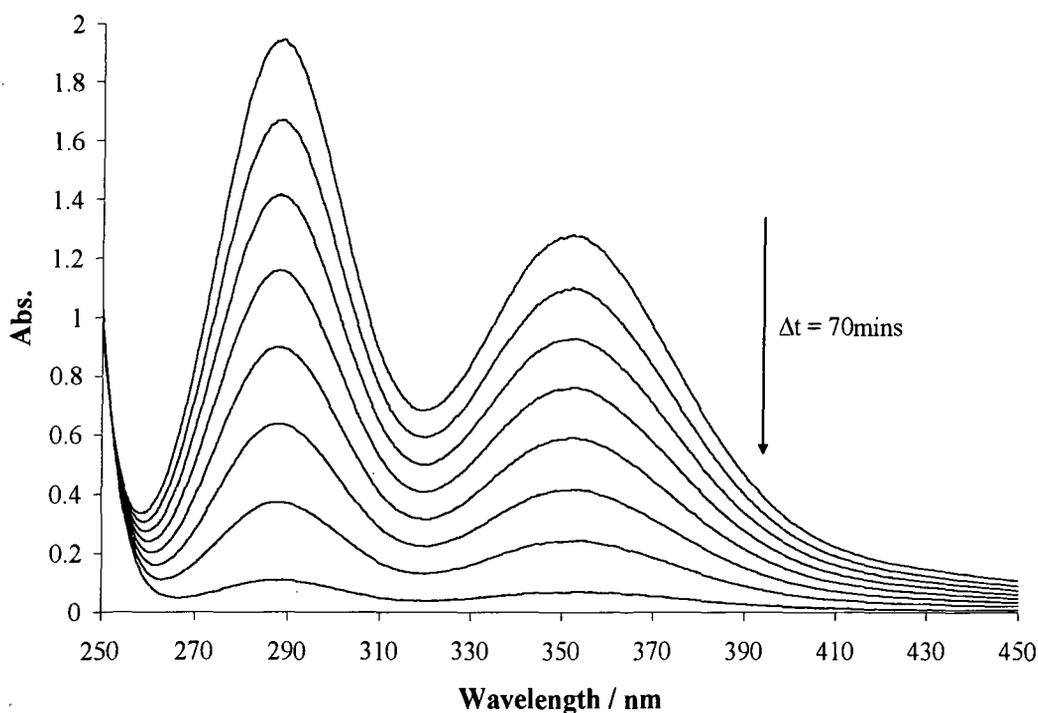
Figure 2.7: Zero order plots for varying HPS concentrations with 1×10^{-4} mol dm^{-3} aqueous iodine solution (KI = 1×10^{-3} mol dm^{-3}) at pH 4.1, 25 °C
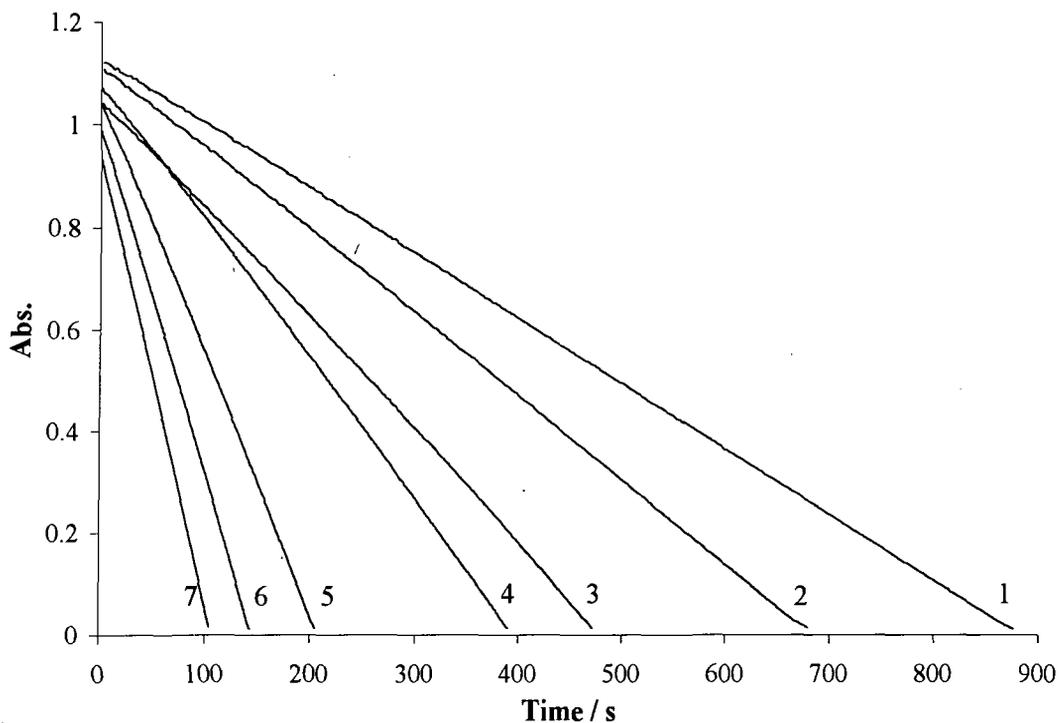
1 = 1.0×10^{-3}M HPS; 2 = 1.5×10^{-3}M; 3 = 2.0×10^{-3}M; 4 = 2.5×10^{-3}M; 5 = 5.0×10^{-3}M; 6 = 7.5×10^{-3}M; 7 = 0.01M

Gradients were obtained by linear regression for the zero order plots. These were divided by the extinction co-efficient of iodine at 350nm, 13400 mol^{-1} dm^3 cm^{-1}, to obtain values for k_{obs} / mol dm^{-3} s^{-1}. The results are shown in table 2.12.

Plotting k_{obs} / mol dm^{-3} s^{-1} versus HPS concentration allowed the calculation of k_b, the first order rate constant, defined in equation 2.6. A typical plot is shown in figure 2.8.

In the more acidic buffers rates of sulfite release were reasonably slow so that complementary measurements were also made using conventional spectrophotometry. Results are shown in table 2.13.

Table 2.12: k_{obs} / mol dm^{-3} s^{-1} obtained at different pH with varied HPS concentration and 1×10^{-4} mol dm^{-3} aqueous iodine solution (KI = 1×10^{-3} mol dm^{-3}), using the Stopped-flow technique

[HPS] / mol dm^{-3}	k_{obs} / mol dm^{-3} s^{-1}					
	pH 0.9	pH 2.9	pH 4.1	pH 5.0	pH 5.9	pH 7.1
1.0×10^{-3}	3.71×10^{-9}	7.23×10^{-9}	9.30×10^{-8}	5.46×10^{-7}	5.60×10^{-6}	7.12×10^{-5}
1.5×10^{-3}	5.56×10^{-9}	1.03×10^{-8}	1.27×10^{-7}	8.47×10^{-7}	7.50×10^{-6}	1.07×10^{-4}
2.0×10^{-3}	7.81×10^{-9}	1.42×10^{-8}	1.65×10^{-7}	1.33×10^{-6}	1.13×10^{-5}	1.37×10^{-4}
2.5×10^{-3}	1.05×10^{-8}	1.65×10^{-8}	2.07×10^{-7}	1.71×10^{-6}	1.25×10^{-5}	1.75×10^{-4}
5.0×10^{-3}	2.04×10^{-8}	3.27×10^{-8}	3.65×10^{-7}	3.21×10^{-6}	2.07×10^{-5}	3.48×10^{-4}
7.5×10^{-3}	4.21×10^{-8}	4.67×10^{-8}	5.21×10^{-7}	4.80×10^{-6}	2.81×10^{-5}	4.42×10^{-4}
0.01	-	5.88×10^{-8}	6.69×10^{-7}	6.30×10^{-6}	3.29×10^{-5}	6.31×10^{-4}

Table 2.13: k_{obs} / mol dm^{-3} s^{-1} obtained at different pH with varied HPS concentration and 1×10^{-4} mol dm^{-3} aqueous iodine solution (KI = 1×10^{-3}), using conventional UV/Vis spectrometry

[HPS] / mol dm^{-3}	k_{obs} / mol dm^{-3} s^{-1}		
	pH 1.5	pH 2.0	pH 3.4
0.01	4.24×10^{-8}	5.35×10^{-8}	2.80×10^{-7}
0.02	8.39×10^{-8}	1.09×10^{-7}	5.22×10^{-7}
0.04	1.66×10^{-7}	2.03×10^{-7}	9.45×10^{-7}
0.06	2.56×10^{-7}	2.91×10^{-7}	1.34×10^{-6}
0.08	3.48×10^{-7}	3.95×10^{-7}	1.69×10^{-6}
0.1	4.27×10^{-7}	4.88×10^{-7}	2.02×10^{-6}

Figure 2.8: Plot of k_{obs} / mol dm^{-3} s^{-1} against HPS / mol dm^{-3} at pH 4.1, 25 °C
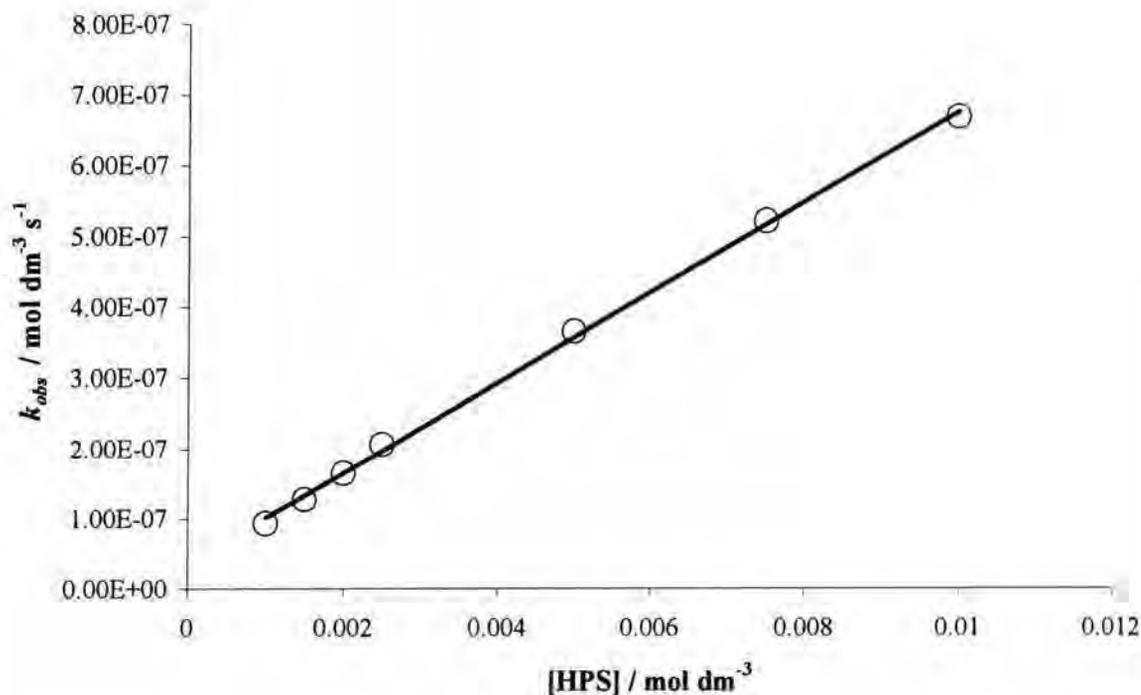
Good linear plots were obtained and correlation coefficients at all pH values were > 0.985. Values obtained for k_b are collected in table 2.14. The plot of Log k_b versus pH is shown in figure 2.9.

Table 2.14: Calculated values of k_b the first order rate constant for the decomposition of HPS at varying pH

pH	k_b / s^{-1}
0.9	4.26×10^{-6}
1.5	4.26×10^{-6}
2.0	4.70×10^{-6}
2.9	5.79×10^{-6}
3.4	1.93×10^{-5}
4.1	7.55×10^{-5}
5.0	6.36×10^{-4}
5.9	4.88×10^{-3}
7.1	6.05×10^{-2}

Figure 2.9: Plot of Log k_b versus pH, with a superimposed fit of equation 2.18 for the decomposition kinetics of HPS
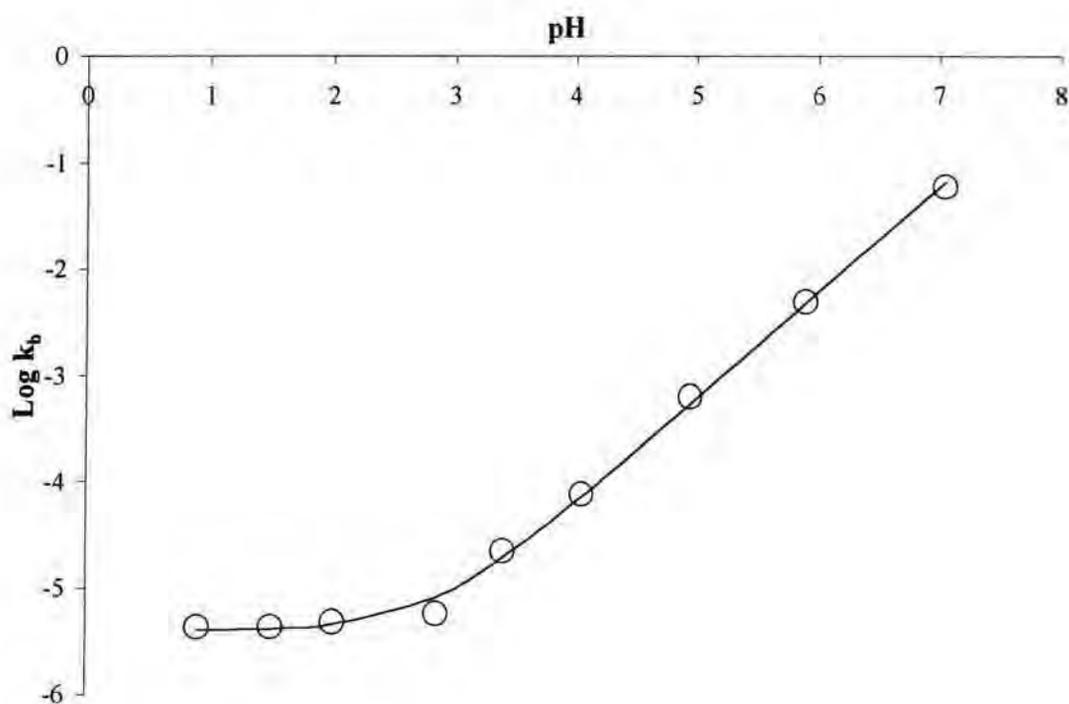
The first order rate constant k_b for decomposition of HPS, clearly shows pH dependency above pH 3. Below this pH, and especially, below pH 2, k_b becomes independent of acidity with values remaining constant within experimental error.

The plot may be discussed in terms of equation 2.18. In acidic solutions where equation 2.20 is true, the equation 2.21 is valid.

$$k_{-1} \gg \frac{k_{-2} K_a}{[H^+]}$$

(2.21)

$$\therefore \quad k_b = k_{-1}$$

(2.22)

This leads to a value for k_{-1} of $(4.0\pm0.4)\times10^{-6}$ s^{-1}.

In less acidic solutions where equation 2.23 holds then equation 2.24 is valid. This leads to equation 2.25.

$$k_{-1} \ll \frac{k_{-2} K_a}{[H^+]}$$

(2.23)

$$k_b = \frac{k_{-2} K_a}{[H^+]}$$

(2.24)

$$\text{Log } k_b = \text{Log } k_{-2} K_a + \text{pH}$$

(2.25)

Extrapolation of the acid dependent part of figure 2.9 to pH = 0 allows the determination of a value for Log $k_{-2} K_a$ of -8.13. This gives a value for $k_{-2} K_a$ of 7.4×10^{-9} mol dm^{-3} s^{-1}, since the value of K_a is known to be 2×10^{-11} mol dm^{-3}, a value for k_{-2} of 370 s^{-1} is found.

Using the results in table 2.14 together with equation 2.18 it is possible to evaluate values for k_{-2} at each pH measured. Using fixed values for k_{-1}, 4.0×10^{-6} s^{-1}, and K_a, 2×10^{-11} mol dm^{-3}, leads to the values given in table 2.15, which are in satisfactory agreement with that obtained by the extrapolation method.

Table 2.15: Calculated values for the first order rate constant for the decomposition of the dianion form of HPS, in the pH range of 3.4 to 7.1

pH	k_{-2} / s^{-1}
3.4	300
4.1	280
5.0	320
5.9	305
7.1	270

The results in figure 2.9 show that values of k_b increase with pH when pH > 3. This is likely to indicate reaction via the dianionic form, path b, in scheme 2.16. Only in acidic solution pH < 3 can reaction via the monoanionic form, path a, compete. It is to be expected, as observed, that the value of k_{-2} for sulfite expulsion from the dianion will be considerable larger than the value of k_{-1} for expulsion from the monoanion. The pK$_a$ value for sulfurous acid[23] is 1.8 so that in these solutions protonation of the sulfonate group is unlikely. Measurements were not made in strongly acidic media where Jencks[17] showed that general acid catalysis of decomposition may be possible.

Scheme 2.16:
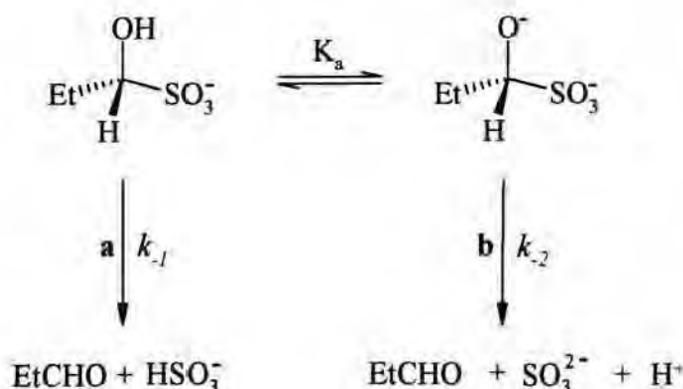
The knowledge of values of k_{-1} and k_{-2} together with values of K_1 and K_2 allows the calculation of values for k_1 ($K_1.k_{-1}$) 1.3 dm^3 mol^{-1} s^{-1} and k_2 ($K_2.k_{-2}$) 3.5x10^4 dm^3 mol^{-1} s^{-1}.

Mechanistically the k_1 and k_{-1} steps are likely to involve rate-limiting attack of sulfite on the protonated aldehyde in the forward direction, and expulsion of sulfite from the monoanion in the reverse direction, (scheme 2.17).

Scheme 2.17:
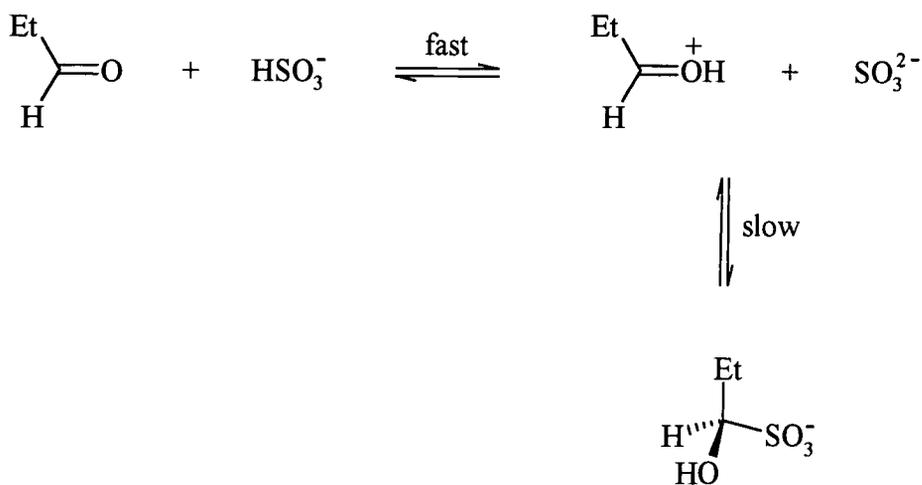
2.2.3: Propanone

2.2.3.1: Formation of hydroxyisopropanesulfonate, HIPS

The UV/Vis spectra provided evidence for interaction between propanone and sulfite. Thus propanone shows a band at λ_{max} 265 nm, ε 16±0.2 dm^3 mol^{-1} cm^{-1} which decreases in the presence of sulfite. For example in the presence of equimolar sodium bisulfuite, 0.1 mol dm^{-3}, the absorbance decreases from 1.6 to 0.3. However since bisulfite itself absorbs in this region with a λ_{max} 257 nm, ε 36±3 dm^3 mol^{-1} cm^{-1}, quantitative measurements of the equilibrium constant were not attempted.

^{1}H NMR measurements were more promising since, as shown in scheme 2.18, single bands are expected for the parent ketone and the adduct.

76

Scheme 2.18:
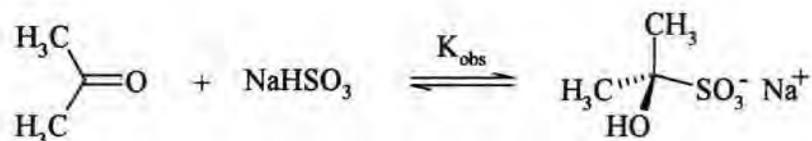
The ^{1}H NMR spectra for propanone and the HIPS adduct can be seen in Figures 2.10 and 2.11 respectively, with assignment detailed in table 2.16. Studies were carried out in D_2O and also, with the presence of 0.1 mol dm^{-3} dioxan. Dioxan was used to quantify the propanone and HIPS concentrations. This was achieved by comparing the relative intensities of the peaks taking account of the number of protons responsible, i.e. 8 for dioxan and 6 for both propanone and HIPS.

Figure 2.10: ^{1}H NMR spectrum of propanone (0.15 mol dm^{-3}) in D_2O with 0.1 mol dm^{-3} dioxan.
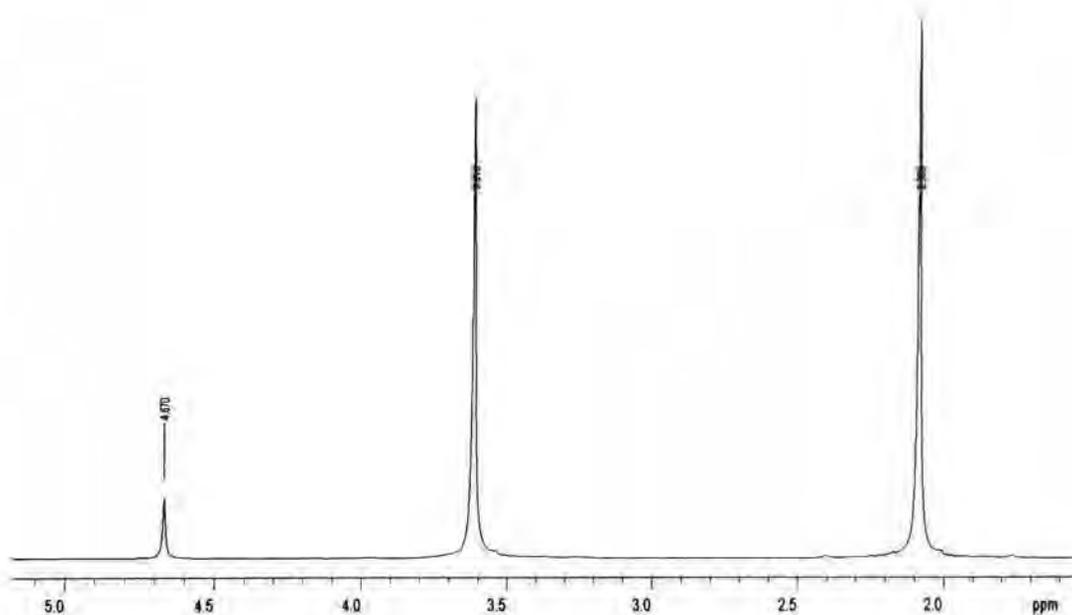
Figure 2.11: ^{1}H NMR spectrum for the reaction of propanone 0.1 mol dm^{-3} and sodium bisulfite 7.5x10^{-2} mol dm^{-3} in D$_2$O with 4.5x10^{-2} mol dm^{-3} dioxan.
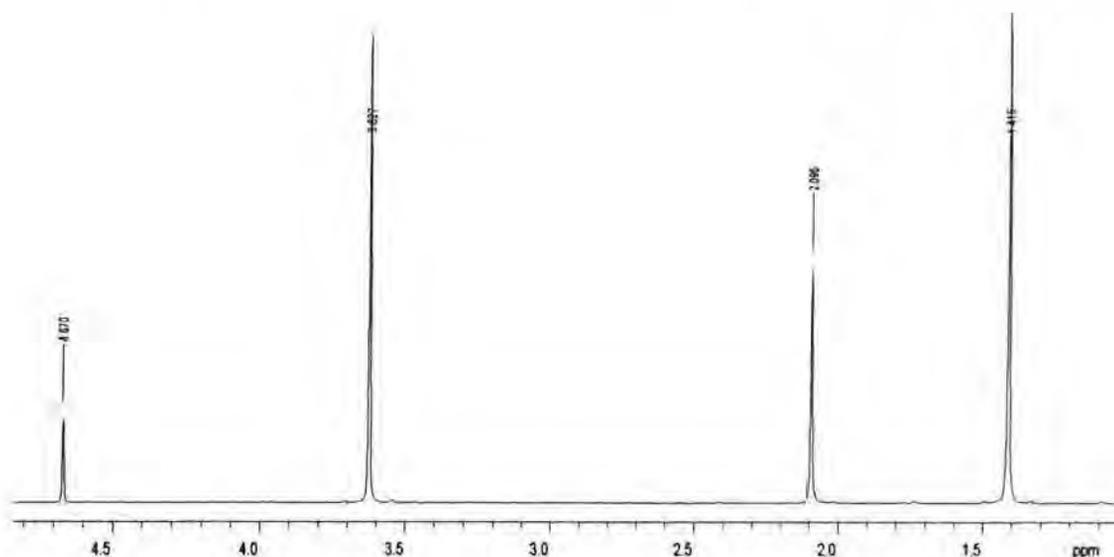
Table 2.16: ^{1}H NMR spectra of propanone in D$_2$O with sodium bisulfite and dioxan: peak assignment

δ / ppm	integrals	multiplicity	assignment
Propanone 0.15 mol dm^{-3} : dioxan 0.1 mol dm^{-3}			
4.67	-	-	H$_2$O
3.62	44	s	Dioxan H$_8$
2.09	50	s	(CH$_3$)$_2$CO
Propanone (0.1 mol dm^{-3}) + NaHSO$_3$ (7.5x10^{-2} mol dm^{-3}) : dioxan 0.045 mol dm^{-3}			
4.67	-	-	H$_2$O
3.62	34	s	Dioxan H$_8$
2.09	19	s	(CH$_3$)$_2$CO
1.42	41	s	(CH$_3$)$_2$C(OH)(SO$_3^-$)

Some problems were encounted due to the volatility of propanone, so that concentrations of stock solutions tend to decrease with time. Hence dioxan, with δ 3.62ppm, was used as an

78

internal reference to allow concentrations to be monitored. Measurements were made in deuterium oxide with propanone 0.1 mol dm^{-3} and with various concentrations of sodium bisulfite. The integrals of the bands due to the adduct and propanone were used to calculate the concentrations on these species. Hence the concentration of free sulfite, and the value of K_{obs} could be calculated. The values in table 2.17 yield a value of *ca.* 350 dm^3 mol^{-1} for K_{obs} under these conditions in D$_2$O.

The value obtained is subject to some error due to some remaining uncertainty in the total concentration of propanone present. Also the solutions were not buffered, and the value of equilibrium constant is expected to be dependent on pH

Table 2.17: Calculation of K_{obs} values from NMR data for formation of HIPS in D$_2$O. The stoichiometric concentration of propanone is 0.1 mol dm^{-3}

[NaHSO$_3$]$_{stoich}$ / mol dm^{-3}	[HIPS]^a / mol dm^{-3}	[propanone]^a / mol dm^{-3}	[SO$_3^{2-}$]$_{free}$^{b} / mol dm^{-3}	K_{obs}^{c} / dm^3 mol^{-1}
0.105	0.0864	0.0136	0.0186	340
0.090	0.0790	0.0210	0.0110	340
0.075	0.0690	0.0310	0.0060	370
0.060	0.0564	0.0436	0.0036	360
0.045	0.0440	0.0560	-	-

^{a} *Determined from the integrals at δ 1.42ppm and 2.09ppm repectively*

^{b} *[SO$_3^{2-}$]$_{free}$ = [SO$_3^{2-}$]$_{stoich}$ − [HIPS]*

^{c} *Calculated as [HIPS]/[propanone]$_{free}$. [SO$_3^{2-}$]$_{free}$*

2.2.3.2: Decomposition of hydroxyisopropanesulfonate, HIPS

2.2.3.2.1: Equilibrium studies of HIPS

Following the method reported in section (2.2.2.2.1), the dissociation of HIPS was observed by titration of the free sulfite with aqueous iodine. HIPS was generated by the addition of

concentration of the original stoichiometric concentration of sulfite added to form the adduct, the value had to be doubled. This value divided by 100 (the volume of the original HPS solution) and then, multiplied by the initial sulfite concentration gave the concentration of the free, unbound sulfite. This value was used to calculate the concentrations of adduct and hence, free propanal, which were used to calculate a value of the equilibrium constant, K_{obs}. In table 2.10, the calculations used to obtain K_{obs} values are shown for several pH values. Experiments, for example B, where the initial propanal concentration was varied yielded concordant values for K_{obs}.

Table 2.10: Specimen calculations for the equilibrium dissociation reactions of HPS. All volumes are in cm^3

Exp. Cond	Total Titre	Vol. acidic I_2	Vol. I_2 used	Vol HSO_3^- (5×10^{-3} M)	$[HSO_3^-]$ / mol dm^{-3}	[adduct] / mol dm^{-3}	[EtCHO] / mol dm^{-3}	K_{obs} / dm^3 mol^{-1}
A	4.5	30	27.75	55.5	2.775×10^{-3}	2.225×10^{-3}	2.775×10^{-3}	288
B	5.0	30	27.5	55.0	2.75×10^{-3}	2.25×10^{-3}	3.25×10^{-3}	252
C	38.3	30	10.85	21.7	1.085×10^{-3}	3.915×10^{-3}	1.085×10^{-3}	3326
D	16.9	30	21.55	43.1	2.155×10^{-3}	2.845×10^{-3}	2.155×10^{-3}	613
E	16.2	50	41.9	83.8	4.19×10^{-3}	8.1×10^{-4}	4.19×10^{-3}	46

Experimental conditions A = Equimolar(0.5 mol dm^{-3}), pH 9.8; B = Propanal 0.55 mol dm^{-3} & Bisulfite 0.5mol dm^{-3}, pH 10.0; C = Equimolar (0.5 mol dm^{-3}), pH 8.5; D = Equimolar (0.5 mol dm^{-3}), pH 9.6; E = Equimolar (0.5 mol dm^{-3}), pH 11.8; concentrations are for the stock solutions before dilution.

Values obtained for K_{obs} for other pH values are summarised in Table 2.11

Table 2.19: K_{obs} values calculated for the HIPS formation reaction at 25 $^{\circ}$C

pH	K_{obs}
5.7	239
5.9	270
6.1	223
6.3	208
6.6	161
6.8	148
7.0	99
7.2	78
7.4	45
7.7	27
7.9	19
8.0	19
8.2	12
8.3	9
8.4	6
8.5	5
8.7	3
8.8	2

Figure 2.12: Plot of Log K_{obs} versus pH for the HIPS formation reaction with a superimposed fit of equation 2.17. $K_a^{HSO3-} = 8.0 \times 10^{-8}$ mol dm^{-3} and $K_1 = 240$ dm^3 mol^{-1}
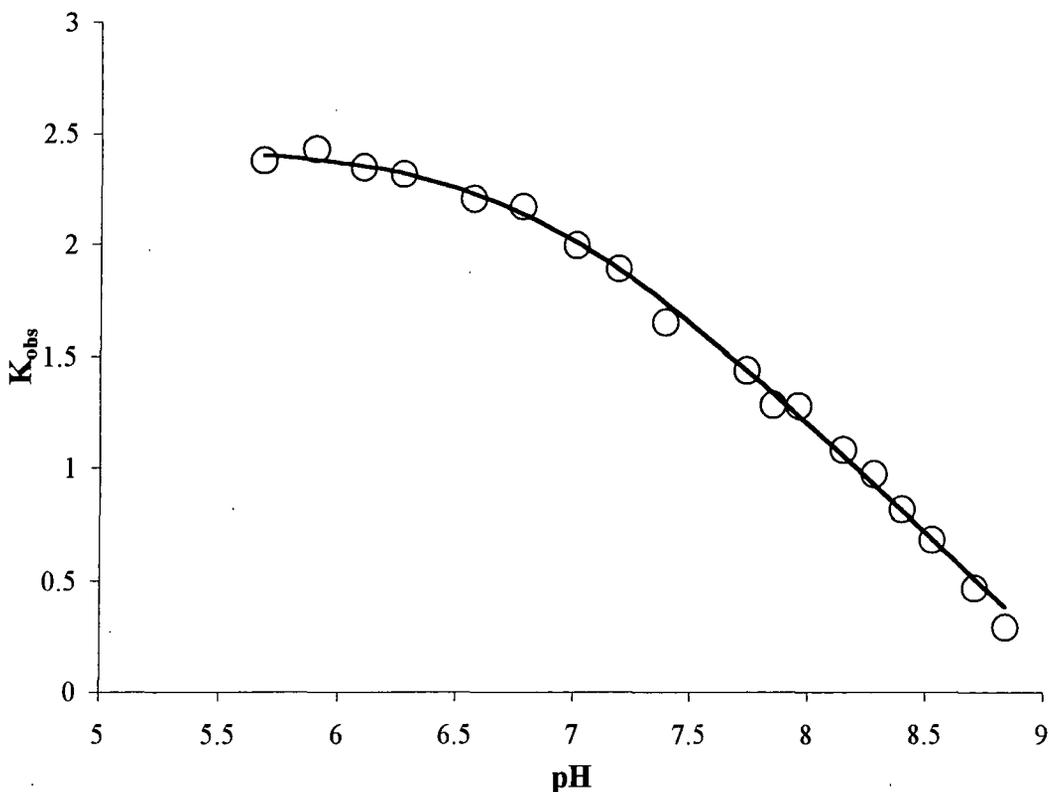
It was not possible to obtain values of K_{obs} at pH values ≥ 9, since they were too small for measurement by this method. Since the pK_a value for dissociation of the HIPS adduct is likely to be > 10, it was not possible to determine the value, i.e. the plateau at high pH was not observable. A likely value for the pK_a will be discussed later in the chapter.

2.2.3.2.2: Kinetic studies of HIPS

The kinetics of the dissociation of HIPS to produce sulfite were followed, as in the case of HPS, by measuring the rate of removal of iodine. Measurements were made with aqueous solutions of HIPS in the concentration range 2.5×10^{-4} to 5.0×10^{-3} mol dm^{-3} in the pH range 1.7 to 7.3. In this range the value of K_{obs} is known to be quite low, *ca.* 200 dm^3 mol^{-1}. Hence it was necessary to work with a large excess of free propanone to ensure virtually complete

conversion of sulfite to the adduct. Thus measurements were made with an excess of 0.1 mol dm^{-3} of propanone. In control experiments it was checked that in the pH range studied there was negligible reaction between propanone, 0.1 mol dm^{-3}, and iodine under the reaction conditions used.

It is evident from equation 2.6 that the reactions will be zero order in iodine, only when the conditions $k_4[I_2]_{stoich} >> k_f[\text{propanone}]$ applies. With the relatively high propanone concentrations used here, it was necessary to use comparatively high concentration of iodine in order to achieve this condition. Hence measurements were made with iodine 5×10^{-4} mol dm^{-3} (KI, 5×10^{-3} mol dm^{-3}). This resulted in unacceptably high absorbance values when measurements were made at 350nm. Hence a compromise was reached whereby measurements were made at 385nm where $\varepsilon = 9115\pm60$ mol^{-1} dm^3 cm^{-1}.

Typical plots obtained at pH 4.6 are shown in figure 2.13. Plots for the pH range 4 -7 show good zero order kinetics, while plots in the pH range 1 -3, obtained at lower concentration of HIPS, change from zero to first order kinetics with increasing time, as the iodine concentration falls. Here the gradients were obtained using the initial slopes of absorbance versus time plots. Values of k_{obs} are given in table 2.20 and were obtained by dividing the gradients by the extinction coefficient of iodine at the appropriate wavelength.

Table 2.20: k_{obs} / mol dm^{-3} s^{-1} obtained at different pH with varied HIPS concentration and 5×10^{-4} mol dm^{-3} aqueous iodine solution (KI = 5×10^{-3} mol dm^{-3})

[HPS] / mol dm^{-3}	k_{obs} / mol dm^{-3} s^{-1}								[HPS] / mol dm^{-3}	k_{obs} / mol dm^{-3} s^{-1}	
	pH 1.7	pH 3.0	pH 4.6	pH 4.95	pH 5.8	pH 6.5	pH 6.7	pH 7.3		pH 1.8	pH 2.2
2.5×10^{-4}	4.96×10^{-8}	-	-	2.51×10^{-7}	-	-	2.81×10^{-5}	-	0.001	1.43×10^{-7}	9.07×10^{-8}
3.75×10^{-4}	6.65×10^{-8}	8.33×10^{-9}	6.97×10^{-7}	8.03×10^{-7}	-	3.08×10^{-5}	9.62×10^{-5}	8.36×10^{-5}	0.0015	2.27×10^{-7}	1.39×10^{-7}
5.0×10^{-4}	7.54×10^{-8}	1.55×10^{-8}	9.35×10^{-7}	1.71×10^{-6}	-	7.13×10^{-5}	2.79×10^{-4}	1.67×10^{-4}	0.002	3.31×10^{-7}	1.95×10^{-7}
1.25×10^{-3}	1.73×10^{-7}	9.26×10^{-8}	3.50×10^{-6}	7.49×10^{-6}	5.49×10^{-5}	2.81×10^{-4}	8.02×10^{-4}	1.14×10^{-3}	0.003	4.87×10^{-7}	2.88×10^{-7}
2.5×10^{-3}	3.34×10^{-7}	1.61×10^{-7}	7.57×10^{-6}	1.66×10^{-5}	1.48×10^{-4}	7.35×10^{-4}	1.70×10^{-3}	3.15×10^{-3}	0.0035	-	3.43×10^{-7}
3.75×10^{-3}	4.81×10^{-7}	3.18×10^{-7}	1.11×10^{-5}	2.64×10^{-5}	2.50×10^{-4}	1.21×10^{-3}	2.52×10^{-3}	5.30×10^{-3}	0.004	6.20×10^{-7}	-
5.0×10^{-3}	6.37×10^{-7}	4.16×10^{-7}	1.49×10^{-5}	3.61×10^{-5}	3.61×10^{-4}	1.69×10^{-3}	3.34×10^{-3}	6.96×10^{-3}	-	-	-

Figure 2.13: Plots of the decomposition reaction of HIPS with aqueous iodine 5×10^{-4} mol dm^{-3} (and KI 5×10^{-4} mol dm^{-3}) at 25 °C
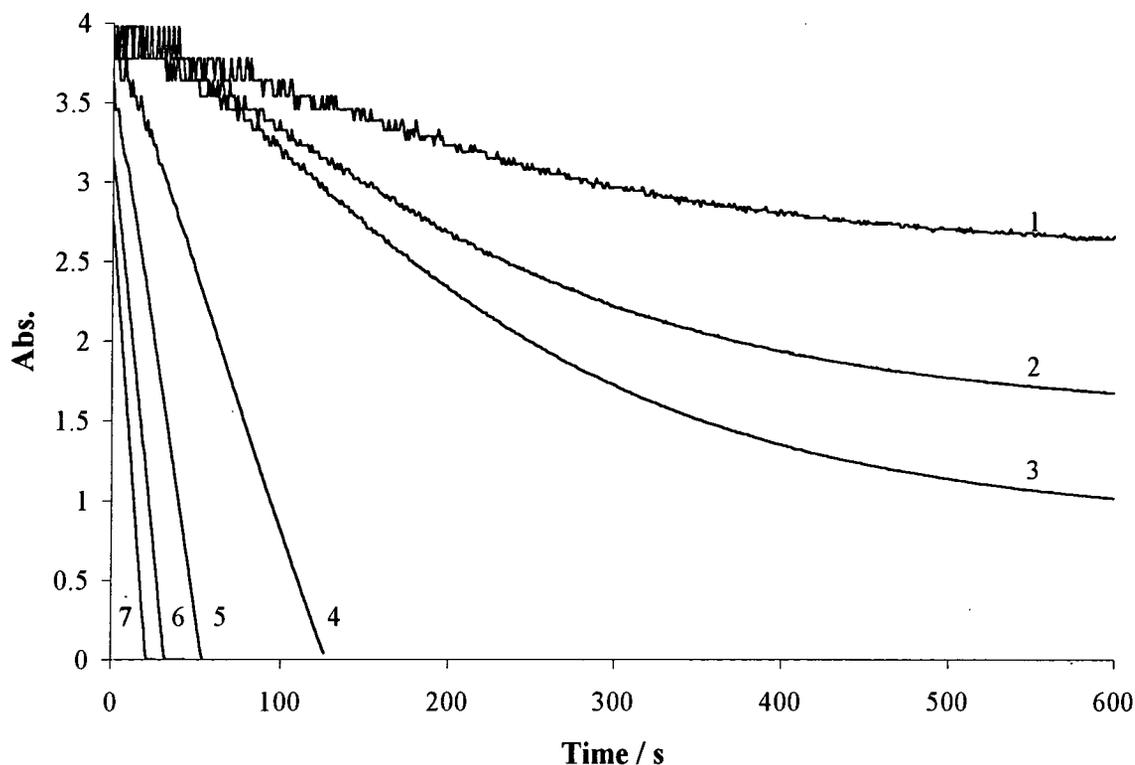
$1 = 2.5 \times 10^{-4}$M HIPS; $2 = 3.75 \times 10^{-4}$M; $3 = 5.0 \times 10^{-4}$M; $4 = 1.25 \times 10^{-3}$M; $5 = 2.5 \times 10^{-3}$M; $6 = 3.75 \times 10^{-3}$M; $7 = 5 \times 10^{-3}$M

Plotting k_{obs} mol dm^{-3} s^{-1} versus HIPS concentration enabled the calculation of the first order rate constant defined in equation 2.7, with k_b equal to the gradient. Linear regression yielded correlation co-efficients between 0.979 and 0.999. The values for k_b are shown in table 2.21, and the plot of Log k_b versus pH with the fit according to equation 2.18, is shown in figure 2.14.

Table 2.21: Calculated values of k_b, the first order rate constant for the decomposition of HIPS, at various pH values

pH	k_b / s^{-1}
1.7	1.24×10^{-4}
1.8	1.57×10^{-4}
2.2	1.00×10^{-4}
2.7	2.52×10^{-4}
3	8.93×10^{-5}
3.8	6.16×10^{-4}
4.6	3.09×10^{-3}
5.0	7.58×10^{-3}
5.8	8.16×10^{-2}
6.5	0.359
6.7	0.698
7.3	1.527

Figure 2.14: Plot of Log k_b versus pH, with a superimposed fit of equation 2.18 for the decomposition kinetics of HIPS
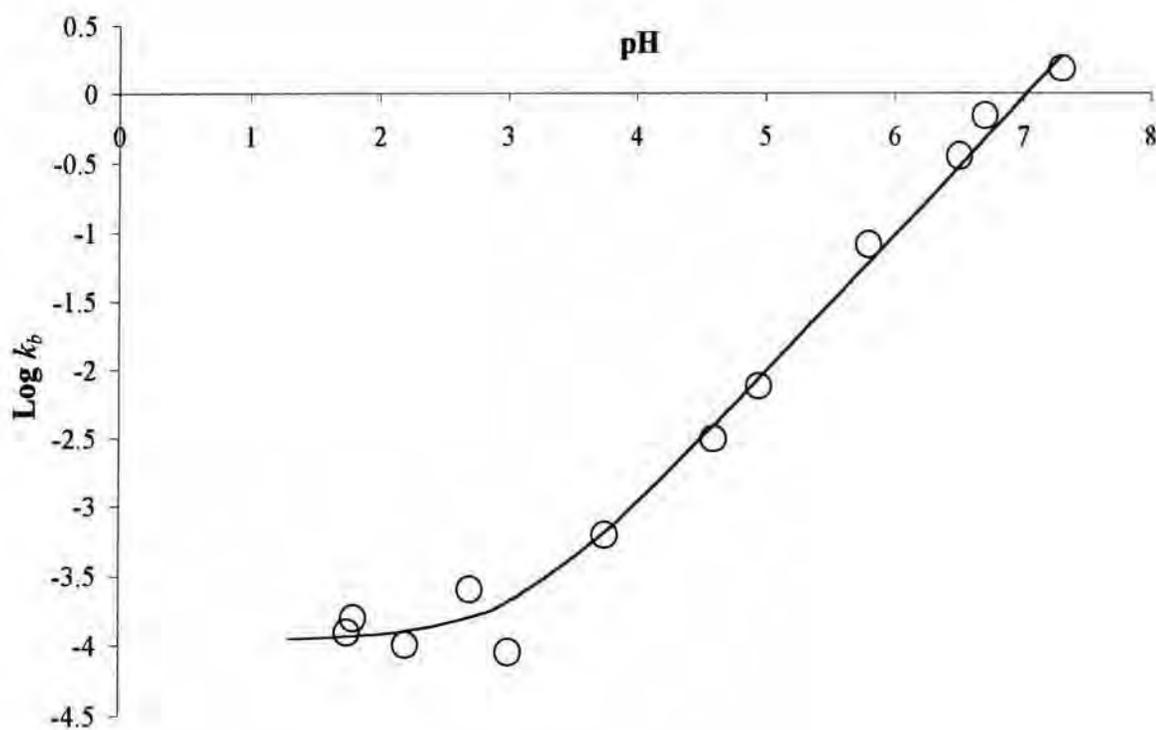
The terms contained in equation 2.18, can again be calculated from the plot, figure 2.14, as in the case of HPS using equations 2.20 to 2.24. k_{-1} was calculated as 1.11×10^{-4} s^{-1}. Extrapolation to pH = 0 of the points obtained with pH > 3 gave an intercept of -7.08. This leads to a value for $k_{-2}K_a$ of $(8\pm2) \times 10^{-8}$ mol dm^{-3} s^{-1}. As a value for the acid dissociation constant could not be determined the term $k_{-2}K_a$ can not be separated.

As stated with the studies for propanal, the Log k_b versus pH plot exhibits two areas that represent two different pathways of dissociation. Below pH 3, the monoanionic form of the adduct dissociates to form propanone and bisulfite (k_{-1}). Above pH 3, the predominant dissociation occurs via the dianion, to give propanone and sulfite ions (k_{-2}). However as the acid dissociation constant for HIPS could not be calculated, values for k_{-2} could not either. The values obtained for K_1 and k_{-1} lead to a value for k_1, = $K_1 \cdot k_{-1}$, of 0.027 dm^3 mol^{-1} s^{-1}. The value of 240 dm^3 mol^{-1} for K_1 obtained by the titration method is preferred to the value of 350 dm^3 mol^{-1} obtained from NMR measurements in D$_2$O. The difference in values may represent a solvent isotope effect.

2.2.4: Chloropropanone

2.2.4.1: Formation of hydroxyiso-1-chloropropanesulfonate, HCPS

Initial observations using UV/Vis spectrometry indicated that chloropropanone, has λ_{max} at 244nm, with an extinction co-efficient of $\varepsilon = 113 \pm 2$ mol^{-1} dm^3 cm^{-1}. On reaction with low concentrations of sodium bisulfite (λ_{max} at 257nm, $\varepsilon = 36 \pm 3$ mol^{-1} dm^3 cm^{-1}) small decreases in absorption (ΔAbs = 0.1) occurred. However, with concentrations of bisulfite 0.04 mol dm^{-3}, in excess of chloropropanone, 0.01 mol dm^{-3}, the absorbance increases with a shift towards that of free sulfite. The interference between the two bands made quantitative measurements unprofitable.

^{1}H NMR studies of chloropropanone showed the presence of both the hydrated and unhydrated forms (figure 2.15 and table 2.22). The parent chloropropanone was in greatest abundance. Bands due to the parent are shifted to higher frequencies compared with the

bands in propanone due to the presence of the electron withdrawing chlorine atom. The value of the equilibrium constant for hydration was calculated to be 0.12. However this value was measured in D_2O, and a slightly lower value[24] is expected in H_2O.

Figure 2.15: ^{1}H NMR spectrum of chloropropanone (0.1 mol dm^{-3}) in D_2O
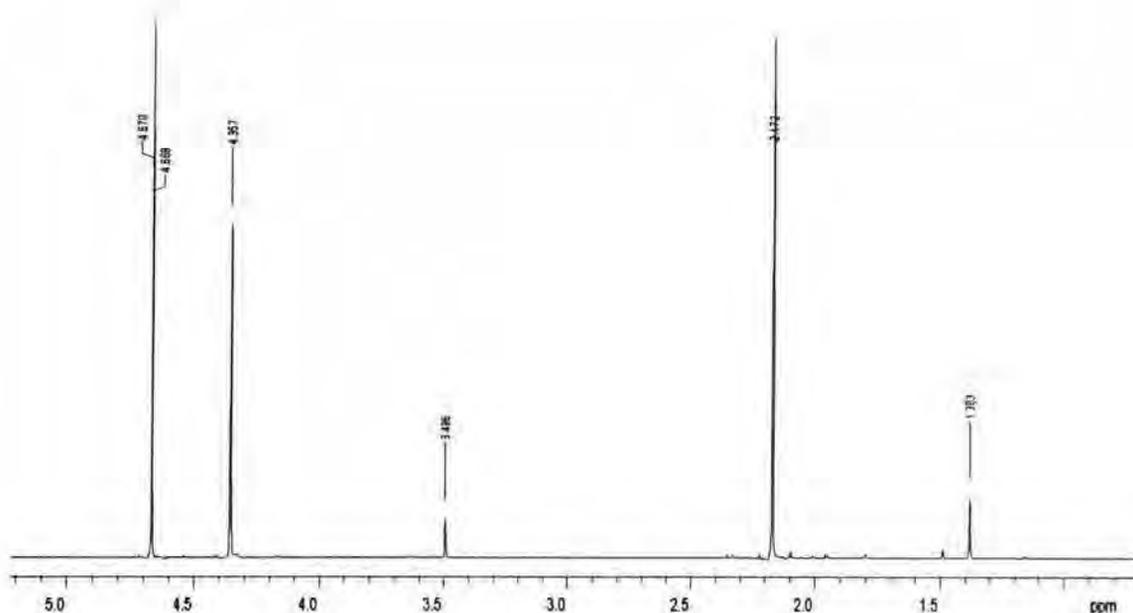
Table 2.22: ^{1}H NMR spectrum of chloropropanone (0.1 mol dm^{-3}) in D_2O; peak assignment

δ / ppm	integral ratio	multiplicity	assignment
4.67	-	-	H_2O
4.36	2	s	$-CH_2Cl$ (unhyd)
3.50	0.24	s	$-CH_2Cl$ (hyd)
2.17	3	s	$-CH_3$ (unhyd)
1.38	0.36	s	$-CH_3$ (unhyd)

The reaction of chloropropanone with sodium bisulfite was also observed using ^{1}H NMR spectroscopy and the formation of hydroxyisochloropropanesulfonate, HCPS, was detected. Spectra were measured where the chloropropanone: bisulfite stoichiometry was 1:1 and 1:2.

In the 1:1 stoichiometry reaction (both 0.1 mol dm^{-3}) bands due to products and reactants, were observed. Bands due to the hydrate were small but observable. Using the relative intensities of the peaks, and the method used in the case of propanone, concentrations were calculated to obtain a rough estimation of the equilibrium constant. A value of *ca.* 450 was calculated for the equilibrium constant for formation. However, this is only an estimate, because, as seen with propanone, this technique can be subject to a relatively large experimental error. In the 1:2 stoichiometry reaction (chloropropanone 0.1 mol dm^{-3} and bisulfite 0.2 mol dm^{-3}) adduct formation was virtually complete, as only bands due to the product were observed. Figures 2.16 and 2.17 show the spectra with peak assignment seen in table 2.23.

Figure 2.16: ^{1}H NMR spectrum for the reaction in 1:1 stoichiometry of chloropropanone and sodium bisulfite (0.1 mol dm^{-3}) in D$_2$O
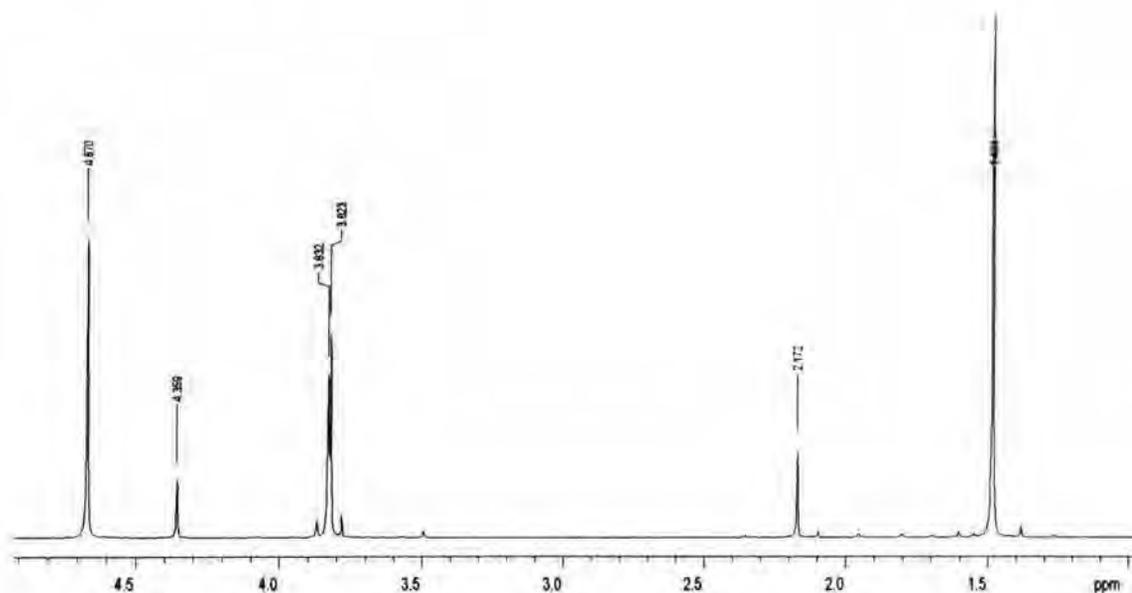
Figure 2.17: ^{1}H NMR spectrum for the reaction in 1:2 stoichiometry of chloropropanone (0.1 mol dm^{-3}) and sodium bisulfite (0.2 mol dm^{-3}) in D_2O
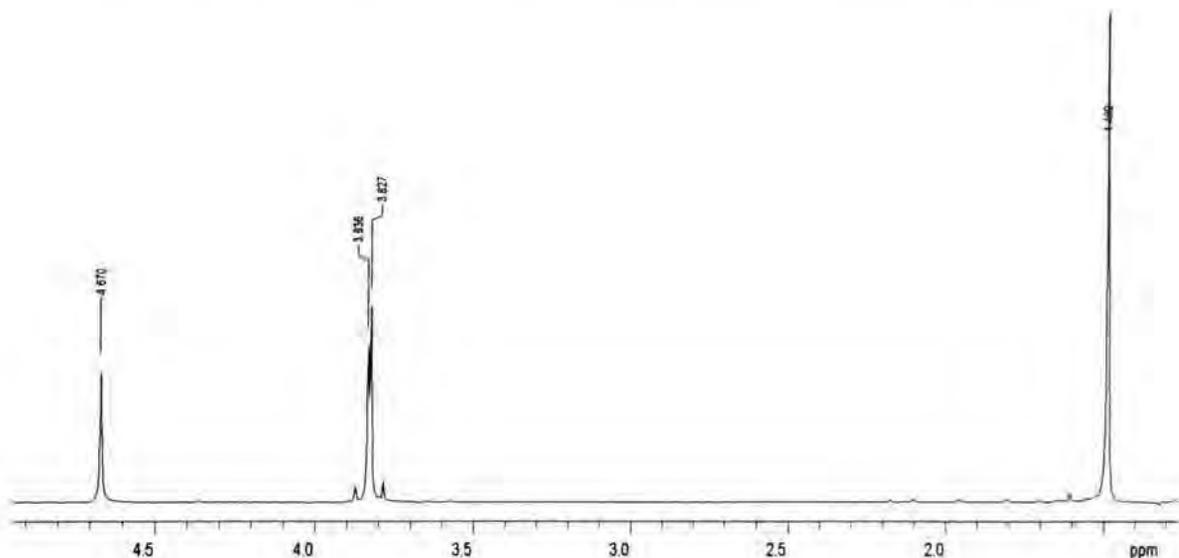
Table 2.23: Peak assignment for 1H NMR spectra; for the reactions of chloropropanone (0.1 mol dm^{-3}) and sodium bisulfite (0.1/0.2 mol dm^{-3}) in D_2O

δ / ppm	multiplicity	1:1 stoichiometry		1:2 stoichiometry		assignment
		Integral ratio	Intens.	Integral ratio	Intens.	
4.67	-	-	-	-	-	H_2O
4.36	s	0.32	4.36	-	-	-CH$_2$Cl (react.)
3.82	s	2	25.66	2	35.16	-CH$_2$Cl (prod.)
2.17	s	0.48	6.43	-	-	-CH$_3$ (react.)
1.49	s	3	41.45	3	51.07	-CH$_3$ (prod.)

The adducts peaks, compared to the unreacted chloropropanone are shifted to lower frequencies as is also the case in the hydration process.

2.2.4.2: Decomposition of hydroxyisochloropropanesulfonate, HCPS

2.2.4.2.1: Equilibrium studies of HCPS

The dissociation of HCPS was observed by titration of the free sulfite against iodine, in exactly the same way as for propanone and described in section (2.2.3.2.1). A stock solution was prepared containing chloropropanone, 0.75 mol dm^{-3}, and NaHSO$_3$, 0.5 mol dm^{-3}, and 1 cm^3 aliquots were diluted to 100 cm^3 using the appropriate buffer solution. Specimen calculations used to determine values of K$_{obs}$ at various pH values are shown in table 2.24. As a result, a summary of values for K$_{obs}$ can be shown tabulated in table 2.25, and plotted in figure 2.18 with a fit line according to equation 2.17. A value of K$_a^{HSO3-}$ 8.0x10^{-8} mol dm^{-3} was used to plot the best fit line however an independent value of 7.66x10^{-8} mol dm^{-3} could have been used to achieve a slightly better fit.

Table 2.24: Specimen calculations for the equilibrium dissociation reactions of HCPS. All volumes are in cm^3

pH	Total Titre	Vol. acidic I$_2$	Vol. I$_2$ used	Vol HSO$_3^-$ (5x10^{-3} M)	[HSO$_3^-$] / mol dm^{-3}	[adduct] / mol dm^{-3}	[ketone] / mol dm^{-3}	K$_{obs}$ / dm^3 mol^{-1}
6.0	42.8	30	8.6	17.2	8.60x10^{-4}	4.14x10^{-3}	3.36x10^{-3}	1433
6.6	61.6	40	9.2	18.4	9.20x10^{-4}	4.08x10^{-3}	3.42x10^{-3}	1297
8.4	46.5	50	26.75	53.5	2.675x10^{-3}	2.325x10^{-3}	5.175x10^{-3}	168
8.0	32.3	50	33.85	67.7	3.385x10^{-3}	1.615x10^{-4}	5.885x10^{-3}	81
8.5	12.9	50	43.55	87.1	4.355x10^{-3}	6.45x10^{-4}	6.855x10^{-3}	21.6

Experimental conditions, initial reaction concentrations; [HSO$_3^-$] = 0.005 mol dm^{-3}, *[chloropropanone]* = 0.0075 mol dm^{-3}

Table 2.25: K_{obs} values calculated for the HCPS formation reaction, at 25 $^{\circ}$C

pH	K_{obs}
5.3	1409
5.5	1483
6.0	1433
6.1	1562
6.6	1297
6.8	833
7.9	275
8.2	236
8.4	168
8.5	144
9.0	81
9.2	75
9.8	22
10.2	22
10.5	22
11.0	20

Figure 2.18: Plot of Log K_{obs} versus pH for the formation reaction superimposing the fit according to equation 2.17. $K_{hyd} = 0.10$ mol dm^{-3}, and $K_a^{HSO3-} = 8.0 \times 10^{-8}$ mol dm^{-3} $K_a = 1.0 \times 10^{-9}$ mol dm^{-3} and $K_1 = 1650$ dm^3 mol^{-1} were used
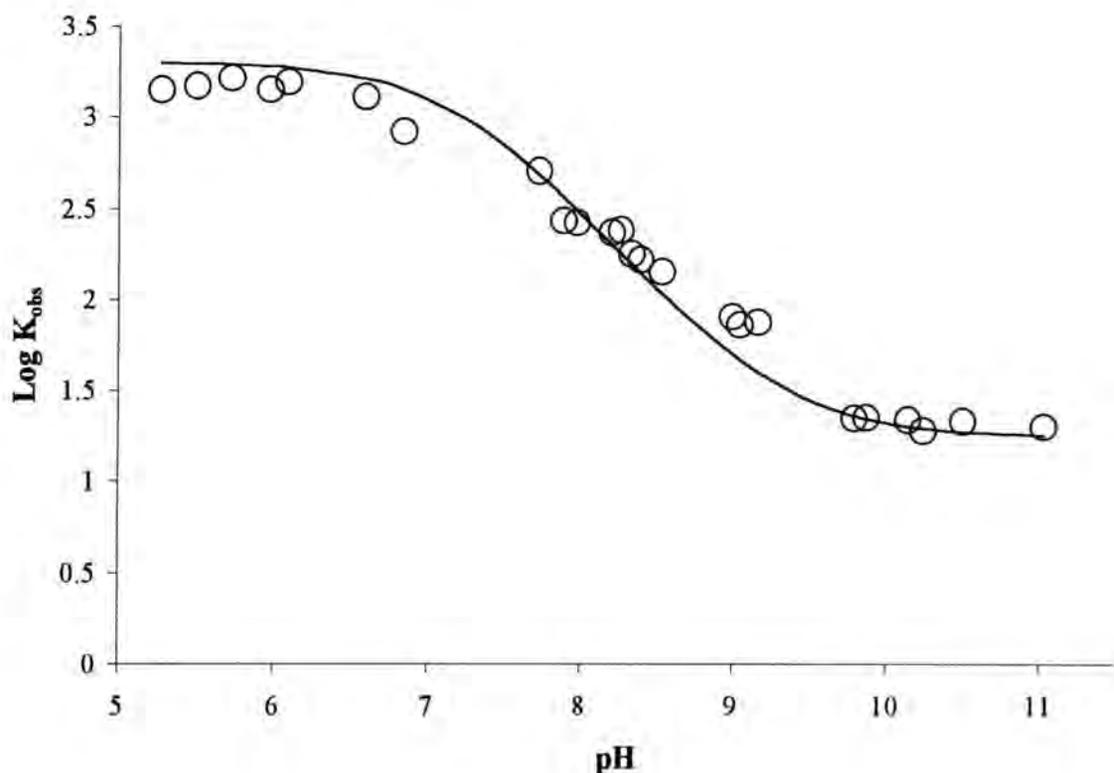
The data give a reasonably good fit with value for K_1, 1650 ± 150 dm^3 mol^{-1}, K_a $(1.0 \pm 0.2) \times 10^{-9}$ mol dm^{-3} using the known values of K_a^{HSO3-} 8.0×10^{-8} mol dm^{-3} and K_{hyd} 0.10 mol dm^{-3}.

An alternative method of treating the data is by plotting the reciprocal of the hydroxide concentration versus K_{obs}. The plot (figure 2.19) shows a linear trend, which relates to equation 2.19 and was derived from scheme 2.15, involving terms for the acid dissociation constant, the hydration equilibrium constant and the formation equilibrium constant.

Figure 2.19: $1 / [OH^-]$ versus Log K_{obs} for the HCPS formation reaction
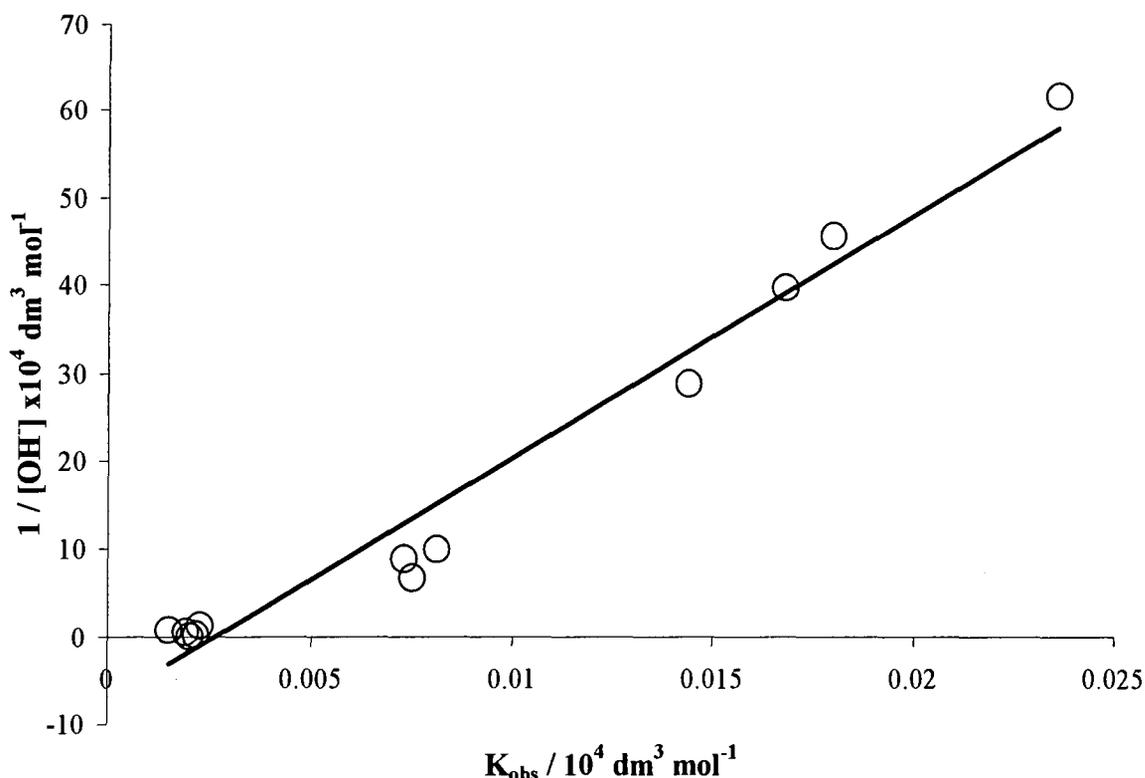
Linear regression produced a gradient of 3050 and the intercept of -1.0×10^5 dm^3 mol^{-1}. With knowledge of scheme 2.15 and equation 2.20, the acid dissociation constant and the equilibrium constant for HCPS formation were calculated. The intercept gave a value for K_a of 1.0×10^{-9} mol dm^{-3} equating to a pK_a for HCPS of 9.0. K_2 was calculated from the gradient, and the value obtained was 35 dm^3 mol^{-1}. This is rather higher than that, 21 dm^3 mol^{-1}, calculated from equation 2.16 using the known values of K_1 and K_a.

2.2.3.2.2: Kinetic studies of HCPS

The reaction of aqueous HCPS at concentrations of 5.0×10^{-4} to 5.0×10^{-3} mol dm^{-3} with 5×10^{-4} M aqueous iodine solution ($KI = 5 \times 10^{-3}$ mol dm^{-3}) at 25 °C was observed in the pH range of 1 to 7. The method that applied to propanone was followed. However since the value of K_{obs} is higher for chloropropanone it was sufficient to have chloropropanone in twice the concentration of bisulfite, when generating HCPS solutions. The iodine decomposition was

Table 2.26: k_{obs} / mol dm^{-3} s^{-1} obtained at different pH with varied HCPS concentration and 5×10^{-4} mol dm^{-3} aqueous iodine solution (KI = 5×10^{-3} mol dm^{-3})

[HPS] / mol dm^{-3}	k_{obs} / mol dm^{-3} s^{-1}										
	pH 1.7	pH 1.9	pH 2.1	pH 2.6	pH 3.4	pH 4.0	pH 4.4	pH 5.0	pH 5.6	pH 6.2	pH 6.8
5.0×10^{-4}	-	-	-	-	-	-	-	-	-	-	7.33×10^{-5}
7.5×10^{-4}	-	-	-	-	-	-	-	-	-	-	5.91×10^{-4}
1.0×10^{-3}	1.65×10^{-8}	1.55×10^{-8}	2.22×10^{-8}	7.33×10^{-8}	-	2.86×10^{-6}	7.99×10^{-6}	3.11×10^{-5}	1.10×10^{-4}	1.35×10^{-4}	1.33×10^{-3}
1.25×10^{-3}	3.00×10^{-8}	2.98×10^{-8}	4.46×10^{-8}	1.57×10^{-7}	-	4.17×10^{-6}	1.23×10^{-5}	2.02×10^{-4}	-	3.87×10^{-4}	3.18×10^{-3}
1.5×10^{-3}	5.39×10^{-8}	5.25×10^{-8}	6.86×10^{-8}	1.94×10^{-7}	1.21×10^{-6}	4.82×10^{-6}	1.52×10^{-5}	2.29×10^{-4}	3.38×10^{-4}	6.72×10^{-4}	4.21×10^{-3}
1.75×10^{-3}	6.48×10^{-8}	6.18×10^{-8}	-	2.53×10^{-7}	-	6.20×10^{-6}	1.98×10^{-5}	-	-	8.56×10^{-4}	-
2.0×10^{-3}	8.51×10^{-8}	8.26×10^{-8}	9.74×10^{-8}	3.22×10^{-7}	1.99×10^{-6}	7.52×10^{-6}	2.46×10^{-5}	4.02×10^{-4}	5.16×10^{-4}	1.06×10^{-3}	5.72×10^{-3}
2.25×10^{-3}	1.06×10^{-7}	9.98×10^{-8}	1.62×10^{-7}	3.66×10^{-7}		9.13×10^{-6}	2.81×10^{-5}	-	-	1.23×10^{-3}	-
2.5×10^{-3}	1.33×10^{-3}	1.25×10^{-7}	-	4.56×10^{-7}	2.65×10^{-6}	1.06×10^{-5}	3.18×10^{-5}	6.81×10^{-4}	7.52×10^{-4}	1.53×10^{-3}	-
5.0×10^{-3}	-	-	-	-	5.25×10^{-6}		-	1.35×10^{-3}	1.54×10^{-3}	-	-

followed at 385nm, and the gradients of the zero order plots were divided by the appropriate extinction co-efficient of iodine to obtain k_{obs} (table 2.26). Values of k_{obs} were then plotted against HIPS concentration, where the gradient was equal to the term k_b. Correlation co-efficients for these linear plots gave values between 0.981 and 0.999 and values obtained for k_b can be seen in table 2.27. The plot of Log k_b versus pH can be seen in figure 2.20, where a fit according to equation 2.18, is superimposed.

Table 2.27: A summary of calculated values for k_b, the first order rate constant for the decomposition of HCPS at varying pH

pH	k_b / s^{-1}
1.7	7.16×10^{-5}
1.9	7.12×10^{-5}
2.1	7.90×10^{-5}
2.6	2.42×10^{-4}
3.4	1.10×10^{-3}
4.0	5.12×10^{-3}
4.4	1.61×10^{-2}
5.0	6.41×10^{-2}
5.6	0.284
6.2	0.895
6.8	4.060

Figure 2.20: Plot of Log k_b versus pH, with a superimposed fit of equation 2.19 for the decomposition kinetics of HCPS
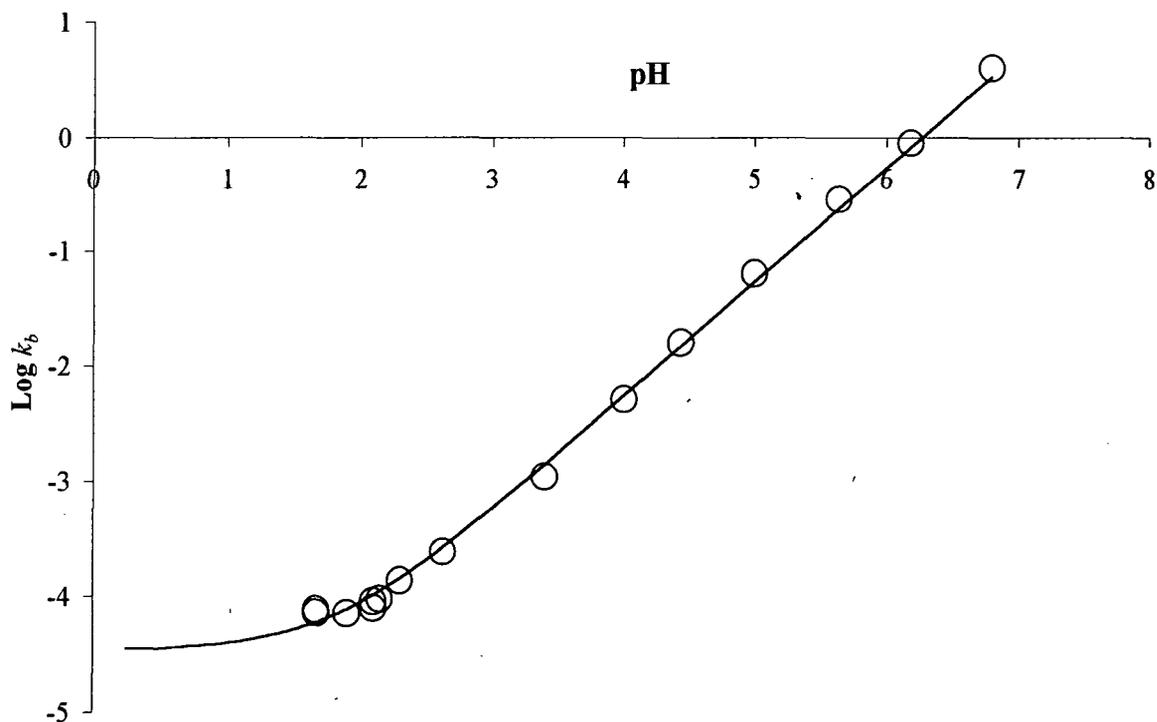
The values of the two terms in equation 2.18 were calculated using equations 2.20 to 2.24. The values obtained are $k_{-1} = (4\pm1)\times10^{-5}$ s^{-1} and $k_{-2}K_a = (5\pm1)\times10^{-7}$ mol dm^{-3} s^{-1}. Since K_a is known to have the value 1×10^{-9} mol dm^{-3} the value obtained for k_{-2} is 500 s^{-1}. Since the values of K_1 and k_{-1} are known it is possible to calculate values for k_1 (=K_1 . k_{-1}) 0.066 dm^{-3} mol^{-1} s^{-1}, and for k_2 (= K_2 . k_{-2}) 1.1×10^4 dm^3 mol^{-1} s^{-1}.

As in the case of the adducts formed from propanal and propanone the two regions of the plot correspond to decomposition of the monoanionic and dianionic forms.

Using the results in table 2.25 together with equation 2.18 it is possible to calculate values for k_{-2} at each pH measured. Using values for k_{-1} 4×10^{-5} s^{-1} and K_a 1×10^{-9} mol dm^{-3} gives the values quoted in table 2.28. These are consistent with that, 500 s^{-1}, obtained using the intercept of the Log plot in figure 2.20.

Table 2.28: Calculated values for the first order rate constant for the decomposition of the dianion form of HIPS (k_{-2}), in the pH range of 2.0 to 7.0

pH	k_{-2} / s^{-1}
2.1	310
2.6	510
3.4	440
4.0	510
5.0	640
5.6	710
6.2	560
6.8	640

2.2.5: Pentane-2,4-dione

2.2.5.1: Equilibrium constant of formation for 1:1 and 1:2 pentane-2,4-dione : bisulfite adducts

It was thought to be of interest to examine the interactions of a β-diketone with sulfite, where there is the possibility of formation of adducts with 1:1 and 1:2 stoichiometry. The symmetrical pentane-2,4-dione was chosen as a suitable example.

It is known[25] that β-diketones are in equilibrium with their enol forms. Enolisation is encouraged by the formation of an intramolecular hydrogen-bond and by resonance stabilisation provided by the possibility of two identical forms of the enol shown in scheme 2.19.

Scheme 2.19:

Literature sources[25] indicate that in aqueous media the enol:keto ratio is *ca.* 80:20.

The ^{1}H NMR spectrum of pentane-2,4-dione in D_2O is shown in figure 2.21. Interestingly only two peaks are observed in addition to solvent (table 2.29). This is due to the rapid H/D exchange of the methylene hydrogens with the solvent. The relative intensities of the methyl resonances lead to a value of K_{enol} of 5.5±0.3.

1H NMR spectra were recorded for pentane-2,4-dione, 0.05 or 0.1 mol dm^{-3} and sodium bisulfite, 0.1 to 0.5 mol dm^{-3}, in D_2O. The spectra showed that bands due to the keto and enol forms of the reactant remain in constant ratio while new bands were observed attributable to 1:1 and 1:2 adducts with sulfite as shown in scheme 2.20. Equilibria were established rapidly and the solution remained stable over time.

Typical spectra are shown in figures 2.22 to 2.24 and peak assignments are in table 2.30. The 1:1 adduct shows two bands of equal intensities at δ 2.18 and 1.45, attributable to the methyl groups of the adduct in its keto form. No bands are observed which may be attributable to the corresponding enol form of the 1:1 adduct. This form lacks the stabilisation possible in a β-diketonic structure and hence is not likely to be favoured.

Figure 2.21: ^{1}H NMR spectrum of pentane-2,4-dione (0.1 mol dm^{-3}) in D_2O
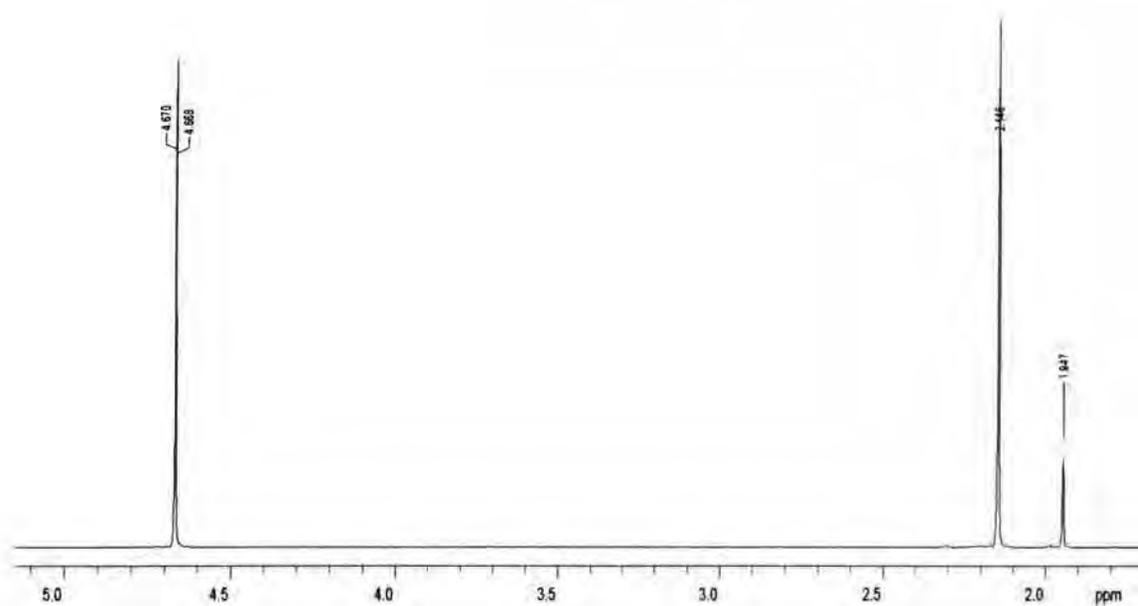
Table 2.29: ^{1}H NMR spectrum of pentane-2,4-dione (0.1 mol dm^{-3}) in D_2O: peak assignment

δ / ppm	integral ratio	multiplicity	assignment
4.67	-	-	H_2O
2.13	5.4	s	CH_3 (enol)
1.93	9.8	s	CH_3 (keto)

Scheme 2.20:

Enol ⇌ Keto + NaHSO₃ ⇌ 1:1 adduct + NaHSO₃ ⇌ 1:2 adduct
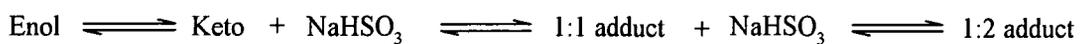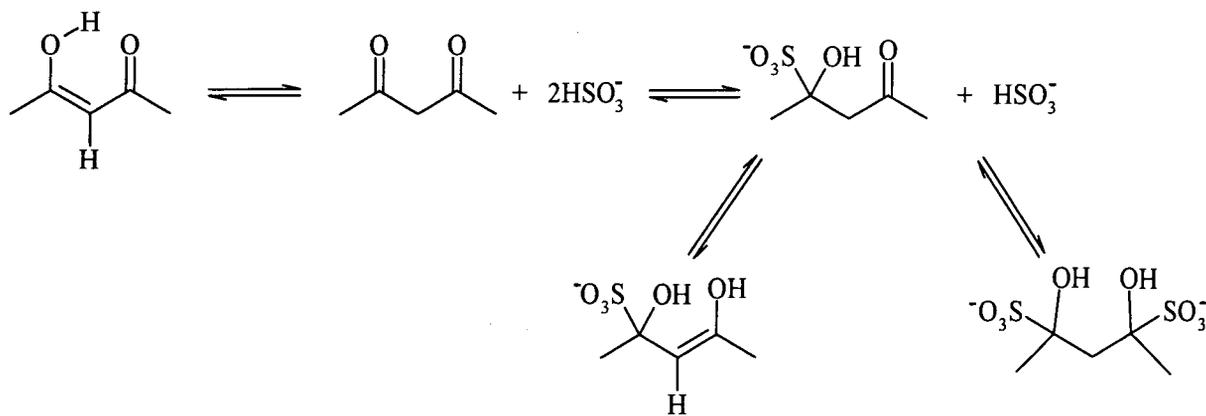
Figure 2.22: ^{1}H NMR spectrum for the reaction of 0.1 mol dm^{-3} pentane-2,4-dione and 0.1 mol dm^{-3} sodium bisulfite in D$_2$O, at 25 °C

Figure 2.23: ^{1}H NMR spectrum for the reaction of 0.1 mol dm^{-3} pentane-2,4-dione and 0.5mol dm^{-3} sodium bisulfite in D$_2$O, at 25 °C
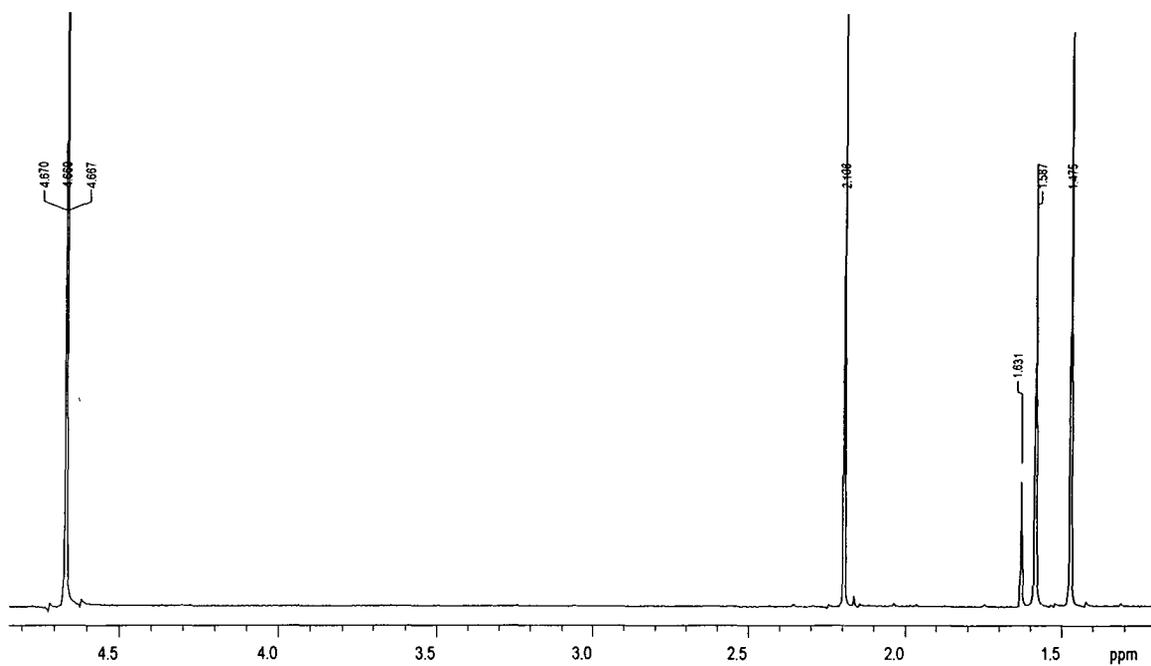
Figure 2.24: ^{1}H NMR spectrum for the reaction of 0.05 mol dm^{-3} pentane-2,4-dione and 0.5mol dm^{-3} sodium bisulfite in D$_2$O, at 25 °C
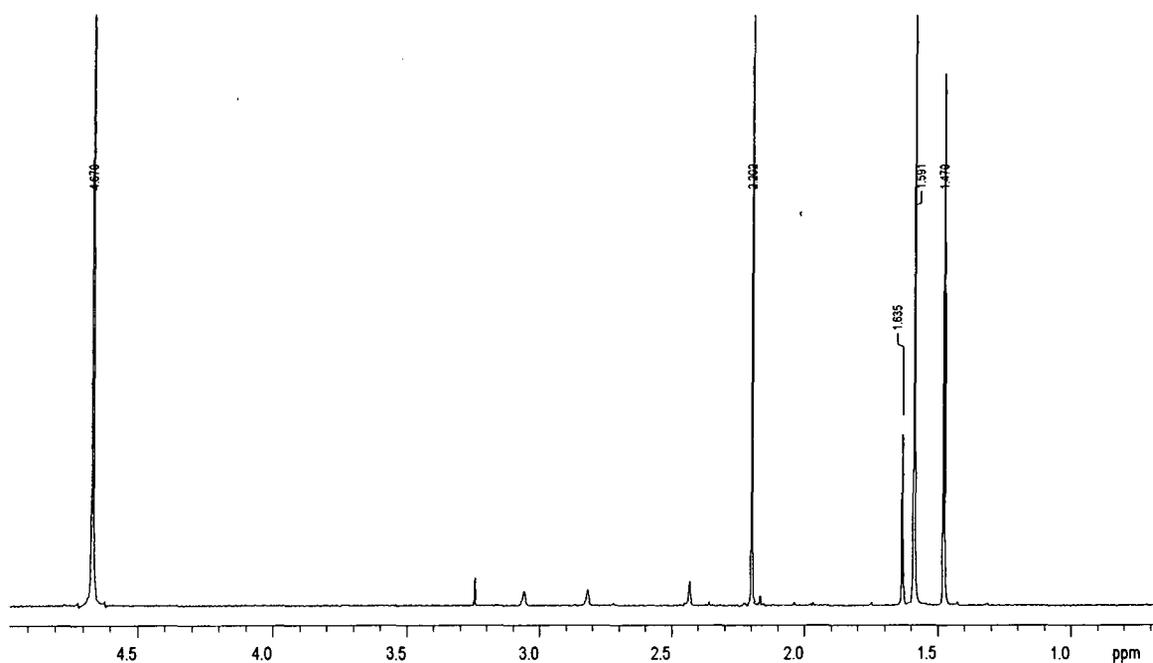
Table 2.30: Peak assignment for the reactions of three different ratios of pentane-2,4-dione and sodium bisulfite in D_2O, at 25 °C
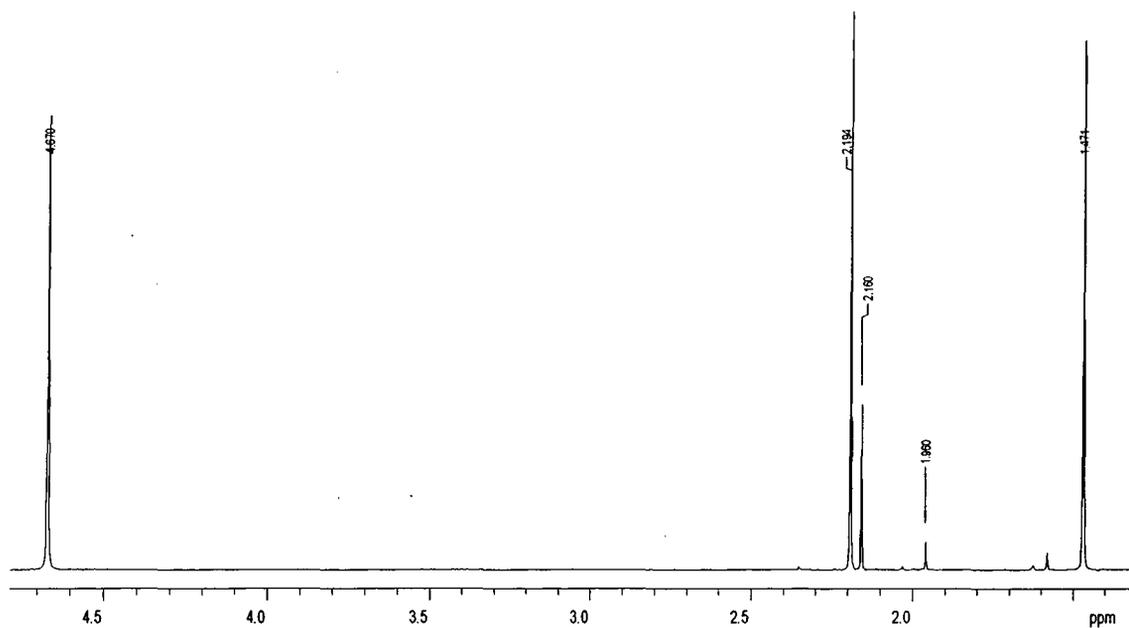
δ / ppm	multiplicity	Intensity			assignment
		1:1 ratio	1:5 ratio	1:10 ratio	
4.67	-	-	-	-	H_2O
2.18	s	24.41	19.14	15.41	$CH_3C=O$ (1:1 adduct)
2.13	s	12.77	0.38	0.24	CH_3 (enol)
1.93	s	2.12	0.06	0.02	CH_3- (keto)
1.61	s	0.21	4.60	5.08	1:2 adduct structure **A**
1.56	s	0.77	17.72	19.11	1:2 adduct structure **B**
1.45	s	25.14	20.46	16.39	$CH_3C(OH)(SO_3^-)$ (1:1 adduct)

The 1:2 adducts show two bands of unequal intensity at δ 1.61 and 1.56. The relative intensities are the same at all sulfite concentrations. The explanation is as follows[26]. The 1:2 adduct has two chiral centres and therefore there are diastereoisomers. Thus, four structures are possible, of which two are érythro isomers and the other two are thréo isomers. However, as the four groups attached to each chiral centre are the same, the case becomes simplified, as structure A is the meso form, however structure B has two enantiomers. Denoted in the table 2.30 for the 1:2 adduct, are structures A and B, and these are shown in scheme 2.14, as Fischer projections and simple structures. As stated these structures display peaks that remain in the same intensity ratios regardless of the sulfite concentration, indicating that both are relatively stable but one is preferred sterically over the other. It would be expected that the thréo enantiomer, **B**, would predominate due to the sulfite groups being a much greater distance away from each other compared to enantiomer **A**. In both representations (scheme 2.21) this is apparent; however **A** is still present due mainly to the methylene group between the two chiral centres. It should be noted that the two methyl groups in structure A are equivalent, as are the two methyl groups in structure B.

Scheme 2.21:

A	**B**
Érythro	Thréo
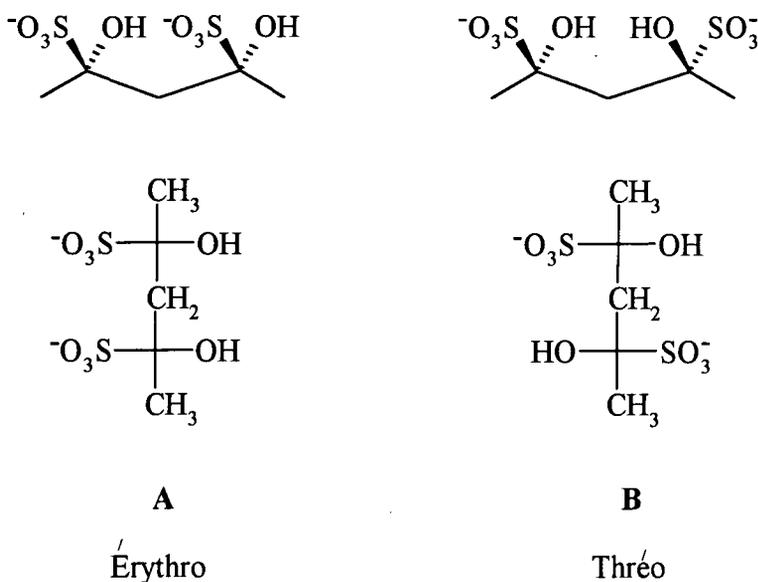
Using the relative intensities of peaks it was possible to calculate concentrations of each compound in the reaction pathway. This was achieved by dividing the intensity of each peak, or in the case of the 1:1 adduct the total CH_3 intensity, by the sum intensity, and then, multiplying the value by the pentane-2,4-dione initial concentration, 0.1 mol dm^{-3}. Calculating the free sulfite concentration was accomplished by subtracting the concentration of the 1:1 adduct plus two times the concentration of the 1:2 adduct from the initial sulfite concentration. Knowing the concentrations, it was possible to calculate the equilibrium constant of formation for both the 1:1 adduct and the 1:2 adducts from equations 2.26 and 2.27, which were derived from scheme 2.13. Equation 2.26 is defined in terms of the concentration of the keto form of the parent rather than the total dione concentration.

$$K_{1:1} = \frac{[1:1 \text{ adduct}]}{[\text{keto}][HSO_3^-]_{\text{free}}}$$

(2.26)

$$K_{1:2} = \frac{[1:2 \text{ adduct}]}{[1:1 \text{ adduct}][HSO_3^-]_{\text{free}}}$$

(2.27)

The experimental error for this type of technique can be relatively large when dealing with very small intensities; therefore two methods of generating the keto intensity were used. Firstly the equilibrium constant was calculated using the measured intensity of the keto peak. Secondly the equilibrium constant was calculated using a value for the intensity for the keto peak calculated using the enol peak intensity and the equilibrium constant of enolization. Using the larger enol peak reduced the experimental error generated when measuring the integral of relatively small peaks. Values calculated for both constants (and with using both methods for $K_{1:1}$) are shown in table 2.31.

Table 2.31: Equilibrium constants for the formation of the 1:1 adducts (by using both methods) and 1:2 adducts for the reaction between pentane-2,4-dione (0.1 mol dm^{-3}) and varying concentrations of sodium bisulfite in D$_2$O, at 25 °C

[NaHSO$_3$] / mol dm^{-3}	$K_{1:1}$ / dm^3 mol^{-1}		$K_{1:2}$ / dm^3 mol^{-1}
	Initial integral intensity [a]	Calculated intensity [b]	
0.1	3653	3962	2.58
0.15	2400	2311	1.54
0.20	2345	2436	1.80
0.25	1850	1850	1.34
0.3	1814	1625	1.32
0.35	1976	1812	1.39
0.40	1459	2673	2.21
0.45	1924	1986	1.41
0.50	1808	1847	1.54

[a] *Direct measurement of keto intensity*

[b] *Using measured intensity of the enol peak and the equilibrium constant for enolisation*

The values obtained are reasonably consistent apart from the value obtained with equimolar parent and bisulfite. The divergence here is likely to stem from the difficulty in obtaining exactly equal concentrations of the two reagents so that errors will be magnified. Overall the values obtained are 1900±200 dm^3 mol^{-1} for $K_{1:1}$ and 1.45±0.15 dm^3 mol^{-1} for $K_{1:2}$.

2.3: Conclusions

The ^{1}H NMR results clearly show the formation of adducts, HXS, from the carbonyl compounds studied and sulfite. Kinetic and equilibrium measurements, obtained using spectrophotometric methods yield the values collected in table 2.32. The nomenclature used is that given in scheme 2.11 on case X. Results are included also for reactions of formaldehyde and of benzaldehyde.

Values of K_1 for bisulfite addition are expected to be affected both by the electronic and steric effects of the groups attached to the carbonyl function. Thus electron-withdrawing groups will reduce electron density at the carbonyl carbon, thus encouraging addition. Sterically, bulky groups should disfavour addition since the bond angles are compressed on going from the parent to the adduct. Attempts to quantify steric and electronic effects in aliphatic systems have been made using the Taft approach[27]. This assigns values of E_s, the steric effect, and σ^*, the electronic effect, for individual groups. The reference is the methyl group for which both E_s and σ^* are zero. Some values are reproduced in table 2.33. Positive values mean that, relative to methyl, addtion should be favoured and the negative value indicates that addition should be disfavoured.

Values of K_1 are broadly in line with expectations of the Taft parameters. Thus for the three aldehydes values fall in the order formaldehyde > propanal > benzaldehyde. The comparatively low value for benzaldehyde confirms the importance of the unfavourable steric effect of the phenyl group. A plot, figure 2.25, of Log K_2 versus the sum of Taft parameters in the form of equation 2.28, shows approximate linearity.

$$\text{Log } K_2 \quad = \quad \sum\sigma^* \quad + \quad (0.6 \times \sum E_s) \qquad \qquad \textbf{(2.28)}$$

Table 2.32: Rate and equilibrium constants obtained at 25 °C, including literature values for two other HXS adducts, for the parent carbonyl compounds stated

Constant	Propanal	Propanone [d]	Chloro-propanone	Formaldehyde [a]	Benzaldehyde [b]
K_1 / mol^{-1} dm^3	3.3×10^5	240	1650	3.4×10^{10}	6400
k_1 / dm^3 mol^{-1} s^{-1}	1.3	0.027	0.066	790	-
k_{-1} / s^{-1}	3.9×10^{-6}	1.11×10^{-4}	4.0×10^{-5}	2.3×10^{-8}	-
K_2 / mol^{-1} dm^3	95	(0.03)	21	2.2×10^5	0.9
k_2 / dm^3 mol^{-1} s^{-1}	3.5×10^4	(240)	1.1×10^4	6.0×10^6	2.1×10^4
k_{-2} / s^{-1}	370	(8000)	500	25	2.3×10^4
$k_{-2}K_a$ / mol dm^{-3} s^{-1}	7.4×10^{-9}	8.0×10^{-8}	5.0×10^{-7}	5.0×10^{-11}	-
K_a / mol dm^{-3}	2.0×10^{-11}	(1×10^{-11})	1.0×10^{-9}	2.0×10^{-12}	2×10^{-11}
pK_a	10.70	(11.0)	9.0	11.70	10.7
K_{hyd} [c] / mol dm^{-3}	1.2	$\sim 2 \times 10^{-3}$	0.10	~2000	0.008

Pentane-2,4,-dione K_{enol} / mol dm^{-3} = 5.9, $K_{1:1}$ = 1900 dm^3 mol^{-1}, $K_{1:2}$ = 1.45 dm^3 mol^{-1}.

[a] *Data from ref 10*

[b] *Data from ref 13*

[c] *Present work or from ref 24*

[d] *Values in parentheses were calculated assuming a pK$_a$ value of 11.0*

Figure 2.25: A plot of Log K_2 versus the sum of Taft parameters

$$\sigma^* + (0.6 \times E_s)$$
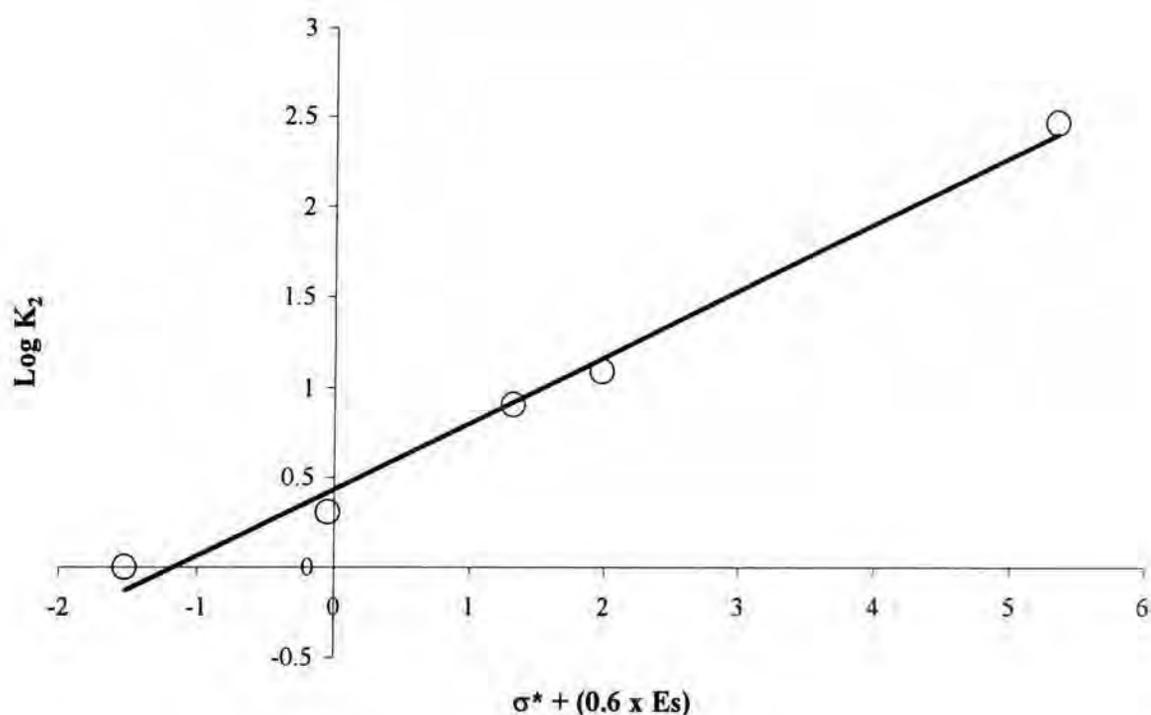
Table 2.33: Values [27] for the Taft parameters E_s and σ^* for carbonyl compounds R,R'C=O

R	R'	σ^*		E_s		$K_1 / mol^{-1} dm^3$
		R	R'	R	R'	
H	H	0.49	0.49	1.24	1.24	3.4×10^{10}
H	Et	0.49	-0.10	1.24	-0.07	3.3×10^5
H	Ph	0.49	0.60	1.24	-2.55	6.4×10^3
CH₃	CH₂Cl	0	1.05	0	-0.24	1.65×10^3
CH₃	Ac	0	0.59		(-0.3)	1.0×10^{3} ᵃ
CH₃	CH₃	0	0	0	0	2.4×10^2

ᵃ *Measured value has been statistically corrected. Value was divided by two to take account of the two carbonyl groups*

Values for the three ketones are all lower than the aldehydes, again confirming the importance of steric effects. There is some evidence that steric effects are more important in sulfite addition than in the formation of hydrates. Thus the value of K_1 is lower for chloropropanone

than for benzaldehyde, while for K_{hyd} this order is reversed. It was not thought to be worthwhile to try and attempt quantitative correlation with the Taft parameters given the limited data.

Interestingly the very much lower value obtained for $K_{1:2}$ than for $K_{1:1}$ in bisulfite addition to pentane-2,4-dione indicates that the steric effect of the added bisulfite group effectively inhibits the addition of the second bisulfite group.

The values obtained for the rate constants, k_1, increase in the same order as K_1, while values of k_{-1} decrease correspondingly.

The values of K_2 are, of course, related to values of K_1 by the dissociation constants K_a as shown in equation 2.16. Values of K_a were obtained experimentally for propanal and for chloropropanone and may be compared with literature values for formaldehyde and benzaldehyde. The values obtained are not easily interpreted. The values are expected to be largely effected by electronic effects of the dianionic species. Steric effects may be important since ionisation produces the dianion and the proximity of negative charges may result in greater steric compression of the substituents. The most acidic adduct, $pK_a = 9$, is that obtained from chloropropanone and indicates the effect of the electron withdrawal by the CH_2Cl group. The values for propanal, $pK_a = 10.7$, and benzaldehyde, $pK_a = 10.7$ are, surprisingly, equal. The higher steric effect of the phenyl group compared to the ethyl group may compensate for its favourable electronic effect. The value obtained for formaldehyde, $pK_a = 11.7$, is surprisingly high in relation to the other compounds, indicating that it may be of questionable validity.

It was not possible to obtain a value for pK_a for the propanone-adduct experimentally. A value of 11 has been used to estimate values for K_2, k_2 and k_{-2} in table 2.32. The combination of electronic effects of the two methyl groups relative to hydrogen plus ethyl, should reduce the acidity somewhat. Hence a slightly higher pK_a than obtained for the propanal adduct has been used.

Values of K_2 follow the same order as values of K_1 except that chloropropanone and benzaldehyde are reversed. This can be viewed as an effect of the higher acidity of the chloropropanone adduct, or as the favourable effect of the CH_2Cl substituent in promoting

SO_3^{2-} addition. Values of k_2 and of k_{-2} again largely reflect values of K_2 for the compounds studied.

The values obtained are of interest in their own right, and in particular the values obtained for propanal will be used in Chapter 3 and 4, where reactions of HPS and aniline are studied.

2.4: References

1) A. Vogel, 'Textbook of Practical Organic Chemistry', 5th Ed., Longman, London, 1991, p. 1289

2) F. Raschig and W. Prahl, *Ann.*, 1926, **448**, 265

3) C. N. Caughlan and H. V. Tartar, *J. Am. Chem. Soc.*, 1941, **63**, 1265

4) W. A. Sheppard and A. N. Bourns, *Can. J. Chem.*, 1954, **32**, 4

5) A. Kh Khusid and N. V. Chizhova, *Zh. Org. Khim.*, 1985, **21**, 43

6) J. B. Ekeley and A. O'Kelly, *J. Am. Chem. Soc.*, 1928, **50**, 2732

7) A. Kondo and S. Iwatsuki, *J. Fluro. Chem.*, 1984, 59

8) T. J. Johnson and R. A. Jones, *Tetrahedron*, 1978, **34**, 547

9) S. D. Boyce and M. R. Hoffmann, *J. Phys. Chem.*, 1984, **88**, 4740

10) (a) J. H. Atherton, K. H. Brown and M. R. Crampton, *J. Chem. Soc., Perkin Trans. 2*, 2000, 941 (b) K. H. Brown, PhD Thesis, University of Durham, 1999

11) P. E. Sørensen and V. S. Andersen, *Acta Chem. Scand.*, 1970, **24**, 1301

12) M. A. Gubareva, *J. Gen. Chem. (U.S.S.R.)*, 1947, **17**, 2259

13) F. C. Kokesh and R. E. Hall, *J. Org. Chem.*, 1975, **40**, 1632

14) (a) T. M. Olson, S. D. Boyce and M. R. Hoffmann, *J. Phys. Chem.*, 1986, **90**, 2488; (b) E. A. Betterton and M. R. Hoffmann, *ibid.*, 1987, **91**, 3011

15) (a) T. D. Stewart and L. H. Donnally, *J. Am. Chem. Soc.*, 1932, **54**, 2333; (b) *ibid.*, 3555; (c) *ibid.*, 3559

16) D. A. Blackadder and C. Hinshelwood, *J. Chem. Soc.*, 1958, 2720

17) P. R. Young and W. P. Jencks, *J. Am. Chem. Soc.*, 1978, **100**, 1228

18) (a) D. A. Palmer, R. W. Ramette and R. E. Mesmer, *J. Solution Chem.*, 1984, **13**, 637; (b) R. W. Ramette and R. W. Sandford, *J. Am. Chem. Soc.*, 1965, **87**, 5001

19) (a) B. S. Yiin and D. W. Margerum, *Inorg. Chem.*, 1990, **29**, 1559; (b) S. Dong and P. K. Dasgupta, *Atmos. Environ.*, 1986, **20**, 1635

20) (a) G. L. Kok, S. N. Gitlin and A. L. Lazrus, *J. Geophys. Res., D*, 1986, **91**, 2801; (b) E. Haydon, A. Treinin and J. Wilf, *J. Am. Chem. Soc.*, 1972, **94**, 47; (c) V. H. Tartar and H. H. Garretson, *ibid.*, 1941, **63**, 808

21) W. Hérold, *Z. physic. Chem.*, 1932, *B.*, **18**, 265

22) L. C. Gruen and P. T. McTigue, *J. Chem. Soc.*, 1963, 5217

23) 'CRC Handbook of Chemistry and Physics', CRC Press, Florida, 1982, 63rd Ed., D173

24) R. P. Bell, *Adv. Phys. Org. Chem.*, 1966, **4**, 1

25) G. M. Loudon, 'Organic Chemistry', The Benjamin/Cummings Publishing company, Inc. Redwood City, CA, 1995, 3rd Ed., p. 1044-1046

26) G. E. Senon, 'L'Indispensable de Chimie Organique', Edition Breg, Paris, 1993, p.15

27) J. Shorter, *Quart. Rev. (London)*, 1970, **24**, 443

Chapter three

3 The reaction of HPS with aniline and its derivatives

3.1: Introduction

Reactions of hydroxyalkanesulfonates, HXS, with amines have been rarely memtioned in the literature, and in fact, only two studies, both concerning hydroxymethanesulfonate, HMS have been reported. These two reported reactions have been mentioned in the section 1.2.2.1; the reaction of HMS with ammonia, carried out by Le Hénaff[1] and the reaction of HMS with aniline and some of its derivatives, observed by Brown and Crampton [2].

Le Hénaff observed kinetically, the reactions of ammonia with HMS, and reported values of several rate and equilibrium constants for the processes at 20 °C, shown in table 3.1. It was postulated (Scheme 3.1) that ammonia reacted with more than one equivalent of HMS, yielding both the 1:1 and 1:2 adducts. Concentrations of intermediates were thought to be small.

Scheme 3.1:

1:1 adduct formation

1:2 adduct formation

$$HCHO + H_2NCH_2SO_3^- \underset{k_{-2}'}{\overset{k_2'}{\rightleftharpoons}} NH(CH_2SO_3^-)(CH_2OH)$$

$$\overset{+}{H_2N}(CH_2SO_3^-)(CH_2OH) \quad +OH^- \| -OH^-$$

$$(CH_2SO_3^-)\overset{+}{N}H{=}CH_2 \underset{k_{-6}'}{\overset{k_6'}{\rightleftharpoons}} NH(CH_2SO_3^-)_2$$

Table 3.1: Literature values [1] for rate and equilibrium constants of the processes as shown in scheme 3.1

Constant	Value
k_{-6}	6.8×10^{-5} s^{-1}
k_{-3} / k_6	40.5
k_{-5} / k_6	2.7×10^{-4} mol dm^{-3}
$K = [NH_3][CH_2(OH)(SO_3^-)] / [H_2NCH_2SO_3^-]$	1.4×10^{-3} mol dm^{-3}
k_{-6}'	2.0×10^{-5} s^{-1}
k_{-3}' / k_6'	320
k_{-5}' / k_6'	2.4×10^{-3} mol dm^{-3}
$K' = [H_2NCH_2SO_3^-][CH_2(OH)(SO_3^-)] / [NH(CH_2SO_3^-)_2]$	2.6×10^{-3} mol dm^{-3}

The mechanisms shown in scheme 3.1 demonstrate both a 1:1 and 1:2 adduct formation. Le Hénaff recognised that the reaction is greatly retarded by sulfite, due to the reduction in concentration of free fomaldehyde, and suggested that formation of the 1:3 adduct $(N(CH_2SO_3^-)_3)$ would be possible.

A reaction of more interest to the current work is Brown and Crampton's study of HMS with aniline and some of its derivatives. The reaction yields anilinomethanesulfonates, AMS, via
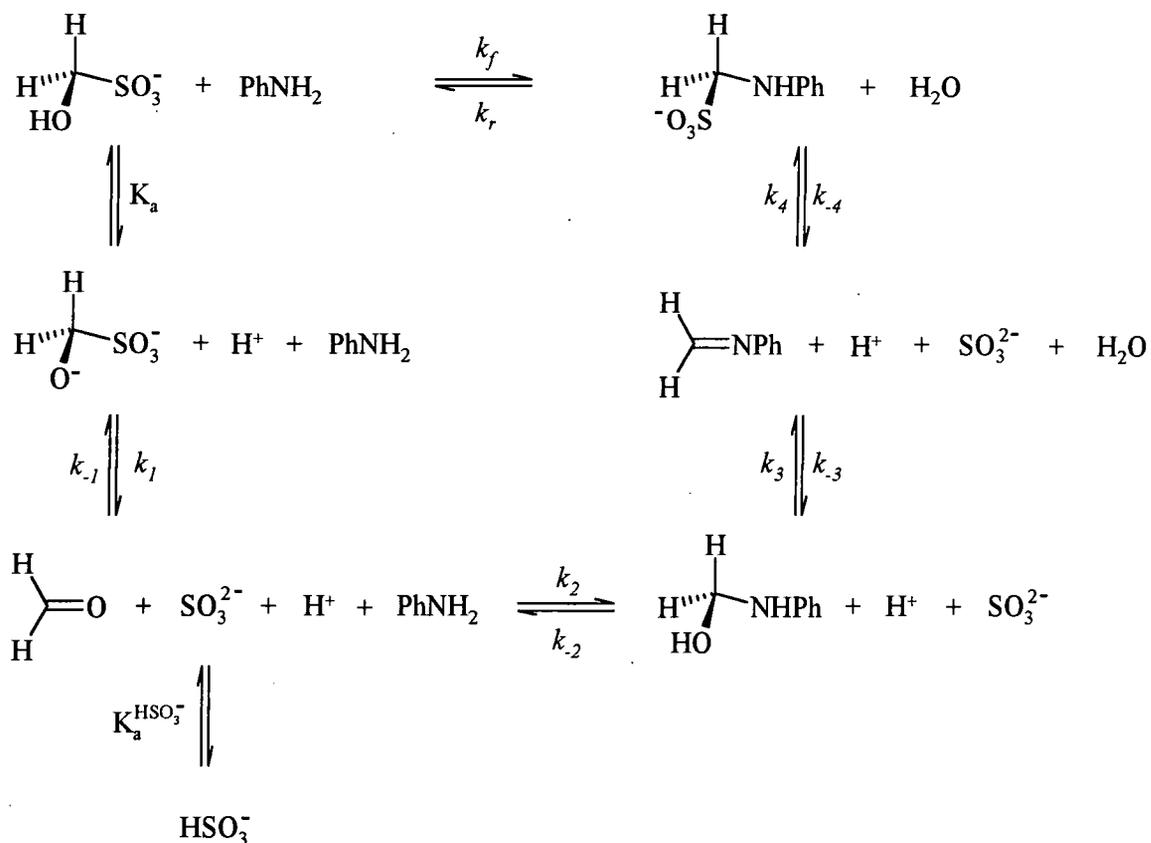
imine or iminium ion intermediates. The reaction of aniline and its derivatives with HMS was observed by both ^{1}H NMR and UV/Vis spectroscopy. ^{1}H NMR studies showed that the formation was relatively slow and took several hours to achieve completion. On the other hand, aniline is a much weaker base than ammonia, so that here, only adducts of 1:1 stoichiometry were observed. UV/Vis studies, when HMS was in large excess, showed first order kinetic behaviour. Values for the overall rate and equilibrium constants were obtained from both methods for aniline and 4-methylaniline, and are shown in table 3.2.

Table 3.2: Rate and equilibrium constants reported in literature for the reactions of HMS with aniline and 4-methylaniline obtained at 25 °C

amine	k_f / dm^3 mol^{-1} s^{-1}	k_r / s^{-1}	K / dm^3 mol^{-1}
aniline	$7.8 \times 10^{-3} \pm 2 \times 10^{-5}$	$1.0 \times 10^{-5} \pm 8 \times 10^{-7}$	780 ± 60
4-methylaniline	$4.9 \times 10^{-2} \pm 6 \times 10^{-5}$	$1.2 \times 10^{-4} \pm 3 \times 10^{-6}$	410 ± 10

A mechanistic view on the reactions was considered, and a scheme was postulated, as shown in 3.2. It shows that the HMS adduct dissociates to reactants, so that the free formaldehyde can react with the amine, to yield a carbinolamine. This undergoes dehydration to yield the imine / iminium ion, which subsequently reacts with the free sulfite to produce the product, anilinomethanesulfonate.

Scheme 3.2:

$$\text{H}^{\prime\prime\prime}\overset{\text{H}}{\underset{\text{HO}}{\bigg|}}\text{SO}_3^- + \text{PhNH}_2 \underset{k_r}{\overset{k_f}{\rightleftharpoons}} \text{H}^{\prime\prime\prime}\overset{\text{H}}{\underset{^-\text{O}_3\text{S}}{\bigg|}}\text{NHPh} + \text{H}_2\text{O}$$

$$\Big\updownarrow K_a \qquad\qquad\qquad \Big\updownarrow k_4 \,\Big\updownarrow k_{-4}$$

$$\text{H}^{\prime\prime\prime}\overset{\text{H}}{\underset{\text{O}^-}{\bigg|}}\text{SO}_3^- + \text{H}^+ + \text{PhNH}_2 \qquad\qquad \overset{\text{H}}{\underset{\text{H}}{\diagdown}}=\text{NPh} + \text{H}^+ + \text{SO}_3^{2-} + \text{H}_2\text{O}$$

$$k_{-1}\,\Big\updownarrow k_1 \qquad\qquad\qquad k_3\,\Big\updownarrow k_{-3}$$

$$\overset{\text{H}}{\underset{\text{H}}{\diagdown}}=\text{O} + \text{SO}_3^{2-} + \text{H}^+ + \text{PhNH}_2 \underset{k_{-2}}{\overset{k_2}{\rightleftharpoons}} \text{H}^{\prime\prime\prime}\overset{\text{H}}{\underset{\text{HO}}{\bigg|}}\text{NHPh} + \text{H}^+ + \text{SO}_3^{2-}$$
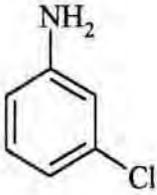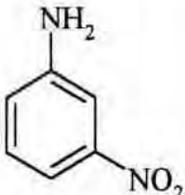
$$K_a^{\text{HSO}_3^-}\,\Big\updownarrow$$
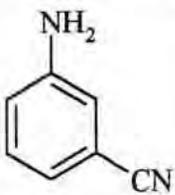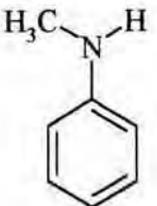
$$\text{HSO}_3^-$$

Evidence was presented to show that the rate determining step, was either the reaction of free formaldehyde with aniline, k_2, or the dehydration of this product, the carbinolamine, k_3. The results illustrated that it was likely that a change in rate determining step occurred from carbinolamine formation, to carbinolamine dehydration with increasing pH.

Here, the reactions of HPS with aniline and its derivatives are investigated. Propanal has the advantage over formaldehyde, in that hydration of the free aldehyde is relatively unimportant. The amines studied are shown in table 3.3.

The reactions of aniline and its derivatives with HPS were studied using ^{1}H NMR spectroscopy. The spectrum of the amine alone was obtained, and then, the spectra in the presence of excess HPS. The kinetics of the reaction were observed using UV/Vis spectroscopy. Sulfite ions were generally added to the system to facilitate the analysis of the kinetics, in terms of the stoichiometric concentration of sulfite.

**Table 3.3:** Amines studied in the reaction with HPS
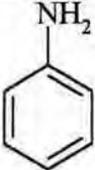
Amine			pK$_a$§
Aniline		**3.2**	4.60
4-methylaniline		**3.3**	5.08
4-chloroaniline		**3.4**	4.15
3-chloroaniline		**3.5**	3.46
3-nitroaniline		**3.6**	2.47
3-cyanoaniline		**3.7**	2.75
N-methylaniline		**3.8**	4.85

§ pK$_a$ values correspond to dissociation of protonated amines at 25 ^{o}C, reference 3

118

3.2: Results and discussion

3.2.1: ^{1}H NMR studies

The reactions of HPS with the anilines were studied using 1H NMR spectroscopy. Initially the spectra for the starting materials were obtained. The spectrum of HPS **3.1** has been explained in detail in section 2.2.2.1, but shifts are shown again, in table 3.4.
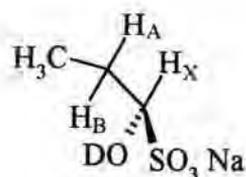
3.1

Table 3.4: ^{1}H NMR peak assignment for 0.1 mol dm^{-3} HPS, **3.1** in D$_2$O

δ / ppm	integral ratio	multiplicity	assignment
4.67	-	-	H$_2$O
4.15	1	dd	-CH(OH)(SO$_3$Na)
1.84	1	m	-CH$_A$H$_B$-
1.53	1	m	-CH$_A$H$_B$-
0.90	3	t	-CH$_3$

Note: refer to table 2.4 for coupling constants

3.2.1.1: Aniline

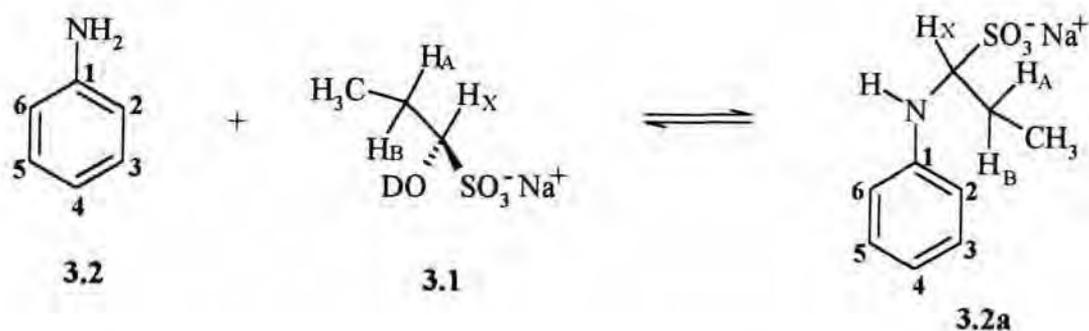Figure 3.1 and table 3.5 describe the ^{1}H NMR spectrum of 0.1 mol dm^{-3} aniline (**3.2**) in D$_2$O.

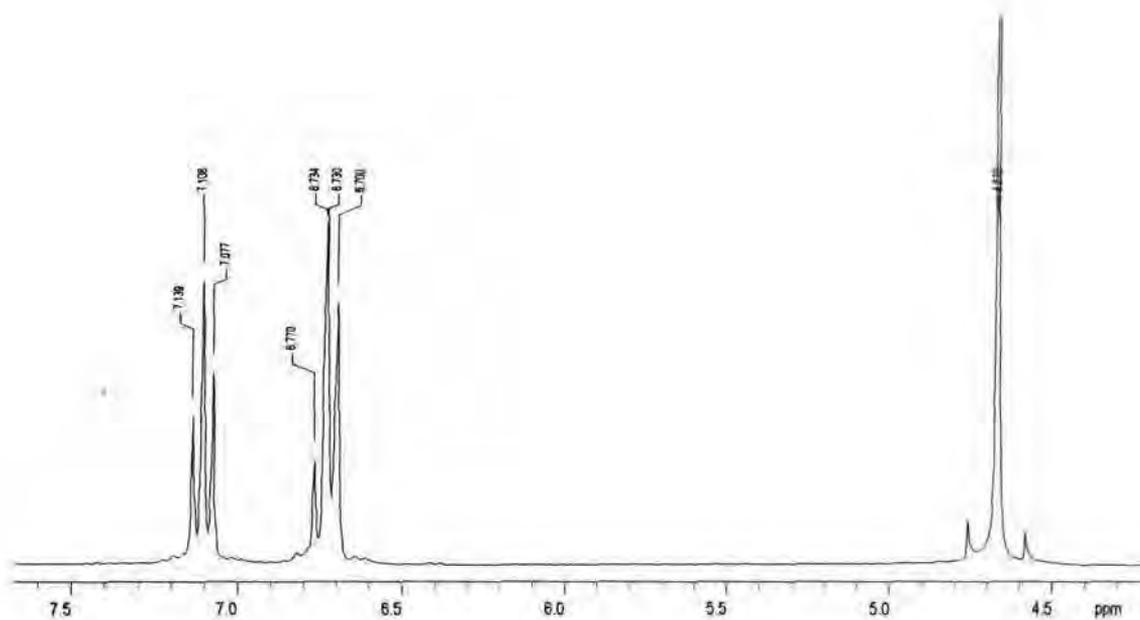**Figure 3.1:** ^{1}H NMR spectrum of 0.1 mol dm^{-3} aniline in D$_2$O

Table 3.5: ^{1}H NMR spectrum of 0.1 mol dm^{-3} aniline in D$_2$O: peak assignment

δ / ppm	integral ratio	multiplicity	J / Hz	assignment
7.11	2	t	8	Ar-H$_3$, H$_5$
6.74	3	t	8	Ar-H$_4$
6.73		d	8	Ar-H$_2$, H$_6$
4.67	-	-	-	H$_2$O, -NH$_2$

The bands due to H$_4$ and to H$_2$ and H$_6$ have similar shifts and give the overlapping triplet and doublet at δ 6.73ppm.

The initial spectra of aniline with HPS, indicated that the reaction was not instantaneous, and therefore, it was observed over time, until no further changes occurred. Reactions were carried out with HPS in large excess of aniline; each reaction contained 0.01 mol dm^{-3} aniline, with HPS concentrations 0.1, 0.2 and 0.5 mol dm^{-3}. Each reaction showed formation of adduct over varying times, and was the fastest when HPS was most concentrated, but essentially the trends were the same. The reaction HPS 0.1 mol dm^{-3} and aniline 0.01 mol dm^{-3} will be discussed in detail. Figures 3.2 and 3.3 show spectra, after 10mins and the spectra after 6hrs, with peak analysis in table 3.6 for all spectra taken.

Figure 3.2: ^{1}H NMR spectrum of 0.01 mol dm^{-3} aniline and 0.1 mol dm^{-3} HPS in D$_2$O, reaction after ten minutes (250Mhz spectrometer)
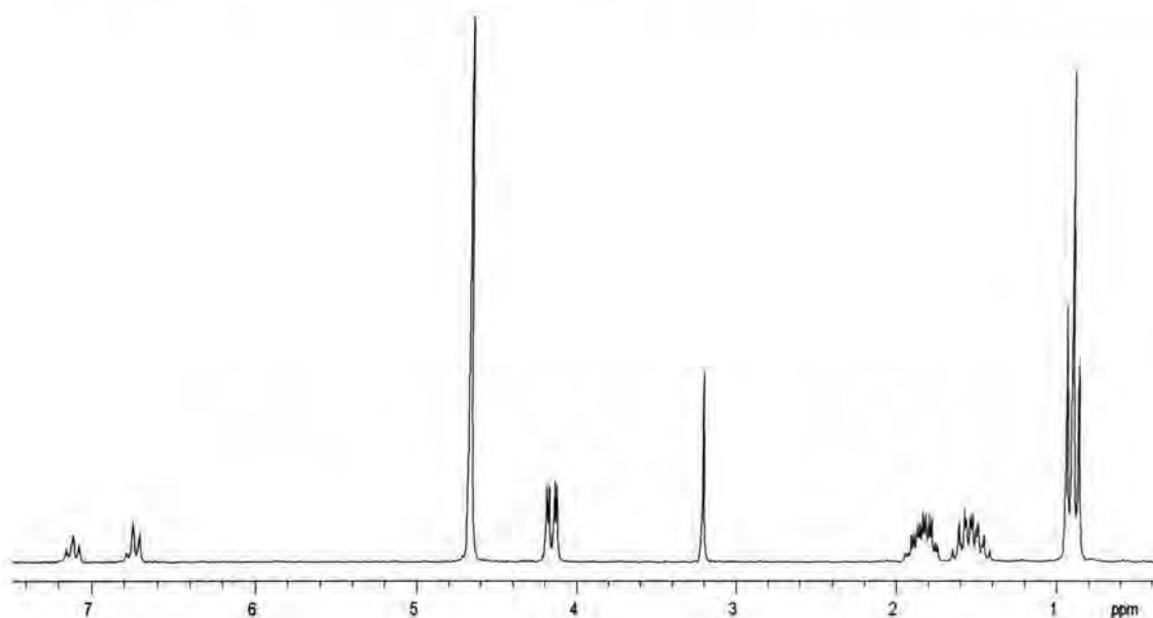

Figure 3.3: ^{1}H NMR spectrum of 0.01 mol dm^{-3} aniline and 0.1 mol dm^{-3} HPS in D$_2$O, reaction after 6hrs (250Mhz spectrometer)
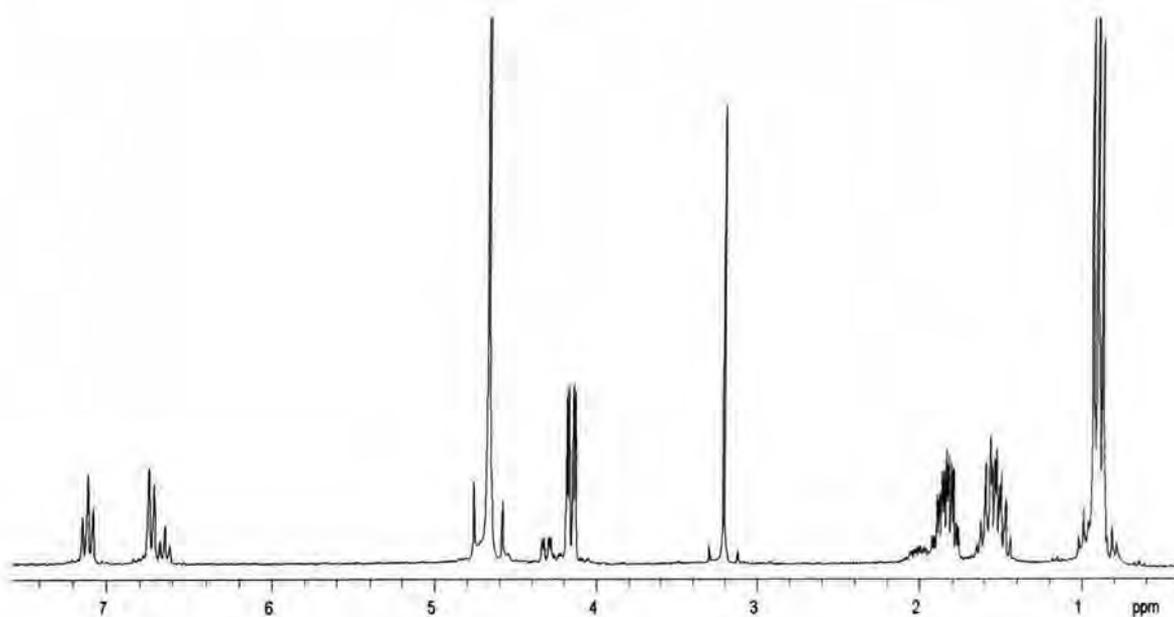
Table 3.6: Peak assignments for 1H NMR taken for the reaction of 0.01 mol dm^{-3} aniline and 0.1 mol dm^{-3} HPS in D_2O, over time (expressed in minutes) with a pH 7 buffer (250Mhz spectrometer)

δ / ppm	Mult.	Variation of intensities of peaks with time					assignment
		10	25	70	200	360	
7.11	t	2.64	2.7	2.85	3.03	2.83	Ar-H$_3$, H$_5$ & Ar-H$_3$, H$_5$ *
6.74	t	3.49	3.52	3.35	3.34	3.19	Ar-H$_4$
6.73	d						Ar-H$_2$, H$_6$ & Ar-H$_2$, H$_6$ *
6.66	t	0	0.45	0.62	1.05	0.97	Ar-H$_4$*
4.67	-	-	-	-	-	-	H$_2$O, -NH$_2$
4.31	dd	0	0.28	0.63	1.12	1.14	-CH$_X$*
4.15	dd	8.88	8.65	8.43	7.89	7.73	-CH$_X$
2.02	m	0	0.17	0.58	1.04	1.31	-CH$_A$H$_B$-*
1.84	m	10.99	10.98	10.84	10.06	9.81	-CH$_A$H$_B$-
1.53	m	11.38	11.33	11.43	11.18	11.06	-CH$_A$H$_B$- & -CH$_A$H$_B$- *
0.90	t	32.15	32.36	32.23	31.79	35.35	-CH$_3$ & -CH$_3$ *

** peaks assigned to product, anilinopropanesulfonate, APS (**3.2a**)*

Due to the complexity of the spectra, integral intensities, rather than ratios, are quoted. They clearly show the products forming with time. At the outset of this experiment, the aim was to firstly obtain evidence for the reaction products being formed, and secondly, to try and obtain values of equilibrium constants for the process. Formation occurs as seen, however attempts to calculate an equilibrium constant proved difficult. This was firstly because, out of the three peaks attributed to the product that were separately visible, two were shouldered by reactants, leaving only the well separated methine peak to observe. Also, due to overlapping of bands due to ring hydrogens, the relative concentrations of free and complexed aniline were difficult to calculate, giving rise to an inherently large experimental error. This, therefore, meant that any values calculated were subject to large error.

Altering the concentrations, so that HPS and aniline were virtually equimolar, 0.05 mol dm^{-3}, was more successful, and spectra were run on a higher resolution NMR spectrometer, in an attempt to achieve greater separation of peaks. Again, the products were observed, and the

higher resolution, indeed produced better separation to the degree, where practically all peaks could be identified and assigned. From the spectrum shown in figure 3.4, and the peak assignment in table 3.7, it was possible to calculate values of the equilibrium constant for the overall reaction.

Figure 3.4: ^{1}H NMR spectrum of 0.05 mol dm^{-3} aniline and 0.04 mol dm^{-3} HPS in D$_2$O (500MHz spectrometer)
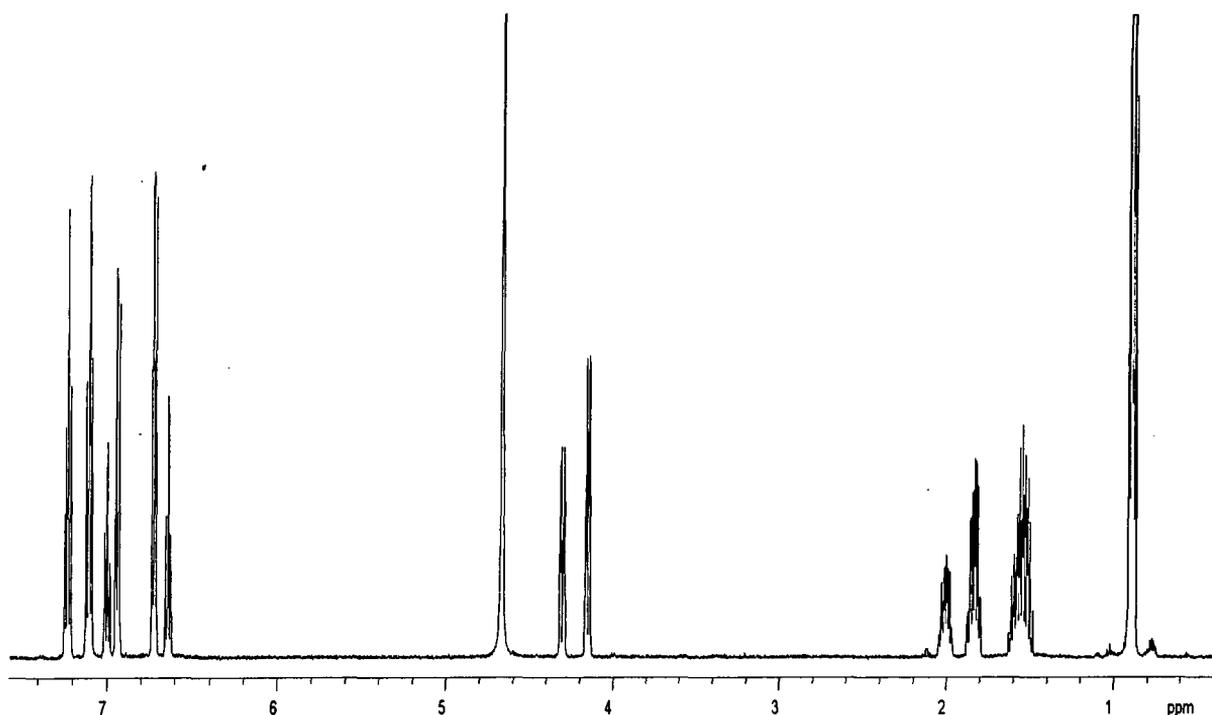
Table 3.7: ^{1}H NMR spectrum of 0.05 mol dm^{-3} aniline and 0.04 mol dm^{-3} HPS in D$_2$O: peak assignment (500MHz spectrometer)

δ / ppm	integral ratio	multiplicity	J / Hz	assignment
7.18	~2.4	t	8	Ar-H$_3$, H$_5$
7.11	2	t	8	Ar-H$_3$, H$_5$*
6.86	~1.2	t	8	Ar-H$_4$
6.82	~2.4	d	8	Ar-H$_2$, H$_6$
6.73	2	d	8	Ar-H$_2$, H$_6$*
6.65	1	t	8	Ar-H$_4$*
4.67	-	-	-	H$_2$O, -NH$_2$
4.31	1.2	dd	†*	-CH$_X$*
4.15	1	dd	†	-CH$_X$
2.02	1	m	†*	-CH$_A$H$_B$-*
1.84	1	m	†	-CH$_A$H$_B$-
1.53	~2.2	m	-	-CH$_A$H$_B$- / -CH$_A$H$_B$-*
0.89	~6.6	-	-	-CH$_3$ / -CH$_3$*

* peaks assigned to products, anilinopropanesulfonates, APS

† coupling constants can be found in table 2.4

*†* products coupling constants are similar to unreacted HPS, table 2.4*

As the aromatic area was well defined, it was possible to calculate the concentrations of the reactants and products, along with the free HPS concentration. The relative intensities were used together with a knowledge of the stoichiometric concentration of aniline and HPS, to calculate the equilibrium concentrations. Values obtained were [Aniline] = 0.027 mol dm^{-3} [APS] = 0.023 mol dm^{-3} and [HPS] = 0.017 mol dm^{-3}. When substituted in equation 3.1, these yielded a value for K of 50±10 dm^3 mol^{-1}.

$$K = \frac{[APS]}{[Aniline][HPS]}$$

(3.1)

The value obtained refers to D_2O as solvent and in unbuffered solutions. Hence, it is likely to be less reliable than values obtained from UV/Visible measurements in water.

3.2.1.2: 4-methylaniline

The ^1H NMR spectrum of **3.3**, 0.01 mol dm^{-3}, in D_2O buffered at pH 8, shows the bands reported in Table 3.8. Spectra obtained in the presence of a tenfold excess of HPS, 0.1 mol dm^{-3} are shown in figures 3.5 and 3.6. These were obtained after 4 minutes and 24 hours, respectively.

3.3   **3.1**

3.3a
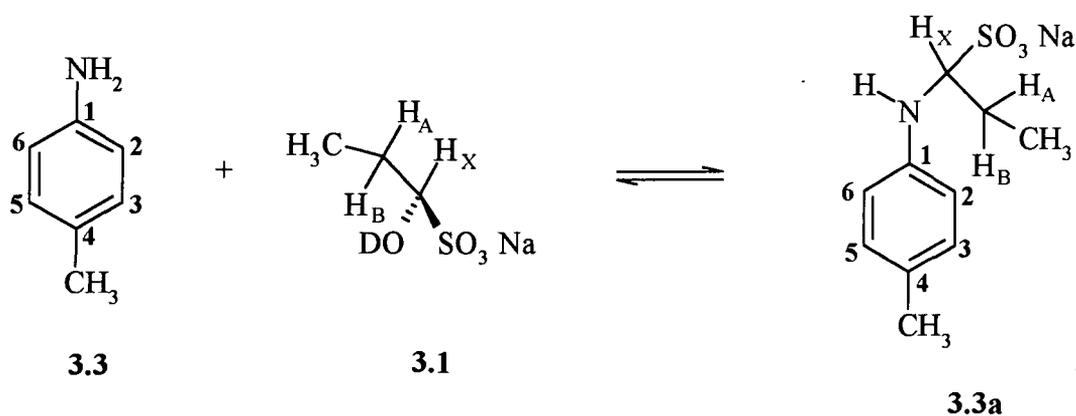
Evidence for adduct formation of **3.3a** is obtained from the development, with time of new bands at *ca.* δ 4.2ppm, attributed to the methine hydrogen H_X*. However, there is little change in the shifts of the ring hydrogens or of the ring methyl group on reaction. Hence, it was not possible to resolve separate bands, due to the two forms present.

126

Figure 3.5: ¹H NMR spectrum of the reaction between 0.01 mol dm⁻³ 4-methylaniline and 0.1 mol dm⁻³ HPS, with a pH 8 buffer after 4 minutes, in D_2O
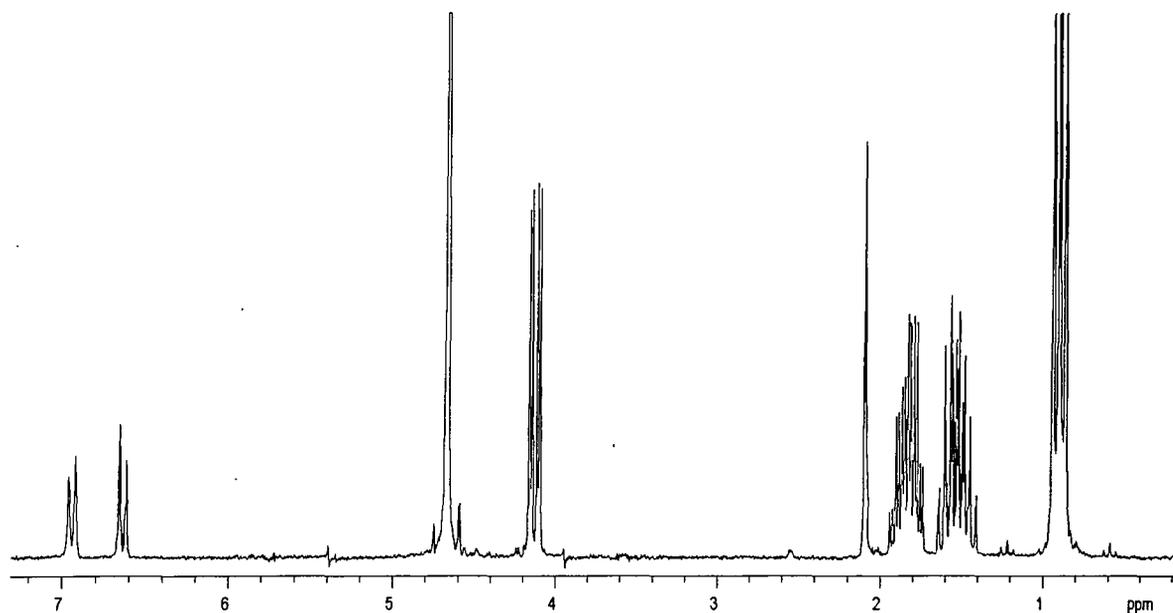

Figure 3.6: ¹H NMR spectrum of the reaction between 0.01 mol dm⁻³ 4-methylaniline and 0.1 mol dm⁻³ HPS, with a pH 8 buffer after 24 hours, in D_2O
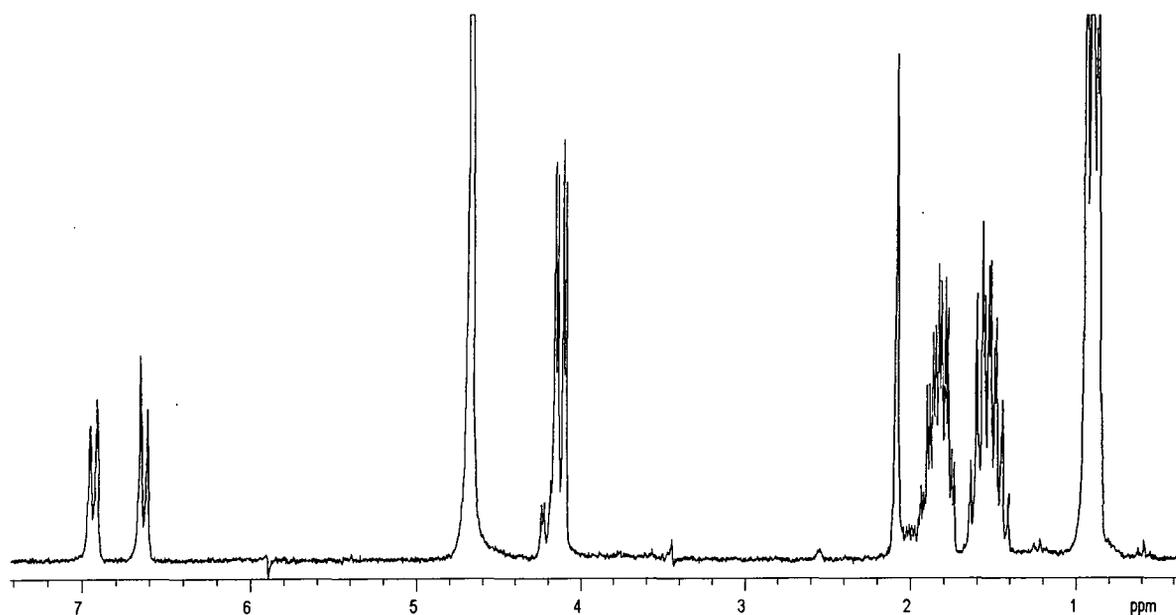
Table 3.8: ^1H NMR spectrum of the reaction between 0.01 mol dm^{-3} 4-methylaniline and 0.1 mol dm^{-3} HPS, with a pH 8 buffer; peak assignment over time

Time	δ / ppm	integral ratio	multiplicity	J / Hz	assignment
4 mins	6.95	2	d	8	Ar-H_3, H_5
	6.65	2	d	8	Ar-H_2, H_6
	4.67	-	-	-	H_2O
	4.15	10	dd	3.4 & 10	-CH_X
	2.10	3	s	-	*para*-CH_3
	1.84	10	m	†	-CH_AH_B-
	1.53	10	m	†	-CH_AH_B-
	0.90	30	t	7.5	-CH_3
24 hours	6.95	2	d	8	Ar-H_3, H_5 & Ar-H_3, H_5*
	6.63	2	d	8	Ar-H_2, H_6 & Ar-H_2, H_6*
	4.67	-	-	-	H_2O
	4.19	$1^\S$	dd	3.4 & 10	-CH_X*
	4.15	$9^\S$	dd	3.4 & 10	-CH_X
	2.10	3	s	-	*para*-CH_3 & *para*-CH_3*
	1.84	$1^\S$	m	†	-CH_AH_B-*
	1.84	$9^\S$	m	†	-CH_AH_B-
	1.53	10	m	†	-CH_AH_B- & -CH_AH_B-*
	0.90	30	t	7.5	-CH_3 & -CH_3*

** peaks assigned to adduct **3.3a***

† coupling constants of HPS peaks, unreacted and present as adduct, are equal to values in table 2.4

§ ratios of peaks calculated using partial integrals of formed peaks

With the large excess of HPS used, the conversion of **3.3** to the adduct **3.3a**, goes very largely to completion, so that calculation of a value for the equilibrium constant, K, was not possible. Due to the very small change in shifts observed on adduct formation, it was not thought profitable to attempt to obtain a value for K, using a smaller excess of HPS.

3.2.1.3: 4-chloroaniline, 3-chloroaniline, 3-nitroaniline, 3-cyanoaniline and 4-nitroaniline

The spectra obtained for the parent molecules in dilute solutions in D_2O are reported in tables 3.9, 3.10, 3.11, 3.12 and 3.13.

Table 3.9: ^1H NMR spectrum of 0.1 mol dm^{-3} 4-chloroaniline **3.3** in D_2O; peak assignment

δ / ppm	integral ratio	multiplicity	J / Hz	assignment
7.05	2	d	8.8	Ar-H_2, H_6
6.60	2	d	8.8	Ar-H_3, H_5
4.67	-	-	-	H_2O

Table 3.10: ^1H NMR spectrum of 0.1 mol dm^{-3} 3-chloroaniline **3.4** in D_2O; peak assignment

δ / ppm	integral ratio	multiplicity	J / Hz	assignment
7.01	1	t	8	Ar-H_5
6.68	1	s	8	Ar-H_2
6.60^a	1	d	8	Ar-H_4
6.58	1	d	8	Ar-H_6
4.67	-	-	-	H_2O

a *on adduct formation peaks shifts to 6.50*

Table 3.11: ^1H NMR spectrum of 0.1 mol dm^{-3} 3-nitroaniline **3.4** in D_2O; peak assignment

δ / ppm	integral ratio	multiplicity	J / Hz	assignment
7.46	2	d	8.4	Ar-H_2
7.49^a				Ar-H_4
7.22	1	t	8	Ar-H_5
7.04	1	d	8.4	Ar-H_6
4.67	-	-	-	H_2O

a *on adduct formation peaks shifts to 7.41*

Table 3.12: ^{1}H NMR spectrum of 0.1 mol dm^{-3} 3-cyanoaniline in D$_2$O: peak assignment

δ / ppm	integral ratio	multiplicity	J / Hz	assignment
7.21	1	t	8	Ar-H$_5$
7.01	1	d	8	Ar-H$_4$
6.96	1	d	8	Ar-H$_2$, H$_6$
4.67	-	-	-	H$_2$O

Table 3.13: ^{1}H NMR spectrum of 0.1 mol dm^{-3} 4-nitroaniline in D$_2$O: peak assignment

δ / ppm	integral ratio	multiplicity	J / Hz	assignment
7.93	2	d	9	Ar-H$_3$, H$_5$
6.60	2	d	9	Ar-H$_2$, H$_6$
4.67	-	-	-	H$_2$O

In the presence of a tenfold excess of HPS, changes in shifts of ring hydrogens were very small. However, in each case, new bands were observed due to the methine hydrogen, H$_X$, in the adduct. Table 3.14, shows shifts of the methine peak in adducts, compared to the unreacted HPS band. There is some variation in the change in shift, Δδ, with the nature of the ring substituent, e.g. the electron withdrawing 4-nitro derivative, resulting in most de-shielding.

Table 3.14: Chemical shifts of methine hydrogen CH$_X$ in aniline adducts

Adduct	δ / ppm	Δδ / ppm
HPS alone	4.15	0
3.2a (aniline)	4.31	+0.16
3.3a (4-methylaniline)	4.19	+0.04
3.4a (4-chloroaniline)	4.24	+0.09
3.5a (3-chloroaniline)	4.28	+0.13
3.6a (3-nitroaniline)	4.34	+0.19
3.7a (3-cyanoaniline)	4.30	+0.15
3.5a (4-nitroaniline)	4.46	+0.31

3.2.1.4: N-methylaniline

Figure 3.7 shows the ^{1}H NMR of N-methylaniline **3.8** with peak assignment in table 3.15.
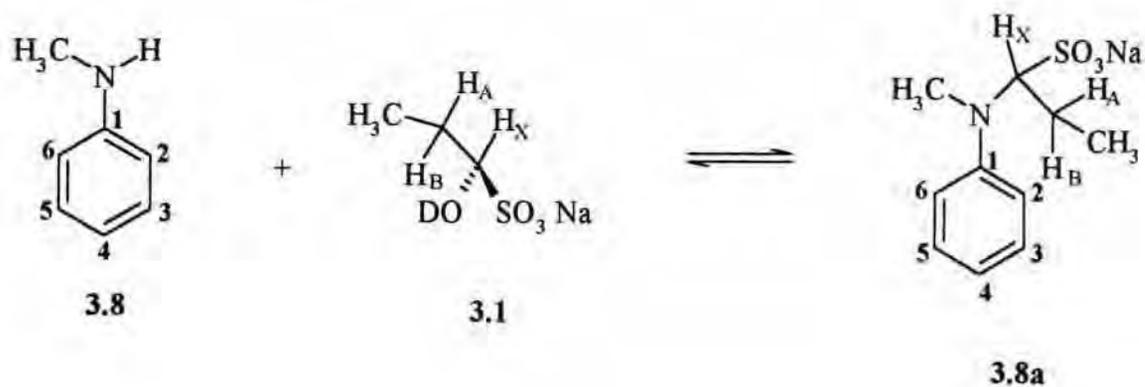

3.8

3.1

3.8a

Figure 3.7: ^{1}H NMR spectrum of 0.1 mol dm^{-3} N-methylaniline in D$_2$O
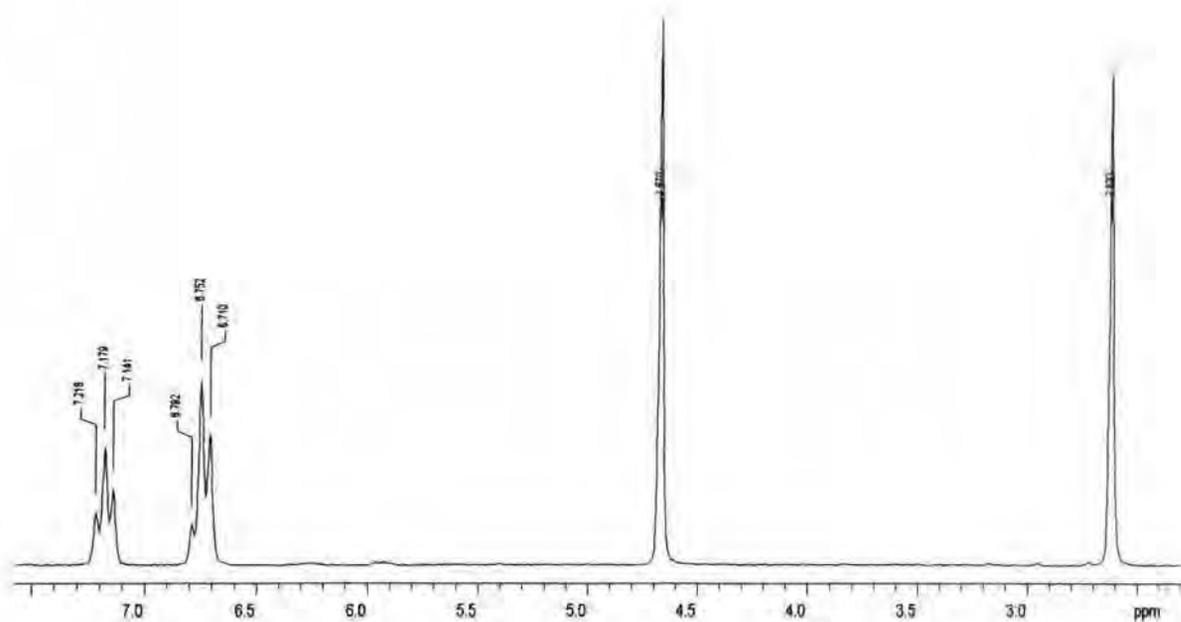
Table 3.15: ^{1}H NMR spectrum of 0.1 mol dm^{-3} N-methylaniline in D$_2$O: peak assignment

δ / ppm	integral ratio	multiplicity	J / Hz	assignment
7.18	2	t	8	Ar-H$_3$, H$_5$
6.76	3	t	8	Ar-H$_4$
6.75		d	8	Ar-H$_2$, H$_6$
4.67	-	-	-	H$_2$O, -NH
2.62	3	s	-	CH$_3$-N(H)-

As with other aniline derivatives reaction with HPS results in only slight changes; little separation is seen within the aromatic hydrogens, except the para hydrogen shifting down field to *ca.* 6.84. The adduct methine peak is hard to distinguish, especially for quantitative measurements. However, separation of the N-methyl peak is observed, and hence, quantitative studies could be undertaken. Figure 3.8 shows the reaction of N-methylaniline 0.01 mol dm^{-3} and HPS 0.1 mol dm^{-3} after 24 hours, and hence, when the reaction was at equilibrium.

Figure 3.8: ^{1}H NMR spectrum for the reaction of 0.01 mol dm^{-3} N-methylaniline with 0.1 mol dm^{-3} HPS in D$_2$O and a pH 7 buffer, reaction time 24 hours
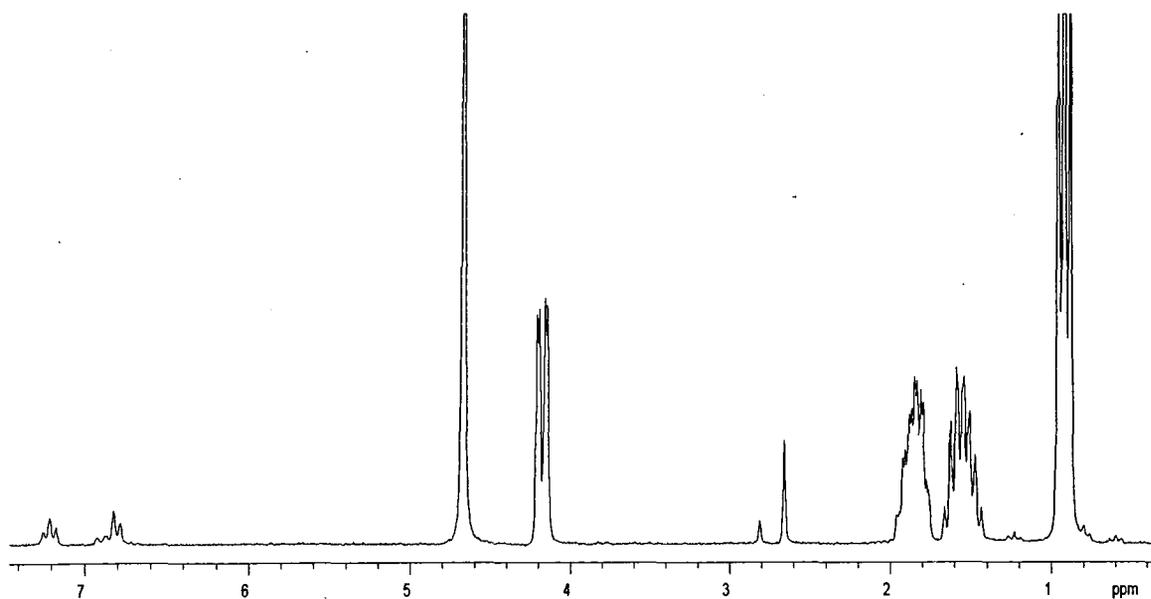
Table 3.16: ^{1}H NMR spectrum for the reaction of 0.01 mol dm^{-3} N-methylaniline with 0.1 mol dm^{-3} HPS in D$_2$O and a pH 7 buffer, reaction time 24 hours: peak assignment

δ / ppm	Int. ratio [§]	Multip	J / Hz	assignment
7.18	2	t	8	Ar-H$_3$, H$_5$ & Ar-H$_3$, H$_5$*
6.84	3	t	8	Ar-H$_4$*
6.76		d	8	Ar-H$_4$ & Ar-H$_2$, H$_6$ & Ar-H$_2$, H$_6$*
4.67	-	-	-	H$_2$O, -NH$_2$
4.17	10	dd	3.2 & 10	C H$_X$ & CH$_X$*
2.82	3	s	-	CH$_3$-N*
2.65		s	-	CH$_3$-N
1.84	10	m	†	-CH$_A$H$_B$- & -CH$_A$H$_B$-*
1.54	10			-CH$_A$H$_B$- & -CH$_A$H$_B$-*
0.90	30			-CH$_3$ & -CH$_3$*

* *peaks assigned to adduct* **3.8a**

† *coupling constants of HPS peaks, unreacted and present as adduct, are equal to values in table 2.4*

§ *integral ratios given as if reaction was virtually complete*

The equilibrium constant for the reaction, could be derived simply using two peaks, namely the unreacted and the adduct N-methyl peaks, at δ 2.65 and δ 2.82, respectively. Since, the concentration of the initially added aniline, **3.8**, was known, the ratio of these two peaks gave their respective concentrations. The total stoichiometeric concentration of HPS was known, and with the knowledge that the reaction with N-methylaniline had 1:1 stoichiometry, the concentration of free HPS could be calculated. Using equation 3.1 enabled values of the equilibrium constant for the process to be obtained.

Since the N-methyl peak is three times greater than the methine peak, the concentration ratio of HPS to **3.8** could be increased from 10:1 (used in other HPS / aniline reactions) to almost 50:1, with the ability still, to obtain equilibrium data. This was done in order to obtain values for K, the equilibrium constant, at various HPS concentrations. Table 3.17 shows the values obtained.

Table 3.17: Equilibrium constants obtained for the reaction of HPS (varying concentrations) with 0.01 mol dm^{-3} N-methylaniline at pH 7, in D$_2$O solutions.

Initial [HPS] /mol dm^{-3}	[HPS]$_{free}$ / mol dm^{-3}	Relative intensities / mol dm^{-3}		K / dm^3 mol^{-1}
		[Adduct, 3.8a]	[Parent, 3.8]	
0.10^a	0.099	1.02x10^{-3}	8.98x10^{-3}	1.15
0.10^b	0.099	1.00x10^{-3}	9.00x10^{-3}	1.12
0.20^a	0.198	1.74x10^{-3}	8.26x10^{-3}	1.06
0.20^b	0.198	1.96x10^{-3}	8.04x10^{-3}	1.23
0.25^a	0.248	1.98x10^{-3}	8.02x10^{-3}	0.99
0.25^b	0.248	2.50x10^{-3}	7.50x10^{-3}	1.35
0.50^a	0.497	3.22x10^{-3}	6.78x10^{-3}	0.96
0.50^b	0.497	3.39x10^{-3}	6.61x10^{-3}	1.03

a *data obtained after ~3hours of reaction*

b *data obtained after ~24hours of reaction*

The values obtained show good consistency with each other, giving an average equilibrium constant for the reaction of HPS with N-methylaniline of 1.11 dm^3 mol^{-1}.

3.2.2: Discussion of the rate determining step for the reaction

Kinetic and equilibrium studies of the formation of APS from HPS and Aniline were made spectrophotometrically, in aqueous buffers. The overall reaction, as in the case of the formation of AMS[2], is likely to involve several steps, and before presenting the results in detail, it is useful to outline the proposed mechanism. This is shown in scheme 3.3.

Scheme 3.3:
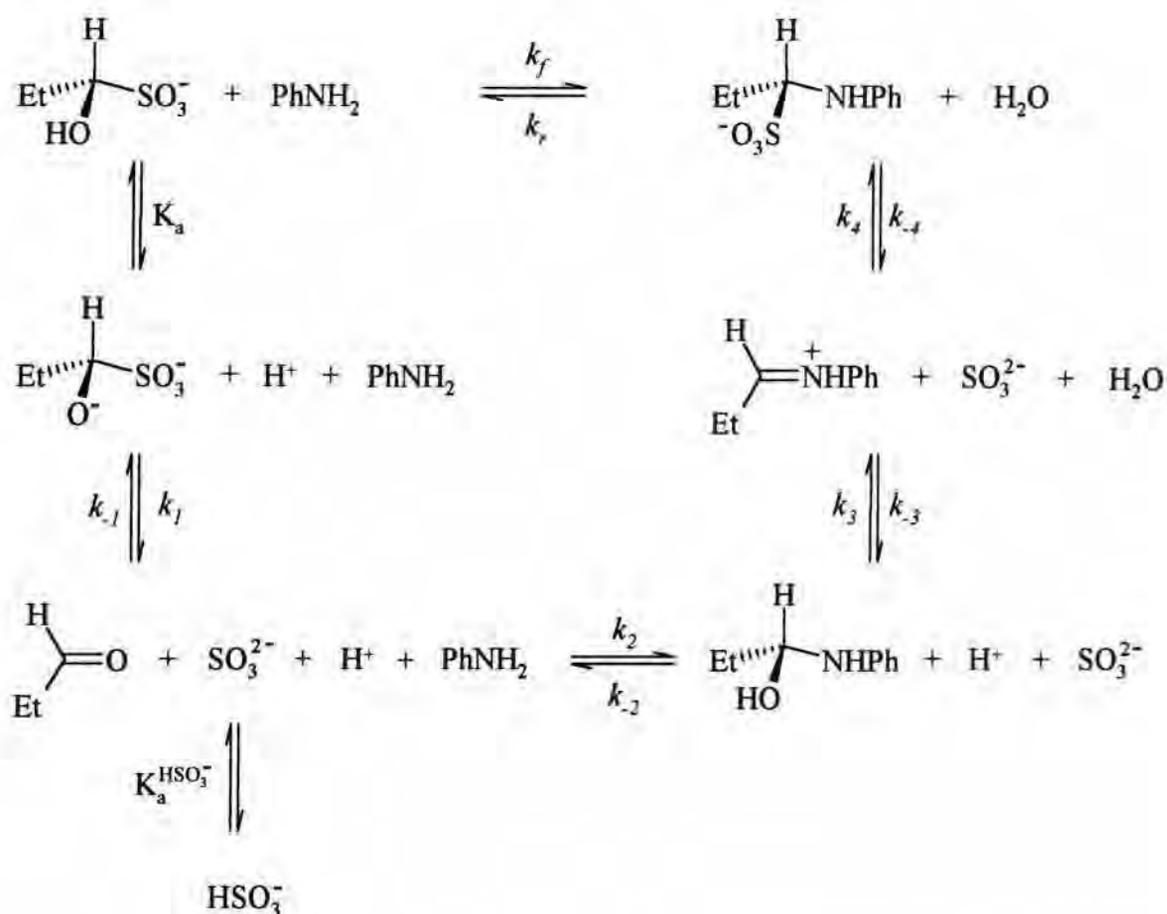
Experimentally, it was possible only to follow the overall interconversion of reactants and products, and thus, reaction intermediates were not observed. Since the process observed, is an equilibrium, the overall velocity is the difference between contributions for the forward and reverse reactions, as shown in equations 3.2 and 3.3
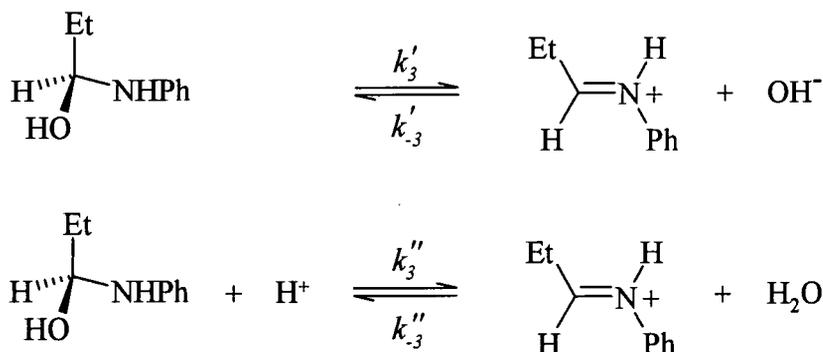
$$v = v_f - v_r \tag{3.2}$$

$$= k_f[\text{HPS}][\text{Aniline}] - k_r[\text{APS}] \tag{3.3}$$

Evidence was produced for the corresponding reaction of HMS, the formaldehyde equivalent, that the dehydration of the carbinolamine intermediate is likely to be rate limiting, in the

forward reaction[2]. The assumption that the rate determining step in the reaction of HPS is also dehydration, leads to scheme 3.4

Scheme 3.4:

$$
\underset{\substack{\text{HO}}}{\overset{\substack{\text{Et}}}{\text{H}''\!\!\diagup\!\!-\text{NHPh}}}
\underset{k'_{-3}}{\overset{k'_{3}}{\rightleftharpoons}}
\underset{\substack{\text{H} \quad \text{Ph}}}{\overset{\substack{\text{Et} \quad \text{H}}}{{=}\text{N}{+}}}
\;+\; \text{OH}^{-}
$$

$$
\underset{\substack{\text{HO}}}{\overset{\substack{\text{Et}}}{\text{H}''\!\!\diagup\!\!-\text{NHPh}}}
\;+\; \text{H}^{+}
\underset{k''_{-3}}{\overset{k''_{3}}{\rightleftharpoons}}
\underset{\substack{\text{H} \quad \text{Ph}}}{\overset{\substack{\text{Et} \quad \text{H}}}{{=}\text{N}{+}}}
\;+\; \text{H}_2\text{O}
$$

This shows the uncatalysed and acid catalysed routes. Since the reactions are reversible, it is possible to define an overall rate constant $k_3 + k_{-3}$ with a dependence on acidity, as shown in equations 3.4 and 3.5.

$$k_3 + k_{-3} = k'_3 + k''_3[\text{H}^+] + k''_{-3} + k'_{-3}[\text{OH}^-] \tag{3.4}$$

$$= k'_3 + k''_{-3} + k''_3[\text{H}^+] + \frac{k'_{-3}\,\text{K}_w}{[\text{H}^+]} \tag{3.5}$$

In terms of the forward reaction, equation 3.6 relates v_f to the rate constants k_3' and k_3''. The assumption is made that the carbinolamine, COH, is in rapid equilibrium with aniline and propanal, leading to equation 3.7.

$$v_f = (k'_3 + k''_3[\text{H}^+])[\text{COH}] \tag{3.6}$$

$$v_f = (k'_3 + k''_3[\text{H}^+])\text{K}_2[\text{Propanal}]_{free}[\text{Aniline}] \tag{3.7}$$

With knowledge of the dissociation equilibrium of HPS, the term for the free propanal concentration can be related to the HPS concentration, producing equations 3.8 and 3.9. At the pH values studied sulfite will exist in both mono- and di-anionic forms. Hence, it is convenient to formulate the expression in terms of the total sulfite concentration, $[SO_3^{2-}]_{stoich}$ and the dissociation constant K_a^{HSO3-}.

$$v_f \; = \; (k_3' + k_3''[H^+])K_2[\text{Aniline}]\left(\frac{K_aK_1[\text{HPS}]}{[SO_3^{2-}]_{\text{stoich}}}\right)\left(\frac{[H^+] + K_a^{HSO_3^-}}{[H^+]K_a^{HSO_3^-}}\right) \tag{3.8}$$

$$v_f \; = \; (k_3' + k_3''[H^+])K_1K_2K_a\left(\frac{[\text{HPS}][\text{Aniline}]}{[SO_3^{2-}]_{\text{stoich}}}\right)\left(\frac{[H^+] + K_a^{HSO_3^-}}{[H^+]K_a^{HSO_3^-}}\right) \tag{3.9}$$

As the above equation is still in terms of velocity, it may be combined with equation 3.3 to obtain an expression (equation 3.10) for k_f.

$$k_f[SO_3^{2-}]_{\text{stoich}} \; = \; (k_3' + k_3''[H^+])K_1K_2K_a\left(\frac{[H^+] + K_a^{HSO_3^-}}{[H^+]K_a^{HSO_3^-}}\right) \tag{3.10}$$

If the acid catalysed dehydration pathway is dominant, so that $k_3''[H^+] \gg k_3'$, then this reduces to equation 3.11.

$$k_f[SO_3^{2-}]_{\text{stoich}} \; = \; k_3''K_1K_2K_a\left(\frac{[H^+] + K_a^{HSO_3^-}}{K_a^{HSO_3^-}}\right) \tag{3.11}$$

The final expression for the forward reaction, involves the term for the acid dissociation of bisulfite[2, 5], which is known to be *ca.* 1×10^{-7} mol dm^{-3}, indicating, that either side of pH 7, the reaction will show different dependences on acidity. When the pH value is greater than 7, the acid dissociation term will outweight the proton concentration, so that the term within the brackets cancels, leaving equation 3.12, which would show an independence on acidity.

$$k_f [SO_3^{2-}]_{stoich} = k_3'' K_1 K_2 K_a \qquad (3.12)$$

However, when the pH value is lower than 7, the acid concentration will be greater than the acid dissociation value, resulting in equation 3.13, which would predict acid catalysis.

$$k_f [SO_3^{2-}]_{stoich} = k_3'' K_1 K_2 K_a \frac{[H^+]}{K_a^{HSO_3^-}} \qquad (3.13)$$

A theoretical plot of log $k_f[SO_3^{2-}]_{stoich}$ versus pH, taking account of these two expressions, would give two distinct areas to the graph. Equation 3.12, being independent of acidity, would show a plateau above pH 7, while below this value, the plot would be dependent on equation 3.13, and hence, increase linearly with acidity.

The above equations have concentrated on the forward reaction. However, related derivations can be attempted for the reverse reaction, to produce a final term for $k_r[SO_3^{2-}]_{stoich}$. The reverse reaction, as with the forward reaction, will involve the carbinolamine. However, instead of dehydration of the carbinolamine, it is the hydration of the iminium ion that is observed for the reverse process. The two reaction pathways shown for the forward reaction have to hold true for the overall reverse process, i.e. the addition of hydroxide ion or the addition of water. If the forward reaction requires acid catalysis, this implies that in the reverse reaction, addition of water dominates. For this reason, the velocity of the reverse reaction can be expressed in terms of addition of water to the iminium ion, as shown in equation 3.14, where [ImH$^+$], represents the concentration of the iminium ion.

$$v_r = k''_{-3}[\text{ImH}^+] = k_r[\text{APS}] \tag{3.14}$$

The expression for K_4, the process of addition of sulfite to the iminium ion, can be incorporated into equation 3.14. The k_4 process in the forward direction is expected to be much faster than the addition of water, since sulfite is a more powerful nucleophile. However, this will be discussed further, in a later chapter. The addition of the expression for K_4 enables the equation to be written in terms of the product, APS, concentration. This is possible since K_4 contains the term $[\text{ImH}^+]$ along with sulfite concentration and final product concentration, $[\text{APS}]$, as shown in equation 3.15, with the new expression in equation 3.16.

$$K_4 = \frac{[\text{APS}]}{[\text{ImH}^+][\text{SO}_3^{2-}]} \tag{3.15}$$

$$[\text{ImH}^+] = \frac{[\text{APS}]}{K_4}\left(\frac{[\text{H}^+] + K_a^{\text{HSO}_3^-}}{K_a^{\text{HSO}_3^-}}\right)\frac{1}{[\text{SO}_3^{2-}]_{\text{stoich}}} \tag{3.16}$$

Use of equation 3.14 followed by rearrangement, leads to equation 3.17.

$$k_r[\text{SO}_3^{2-}]_{\text{stoich}} = k''_{-3}\frac{1}{K_4}\left(\frac{[\text{H}^+] + K_a^{\text{HSO}_3^-}}{K_a^{\text{HSO}_3^-}}\right) \tag{3.17}$$

The expression again, contains the acid dissociation constant for sodium bisulfite, as in the equation for the forward reaction, (equation 3.11), suggesting that different acidity dependence will be observed above and below pH 7. Above pH 7, the reaction will be independent of acidity, as the term in brackets, becomes equal to ~1, thus, producing a plateau when plotting Log $k_r[\text{SO}_3^{2-}]_{\text{stoich}}$ versus pH (>7). In contrast, below pH 7, the bracketed term becomes acid dependent. In this region a plot of Log $k_r[\text{SO}_3^{2-}]_{\text{stoich}}$ versus pH (<7) would show a linear slope, with a gradient of one.

The overall expression for the equilibrium constant for the reaction, K, can now be derived via combination of the terms, derived for the forward and reverse processes, (equations 3.11 and 3.17) since, $K = k_f / k_r$. The overall expression can be seen in equation 3.19.

$$K = \frac{k_3'' K_1 K_2 K_a \left(\dfrac{[H^+] + K_a^{HSO_3^-}}{K_a^{HSO_3^-}} \right)}{k_{-3}'' \dfrac{1}{K_4} \left(\dfrac{[H^+] + K_a^{HSO_3^-}}{K_a^{HSO_3^-}} \right)}$$

(3.18)

$$K = \frac{k_3''}{k_{-3}''} K_1 K_2 K_a K_4$$

(3.19)

Since, in the pH region under study, none of the species HPS, aniline or APS, will be significantly ionised (either protonated or deprotonated) the value of K, as distinct from the values of k_f and k_r, is expected to be independent of acidity.

It should be noted that in scheme 3.3, K_1 is written as the dissociation of the dianionic form of HPS to give propanal and sulfite. The valued K_1, here, corresponds to $1/K_2$, as written in scheme 2.10 in chapter 2.

3.2.3: UV/Visible kinetic studies of the forward reaction

The reactions between HPS and aniline, as well as some aniline derivatives, were observed by UV/Vis spectroscopy. Firstly, absorbance versus wavelength scans, were obtained for the reacting system, and then compared to the parent amine spectrum, to observe any change. Secondly absorbance versus time plots at varying pH values, were acquired, once a suitable wavelength, showing the greatest absorbance change, was known. These absorbance versus

time plots were run with constant amine concentration, usually 1×10^{-4} mol dm^{-3}, and with varying HPS concentration, where the HPS concentration was always in at a least hundred fold excess. The results obtained showed first order kinetic behaviour and using absorbance data, it was possible to obtain values for the overall equilibrium constant, K, for each aniline.

Equations 3.9, 3.10, and 3.17, show that the observed rate constant will depend on the concentration of sulfite present. Hence, in order to interpret the kinetics, this value needs to be known. In the absence of added sulfite some will be produced through dissociation of HPS. However, this concentration will be small and uncertain. Therefore, measurements were made in the presence of added sulfite, so that the concentration was more accurately known.

Reactions were carried out with an amine concentration of 1×10^{-4} mol dm^{-3}and with HPS concentrations in the range 0.01 to 0.1 mol dm^{-3}. Sulfite was added, either in constant amounts, or as a fixed proportion of the HPS concentration and account was taken, where necessary, of the sulfite produced from dissociation of HPS. As predicted, values of rate constants decreased with increasing concentration of added sulfite. The ionic strength was maintained at 0.1 mol dm^{-3}, using sodium chloride as the added electrolyte.

Under these conditions, first order kinetics were observed and the value of k_{obs} is related to the forward and reverse rate constants by equation 3.20.

$$k_{obs}[SO_3^{2-}]_{\text{stoich}} \quad = \quad k_f[SO_3^{2-}]_{\text{stoich}}[HPS] \quad + \quad k_r[SO_3^{2-}]_{\text{stoich}} \tag{3.20}$$

Values were obtained in the pH range 4 – 10 and values of $k_f[SO_3^{2-}]_{\text{stoich}}$ and $k_r[SO_3^{2-}]_{\text{stoich}}$ versus acidity were plotted in logarithmic forms. For each plot, two fit lines were superimposed, one giving the best fit, treating K_a^{HSO3-} as a variable, and the other using a fixed value of 8.0×10^{-8} mol dm^{-3}, the value that is believed to be the true dissociation constant of hydrogen sulfite, at this ionic strength. Values of the equilibrium constant, K, were calculated, either using the ratio of the kinetic parameters, or by using absorbance values obtained at equilibrium.

Each aniline studied (table 3.3) will be discussed in turn and the results compared at the end.

3.2.3.1: Aniline

An initial absorbance versus wavelength scan was obtained for the reaction of 1×10^{-4} mol dm^{-3} aniline with HPS 0.01 to 0.1 mol dm^{-3} at 25 °C in aqueous solution. The spectrum of 1×10^{-4} mol dm^{-3} aniline alone was obtained for comparison. The spectra with aqueous HPS added, showed a shift to a higher wavelength, with a corresponding increase in absorbance, compared to the spectrum of aniline alone. The higher the concentration of aqueous HPS, the greater the change in spectrum observed. However, due to sulfite being strongly absorbing, the spectra can get swamped by the free sulfite absorption band 200 – *ca.* 240nm. All reactions are complete after 80 minutes. Figure 3.9 shows an example of this reaction at pH 8, along with a spectrum of aniline alone; table 3.18 shows peak positions and extinction coefficients (ε) for the two spectra.

Figure 3.9: Spectra of 1×10^{-4} mol dm^{-3} aniline alone, and for the reaction of 1×10^{-4} mol dm^{-3} aniline and 0.01 mol dm^{-3} HPS after 60 minutes, 25 °C, pH 8 aqueous buffer solution
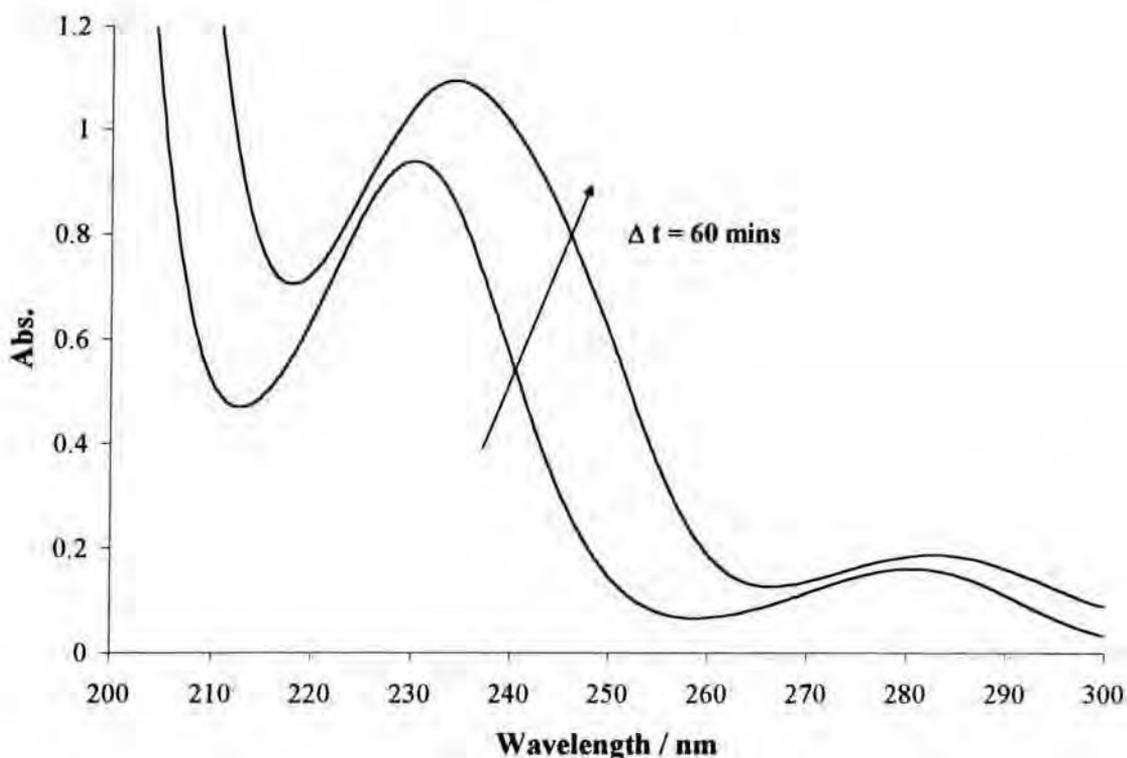
Table 3.18: Spectral appearance in aqueous solution of 1×10^{-4} mol dm^{-3} aniline and the final spectrum in the presence of 0.01 mol dm^{-3} HPS

HPS / mol dm^{-3}	λ_{max} / nm ($\varepsilon^{\dagger}$ / mol^{-1} dm^{3} cm^{-1})
none	230 (9400); 280 (1600)
0.01	234 (10900); 282 (1870)

† *Based on the assumption that all the aniline reacts to give 1×10^{-4} mol dm^{-3} product*

The above spectra were used to determine a suitable wavelength where the greatest change of absorbance occurred; the selected wavelength was 250nm. This wavelength was used when observing absorbance versus time plots.

143

Plots of absorbance against time were obtained for the reaction of 1×10^{-4} mol dm^{-3} aniline with HPS, 0.005 to 0.1 mol dm^{-3}, over a pH range 4 to 10 at 25 °C. Formation, as stated, was followed at 250nm. k_{obs} / s^{-1} values were obtained from first order fits of the plots of absorbance, versus time for each reaction. From these data, it was possible to calculate the values for $k_{obs}[SO_3^{2-}]_{stoich}$ which were plotted against HPS concentration, in order to get values for the forward and reverse reactions, in terms of total sulfite concentration, and hence, an equilibrium constant. Overall equilibrium constants were calculated from the absorbance data. These values, should in theory, be constant, since they are unaffected by acidity

As stated, reactions were conducted using a wide range of pH values. However, the reaction at pH 7.6 will be used as an example. Figure 3.10 shows the spectral plots at this pH value. Table 3.19 shows the concentrations of reactants with observed rate constants (both in terms of sulfite and independent of sulfite), along with the overall equilibrium constant for the reaction, calculated from the absorbance changes. The equilibrium constant is calculated by equation 3.21, where the overall change of absorbance is divided by a term containing, ΔAbs_{inf}, which is the change in absorbance calculated for complete reaction, and by the HPS concentration.

$$K = \frac{\Delta Abs}{(\Delta Abs_{inf} - \Delta Abs)[HPS]}$$

(3.21)

144

Figure 3.10: Plots of the reactions between HPS 0.005 to 0.05 mol dm^{-3} with 1x10^{-4} mol dm^{-3} aniline along with added sodium bisulfite, at pH 7.6, at 25 °C
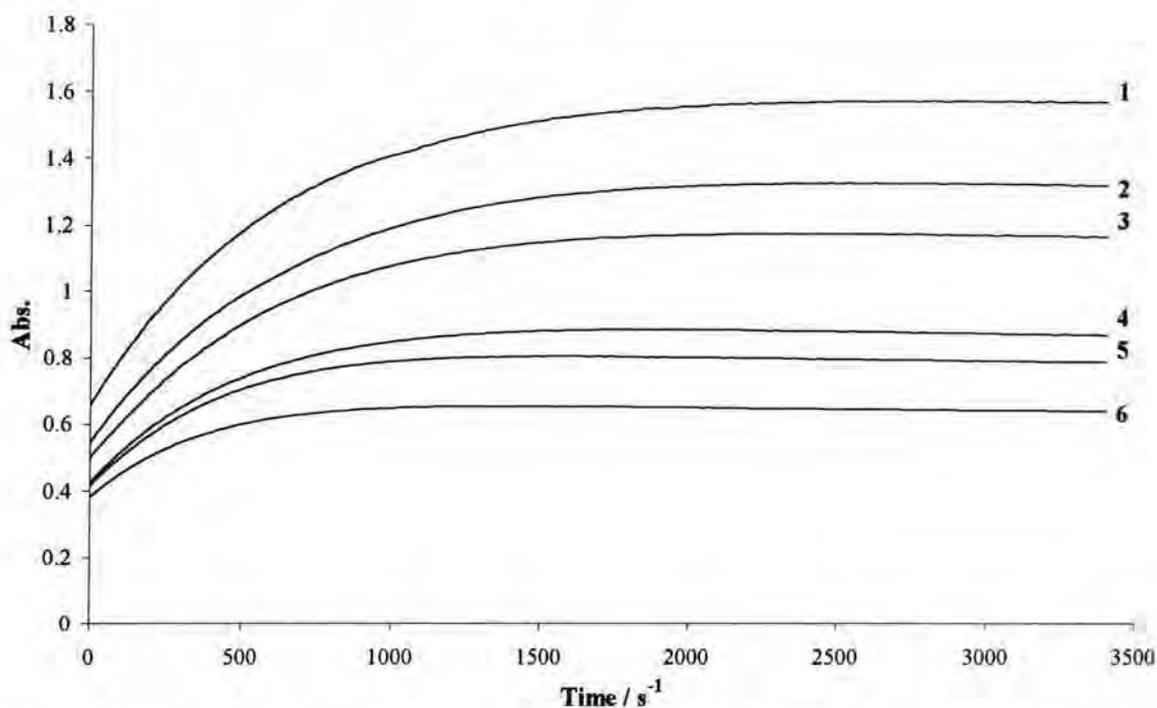
1 = 0.044 mol dm^{-3} HPS; 2 = 0.027 mol dm^{-3}; 3 = 0.017 mol dm^{-3}; 4 = 0.0080 mol dm^{-3}; 5 = 0.0063 mol dm^{-3}; 6 = 0.0039 mol dm^{-3}. HPS shows some absorbance at 250nm.

Table 3.19: Kinetic data obtained from the spectral plots for the reaction of HPS (varying concentrations) and 1x10^{-4} mol dm^{-3} aniline with added sodium sulfite and an aqueous pH 7.6 buffer, 25 °C, ΔAbs_{inf} = 1.25

[HPS] / mol dm^{-3}	[SO$_3^{2-}$] / mol dm^{-3}	k_{obs} / 10^{-3} s^{-1}	k_{obs}[SO$_3^{2-}$]$_{stoich}$ / 10^{-6} mol dm^{-3} s^{-1}	ΔAbs	K / dm^3 mol^{-1}
0.0039	0.0022	1.48	3.18	0.286	77.1
0.0063	0.0027	1.22	3.27	0.412	78.0
0.0080	0.0030	1.12	3.42	0.481	78.2
0.0170	0.0044	1.09	4.89	0.709	77.1
0.0260	0.0054	1.12	6.06	0.811	71.0
0.0440	0.0065	1.30	8.46	0.933	67.7

The plot of $k_{obs}[SO_3^{2-}]_{stoich}$ versus HPS concentration using the data in table 3.19, is shown in figure 3.11. The gradient of the slope is equal to the term $k_f[SO_3^{2-}]_{stoich}$, and the intercept equal to $k_r[SO_3^{2-}]_{stoich}$. The linear correlation coefficient for these plots for aniline gave values of 0.985 to 0.999.

Figure 3.11: A plot of calculated values of $k_{obs}[SO_3^{2-}]_{stoich}$ / mol dm^{-3} s^{-1} versus HPS / mol dm^{-3} for the reaction of HPS and aniline 1×10^{-4} mol dm^{-3} with an aqueous pH 7.6 buffer, 25 °C
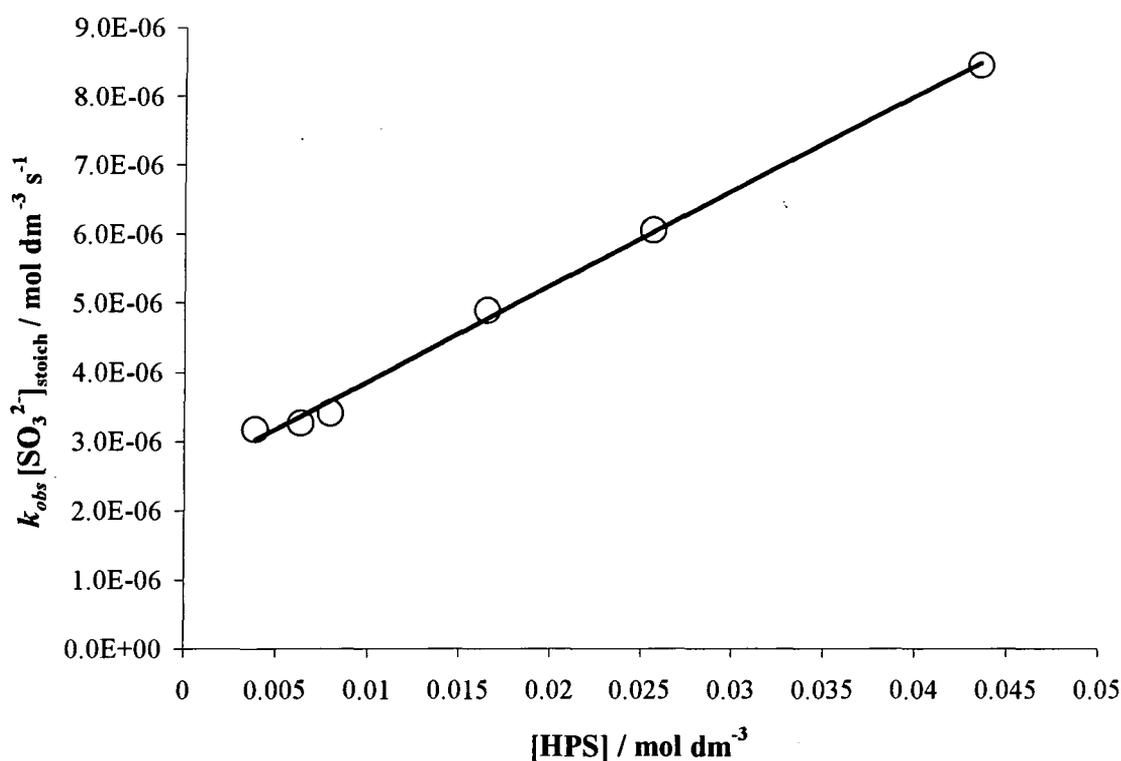
The gradient of this plot, which is equal to the value of $k_f[SO_3^{2-}]_{stoich}$, was 1.85×10^{-4} s^{-1}. The intercept being equal to $k_r[SO_3^{2-}]_{stoich}$, was, at this pH, 2.20×10^{-6} mol dm^{-3} s^{-1}. This gave an equilibrium constant at this pH, of 84 mol dm^{-3} in reasonable agreement with values obtained from absorbance data. Other calculated values for both expressions at various pH values, are shown in table 3.20, with the corresponding plots against acidity in figure 3.12 and 3.13. The plots shown do follow the predicted trends; acid catalysis below pH 7 shown by the values increasing with acidity, and acid independence above pH 7 shown by the plateau. Values

calculated for $k_f[SO_3^{2-}]_{stoich}$ and $k_r[SO_3^{2-}]_{stoich}$ are subject to some experimental error, as they depend markedly on the concentration of sulfite.

Table 3.20: Variation with pH of calculated values of rate and equilibrium constants for reaction of aniline and HPS

pH	$k_f[SO_3^{2-}]_{stoich}$ / 10^{-4} s^{-1}	$k_r[SO_3^{2-}]_{stoich}$ / 10^{-6} mol dm^{-3} s^{-1}	K (kinetic) / dm^3 mol^{-1}	K (Abs.) / dm^3 mol^{-1}
5.2	14.0	18.0	77	60
5.9	3.70	4.70	78	52
7.0	1.85	2.20	84	76
7.6	1.37	2.50	55	76
8.0	1.90	2.30	84	71
9.1	0.74	1.00	74	68
10.0	0.88	1.20	73	70

The plots versus pH are shown in figures 3.12, for the forward reaction, and 3.13, for the reverse. Both plots have two theoretical fits superimposed; each plot is fitted by the respective derived equation, either for forward (equation 3.11) or reverse (equation 3.17) rates. However, for the forward reaction k_3'', K_1, K_2 and K_a and similarly k_{-3}'' and $1/K_4$ for the reverse reaction, cannot be separated from each other when obtaining values from the fits. The two fitted plots differ in the value used for the acid dissociation constant of sodium bisulfite. The dashed fit line represented, is the data best fit, where values of 5.59×10^{-7} mol dm^{-3} and 6.21×10^{-7} mol dm^{-3} are used for K_a^{HSO3-} in the forward and reverse reactions, respectively. The value obtained for $k_3''.K_1.K_2.K_a$ was 1.41×10^{-4} s^{-1} and for k_{-3}''/K_4 was 4.95×10^{-6} mol dm^{-3} s^{-1}. The full lines represent the fits when K_a^{HSO3-} is kept constant at 8.0×10^{-8} mol dm^{-3}. The value obtained for $k_3''.K_1.K_2.K_a$ was 1.16×10^{-4} s^{-1} and for k_{-3}''/K_4 in the same conditions was 1.59×10^{-6} mol dm^{-3} s^{-1}.

Figure 3.12: A plot of $k_f[SO_3^{2-}]_{stoich}$ versus pH for the reaction of aniline and HPS with added sodium bisulfite.
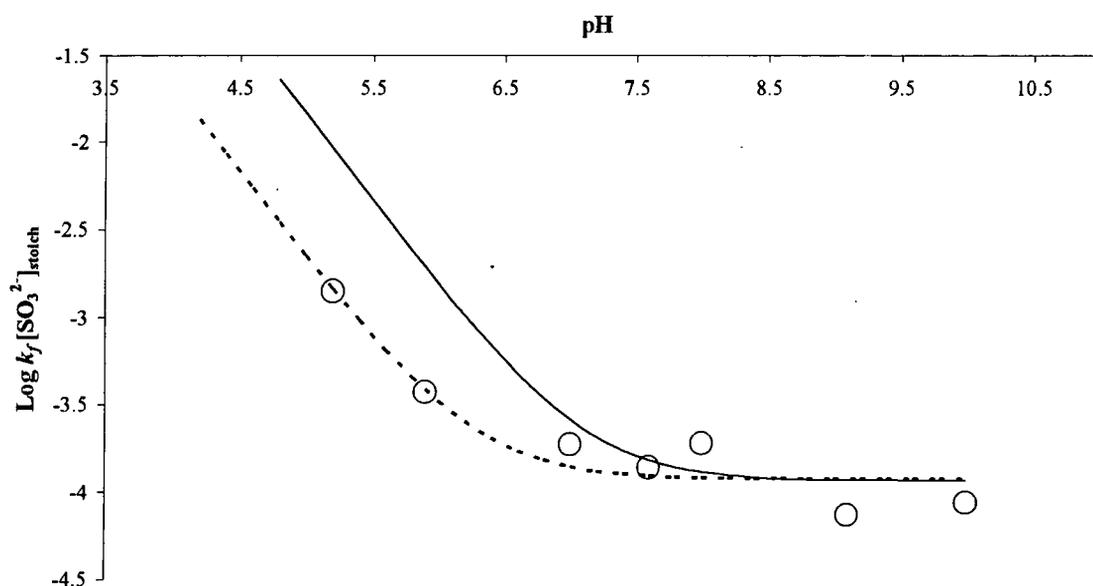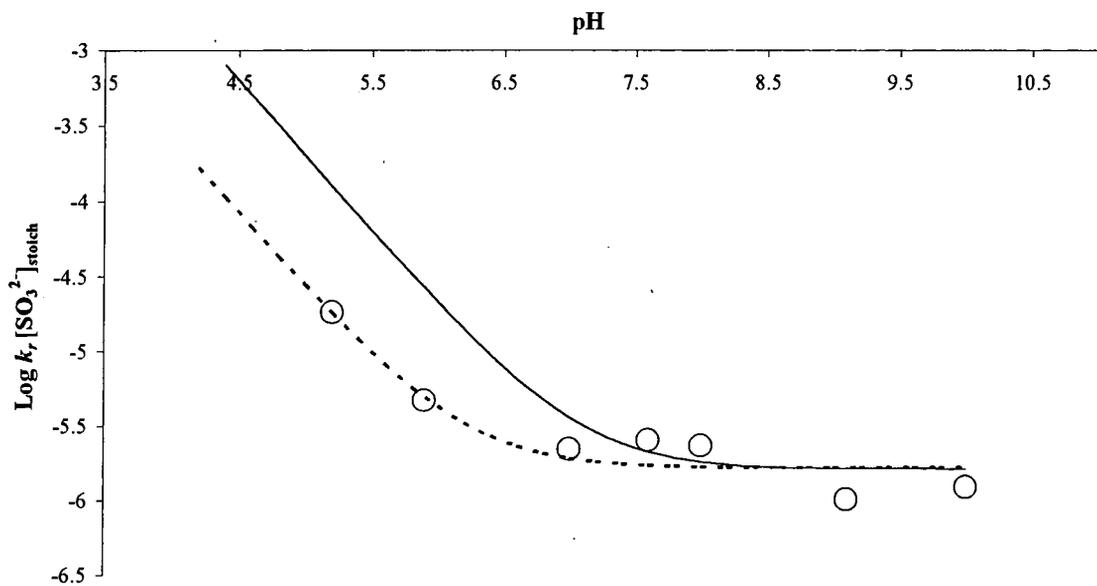

Figure 3.13: A plot of $k_r[SO_3^{2-}]_{stoich}$ versus pH for the reaction of aniline and HPS with added sodium bisulfite.

The plots shown above are consistent with each other, in that both show an independence to acidity above pH 7, and show some sort of increase when acidity increases. However, both do not agree fully with their respective equations, in that the best fits are obtained with

unrealistically high values for the dissociation constant of bisulfite. The reasons for this will be considered in the discussion at the end of chapter 4.

The addition of sulfite ions to the system as stated retards the reaction and hence alters, the k_{obs} values obtained. To avoid this complication, the term $k_{obs}[SO_3^{2-}]_{stoich}$ is derived, to show that the value of this term is independent of the added sulfite measurements were made, where the concentration of HPS and aniline were kept constant, but the concentration of sulfite was varied. The example shown in table 3.21 is at pH 7; two sets of data were obtained, where HPS was either 0.008 mol dm^{-3} or 0.044 mol dm^{-3}, aniline was a constant 1×10^{-4} mol dm^{-3} and sodium bisulfite was varied. Values for both k_{obs} (independent of bisulfite) and $k_{obs}[SO_3^{2-}]_{stoich}$ were calculated. The concentrations of bisulfite in table 3.21 include an estimation for the concentration of sulfite liberated from HPS.

Table 3.21: Values for the observed rate constants (dependent and independent of bisulfite) for the reaction of HPS 0.008 or 0.044 mol dm^{-3} with aniline 1×10^{-4} mol dm^{-3} and varying concentrations of sodium bisulfite, at pH 7, 25 °C

[HPS] / mol dm^{-3}	[HSO$_3^-$] / mol dm^{-3}	k_{obs} / $\times 10^{-3}$ s^{-1}	$k_{obs}[SO_3^{2-}]_{stoich}$ / 10^{-6} mol dm^{-3} s^{-1}	ΔAbs
0.008	0.002	2.11	4.22	0.704
	0.003	1.40	4.20	0.726
	0.004	1.16	4.64	0.720
	0.005	0.89	4.45	0.729
	0.006	0.75	4.52	0.729
	0.007	0.69	4.82	0.673
0.044	0.006	2.67	16.02	1.025
	0.007	2.32	16.24	1.047
	0.008	2.10	16.78	1.042
	0.009	1.91	17.16	1.078
	0.010	1.75	17.50	1.085
	0.011	1.60	17.59	1.135

The results clearly show, that although values of k_{obs} vary, the value of $k_{obs}[SO_3^{2-}]_{stoich}$ are constant at a given concentration of HPS. This justifies the treatment of the data in this section.

3.2.3.2: 4-Methylaniline

An initial scan of absorbance against wavelength was obtained for the reaction of 1×10^{-4} mol dm^{-3} 4-methylaniline with HPS, 0.01 to 0.1 mol dm^{-3}, at 25 °C in aqueous solution. The spectrum of 1×10^{-4} mol dm^{-3} 4-methylaniline alone was obtained for comparison. As with aniline, an increase in absorption, with a shift to longer wavelength, was observed when 4-methylaniline reacted with HPS. However, there was some interference from the HPS absorption. The trend of increasing absorption, with increasing HPS concentration, was obeyed as well. All reactions were over within 30 minutes, much faster than aniline, which might be expected, due to the electron donating para-methyl group. Figure 3.14 shows an example of this reaction with a spectrum of 4-methylaniline alone; table 3.22 shows peak positions and extinction coefficients (ε) for the two spectra.

Figure 3.14: Spectrum of 1×10^{-4} mol dm^{-3} 4-methylaniline alone, and the spectrum for the reaction of 1×10^{-4} mol dm^{-3} 4-methylaniline and 0.01 mol dm^{-3} HPS after 30 minutes, 25 °C, aqueous solution
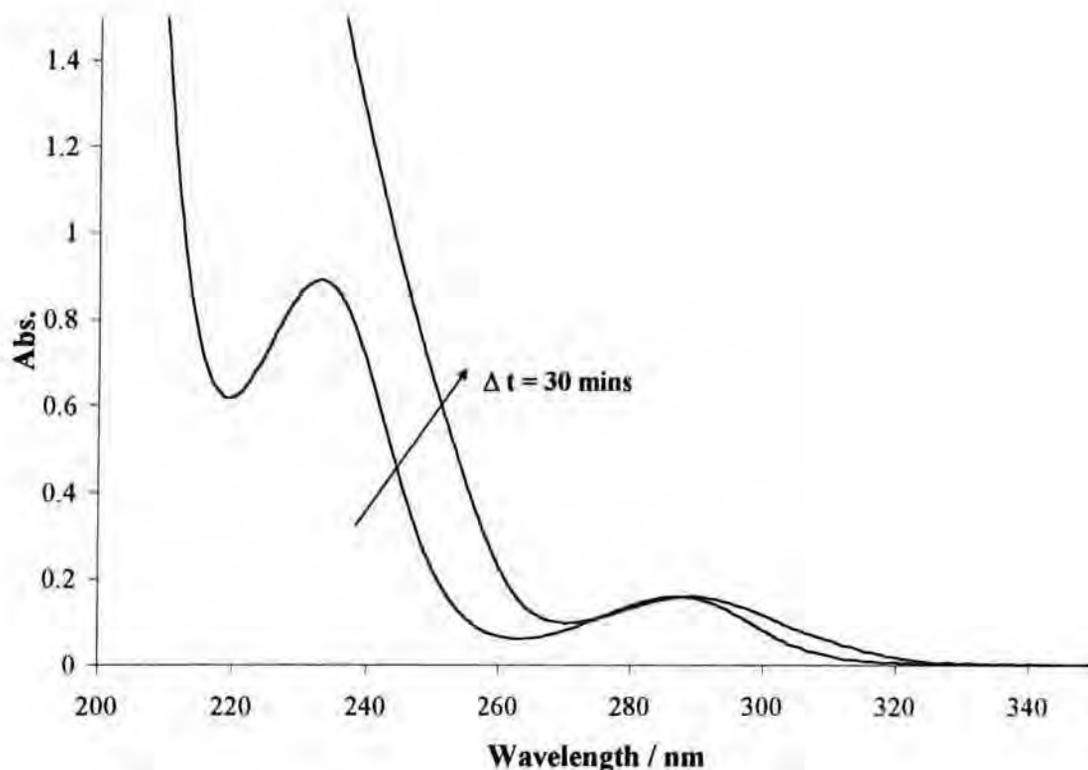
Table 3.22: Spectral appearance in aqueous solution of 1×10^{-4} mol dm^{-3} 4-methylaniline and the final spectrum in the presence of 0.01 mol dm^{-3} HPS

HPS / mol dm^{-3}	λ_{max} / nm ($\varepsilon^{\dagger}$ / mol^{-1} dm^{3} cm^{-1})
none	232 (8860); 287 (1600)
0.01	287 (1600)

† *Based on the assumption that all the aniline reacts to give 1×10^{-4} mol dm^{-3} product*

Plots of absorbance versus time were obtained for the reaction of 4-methylaniline 1×10^{-4} mol dm^{-3} with HPS 0.01 to 0.1 mol dm^{-3} in the pH range of 4.7 to 10. The wavelength used for observations was 255nm. Observed rate constants were obtained from the first order fits,

which enabled the observed rate constants, in terms of the total sulfite concentration to be calculated. Figure 3.15 shows the absorbance versus times plots for these reactions at pH 8; calculated rate constants with values for the overall equilibrium constant, K, are shown in table 3.23.

Figure 3.15: Spectral plots of the reactions between HPS 0.01 to 0.1 mol dm^{-3} with 1x10^{-4} mol dm^{-3} 4-methylaniline along with added sodium bisulfite, at pH 8, at 25 °C
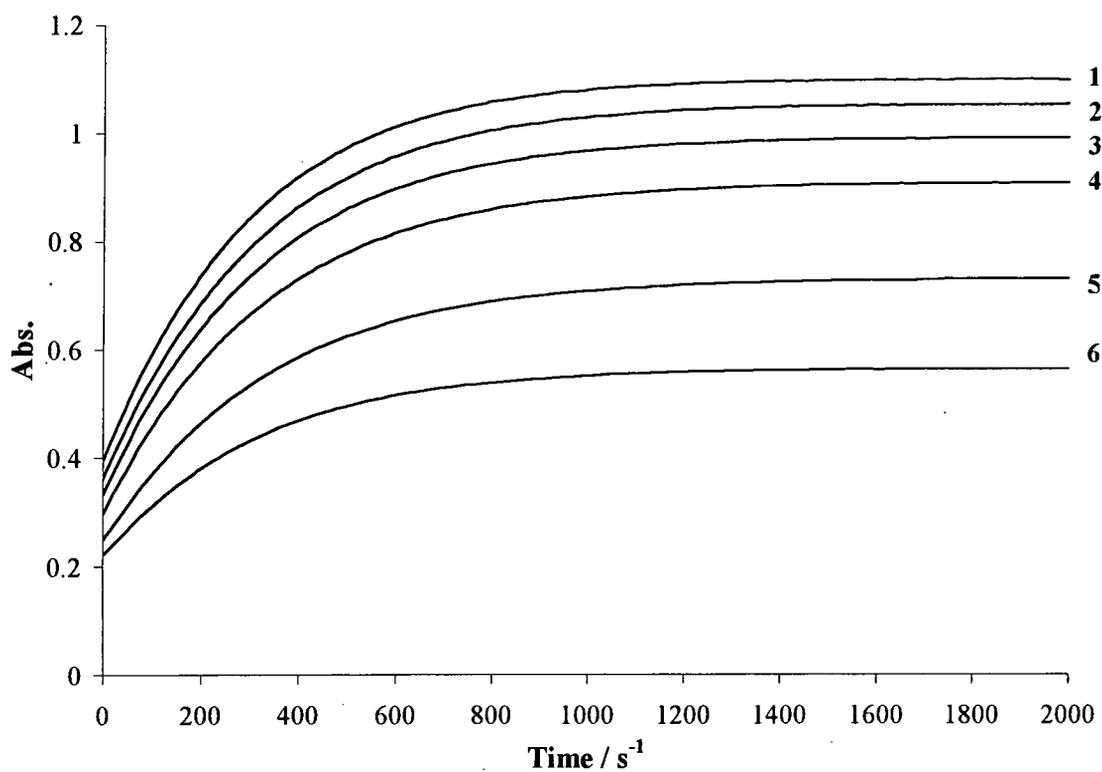
1 = 0.09 mol dm^{-3} HPS; 2 = 0.071 mol dm^{-3}; 3 = 0.053 mol dm^{-3}; 4 = 0.034 mol dm^{-3}; 5 = 0.017 mol dm^{-3}; 6 = 0.008 mol dm^{-3}

Table 3.23: Kinetic data obtained from the spectral plots for the reaction of HPS (varying concentrations) and 1×10^{-4} mol dm^{-3} 4-methylaniline with added sodium sulfite and an aqueous pH 8 buffer, 25 °C, $\Delta Abs_{inf} = 1.00$

[HPS] / mol dm^{-3}	[SO$_3^{2-}$] / mol dm^{-3}	k_{obs} / 10^{-3} s^{-1}	k_{obs}[SO$_3^{2-}$]$_{stoich}$ / 10^{-6} mol dm^{-3} s^{-1}	ΔAbs	K / dm^{3} mol^{-1}
0.008	0.003	3.26	9.79	0.342	65
0.017	0.004	3.07	12.3	0.509	61
0.034	0.007	3.19	22.3	0.683	63
0.053	0.008	3.31	26.5	0.764	61
0.071	0.010	3.37	33.7	0.823	65
0.090	0.011	3.44	37.8	0.866	72

Figure 3.16: A plot of values of k_{obs}[SO$_3^{2-}$]$_{stoich}$ / mol dm^{-3} s^{-1} versus [HPS] /mol dm^{-3} for the reaction of HPS and 4-methylaniline 1×10^{-4} mol dm^{-3} in an aqueous pH 8 buffer, 25 °C
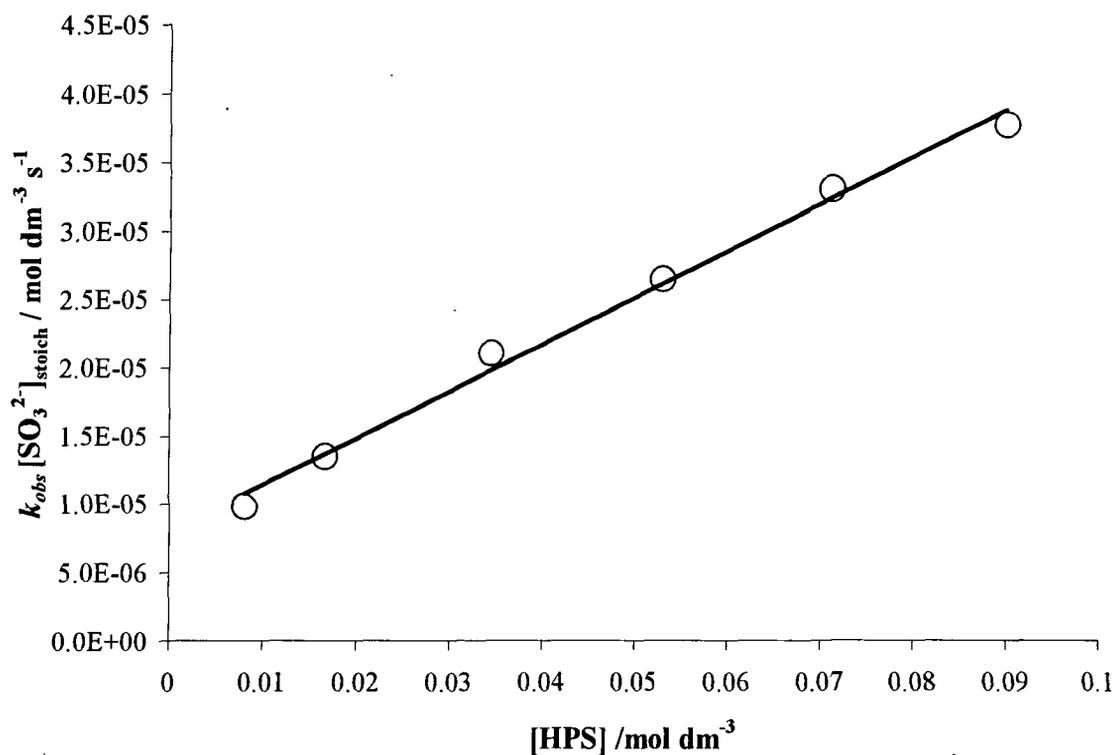
From this plot, the gradient and intercept, being equal to the rate terms for the forward and reverse reactions, were calculated as 3.43×10^{-4} s^{-1} and 7.0×10^{-6} mol dm^{-3} s^{-1} respectively. This yields an overall equilibrium constant of 49 dm^3 mol^{-1}, which is lower than that calculated from the absorbance data. Table 3.24 shows other values for $k_f[SO_3^{2-}]_{stoich}$ and $k_r[SO_3^{2-}]_{stoich}$ along with equilibrium constants, calculated at various pH values. Other data obtained at pH 8 in table 3.25, yield 'best' values for the forward and reverse reactions of $3.6 \pm 0.3 \times 10^{-4}$ s^{-1} and $(6.0 \pm 1.0) \times 10^{-6}$ mol dm^{-3} s^{-1} respectively.

Table 3.24: Summary of rate and equilibrium constants for the reaction of 4-methylaniline with HPS, over the pH range 4.7 to 10.0

pH		$k_f[SO_3^{2-}]_{stoich} / 10^{-4}$ s^{-1}	$k_r[SO_3^{2-}]_{stoich} / 10^{-6}$ mol dm^{-3} s^{-1}	K (kinetic) / dm^3 mol^{-1}	K (Abs.) / dm^3 mol^{-1}
4.7	1	5.80 (20.0)	41.6	(48)	26
5.8	1	8.96	22.3	40	58
	2	9.39	24.7	38	65
8.0	1	3.62	5.61	65	61
	2	3.46	7.00	49	65
9.2	1	1.84	2.73	67	65
10.0	1	1.41	2.77	51	51

[1] *sulfite added was a constant 1×10^{-3} mol dm^{-3}*; [2] *sulfite added was 10% of [HPS]*

The values in table 3.24 are in general accord with equations 3.11 and 3.17, in that values of the rate parameter decrease with increasing pH, and then level off at higher pH.

It should be noted, that since the pK$_a$ of 4-methylaniline is 5.08, there will be considerable protonation at pH = 4.7. The relation between the free and stoichiometric amine concentrations is shown in equation 3.22.

$$[amine]_{free} = [amine]_{stoich} \frac{K_a}{K_a + [H^+]}$$

$$(3.22)$$

At pH 4.7, [amine]$_{free}$ = [amine]$_{stoich}$ x 0.29. Making this correction in table 3.24, would give values at pH 4.7 of k_f[SO$_3^{2-}$]$_{stoich}$ = 20.0x10^{-4} s^{-1} and hence, K (kinetic) = 48 dm^3 mol^{-1}.

Logarithmic plots of rate parameters versus pH are shown in figures 3.17 and 3.18. The dashed lines are best fits to equation 3.11 and 3.17, allowing K$_a^{HSO3-}$ to be a variable. Values obtained are k_3''.K$_1$.K$_2$.K$_a$ = 2.4x10^{-4} s^{-1} and K$_a^{HSO3-}$ = 1.98x10^{-6} mol dm^{-3}; and k_{-3}''/K$_4$ = 3.5x10^{-6} mol dm^{-3} s^{-1} with K$_a^{HSO3-}$ = 3.1x10^{-7} mol dm^{-3}. With K$_a^{HSO3-}$ fixed at 8.0x10^{-8} mol dm^{-3}, the full lines are obtained, giving k_3''.K$_1$.K$_2$.K$_a$ = 2.0x10^{-4} s^{-1} and k_{-3}''/K$_4$ = 3.45x10^{-6} mol dm^{-3} s^{-1}.

Figure 3.17: A plot of k_f[SO$_3^{2-}$]$_{stoich}$ versus pH for the reaction of 4-methylaniline and HPS with added sodium bisulfite. k_3''.K$_1$.K$_2$.K$_a$ = 2.0x10^{-4} s^{-1} with K$_a^{HSO3-}$ 8.0x10^{-8} mol dm^{-3}
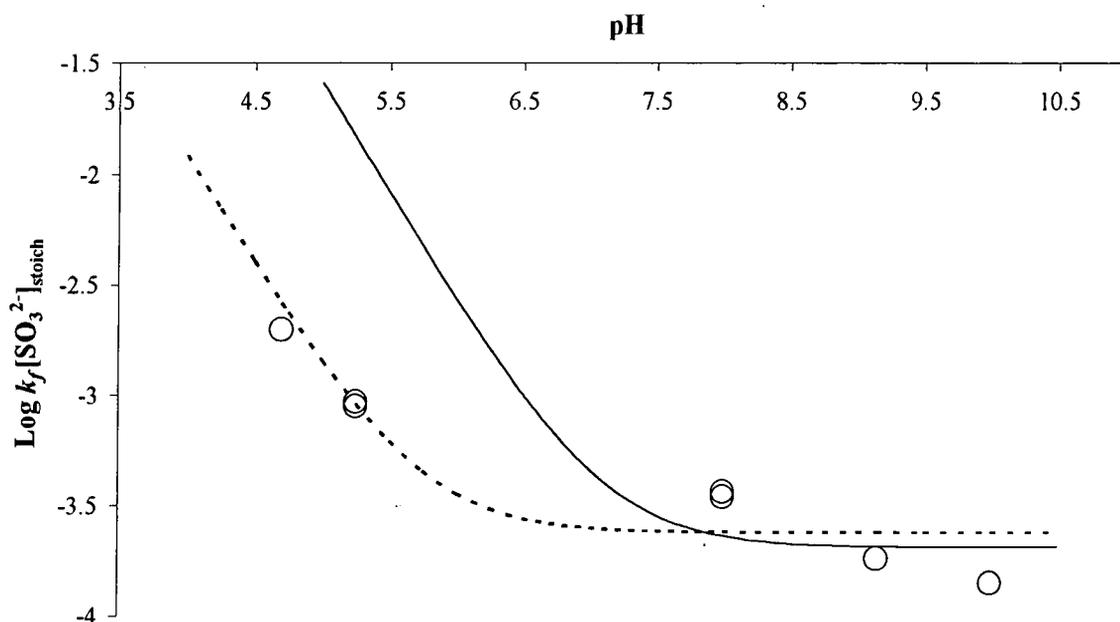
Figure 3.18: A plot of $k_r[SO_3^{2-}]_{stoich}$ versus pH for the reaction of 4-methylaniline and HPS with added sodium bisulfite. $k_{-3}{''}/K_4 = 3.45 \times 10^{-6}$ mol dm^{-3} s^{-1} and K_a^{HSO3-} 8.0×10^{-8} mol dm^{-3}
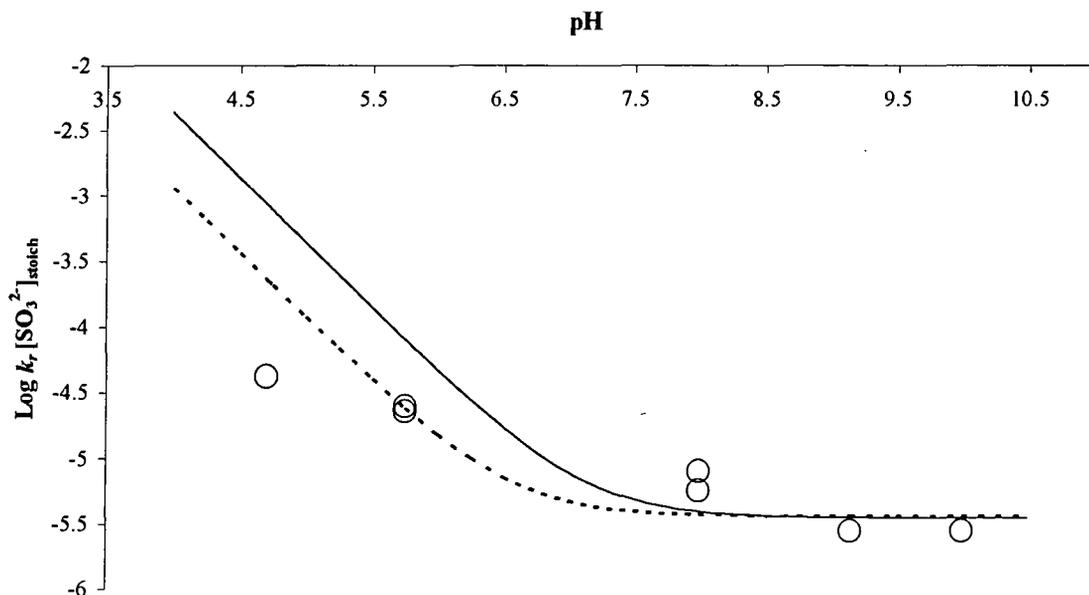
The results in table 3.25, indicate that the value of the parameter $k_{obs}[SO_3^{2-}]_{stoich}$ is independent of the concentration of added sulfite.

Table 3.25: Values for the observed rate constants (in the presence of added bisulfite) for the reaction of HPS 0.01 to 0.1 mol dm^{-3} with 4-methylaniline 1×10^{-4} mol dm^{-3}, at pH 8, 25 °C

[HPS] / mol dm^{-3}	[SO$_3^{2-}$] / mol dm^{-3}	k_{obs} / x10^{-3} s^{-1}	k_{obs}[SO$_3^{2-}$]$_{stoich}$ / 10^{-6} mol dm^{-3} s^{-1}	ΔAbs
0.008	0.003	3.26	9.79	0.347
0.008	0.003	2.59	7.77	0.359
0.017	0.004	3.07	12.3	0.487
0.017	0.005	2.22	12.0	0.504
0.034	0.007	3.19	22.3	0.615
0.034	0.010	1.89	18.9	0.642
0.053	0.008	3.31	26.5	0.666
0.053	0.013	1.85	24.1	0.700
0.071	0.01	3.37	33.7	0.699
0.071	0.017	1.86	31.2	0.734
0.090	0.011	3.44	37.8	0.713
0.090	0.02	1.91	38.3	0.746

3.2.3.3: 4-Chloroaniline

The initial spectrum of 4-chloroaniline was compared with the spectral scans for the reaction between 1×10^{-4} mol dm^{-3} 4-chloroaniline with 0.01 mol dm^{-3} HPS, in an aqueous solution at 25 °C. Figure 3.19 shows 4-chloroaniline alone and then combined with HPS, after reaction for 80 minutes. Table 3.26 shows the λ_{max} values, along with the extinction coefficients of the peaks concerned.

Figure 3.19: Spectra of 1×10^{-4} mol dm^{-3} 4-chloroaniline alone, and for the reaction of 1×10^{-4} mol dm^{-3} 4-chloroaniline and 0.01 mol dm^{-3} HPS after 80 minutes, 25 °C, aqueous solution
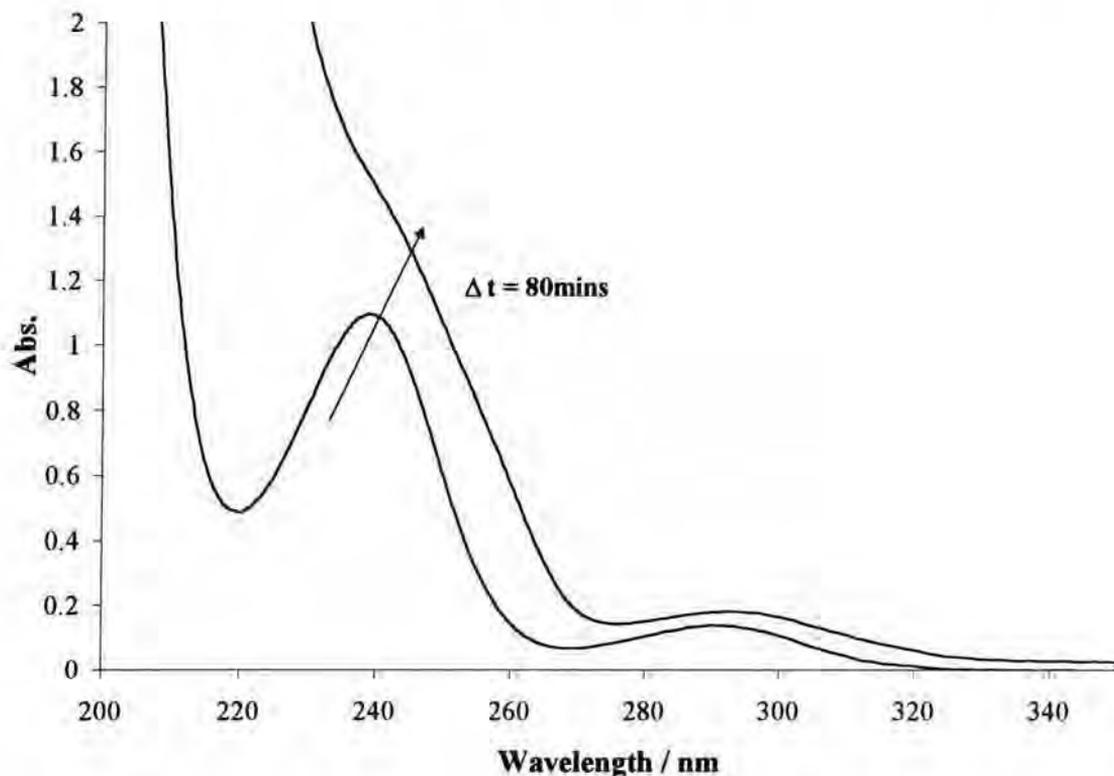
Table 3.26: Spectral appearance in aqueous solution of 1×10^{-4} mol dm^{-3} 4-chloroaniline and the final spectrum in the presence of 0.01 mol dm^{-3} HPS

HPS / mol dm^{-3}	λ_{max} / nm ($\varepsilon^{\dagger}$ / mol^{-1} dm^3 cm^{-1})
none	238 (10900); 290 (1400)
0.01	(~241 (14400)*); 293 (1810)

† *Based on the assumption that all the aniline reacts to give 1×10^{-4} mol dm^{-3} product*

* *Assumption of λ_{max} and ε since interference from HPS*

As can be seen, on reaction with HPS the peak at 240nm intensifies with a shift to longer wavelength, and this is heightened even further, when the HPS concentration is increased. Reactions were all complete after 80 minutes, when no changes in spectral scans were

observed. The greatest increase in absorbance occurred at 255nm, and hence, this wavelength was used to observe the reaction. The reaction between HPS 0.01 to 0.1 mol dm^{-3} with 4-chloroaniline 1x10^{-4} mol dm^{-3} and varying amounts of sodium sulfite, were observed over the pH range 4.7 to 9, and the reaction at pH 8, is shown in figure 3.20.

Figure 3.20: Spectral plots of the reactions between HPS 0.01 to 0.1 mol dm^{-3} with 1x10^{-4} mol dm^{-3} 4-chloroaniline along with added sodium bisulfite, at pH 8, at 25 °C
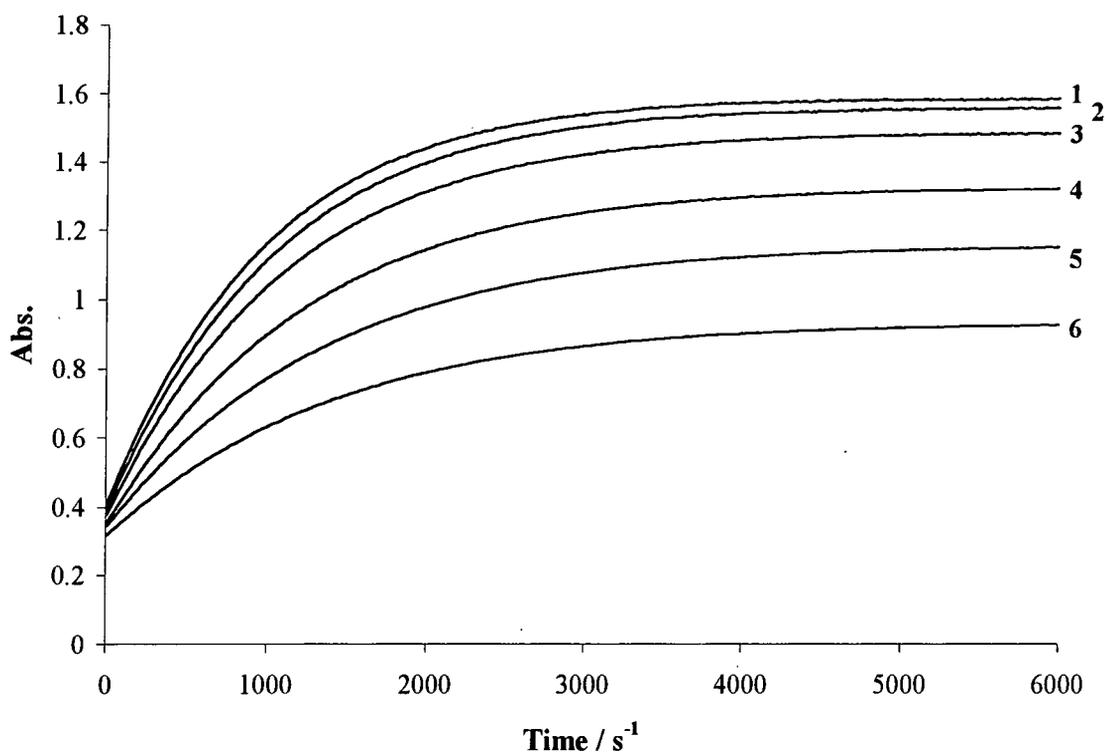
1 = 0.09 mol dm^{-3} HPS; 2 = 0.071 mol dm^{-3}; 3 = 0.053 mol dm^{-3}; 4 = 0.034 mol dm^{-3}; 5 = 0.017 mol dm^{-3}; 6 = 0.008 mol dm^{-3}

Values for the observed rate constants for this reaction, and at all other pH values, were obtained from the first order fits of the plots. The same estimations of liberated sulfite concentrations were used in order to produce values for the observed rate of reaction, in terms of total sulfite concentration. The values calculated for the pH 8 reaction, along with equilibrium constants calculated from absorbances and equation 3.20, are shown in table 3.27.

Table 3.27: Kinetic and equilibrium data for the reaction of HPS (various concentrations) and 1×10^{-4} mol dm^{-3} 4-chloroaniline with added sodium sulfite in an aqueous pH 8 buffer, 25 °C, $\Delta Abs_{inf} = 1.375$

[HPS] / mol dm^{-3}	[SO$_3$$^{2-}$] / mol dm^{-3}	k_{obs} / 10^{-4} s^{-1}	k_{obs}[SO$_3$$^{2-}$]$_{stoich}$ / 10^{-6} mol dm^{-3} s^{-1}	ΔAbs	K / dm^3 mol^{-1}
0.008	0.003	7.30	2.19	0.623	103
0.017	0.004	7.66	3.37	0.825	88
0.034	0.007	8.48	5.43	0.988	75
0.053	0.008	9.27	7.44	1.129	86
0.071	0.010	9.87	9.67	1.188	89
0.090	0.011	10.49	11.54	1.198	75

Values calculated for the overall equilibrium constant give an average value for K, as 83. Values calculated for the observed rate constants, in terms of total sulfite concentration, were plotted against pH to obtain values for the respective forward and reverse rates. Figure 3.21 shows this particular plot for the reaction at pH 8.

k_f[SO$_3$$^{2-}$]$_{stoich}$ equal to the gradient, was given as 1.14×10^{-4} s^{-1} and k_r[SO$_3$$^{2-}$]$_{stoich}$ equal to the intercept, was obtained as 1.41×10^{-6} mol dm^{-3} s^{-1}. These values therefore, give the overall equilibrium constant for the reaction at pH 8, of 81 mol dm^{-3} (since K = k_f / k_r), which is in fair agreement with the values calculated from the absorbance data. Values for all these constants are shown in table 3.28.

Figure 3.21: A plot of values of $k_{obs}[SO_3^{2-}]_{stoich}$ / mol dm^{-3} s^{-1} versus [HPS] / mol dm^{-3} for the reaction of HPS and 4-chloroaniline 1×10^{-4} mol dm^{-3} with an aqueous pH 8 buffer, 25 °C
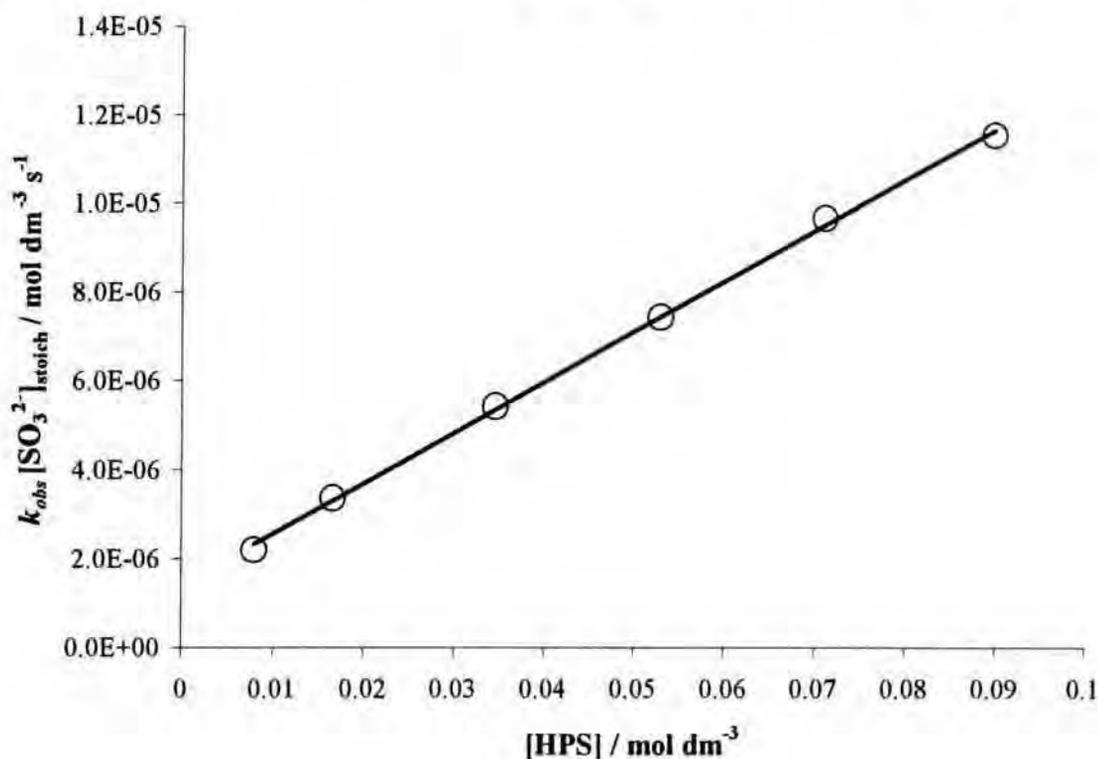

Table 3.28: Rate and equilibrium constants for the reaction of HPS and 4-chloroaniline with added sulfite over the pH range 4.7 to 9.2, in aqueous solutions at 25 °C

pH		$k_f[SO_3^{2-}]_{stoich}$ x10^{-4} / s^{-1}	$k_r[SO_3^{2-}]_{stoich}$ x10^{-6} / mol dm^{-3} s^{-1}	K (kinetic) / mol dm^{-3}	K (Abs.) / mol dm^{-3}
4.7	1	4.20	10.50	40	89
	2	5.15	8.63	60	86
5.8	1	4.36	5.48	80	89
	2	4.01	4.99	80	84
6.0	1	5.10	8.11	63	76
7.0	1	1.94	2.82	69	81
8.0	1	1.14	1.41	81	83
	2	1.21	1.49	81	82
9.2	1	0.46	0.42	111	90
10.0	1	0.37	0.45	81	67

[1] *sulfite added was a constant 1×10^{-3} mol dm^{-3}*; [2] *sulfite added was 10% of [HPS]*

The value obtained at a given pH, again show a fair level of self-consistency. The plots for the forward reaction in figure 3.22, show that at higher pH values, there is little dependence on acidity. At lower pH, the observed values show some increase, but not in line with the prediction of equation 3.1. Since the pK_a value of the amine is 4.15, applying a correction for protonation of the amine, would slightly increase the experimental value obtained at pH 4.7, but would not significantly affect the fit.

Similarly, values for the reverse reaction, in figure 3.23, do not increase as predicted by equation 3.17, at lower pH values.

Allowing for the value of K_a^{HSO3-} to be variable, yielded values as follows; $k_3''.K_1.K_2.K_a = 9.38 \times 10^{-5}$ s^{-1} with $K_a^{HSO3-} = 2.38 \times 10^{-7}$ mol dm^{-3}, $k_{-3}''/K_4 = 8.34 \times 10^{-7}$ mol dm^{-3} s^{-1} with $K_a^{HSO3-} = 7.09 \times 10^{-7}$ mol dm^{-3}.

Figure 3.22: A plot of $k_f[SO_3^{2-}]_{stoich}$ versus pH for the reaction of 4-chloroaniline and HPS with added sodium sulfite. $k_3''.K_1.K_2.K_a = 7.1 \times 10^{-5}$ s^{-1} when $K_a^{HSO3-} = 8.0 \times 10^{-8}$ mol dm^{-3}
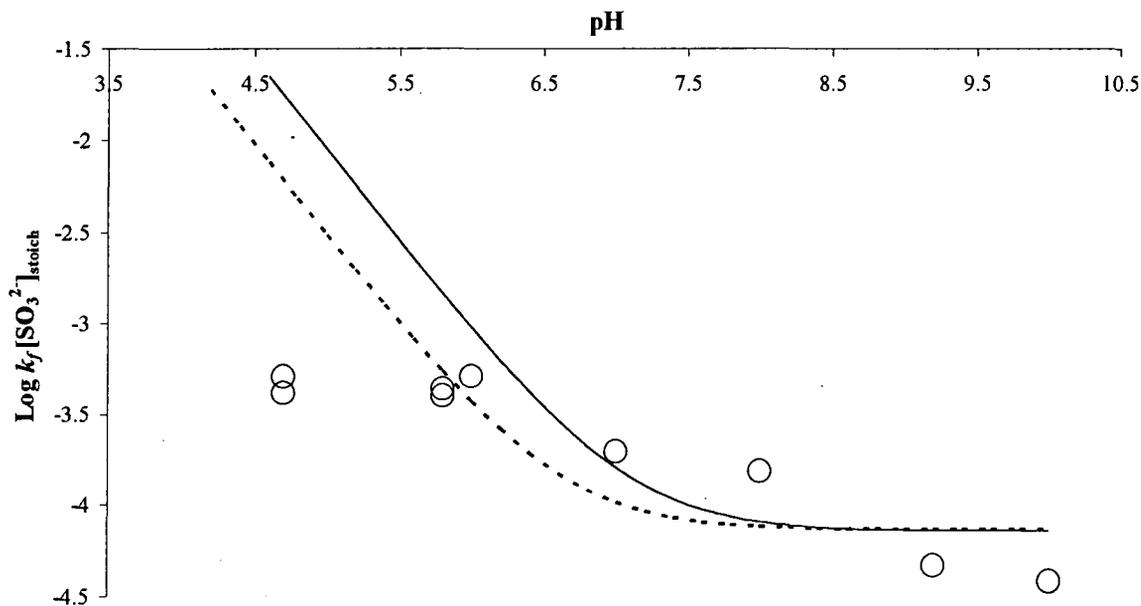
Figure 3.23: A plot of $k_r[SO_3^{2-}]_{stoich}$ versus pH for the reaction of 4-chloroaniline and HPS with added sodium sulfite. $k_{-3}''/K_4 = 8.5 \times 10^{-7}$ mol dm^{-3} s^{-1} with $K_a^{HSO3-} = 8.0 \times 10^{-8}$ mol dm^{-3}.
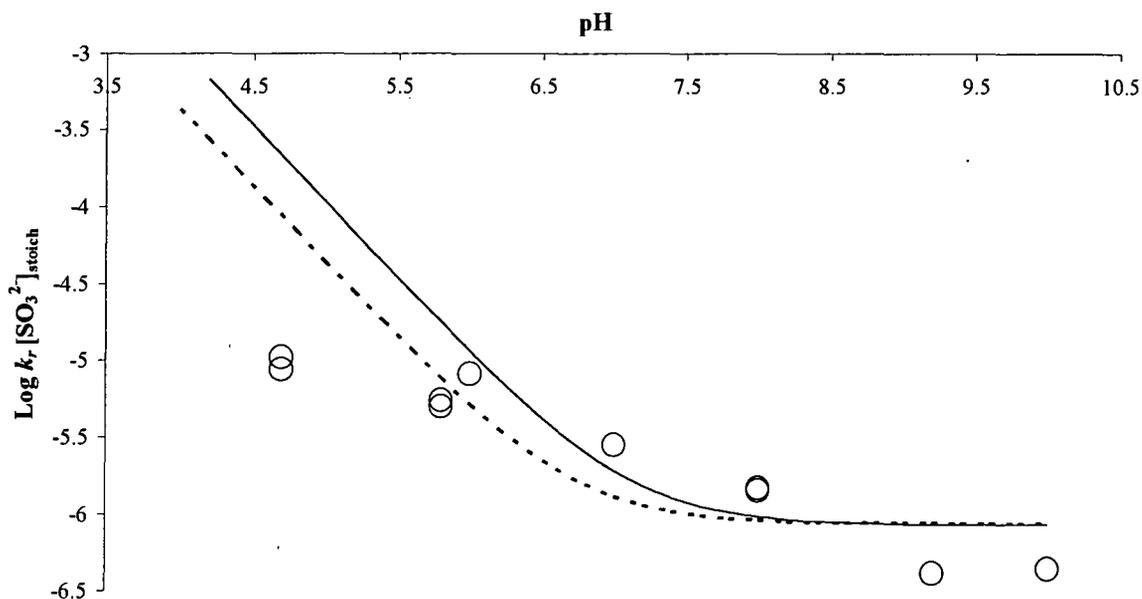
3.2.3.4: 3-Chloroaniline

The spectra of 3-chloroaniline, 1×10^{-4} mol dm^{-3}, alone and with HPS 0.01mol dm^{-3} were observed, and are shown in figure 3.24. It was clear that 3-chloroaniline followed similar trends to the previous anilines studied, in the sense that on reaction, the formation of the products causes the initial peak to shift to a longer wavelength and increase in absorbance over time. Reactions were complete after 100 minutes.

Figure 3.24: Spectra of 1×10^{-4} mol dm^{-3} 3-chloroaniline alone, and after reaction with 0.01 mol dm^{-3} HPS after 100 minutes, 25 °C, aqueous solution
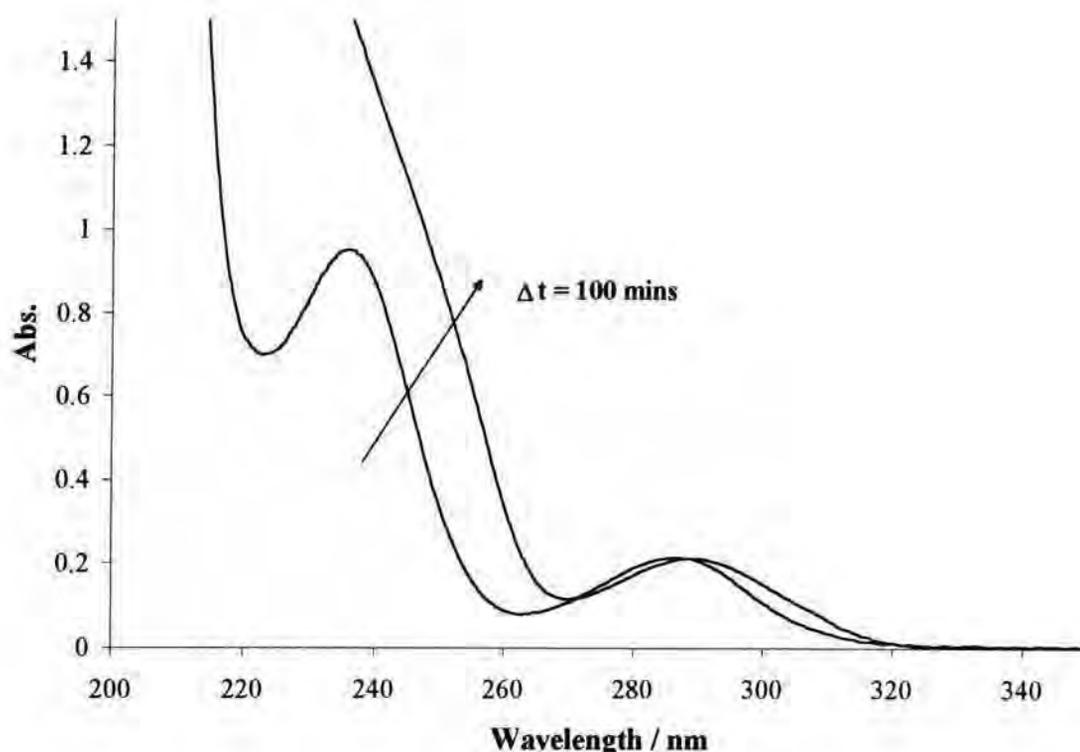
Table 3.29: Spectrum in aqueous solution of 1×10^{-4} mol dm^{-3} 3-chloroaniline and the final spectrum in the presence of 0.01 mol dm^{-3} HPS

HPS / mol dm^{-3}	λ_{max} / nm ($\varepsilon^{\dagger}$ / mol^{-1} dm^{3} cm^{-1})
none	235 (9500); 286 (2060)
0.01	289 (2150)

† *Based on the assumption that all the aniline reacts to give 1×10^{-4} mol dm^{-3} product*

Main absorbance peak swamped by sulfite

The plot suggested that the greatest change in absorption was at 250nm. Therefore, measurements to observe the formation of products were made at this wavelength over time.

Reactions were studied over the pH range 4.7 to 9, where 3-chloraniline was a constant 1×10^{-4} mol dm^{-3} but HPS varied from 0.01 to 0.1 mol dm^{-3}. The reaction at pH 8 is typical and the absorbance versus time plots are shown in figure 3.25. Values of k_{obs} calculated from first order plots, also these values multiplied by the total sulfite concentration are shown in table 3.30. Using the change in absorbance for the plots and equation 3.20, the overall equilibrium constant was calculated for the reaction; values calculated for pH 8 are also displayed in table 3.30.

Figure 3.25: Spectral plots of the reactions between HPS 0.01 to 0.1 mol dm^{-3} with 1×10^{-4} mol dm^{-3} 3-chloroaniline along with added sodium bisulfite, at pH 8, at 25 °C
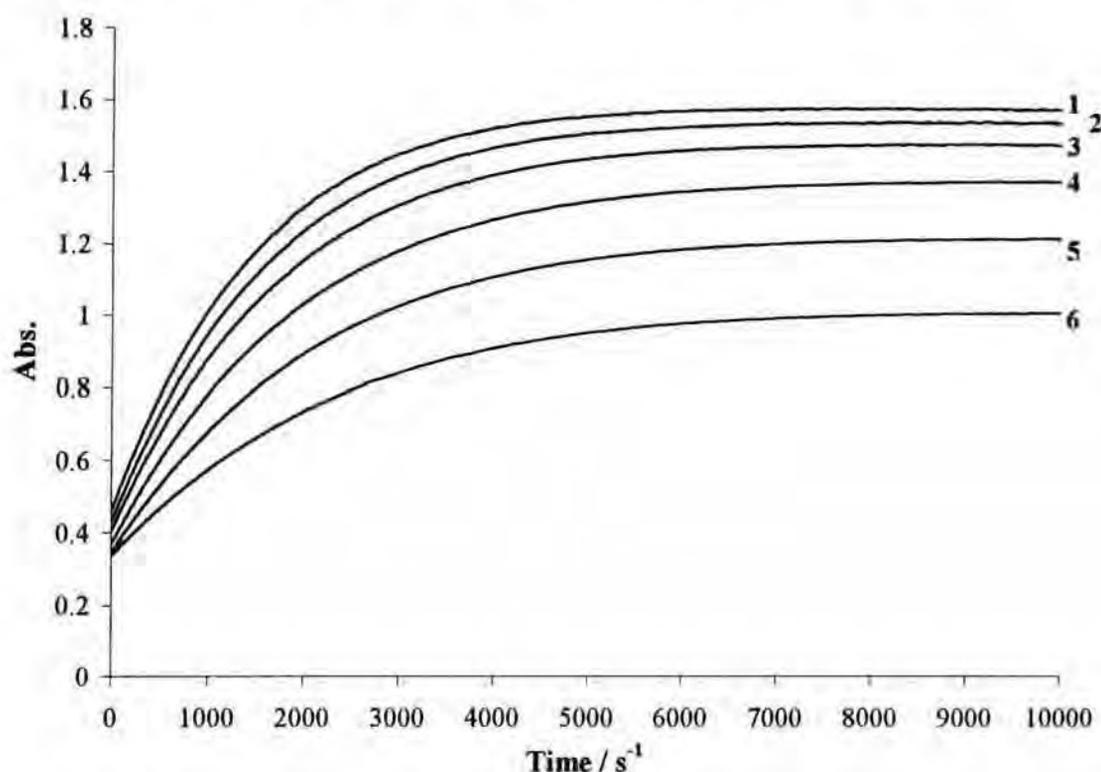
1 = 0.09 mol dm^{-3} HPS; 2 = 0.071 mol dm^{-3}; 3 = 0.053 mol dm^{-3}; 4 = 0.034 mol dm^{-3}; 5 = 0.017 mol dm^{-3}; 6 = 0.008 mol dm^{-3}

Table 3.30: Kinetic and equilibrium data for the reaction of HPS (various concentrations) and 1×10^{-4} mol dm^{-3} 3-chloroaniline with added sodium sulfite in an aqueous pH 8 buffer, 25 °C, $\Delta Abs_{inf} = 1.35$

[HPS] / mol dm^{-3}	[SO$_3^{2-}$] / mol dm^{-3}	k_{obs} / 10^{-4} s^{-1}	k_{obs}[SO$_3^{2-}$]$_{stoich}$ / 10^{-6} mol dm^{-3} s^{-1}	ΔAbs	K / dm^3 mol^{-1}
0.008	0.003	4.65	1.40	0.650	116
0.017	0.004	5.09	2.24	0.870	106
0.034	0.007	5.49	3.62	1.020	91
0.053	0.008	6.17	4.95	1.120	92
0.071	0.010	6.69	6.56	1.180	97
0.090	0.011	7.23	7.95	1.210	96

From the results, the equilibrium constant can be estimated as *ca.* 94 dm^3 mol^{-1}. The values calculated for the observed rate, in terms of total sulfite concentration, were plotted against the HPS concentration (figure 3.26). This was carried out in order to obtain values for the forward and reverse rates and hence, a value for the equilibrium constant, which could be compared with, the value calculated from the absorbance data.

Figure 3.26: A plot of $k_{obs}[SO_3^{2-}]_{stoich}$ / mol dm^{-3} s^{-1} versus [HPS] / mol dm^{-3} for the reaction of HPS and 3-chloroaniline 1×10^{-4} mol dm^{-3} with an aqueous pH 8 buffer, 25 °C
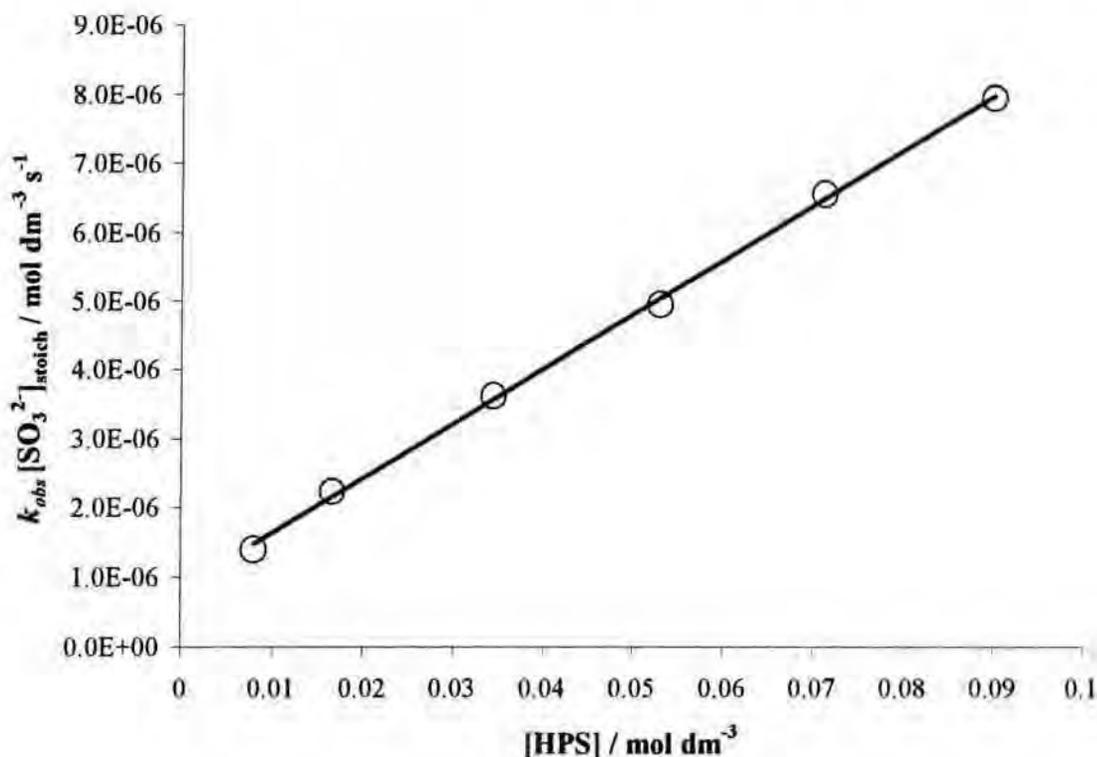
The value obtained for the gradient, equal to $k_f[SO_3^{2-}]_{stoich}$, was $7.93 \pm 0.12 \times 10^{-5}$ s^{-1}, and for the intercept, $k_r[SO_3^{2-}]_{stoich}$, was $8.42 \pm 0.67 \times 10^{-7}$ mol dm^{-3} s^{-1}. These were combined to give a value for the equilibrium constant, K, which was 94 ± 10 mol dm^{-3}. This value was again similar to that obtained from the absorbance data

Values for these terms calculated at other pH values, are summarised in table 3.31.

Table 3.31: Rate and equilibrium constants for the reaction of HPS and 3-chloroaniline with added sulfite over the pH range 4.7 to 10.0, in aqueous solutions at 25 °C

pH		$k_f[SO_3^{2-}]_{stoich}$ / 10^{-4} s^{-1}	$k_r[SO_3^{2-}]_{stoich}$ / 10^{-6} mol dm^{-3} s^{-1}	K (kinetic) / dm^3 mol^{-1}	K (Abs.) / dm^3 mol^{-1}
4.7	1	2.59	4.5	58	85
	2	2.90	4.27	68	87
	3	3.46	3.93	88	95
5.8	1	2.32	2.39	97	90
	2	2.32	2.21	92	89
6.0	4	2.73	2.94	93	99
	1	0.79	0.84	94	94
8.0	2	0.62	0.77	80	98
	4	0.64	0.53	84	95
	1	0.26	0.18	92	95
9.2	2	0.42	0.62	68	87
10.0	1	0.19	0.20	97	84

[1] *sulfite added was a constant 1×10^{-3} mol dm^{-3};* [2] *sulfite added was 10% of [HPS];* [3] *sulfite added was a constant 0.01 mol dm^{-3};* [4] *no extra sulfite was added*

Values shown above for the equilibrium constants give very good consistency; the values for the forward and reverse reactions can be seen plotted against pH in figures 3.27 and 3.28. Two fitted plots are also given for each process; the dashed being the best fit, with K_a^{HSO3-} unfixed (2.77×10^{-7} and 1.94×10^{-6} mol dm^{-3} for the forward and reverse reactions respectively), and the full line fitted with K_a^{HSO3-} fixed at a constant 8.0×10^{-8} mol dm^{-3}. Values obtained for the kinetic and equilibrium terms for the forward and reverse reactions when K_a^{HSO3-} was variable, equalled; $k_3''.K_1.K_2.K_a = 4.39 \times 10^{-5}$ s^{-1} for the forward, and $k_{-3}''/K_4 = 5.66 \times 10^{-7}$ mol dm^{-3} s^{-1} for the reverse.

Figure 3.27: A plot of $k_f[SO_3^{2-}]_{stoich}$ versus pH for the reaction of 3-chloroaniline and HPS with extra added sodium sulfite. $k_3''.K_1.K_2.K_a = 3.80 \times 10^{-5}$ s^{-1} when $K_a^{HSO3-} = 8.0 \times 10^{-8}$ mol dm^{-3}

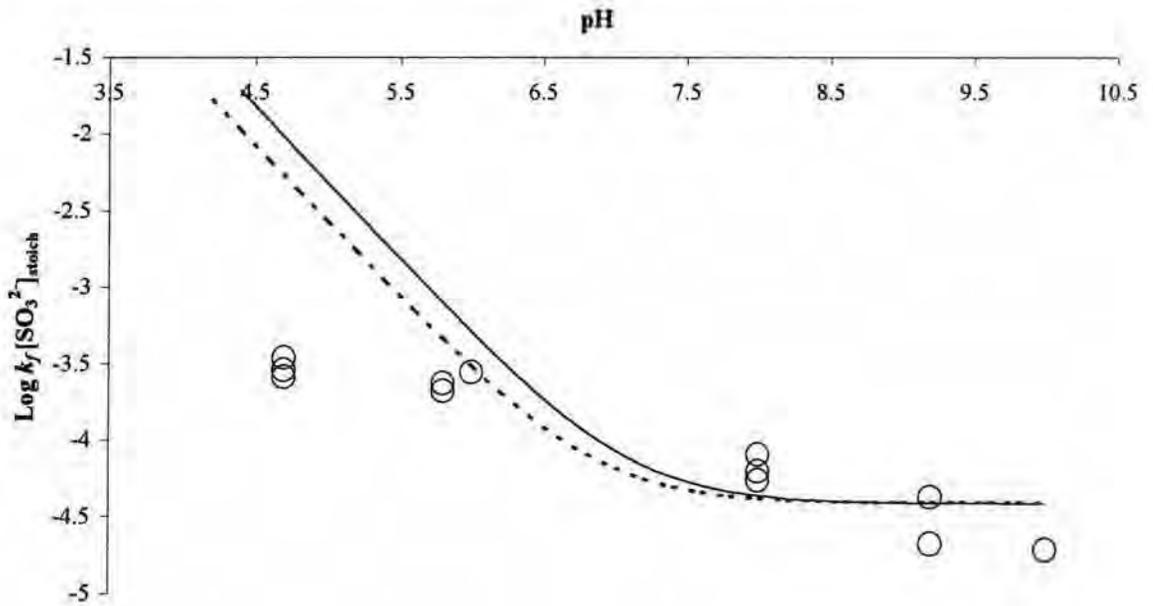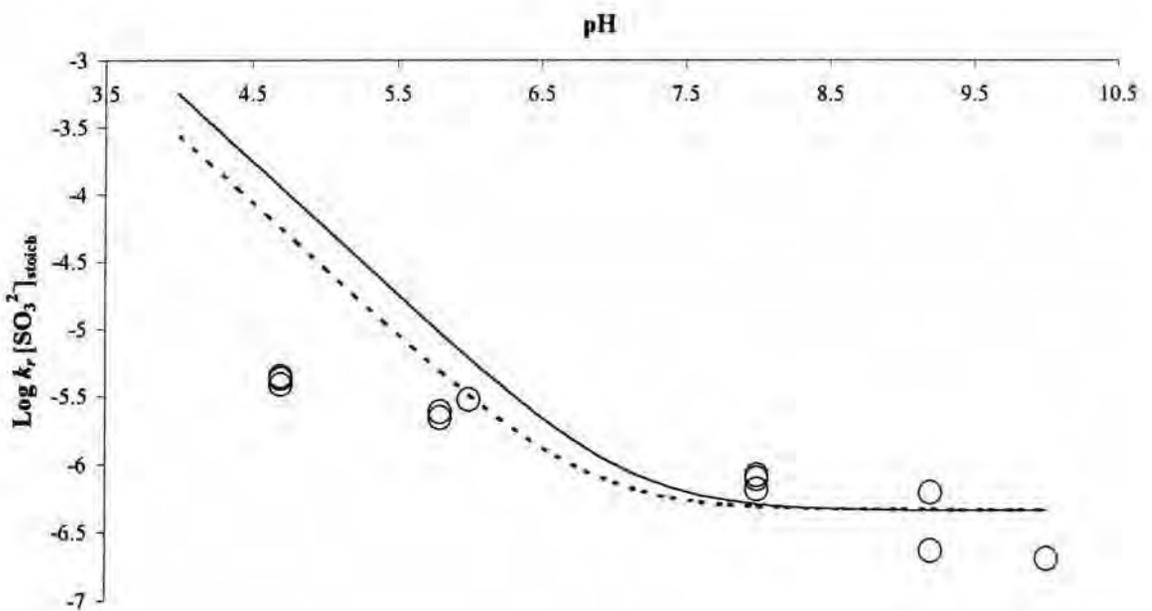**Figure 3.28:** A plot of $k_r[SO_3^{2-}]_{stoich}$ versus pH for the reaction of 3-chloroaniline and HPS with extra added sodium sulfite. $k_{-3}''/K_4 = 4.50 \times 10^{-7}$ mol dm^{-3} s^{-1} when $K_a^{HSO3-} = 8.0 \times 10^{-8}$ mol dm^{-3}

As with 4-chloroaniline, fitted plots fail to show close relations with experimental values below pH 7. Experimental values are lower than those expected from the respective equations, 3.11 or 3.17.

3.2.3.5: 3-Nitroaniline

The spectra in figure 3.29 for 3-nitroaniline, 1×10^{-4} mol dm^{-3}, show that only small changes occur in the presence of HPS, 0.01 mol dm^{-3}. Detailed analysis of the absorption maxima is not warranted, but it was found that measurable changes in absorbance occurred at 260nm. Reactions were considerably slower that for the corresponding reactions with aniline. Typical plots of absorbance versus time measured at pH = 8 are shown in figure 3.30. Good fits to first order kinetics were obtained, and values of k_{obs} are given in table 3.32.

Figure 3.29: Spectra of 1×10^{-4} mol dm^{-3} 3-nitroaniline alone, and after reaction with 0.01 mol dm^{-3} HPS after 200 minutes, 25 °C, aqueous solution

170
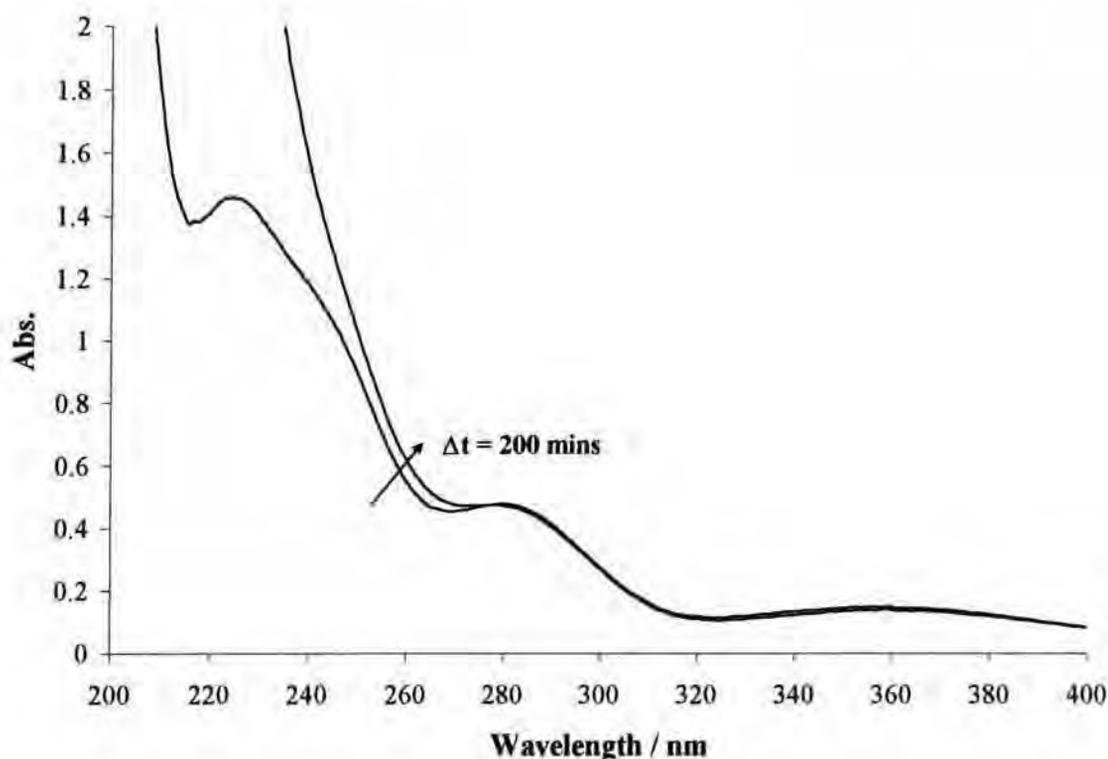
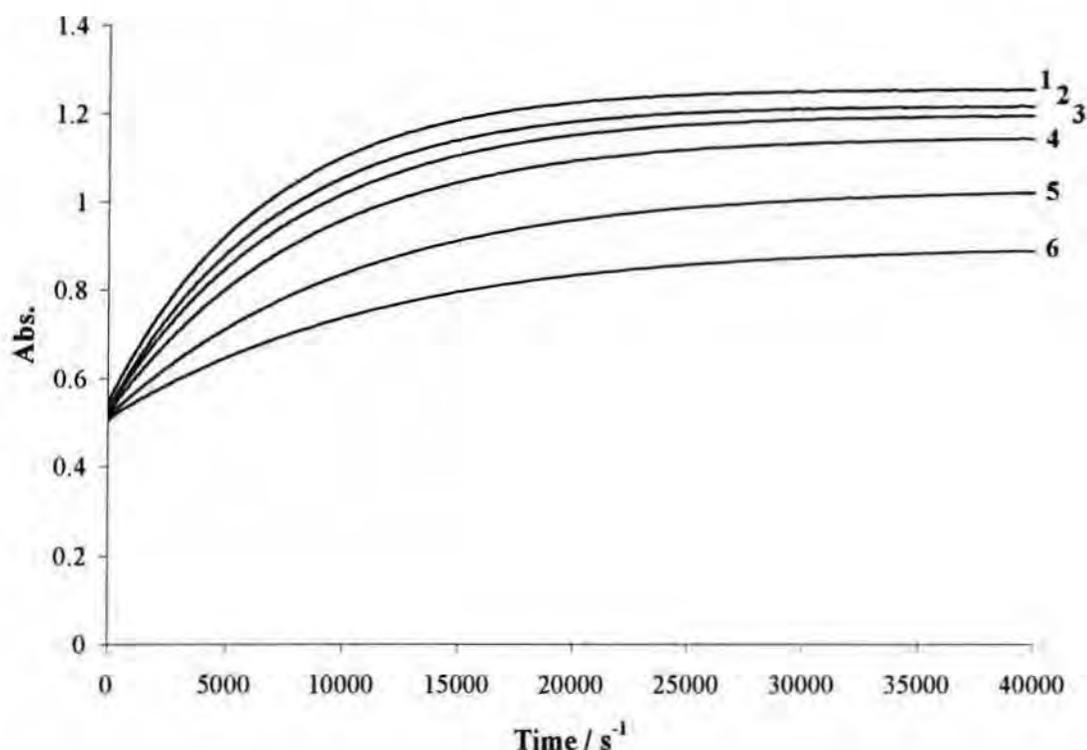**Figure 3.30:** Spectral plots of the reactions between HPS 0.01 to 0.1 mol dm^{-3} with 1×10^{-4} mol dm^{-3} 3-nitroaniline along with added sodium bisulfite, at pH 8, at 25 °C

1 = 0.09 mol dm^{-3} HPS; 2 = 0.071 mol dm^{-3}; 3 = 0.053 mol dm^{-3}; 4 = 0.034 mol dm^{-3}; 5 = 0.017 mol dm^{-3}; 6 = 0.008 mol dm^{-3}

Table 3.32: Kinetic and equilibrium data for the reaction of HPS (various concentrations) and 1×10^{-4} mol dm^{-3} 3-nitroaniline with added sodium sulfite in an aqueous pH 8 buffer, 25 °C, $\Delta Abs_{inf} = 0.775$

[HPS] / mol dm^{-3}	[SO_3^{2-}] / mol dm^{-3}	k_{obs} / 10^{-5} s^{-1}	k_{obs}[SO_3^{2-}]$_{stoich}$ / 10^{-7} mol dm^{-3} s^{-1}	ΔAbs	K / dm^3 mol^{-1}
0.008	0.003	8.78	2.63	0.394	129
0.017	0.004	9.74	4.29	0.521	121
0.034	0.007	11.99	8.39	0.632	130
0.053	0.008	13.17	10.56	0.674	126
0.071	0.010	14.42	14.13	0.693	119
0.090	0.011	15.26	16.79	0.714	130

Values of the overall equilibrium constant calculated via equation 3.20, using absorbance data are very consistent, with the average being 126 dm^3 mol^{-1}. A comparison to this can be made by plotting k_{obs}[SO$_3$$^{2-}$]$_{stoich}$ against the stoichiometric concentration of HPS. Values for the forward and reverse rates of reaction in terms of total sulfite are obtained from the plot, hence, producing a value of the kinetic equilibrium constant (since K = k_f / k_r). Figure 3.31 shows this plot for the reaction at pH 8.

Figure 3.31: A plot of k_{obs}[SO$_3$$^{2-}$]$_{stoich}$ / mol dm^{-3} s^{-1} versus [HPS] / mol dm^{-3} for the reaction of HPS and 3-nitroaniline 1×10^{-4} mol dm^{-3} with an aqueous pH 8 buffer, 25 °C
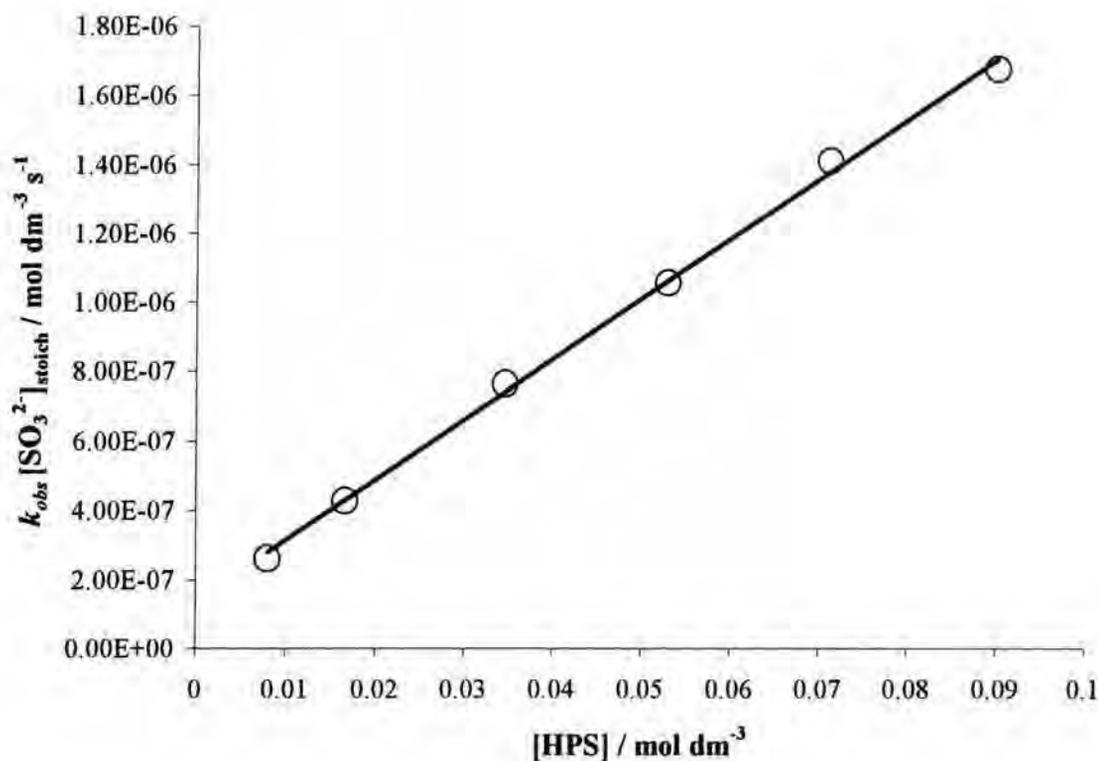
The value obtained for the gradient equalled $1.79 \pm 0.08 \times 10^{-5}$ mol dm^{-3}, with the value for the intercept, equalling $1.35 \pm 0.4 \times 10^{-7}$ mol dm^{-3}. Those values correspond to k_f[SO$_3$$^{2-}$]$_{stoich}$ and k_r[SO$_3$$^{2-}$]$_{stoich}$ respectively, and as it has been stated, K = k_f / k_r indicating that the equilibrium constant calculated from kinetic data, equals 133 ± 30 dm^3 mol^{-1}. This value agrees well with the values of K calculated from absorbance data. Values calculated from both methods, along with data from k_{obs}[SO$_3$$^{2-}$]$_{stoich}$ versus HPS concentration plots at other pH values, are shown in table 3.33.

Table 3.33: Rate and equilibrium constants for the reaction of HPS and 3-nitroaniline with added sulfite over the pH range 4.7 to 9.2, in aqueous solutions at 25 °C

pH		$k_f[SO_3^{2-}]_{stoich}$ x10^{-5} /s^{-1}	$k_r[SO_3^{2-}]_{stoich}$ x10^{-7} / mol dm^{-3} s^{-1}	K (kinetic) / mol dm^{-3}	K (Abs.) / mol dm^{-3}
4.7	1	9.29	7.39	126	137
5.8	1	5.73	4.83	119	138
	2	6.49	3.95	164	138
6.0	3	6.89	5.64	122	125
	1	1.79	1.35	133	126
8.0	2	1.64	1.27	129	128
	3	2.25	1.94	116	134
9.2	1	0.60	0.45	134	121

[1] *sulfite added was a constant $1x10^{-3}$ mol dm^{-3};* [2] *sulfite added was 10% of [HPS];* [3] *no extra sulfite was added*

Reasonable consistency of the data obtained, at a given pH is observed for 3-nitroaniline as shown above. Plots of the forward and reverse rate constants versus pH are shown in figures 3.32 and 3.33. The two fitted lines in each figure differ in the value used for K_a^{HSO3-}, the full line used a constant $8.0x10^{-8}$ mol dm^{-3}, whereas, the dashed line, uses an unfixed value, determined by the best fit. In the case of the forward process, $3.8x10^{-7}$ mol dm^{-3} was determined, and in the reverse, a value of $4.06x10^{-7}$ mol dm^{-3} was obtained. Values obtained for the kinetic and equilibrium terms for the forward and reverse reactions when, K_a^{HSO3-} was variable, equalled: $k_3''.K_1.K_2.K_a = 1.3x10^{-5}$ s^{-1} for the forward and $k_{-3}''/K_4 = 1.2x10^{-7}$ mol dm^{-3} s^{-1} for the reverse.

The plots obtained clearly show that the increases in value of rate constants at pH ≤ 7 predicted by equations 3.11 and 3.17, are not observed

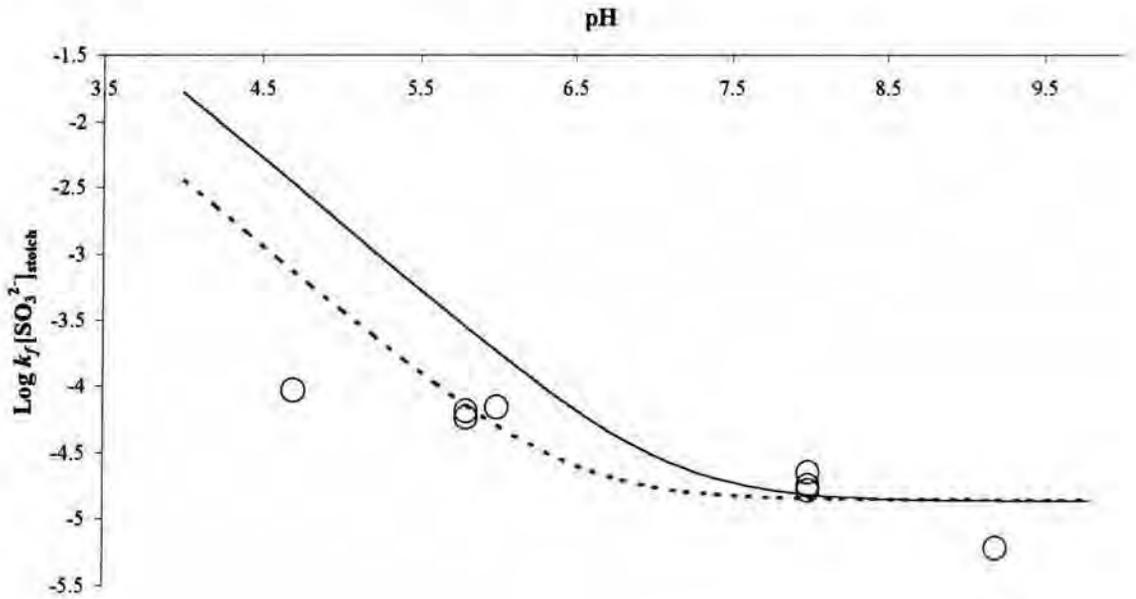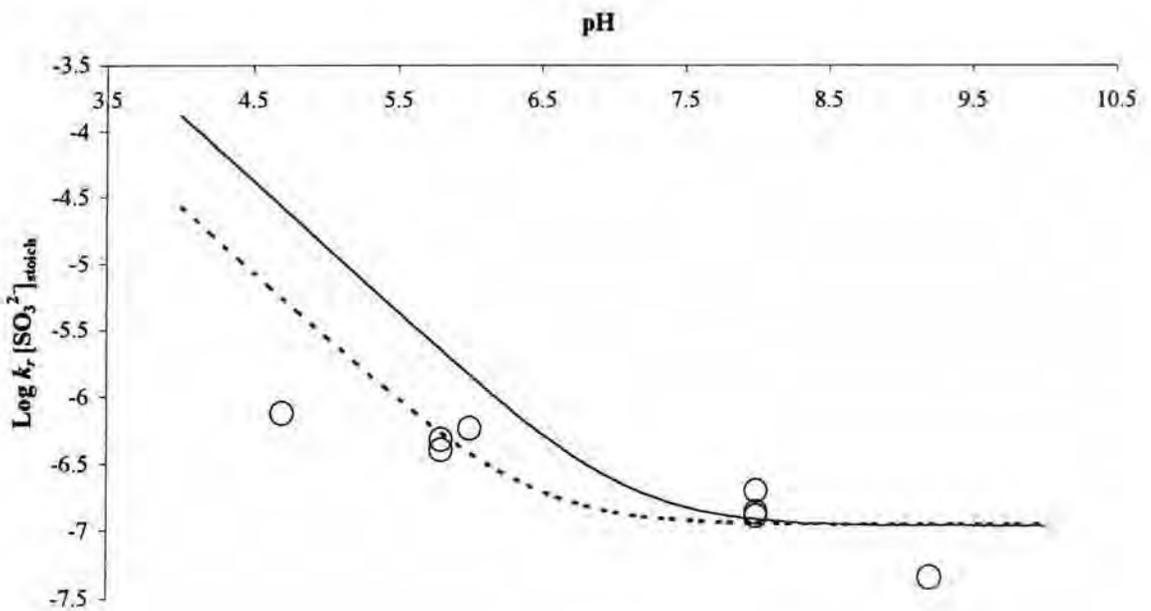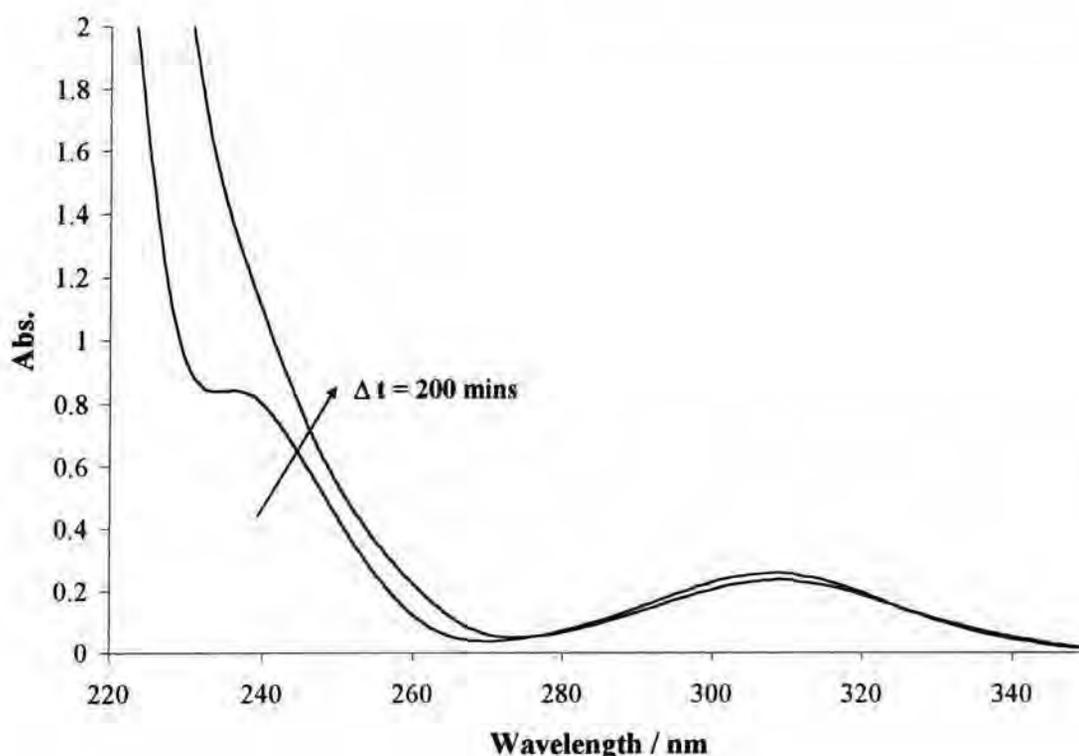**Figure 3.32:** A plot of $k_f[SO_3^{2-}]_{stoich}$ versus pH for the reaction of 3-nitroaniline and HPS with extra added sodium sulfite. $k_3''.K_1.K_2.K_a = 1.35 \times 10^{-5}$ s^{-1} when $K_a^{HSO3-} = 8.0 \times 10^{-8}$ mol dm^{-3}

Figure 3.33: A plot of $k_r[SO_3^{2-}]_{stoich}$ versus pH for the reaction of 3-nitroaniline and HPS with extra added sodium sulfite. $k_{-3}''/K_4 = 1.06 \times 10^{-5}$ mol dm^{-3} s^{-1} when $K_a^{HSO3-} = 8.0 \times 10^{-8}$ mol dm^{-3}

3.2.3.6: 3-cyanoaniline

Initial UV/Vis spectral plots of the reactions of 3-cyanoaniline and HPS, suggested that the reaction rate was slow, with completion, taking well over 10 hours. Figure 3.34 shows spectra of 1×10^{-4} mol dm^{-3} 3-cyanoaniline alone, and with 0.01 mol dm^{-3} HPS, after 200 minutes. Even though reaction rates were slow, investigations at one wavelength were conducted in the attempt to find equilibrium and rate constants for the process. The wavelength used for observation of these reactions was 257nm, which, as figure 3.34 suggests, gives the greatest increase in absorbance.
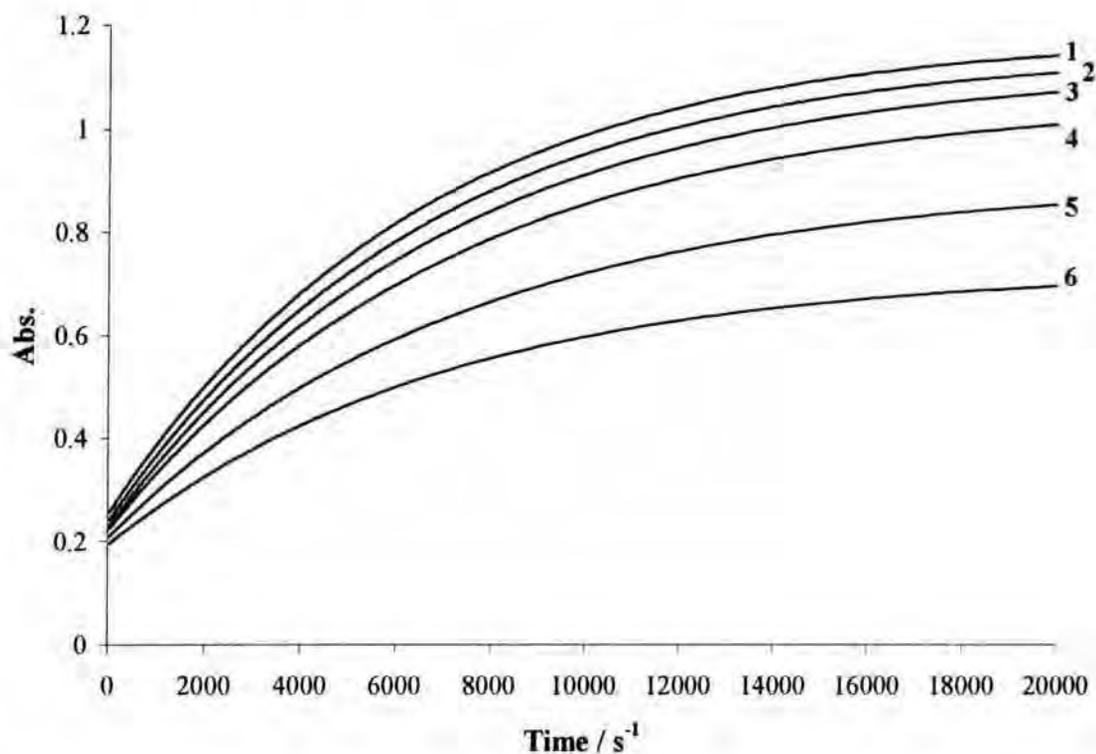
Figure 3.34: Spectra of 1×10^{-4} mol dm^{-3} 3-cyanoaniline alone, and with 0.01 mol dm^{-3} HPS after 200 minutes, 25 °C, aqueous solution

Absorbance versus time plots were obtained for the reactions of 3-cyanoaniline (1×10^{-4} mol dm^{-3}) and HPS, in varying concentration from 0.01 to 0.1 mol dm^{-3}, over the pH range of 4.7 to 9.2, in aqueous solution at 25 °C. Sodium sulfite was also added to the reaction. The plots for the reaction at pH 8 are shown in figure 3.35. Values for the observed rate constants were

obtained from first order fits of the plots, which, when combined with the total sulfite concentration, gave values for $k_{obs}[SO_3^{2-}]_{stoich}$. Table 3.34 shows values of these terms at pH 8, along with overall equilibrium constants calculated, using equation 3.20 and the absorbance data obtained from figure 3.30.

Figure 3.35: Spectral plots of the reactions between HPS 0.01 to 0.1 mol dm^{-3} with 1x10^{-4} mol dm^{-3} 3-cyanoaniline with added sodium bisulfite, at pH 8, at 25 °C
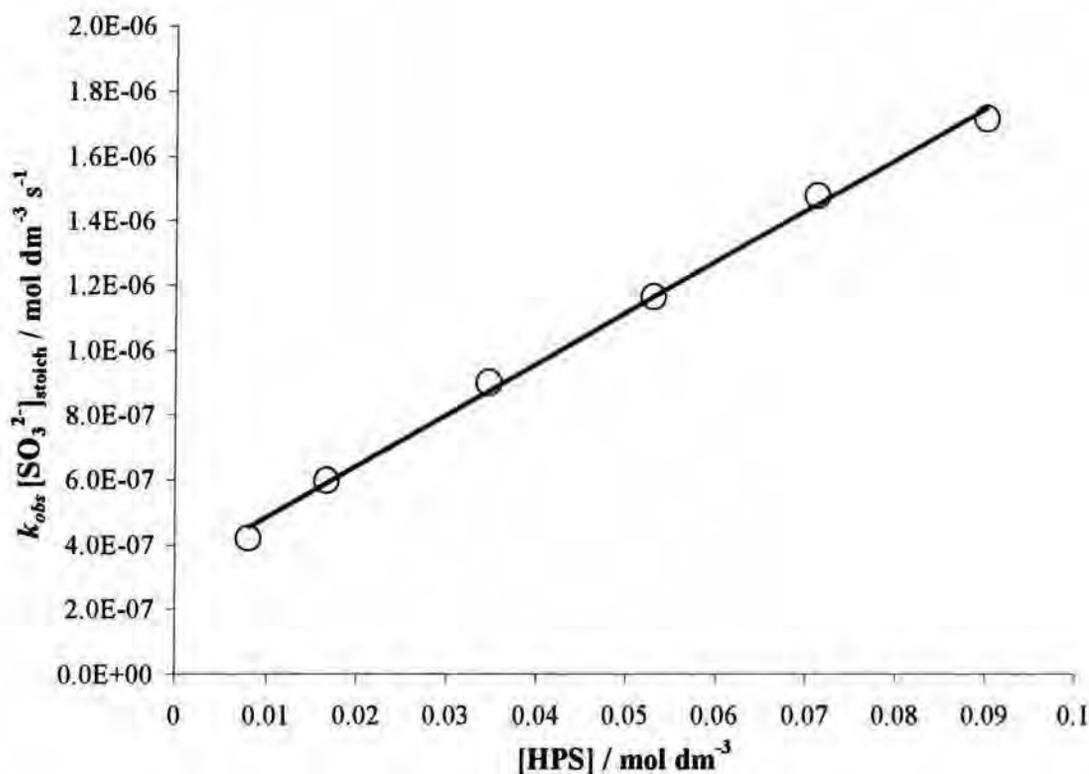

1 = 0.09 mol dm^{-3} HPS; 2 = 0.071 mol dm^{-3}; 3 = 0.053 mol dm^{-3}; 4 = 0.034 mol dm^{-3}; 5 = 0.017 mol dm^{-3}; 6 = 0.008 mol dm^{-3}

Table 3.34: Kinetic and equilibrium data for the reaction of HPS (various concentrations) and 1×10^{-4} mol dm^{-3} 3-cyanoaniline with added sodium sulfite in an aqueous pH 8 buffer, 25 °C, $\Delta Abs_{inf} = 1.025$

[HPS] / mol dm^{-3}	[SO$_3^{2-}$] / mol dm^{-3}	k_{obs} / 10^{-4} s^{-1}	k_{obs}[SO$_3^{2-}$]$_{stoich}$ / 10^{-7} mol dm^{-3} s^{-1}	ΔAbs	K / dm^3 mol^{-1}
0.008	0.003	1.40	4.21	0.535	136
0.017	0.004	1.36	5.98	0.691	122
0.034	0.007	1.41	9.01	0.838	132
0.053	0.008	1.46	11.7	0.893	128
0.071	0.010	1.51	14.8	0.917	120
0.090	0.011	1.56	17.2	0.932	111

Values calculated for the overall equilibrium constant, K, using the absorbance data, gave a value of 125 ± 10 dm^3 mol^{-1}. Values calculated for the observed rate constants, in terms of total sulfite concentration, were plotted against pH, in order to obtain values for the respective forward and reverse rates. Figure 3.36 shows this particular plot for the reaction at pH 8.

177

Figure 3.36: A plot of the HPS concentration versus calculated values of $k_{obs}[SO_3{}^{2-}]_{stoich}$ / mol dm^{-3} s^{-1} for the reaction of HPS and 3-cyanoaniline 1×10^{-4} mol dm^{-3} with an aqueous pH 8 buffer, 25 °C

$k_f[SO_3{}^{2-}]_{stoich}$ equal to the gradient, was found to be 2.41×10^{-5} s^{-1} and $k_r[SO_3{}^{2-}]_{stoich}$ equal to the intercept, was obtained as 2.09×10^{-7} mol dm^{-3} s^{-1}. These values therefore, give the overall equilibrium constant for the reaction at pH 8, as 115 mol dm^{-3} (since K = k_f / k_r). This is in reasonable agreement with the values calculated from the absorbance data. Values obtained at other pH values are shown in table 3.35.

Table 3.35: Rate and equilibrium constants for the reaction of HPS and 3-cyanoaniline with added sulfite over the pH range 4.7 to 9.2, in aqueous solutions at 25 °C

pH	$k_f[SO_3^{2-}]_{stoich} / 10^{-5}$ s^{-1}	$k_r[SO_3^{2-}]_{stoich} / 10^{-7}$ mol dm^{-3} s^{-1}	K (kinetic) / dm^3 mol^{-1}	K (Abs.) / dm^3 mol^{-1}
4.7	12.60	9.62	131	119
5.8	9.92	7.69	129	123
8.0	2.41	2.09	115	125
9.2	0.69	0.52	132	122

Plots of rate constants versus pH are shown in figures 3.37 and 3.38. As before, the dashed line is the best fit, allowing K_a^{HSO3-} to vary, whilst the full line, uses a fixed value of 8.0×10^{-8} mol dm^{-3}. When K_a^{HSO3-} was variable, values for the forward and reverse rate and equilibrium terms were obtained as; $k_3''.K_1.K_2.K_a = 1.1 \times 10^{-5}$ s^{-1} for the forward and $k_{-3}''/K_4 = 1.01 \times 10^{-7}$ mol dm^{-3} s^{-1} for the reverse.
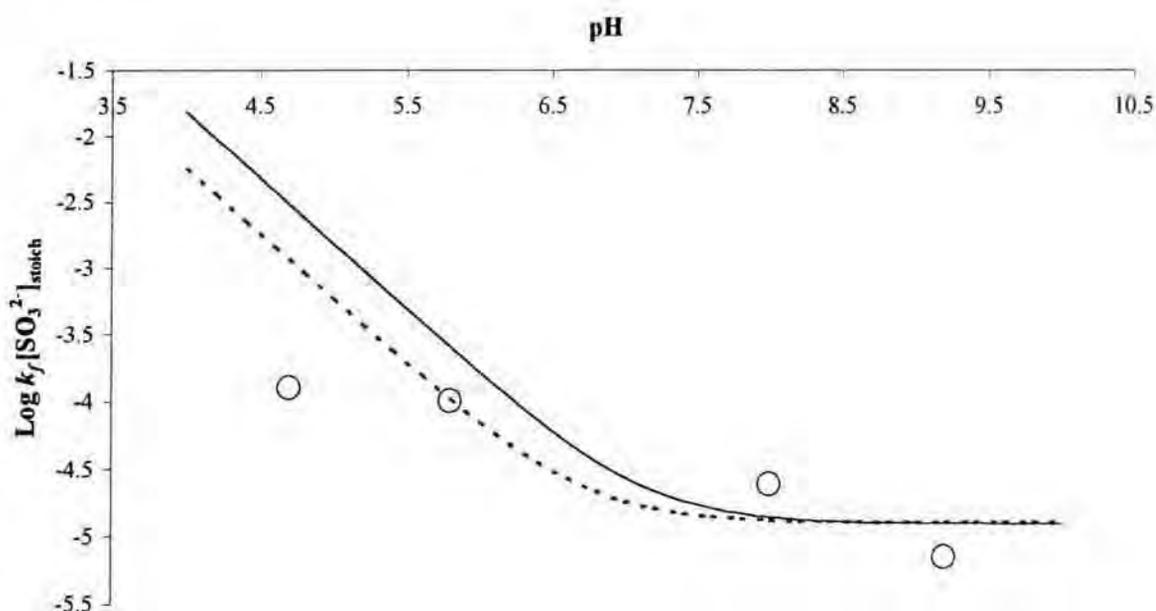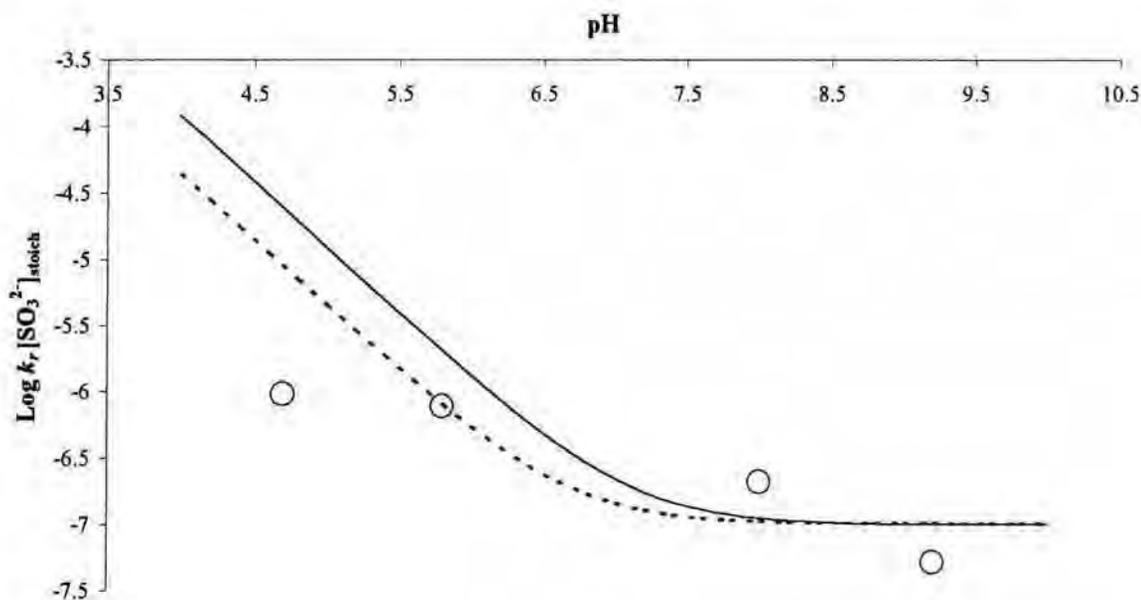
Figure 3.37: A plot of $k_f[SO_3^{2-}]_{stoich}$ versus pH for the reaction of 3-cyanoaniline and HPS with extra added sodium sulfite $k_3''.K_1.K_2.K_a = 1.22 \times 10^{-5}$ s^{-1} when $K_a^{HSO3-} = 8.0 \times 10^{-8}$ mol dm^{-3}

Figure 3.38: A plot of $k_r[SO_3^{2-}]_{stoich}$ versus pH for the reaction of 3-cyanoaniline and HPS with extra added sodium sulfite. $k_{-3}''/K_4 = 9.77 \times 10^{-8}$ mol dm^{-3} s^{-1} when when $K_a^{HSO3-} = 8.0 \times 10^{-8}$ mol dm^{-3}

Values for the equilibrium constants shown in Table 3.35 show good self consistency.

3.2.3.7: N-Methylaniline and 4-nitroaniline

Initial UV/Vis spectra were obtained for both these aniline derivatives. However, further kinetic studies for the reaction with HPS could not be carried out by UV/Vis spectroscopy. This was mainly due to the fact that adduct formation could not be observed, as spectral changes were very small. The change that is seen is close to where sulfite starts to absorb, suggesting that the spectral change due to formation is negligible when observing it using UV/Vis spectroscopy. Formation of the adducts, from the reaction of these aniline derivatives with HPS, is known to occur as it has been observed via ^{1}H NMR, in earlier sections. Calculation of the equilibrium constant for N-methylaniline was possible via 1H NMR. However, neither method can be used to determine the value for 4-nitroaniline.

Figure 3.39: Spectral plots of the reaction of N-methylaniline 1×10^{-4} mol dm^{-3} with HPS 0.05 mol dm^{-3}, 25 °C, unbuffered
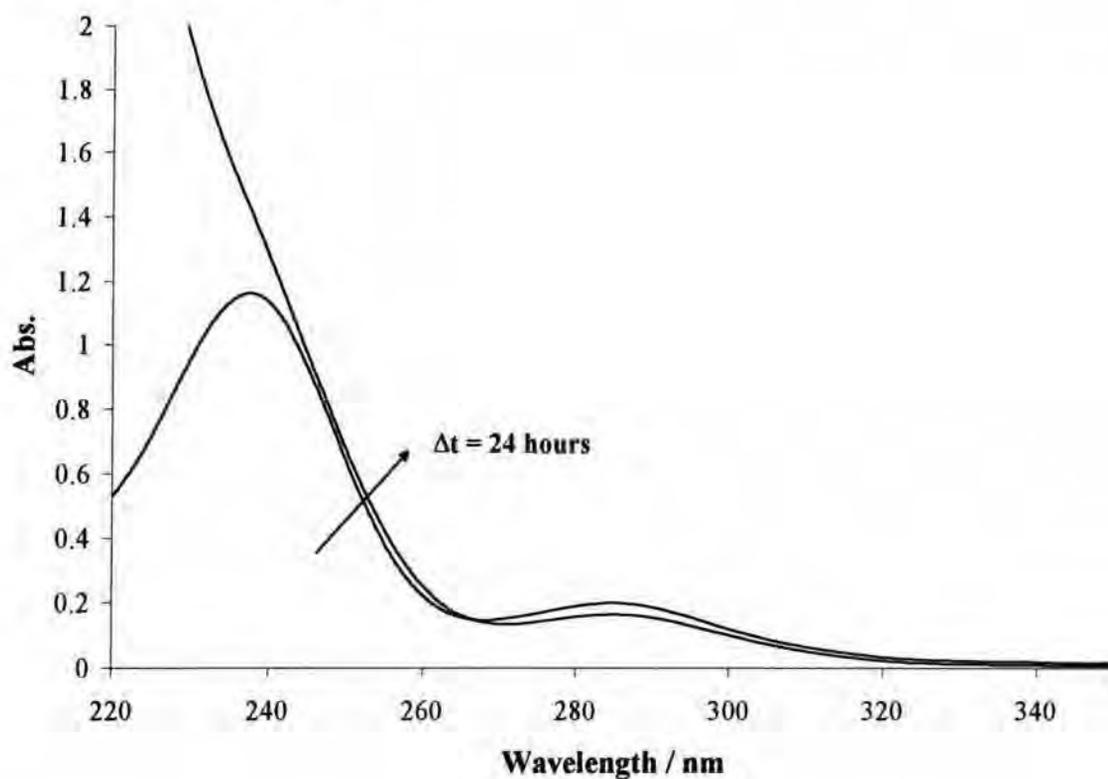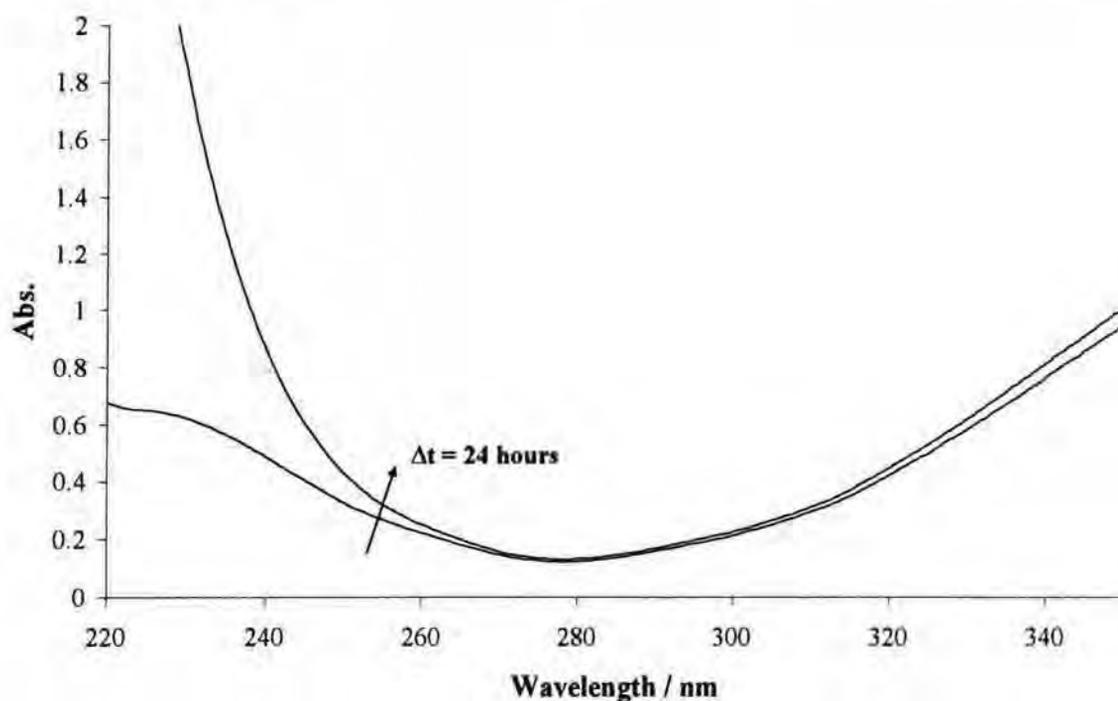

Figure 3.40: Spectral plots of the reaction of 4-nitroaniline 1×10^{-4} mol dm^{-3} with HPS 0.05 mol dm^{-3}, 25 °C, unbuffered
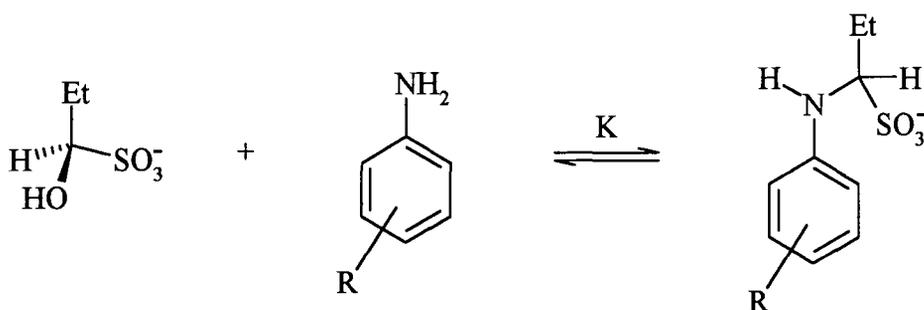
3.2.4: Comparison of results: Hammett plots

The ^1H NMR spectra, gave clear evidence for the formation of anilinopropanesulfonates from HPS and aniline and its derivatives. There is no evidence for the formation of adducts with 1:2 stoichiometery, in observable concentrations.

The UV/Vis data allows examination of the kinetics of the overall process and yield values of the equilibrium constant, K, defined by scheme 3.5.

Scheme 3.5:

Values for aniline and its derivatives are collected in table 3.36, where Hammett σ values[4] are given.

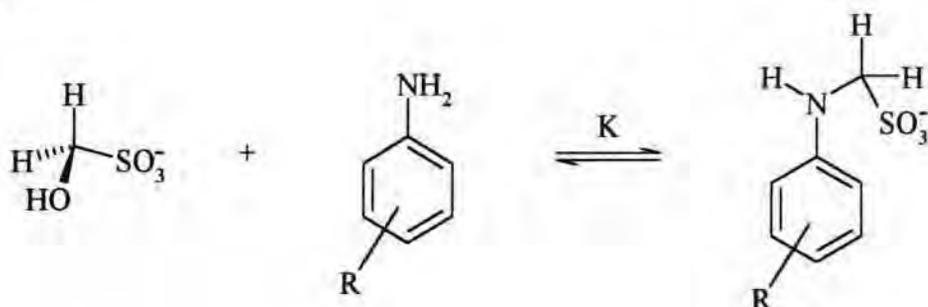The results show that there are relatively small changes in the value of K, as the substituent, R, is varied. The change is only by a factor of *ca.* 2, as the substituent is changed from 4-Me to 4-NO$_2$. This may indicate, that the overall electronic effect of the CHEt(SO$_3^-$) group is rather similar to that of hydrogen, so that the electron demand from the ring varies little on adduct formation.

Table 3.36: Summary of rate and equilibrium constants obtained experimentally, and pK_a values[3] and σ values[4], for $RC_6H_4NH_2$

R	pK_a	σ	$k_f[SO_3^{2-}]_{stoich}$ / s^{-1}	$k_r[SO_3^{2-}]_{stoich}$ / mol dm^{-3} s^{-1}	K / dm^3 mol^{-1}
H	4.60	0	1.9×10^{-4}	2.3×10^{-6}	84
4-CH_3	5.08	-0.17	3.6×10^{-4}	6.0×10^{-6}	60
4-Cl	4.15	0.23	1.1×10^{-4}	1.4×10^{-6}	81
3-Cl	3.46	0.37	7.9×10^{-5}	8.4×10^{-7}	94
3-CN	2.75	0.61	2.4×10^{-5}	2.1×10^{-7}	115
3-NO_2	2.47	0.71	1.8×10^{-5}	1.4×10^{-7}	133
N-Me	4.85	-	-	-	1.1*

* denotes the value of K was obtained from ^1H NMR results

Interestingly, the value for K for N-methyl aniline is considerably reduced, even allowing for the statistical factor of 2, relative to aniline. This is probably a consequence of increased steric repulsion with the ethyl and sulfite groups, as the substituent on the nitrogen is changed from a proton to a methyl group. Further evidence that steric effects may be important in these systems comes from the knowledge in the reaction with HMS, scheme 3.6.

Scheme 3.6:

Values of K are reported[2] as 780 dm^3 mol^{-1} when R= H and 550 dm^3 mol^{-1} when R = 4 – Me. These values are larger by a factor of *ca.* 10 than those for the corresponding reactions with
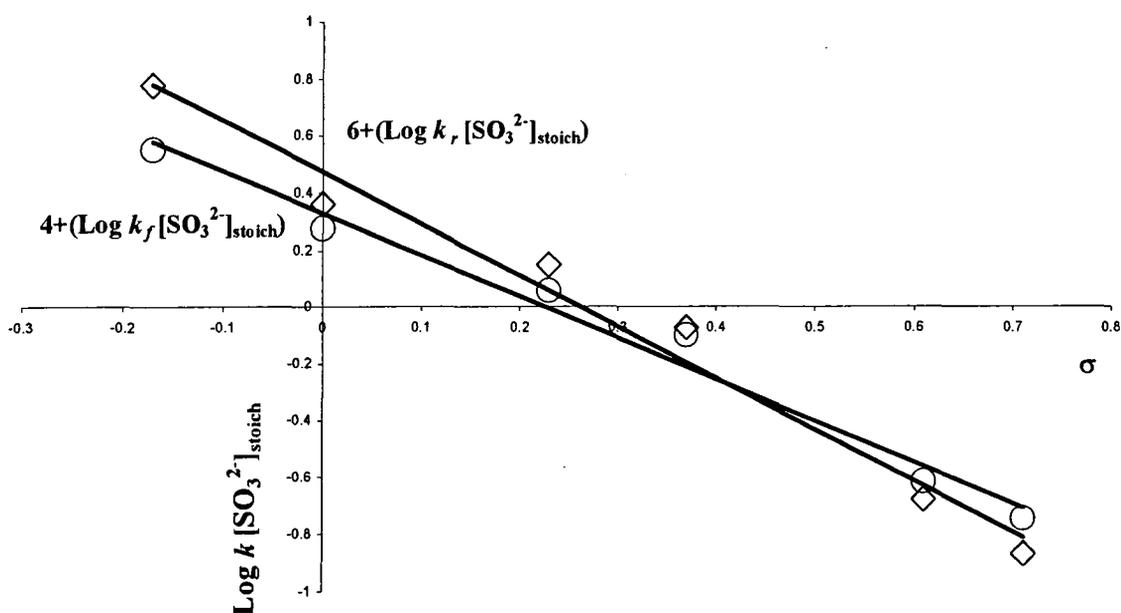
HPS. This may be attributed to the greater steric requirements of the anilinoalkanesulfonates, compared to the corresponding hydroxyalkanesulfonate.

Discussion of the acidity dependence of the kinetic results will be delayed until chapter 4. Additional information is described in that chapter. Values of the term $k_r[SO_3^{2-}]_{stoich}$ were obtained by preforming the imine and following its decomposition, in the presence of sulfite.

The present results show that when above pH 7, values of $k_f[SO_3^{2-}]_{stoich}$ and $k_r[SO_3^{2-}]_{stoich}$ become approximately independent of pH. This is consistent with the rate determining step in the overall reaction being the acid catalysed dehydration of the carbinolamine intermediate. This is further justified in chapter 4.

In table 3.33, values of kinetic parameters at the same pH, pH = 8, are compared. Hammett plots are shown in figure 3.41. These show good correlations with ρ values of -1.47 for the forward reaction and -1.81 for the reverse reaction.

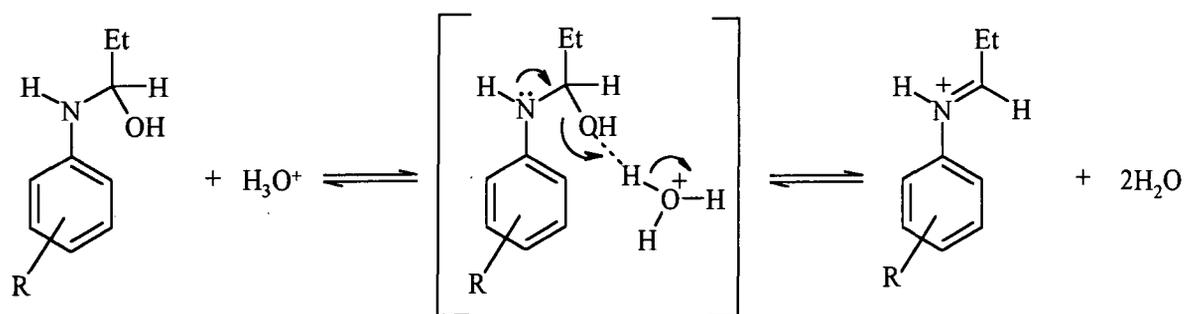**Figure 3.41:** Hammett plots for the forward and reverse rate constants

If carbinolamine dehydration is rate-limiting, then equation 3.23 is valid

$$k_f[SO_3^{2-}]_{stoich} = k_3''K_1K_2K_a$$

Reference to scheme 3.3 shows that values of K_1 and K_a, referring to HPS alone, will be invariant. So, it is the values of k_3'' and K_2 which may be affected by ring substitution. K_2 is the equilibrium constant for carbinolamine formation, and the data for the corresponding reaction, involving formaldehyde[2], shows no variation, in values, within experimental error, with ring substitution. Hence, it is likely in the present system, that values of K_2 will be unaffected and that changes will reflect variations of values of k_3'' with the nature of R. The k_3'' step is the acid catalysed dehydration of the carbinolamine, and the likely mechanism (shown in scheme 3.7) will involve transfer of positive charge to the aniline ring. Hence, a negative value ρ is expected.

Scheme 3.7:

For comparison, a Hammett plot for the protonation of the parent anilines, constructed using the data in table 3.3 gives a ρ value of -2.8.

For the reverse reaction, the rate determining step will be hydration of the iminium ion, with the relation shown in equation 3.24.

$$k_r[SO_3^{2-}]_{stoich} = \frac{k_{-3}''}{K_4}$$

(3.24)

Hence, the ρ value obtained of -1.81, reflects the change in value of k_{-3}'' and K_4 with the nature of the substituent R. The observed ρ value may be written in terms of the ρ value for the two processes involved, as shown in equation 3.25.

$$\rho\text{ [observed]} = \rho\text{ } [k_{-3}''\text{ step}] - \rho\text{ } [K_4\text{ process}]$$

(3.25)

The values of ρ, both for the k_{-3}'' step and the K_4 process, will be expected to have positive values, since each process involves reduction of positive charge on the iminium ion. However, K_4 is the equilibrium constant for addition of sulfite, while, k_{-3}'' refers to a kinetic process, addition of water. In the latter process, only partial neutralisation of charge will have occurred in the transition state, hence giving a lower ρ value. Put another way, the effect of adding the 3-nitro substituent to the aromatic ring will increase the value of K_4, more than it increases the value of k_{-3}''. Hence overall, ρ is negative.

186

3.3: References

1) P. Le Hénaff, *C. R. Acad. Sci.*, 1963, **256**, 3090

2) J. H. Atherton, K. H. Brown and M. R. Crampton, *J. Chem. Soc. Perkin Trans. 2*, 2000, 941

3) D. D. Perrin, 'Dissociation Constants of Organic Bases in Aqueous Solution', Butterworths, London, 1965 and 1972 Supplement

4) D. D. Perrin and G. B. Barlin, *Quart. Rev., Chem. Soc. London*, 1966, **20**, 75

5) (a) G. L. Kok, S. N. Gitlin and A. L. Lazrus, *J. Geophys. Res.,D*, 1986, **91**, 2801; (b) E. Haydon, A. Treinin and J. Wilf, *J. Am. Chem. Soc.*, 1972, **94**, 47; (c) V. H. Tartar and H. H. Garretson, *ibid.*, 1941, **63**, 808

Chapter four

4 The decomposition of APS in the presence of sulfite

4.1: Introduction

In chapter 3, the overall equilibrium between anilines and HPS, to give APS, has been studied, and values for the parameters $k_f[SO_3^{2-}]_{stoich}$ and $k_r[SO_3^{2-}]_{stoich}$ have been evaluated. It is known that imines may be produced and isolated from reactions of carbonyl compounds and amines (refer to chapter 1.3, 1.4). It was thought to be of interest to try to produce the imine from propanal and aniline, and to investigate its reaction with sulfite. It is to be expected that a rapid reaction would occur to give anilinopropanesulfonate, APS, but slow decomposition would eventually yield aniline and propanal, in the form of its sulfite adduct. These steps are shown in scheme 3.3. Starting with low concentration, 1×10^{-4} mol dm^{-3}, of imine, then the reversal should be almost complete at equilibrium. Hence it might be possible to isolate the reverse reaction, and obtain values for the parameter $k_r[SO_3^{2-}]_{stoich}$ at different pH values. These would give, by an independent method, a check on the values obtained in chapter 3.

4.2: Preparation of the imine

4.2.1: ^{1}H NMR studies

Studies were all made in deuterated acetonitrile, since it was predicted that water would cause decomposition of the imine. Initially, the reactants, aniline (**4.1**) and propanal (**4.2**) were observed independently by ^{1}H NMR in CD$_3$CN. Spectra are similar to those shown in chapter 3 and 2, respectively, and therefore, only shifts are shown (tables 4.1 and 4.2). Propanal, when in CD$_3$CN, will only show peaks for unhydrated **4.2**, and thus, table 4.2 is greatly reduced from that shown in table 2.8, where the hydrate is also observed.

Table 4.1: ^{1}H NMR of 0.2 mol dm^{-3} aniline, **4.1**, in CD$_3$CN: peak assignment

δ / ppm	multiplicity	integral ratio	coupling / Hz	assignment
7.09	t	2	8	Ar-H$_3$, H$_5$
6.65	t	3	8	Ar-H$_4$
6.63	d		8	Ar-H$_2$, H$_6$
4.09	broad s	2	-	NH$_2$
2.24	-	-	-	HOD
1.94	-	-	-	CD$_3$CN

Table 4.2: ^{1}H NMR of 0.2 mol dm^{-3} propanal, **4.2**, in CD$_3$CN: peak assignment

δ / ppm	multiplicity	integral ratio	coupling / Hz	assignment
9.70	s	1	-	CH=O
2.40	quintet	2	7.5	-CH$_2$-
1.94	-	-	-	CD$_3$CN
1.01	t	3	7.5	-CH$_3$

The ^{1}H NMR spectrum of aniline, 0.2 mol dm^{-3}, and propanal, 0.2 mol dm^{-3}, is shown in figure 4.1. New bands attributable to the imine, **4.3**, are observed and peak assignment is in table 4.3.
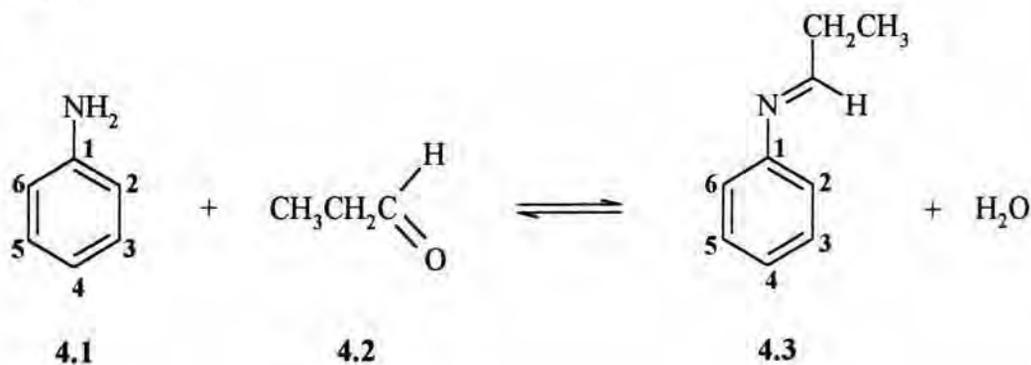
Scheme 4.1:

| **4.1** | **4.2** | **4.3** |

Figure 4.1: 1H NMR spectrum of the reaction between equimolar 0.2 mol dm^{-3} aniline and propanal, yielding the imine **4.3**, in CD$_3$CN
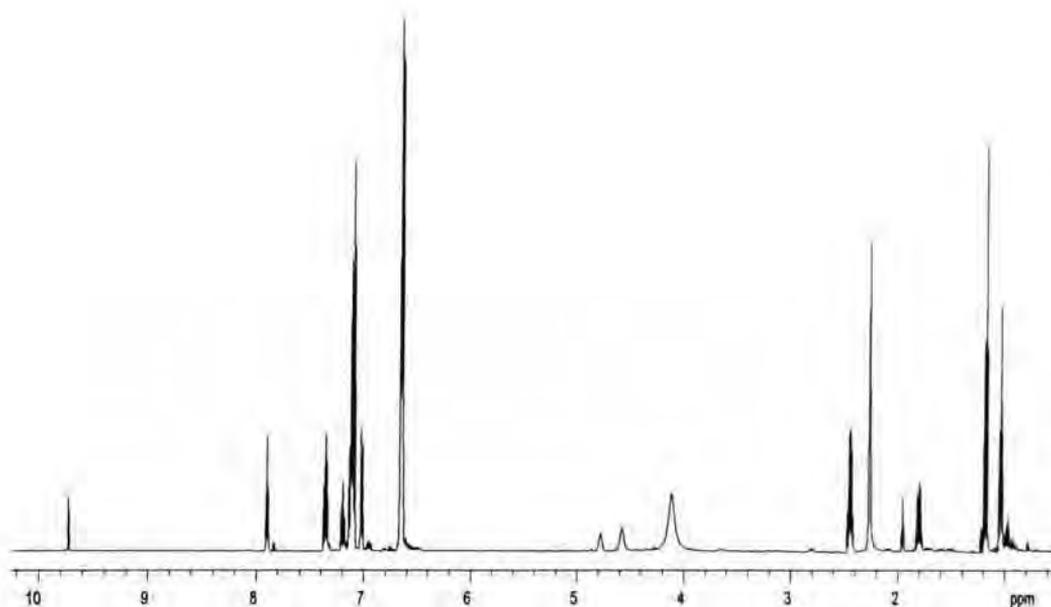

Table 4.3: 1H NMR spectrum of the reaction between equimolar 0.2 mol dm^{-3} aniline and propanal, yielding the imine **4.3**, in CD$_3$CN: peak assignment for the imine

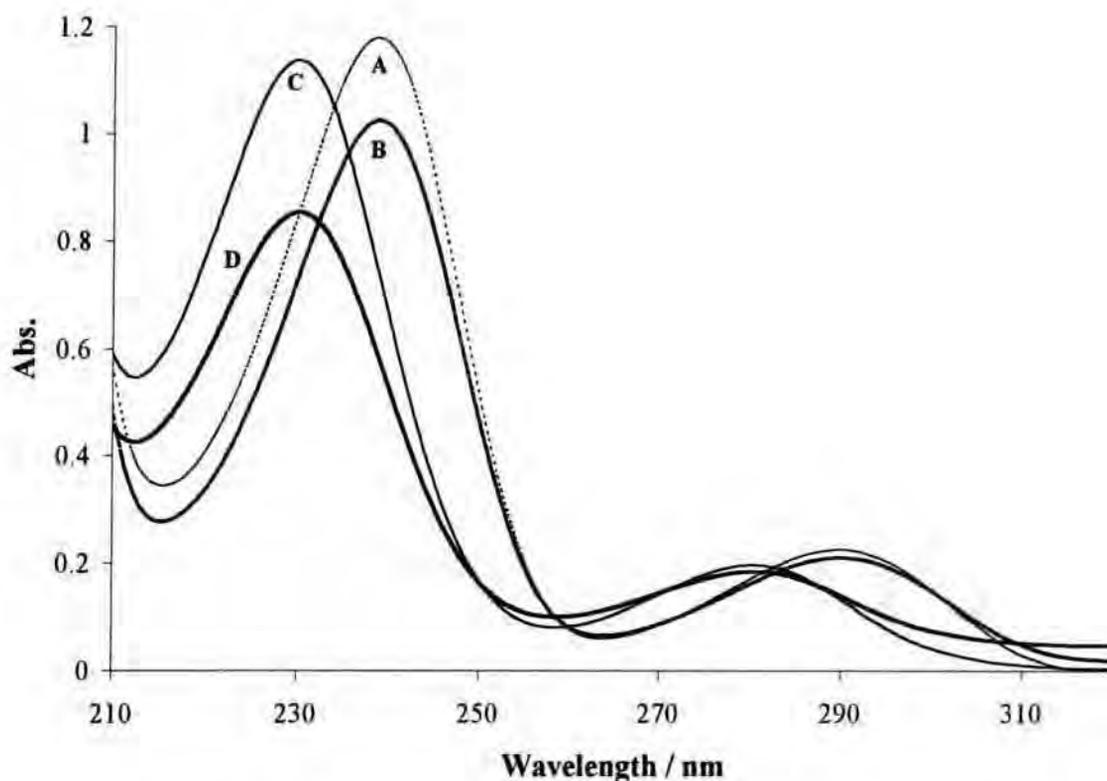| δ / ppm	multiplicity	integral ratio	coupling / Hz	assignment
7.90	t	1	5.0	N=CH(Et)
7.36	t	2	7.5	Ar-H$_3$, H$_5$
7.21	t	1	7.5	Ar-H$_4$
7.03	d	2	7.5	Ar-H$_2$, H$_6$
1.81	quintet	2	7.5	N=CHCH$_2$CH$_3$
1.19	t	3	7.5	N=CHCH$_2$CH$_3$

There is evidence for formation of the imine from aniline and propanal, but the reaction does not go to completion. An equilibrium constant for formation could not be obtained, as there was evidence for some decomposition of the unreacted propanal. Secondary reactions were

possible due to the acidity of solution, since the system was not buffered, leading to a reaction pH of *ca.* 3.5. Reactions that might occur at this pH are; aldol condensation, proton/deuterium exchange on methylene carbon in propanal, due to internal rearrangement of the double bond, and lastly, formation of the carbinolamine analogous to this reaction.

4.2.2: UV/Vis spectrometric studies

The same reaction to produce the imine from aniline and propanal was observed by UV/Vis spectrometry. From the knowledge of the ^{1}H NMR observations, aniline and propanal were mixed in 0.2 mol dm^{-3} concentrations in acetonitrile. Dilution of this solution to 1×10^{-4} mol dm^{-3} was firstly made in acetonitrile and secondly, in water, in order to observe the effect of solvent. The spectra of aniline at the same, 1×10^{-4} mol dm^{-3}, concentration in both acetonitrile and water, are shown for comparison; all four plots are illustrated in figure 4.2. Extinction coefficients with the respective λ_{max} for all spectra are shown in table 4.4. Propanal does not absorb greatly in the areas of observation.

Figure 4.2: UV/Vis spectra of the aniline/propanal imine 1×10^{-4} mol dm^{-3} in acetroniltrile as well as water, with spectra of aniline 1×10^{-4} mol dm^{-3} in both solvents

A = Aniline 1×10^{-4} mol dm^{-3} (CH$_3$CN); B = Imine 1×10^{-4} mol dm^{-3} (CH$_3$CN); C = Aniline 1×10^{-4} mol dm^{-3} (H$_2$O); D = Imine 1×10^{-4} mol dm^{-3} (H$_2$O)

Table 4.4: λ_{max} values with the extinction coefficients of all peaks shown in figure 4.2

Species	Solvent	λ_{max} with the extinction coefficient, ε
Aniline	CH$_3$CN	(239nm), ε = 11800 / (290nm), ε = 2250
Imine	CH$_3$CN	(239nm), ε = 10240 / (290nm), ε = 2100
Aniline	H$_2$O	(230nm), ε = 11400 / (280nm), ε = 1970
Imine	H$_2$O	(230nm), ε = 8550 / (280nm), ε = 1850

Figure 4.2 shows quite a large solvent effect, when changing from acetonitrile to water. As discussed in chapter 1, imines undergo ready hydrolysis. Evidence for hydrolysis was

obtained by observing the spectral changes over time of the imine in water. The hydrolysis reaction of 1×10^{-4} mol dm^{-3} imine was observed over 6 hours. Figure 4.3 shows the spectral change over this time together with a spectrum of aniline, at the same concentration.

Figure 4.3: Spectral plots for the hydrolsis of the aniline/propanal imine 1×10^{-4} mol dm^{-3} over 6 hours, with a spectrum of aniline 1×10^{-4} mol dm^{-3}
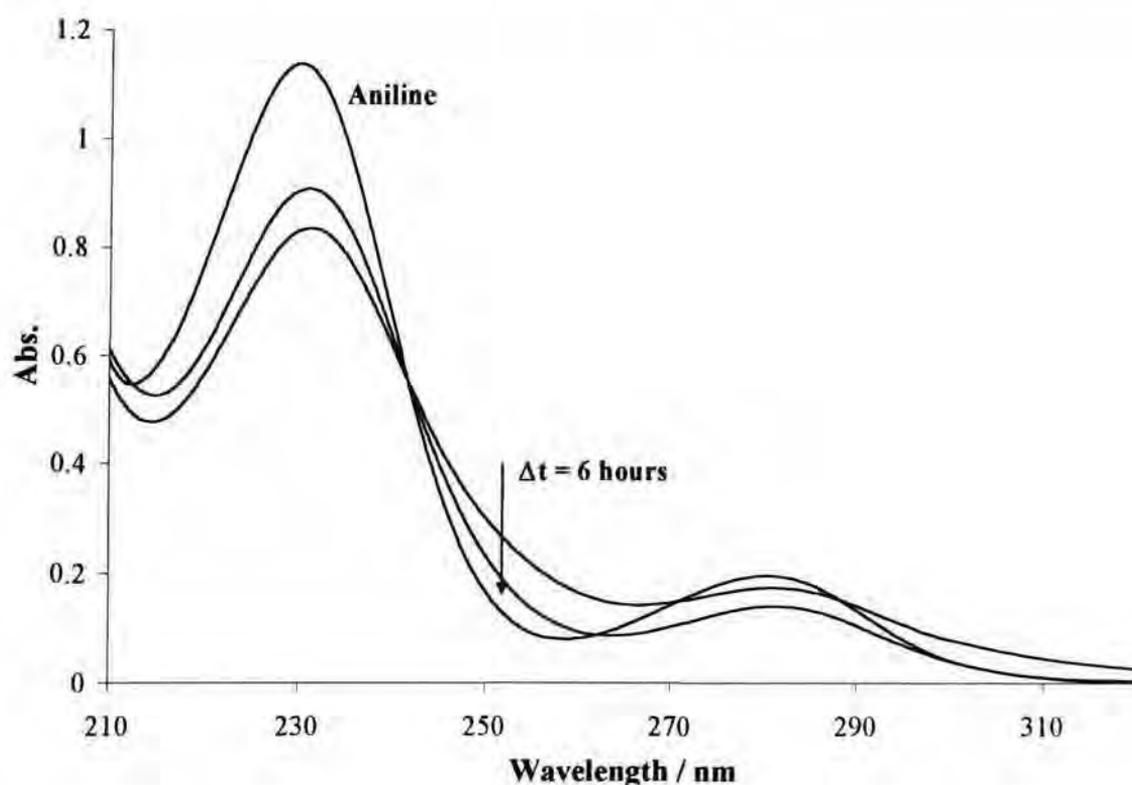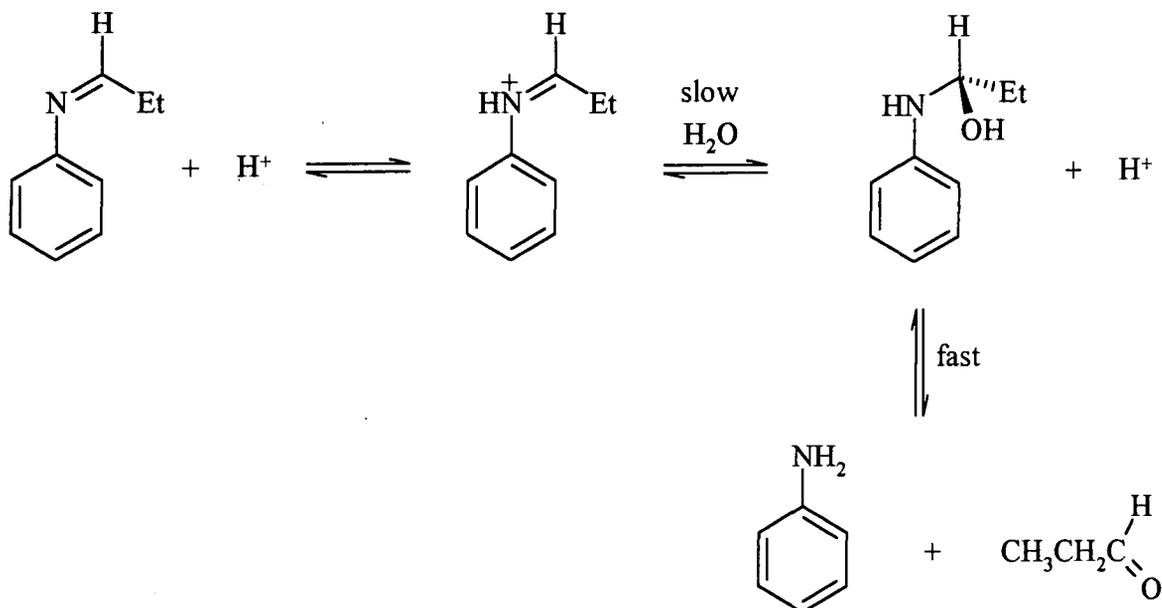

Table 4.5: λ_{max} values with the extinction coefficients of all peaks shown in figure 4.3

Species	λ_{max} with the extinction coefficient, ε
Imine + H_2O (0 mins)	(231nm), $\varepsilon = 8350$ / (281nm), $\varepsilon = 1750$
Imine + H_2O (6 hrs)	(231nm), $\varepsilon = 9080$ / (281nm), $\varepsilon = 1400$
Aniline	(230nm), $\varepsilon = 11400$ / (280nm), $\varepsilon = 1970$

The hydrolysis is clearly not complete, as the imine should eventually revert back to reactants, and in this case, aniline and propanal. The pH of this system was found to be <4, and a proposed mechanism for the hydrolysis of this imine can be seen in scheme 4.2.

Scheme 4.2:

Despite hydrolysis of the imine having being shown to occur, it was decided not to investigate this process in detail, but to study the reaction in the presence of sulfite ions.
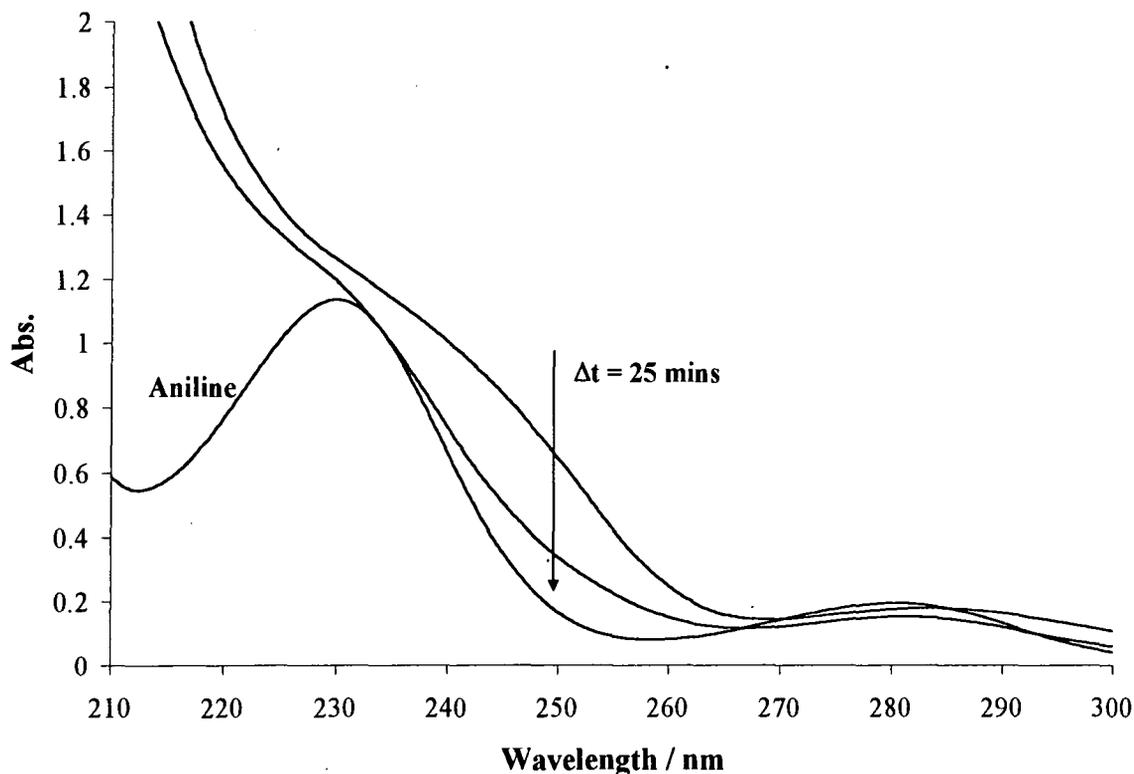
4.3: Reaction with sulifte

4.3.1: Initial Studies

^{1}H NMR studies of the reactions of imine with sulfite were not attempted, due to hydrolysis being too much of a factor at the necessarily high imine concentrations required. Imine concentrations, when studying its formation, were 0.2 mol dm^{-3}, compared to UV/Vis spectroscopy observations at 1x10^{-4} mol dm^{-3}. The other major limiting factor was the lack of

solubility for sulfite in acetonitrile, which precluded studies in acetonitrile rich solvent systems.

Initial UV/Visible studies showed that reaction with sulfite in a tenfold excess caused a relatively quick decomposition. Figure 4.4 shows a spectral plot for the reaction of imine 1×10^{-4} mol dm^{-3} with 5×10^{-3} mol dm^{-3} sodium sulfite initially and after 25 minutes. A spectrum of aniline 1×10^{-4} mol dm^{-3} is also shown.

Figure 4.4: Spectra plots of 1×10^{-4} mol dm^{-3} aniline, imine 1×10^{-4} mol dm^{-3} reacted with 5×10^{-3} mol dm^{-3} sodium bisulfite initially and after 25 minutes, in an aqueous pH 7 buffer solutions

The spectrum initially obtained on mixing the imine with excess sulfite, is not that of the imine alone. Comparison with the spectra in figure 3.9, indicates that there is an initial rapid reaction to yield anilinopropanesulfonates with absorbance at 250nm. Slowly, decomposition

occurs, so that the eventual spectrum is consistent with regeneration of aniline. Measurements were made at 250nm, where the largest change in absorbance occurred.
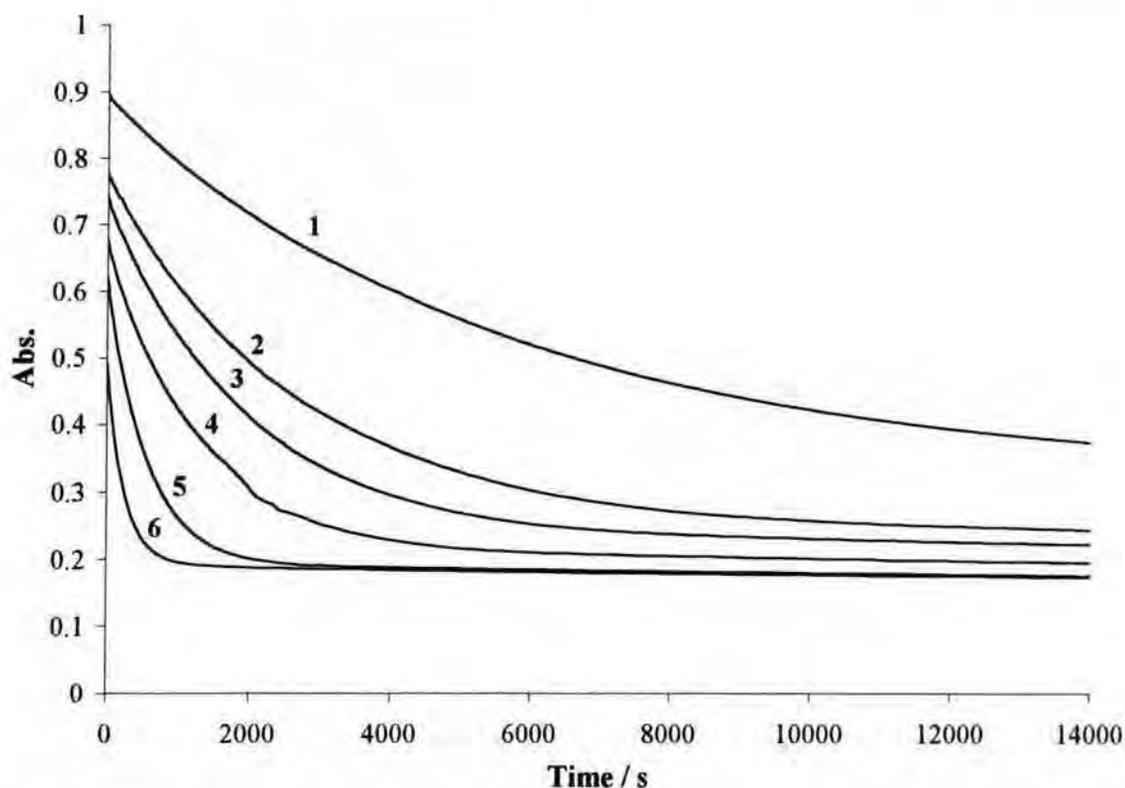
4.3.2: Determination of $k_r[SO_3^{2-}]_{stoich}$

The reaction of imine 1×10^{-4} mol dm^{-3} with sodium sulfite (or bisulfite depending on pH) in varying concentrations was measured, with a number of buffers at different pH, with the ionic strength kept constant at KCl 0.1 mol dm^{-3}. The imine was made initially, with equimolar propanal and aniline 0.2 mol dm^{-3} in acetonitrile. Further dilution was made in acetonitrile, so that the aliquot needed for reaction was small enough to ensure that the ratio of acetonitrile to water in the final solution was very small. However, this ratio was constant for all reactions carried out.

At the very low concentration of imine used, 1×10^{-4} mol dm^{-3}, the concentration of aniline and propanal produced by hydrolysis will also be very small. Hence, the forward reaction will involve a negligible contribution to the overall velocity, allowing the reverse reaction to be isolated.

Reactions were carried out over a pH range of 5.8 to 10.8. The reaction at pH 6.6 will now be discussed in detail. Figure 4.5 shows the absorbance versus time plots for the first order decomposition reaction of 1×10^{-4} mol dm^{-3} imine with sodium bisulfite 1×10^{-3} to 0.02 mol dm^{-3}, with a pH 6.6 buffer and with I = 0.1 mol dm^{-3}. Curves obeyed good first order behaviour and the k_{obs} values obtained, are shown in table 4.6, together with values calculated for $k_{obs}[SO_3^{2-}]_{stoich}$. These values were calculated, by multiplying values obtained from the first order fits with the stoichiometric concentration of sulfite, for that particular reaction. These values should show good consistency and the mean can be expressed, as the term $k_r[SO_3^{2-}]_{stoich}$.

Figure 4.5: Absorbance versus time plots for the reaction of imine 1×10^{-4} mol dm^{-3} and sodium bisulfite 1×10^{-3} to 0.02 mol dm^{-3}, with a pH 6.6 buffer, I = 0.1 mol dm^{-3}

1 = sodium bisulfite 0.02 mol dm^{-3}; 2 = 0.01 mol dm^{-3}; 3 = 0.0075 mol dm^{-3}; 4 = 0.005 mol dm^{-3}; 5 = 0.0025 mol dm^{-3}; 6 = 0.001 mol dm^{-3}

Table 4.6: Values calculated for k_{obs} and $k_{obs}[SO_3^{2-}]_{stoich}$ at varying sodium sulfite concentrations, at pH 6.6, I = 0.1 mol dm^{-3}

[NaHSO$_3$] / mol dm^{-3}	ΔAbs	k_{obs} / 10^{-4} s^{-1}	$k_{obs}[SO_3^{2-}]_{stoich}$ / 10^{-6} mol dm^{-3} s^{-1}
0.001	0.296	39.5	3.95
0.0025	0.426	17.4	4.36
0.005	0.461	7.43	3.71
0.0075	0.504	5.07	3.80
0.01	0.524	3.65	3.65
0.02	0.555	1.80	3.60

The mean value for the reaction at pH 6.6, is 3.85×10^{-6} mol dm^{-3} s^{-1}, giving the value for $k_r[SO_3^{2-}]_{stoich}$ at this acidity. Values obtained at other pH are shown in table 4.7. These $k_r[SO_3^{2-}]_{stoich}$ values were plotted against pH (figure 4.6), along with superimposed fits obtained from equation 3.17. As in chapter 3, two fits were attempted, one where the K_a^{HSO3-} value is allowed to vary, hence the best fit is obtained, and secondly, where the acid dissociation constant of bisulfite is kept at the known constant[1] 8.0×10^{-8} mol dm^{-3}.

Table 4.7: Values obtained for $k_r[SO_3^{2-}]_{stoich}$ / mol dm^{-3} s^{-1} at varying pH

pH	$k_r[SO_3^{2-}]_{stoich}$ / 10^{-6} mol dm^{-3} s^{-1}
5.8	8.56
6.3	5.48
6.6	3.85
7.0	2.57
7.5	1.94
8.3	1.81
8.5	2.18
8.9	2.22
9.0	2.40
9.6	2.50
9.9	3.15
10.4	4.80
10.8	7.10

The effects of varying the ionic strength were examined, by changing the concentration of added potassium chloride. Values obtained at pH 9.7 are shown in table 4.8. They indicate no large ionic strength effects, with the possibility of somewhat higher values, at higher ionic strength.

Table 4.8: Effects of ionic strength on the value of $k_r[SO_3^{2-}]_{stoich}$ at pH 9.7

$[SO_3^{2-}]_{stoich}$ / mol dm^{-3}	$I^{\dagger}$ / mol dm^{-3}	$K_{obs}[SO_3^{2-}]_{stoich}$ / 10^{-6} mol dm^{-3} s^{-1}
0.006	0.05	5.4
0.010	0.05	5.2
0.006	0.10	6.0
0.010	0.10	6.0
0.006	0.20	(8.9)
0.010	0.20	6.8

$\dagger$ $I = \sum \frac{1}{2}.c_i.z_i^2$ *(Ref 2)* *KCl is the added electrolyte*

Figure 4.6: Plot of $k_r[SO_3^{2-}]_{stoich}$ / mol dm^{-3} s^{-1} versus pH, with superimposed fits obtained from equation 3.17

The two fits as stated, were constructed using equation 3.17. As in chapter 3, values for the individual rate and equilibrium constants cannot be obtained independently. Hence, values for the term k_{-3}''/K_4 are shown. The best fit line (dashed line), where K_a^{HSO3-} treated as a variable, gave a value of 3.99×10^{-7} mol dm^{-3} for the acid dissociation, and a value of 2.05×10^{-6} mol dm^{-3} s^{-1} for k_{-3}''/K_4. Since the value for K_a^{HSO3-} is known, 8.0×10^{-8} mol dm^{-3}, the full line, was fitted with this value fixed; the resultant value for k_{-3}''/K_4 was found to be 2.00×10^{-6} mol dm^{-3} s^{-1}.

In the range pH 5.8 – 9.5, the results in figure 4.6 are in good agreement with those shown in figure 3.15 and obtained, starting from aniline and HPS. The independence of the "reverse" term, $k_r[SO_3^{2-}]_{stoich}$, on pH in the range 7 – 9.5 is in accord with the rate limiting reaction of the iminium ion with water. The results in the pH range 10 – 11 shown in figure 4.6 indicate increases in value of the rate term, with increasing pH. These increases may be attributed to a contribution to the reverse term from the reaction of hydroxide ions with the iminium ion (the k_{-3}' term in scheme 3.4).

4.4: Acidity dependence

The results obtained in chapter 3 for the $k_f[SO_3^{2-}]_{stoich}$ and $k_r[SO_3^{2-}]_{stoich}$ terms, and those presented in this chapter for the reverse term, have been discussed in terms of rate determining acid catalysed dehydration of the carbinolamine. This assumption leads to equations 3.11 and 3.17, respectively. In agreement with expectation, the values obtained experimentally, are independent of acidity when pH > 7. However, experimental values are lower than those predicted, when pH < 7. The possible explanations for this, in terms of mechanism, are now considered.

4.4.1: Uncatalysed dehydration of the carbinolamine is rate limiting (scheme 3.4)

This corresponds to reaction of the iminium ion, with hydroxide being rate-limiting in the reverse direction. This leads, from equation (3.10), to equation 4.1 for the forward term and to equation 4.2, for the reverse term.

$$k_f[SO_3^{2-}]_{stoich} = k_3' \, K_1 K_2 K_a \left(\frac{[H^+] + K_a^{HSO_3^-}}{[H^+] \, K_a^{HSO_3^-}} \right)$$

$$(4.1)$$

$$k_r[SO_3^{2-}]_{stoich} = k'_{-3} \frac{K_w}{K_4} \left(\frac{[H^+] + K_a^{HSO_3^-}}{[H^+] K_a^{HSO_3^-}} \right)$$

(4.2)

These expressions predict, that above pH 7, where $K_a^{HSO3-} > [H^+]$, values should be inversely proportional to $[H^+]$. There is evidence from figure 4.6 that at pH values greater than 10, this becomes true. However, between 7< pH > 10 the values are independent of pH.

The expressions also predict, that below pH 7, where $K_a^{HSO3-} < [H^+]$, the values should become independent of pH. The results presented in chapter 3 and in figure 4.6, do show that using the known value for K_a^{HSO3-} (8×10^{-8} mol dm^{-3}), experimental values are lower that these predicted by equation 3.11 and 3.17 and do tend to level off. However, it is unrealistic to postulate that the rate limiting step should change from acid catalysed dehydration of the carbinolamine, to uncatalysed dehydration with increasing acidity. This would correspond in the reverse reaction, to reaction of the iminium ion with hydroxide ions becoming more important with increasing acidity.

Therefore, the acidity dependence below pH 7 cannot be attributed to a change to uncatalysed dehydration of the carbinolamine.

4.4.2: Reaction of the amine with propanal is rate limiting (scheme 3.3)

This leads to equation 4.3 for the forward reaction. Assuming that propanal and HPS are in rapid equilibrium, and writing the expression in terms of the stoichiometric sulfite concentration leads to equation 4.4.

$$v_f = k_2[\text{aniline}][\text{propanal}]_{\text{free}}$$

(4.3)

$$k_f[SO_3^{2-}]_{stoich} = k_2 K_1 K_a \left(\frac{[H^+] + K_a^{HSO_3^-}}{[H^+] K_a^{HSO_3^-}} \right)$$

(4.4)

Similarly, assuming that cleavage of the carbinolamine to give aniline and propanal is the rate limiting, leads to equations 4.5 and 4.6 for the reverse reaction, where [COH] is the concentration of the carbinolamine.

$$v_r = k_{-2}[COH] \tag{4.5}$$

$$k_r[SO_3^{2-}]_{stoich} = \frac{k_{-2}}{K_3 K_4} \left(\frac{[H^+] + K_a^{HSO_3^-}}{[H^+] \, K_a^{HSO_3^-}} \right) \tag{4.6}$$

Equations 4.4 and 4.6 show a similar acidity dependence. Above pH 7, there is an inverse dependence on [H⁺]. Below pH 7, values are predicted to be independent of pH. Clearly, the acidity dependence above pH 7 is not that found experimentally. However, below pH 7, experimental values do tend to linearity as can be seen by examination of figures 3.22, 3.23, 3.26, 3.27, and 3.29.

Thus, the most reasonable explanation of the experimental results is that a change in rate-limiting step occurs in the pH region 6 -7. At higher pH values, acid catalysed dehydration of the carbinolamine is the slow step. At lower pH values, the reaction of aniline with propanal is rate determining.

The results in chapter 3 give values for one term of $k_f[SO_3^{2-}]_{stoich}$ at pH 4.7 – 5.0. At this pH, equation 4.4 will reduce to equation 4.7.

$$k_f[SO_3^{2-}]_{stoich} = \frac{k_2 K_1 K_a}{K_a^{HSO_3^-}} \tag{4.7}$$

K_1 corresponds to dissociation of the dianionic form of HPS and is equivalent to the value of $1/K_2$, as defined in chapter 2; the value is 0.0105 mol dm⁻³. The value of K_a is 2.0×10^{-11} mol

dm^{-3}, also available from the results in chapter 2. Using these values together, with a value for K_a^{HSO3-} of 8×10^{-8} mol dm^{-3}, leads to the values of k_2 given in table 4.9.

Table 4.9: Values at pH 4.7 – 5.0 for the forward and reverse reactions, and values calculated for k_2

$(R)C_6H_4NH_2$	$k_f[SO_3^{2-}]_{stoich} / 10^{-4} s^{-1}$	$k_r[SO_3^{2-}]_{stoich} / 10^{-6} s^{-1}$	$k_2^{\dagger} / dm^3 mol^{-1} s^{-1}$
4 – Me	20	40	760
H	14	18	530
4 – Cl	5.0	9.0	190
3 – Cl	3.0	4.3	110
3 – CN	1.3	1.0	50
3 – NO_2	1.0	0.74	38

† *calculation from equation 4.7 with K_1 0.0105 mol dm^{-3}, K_a 2.0×10^{-11} mol dm^{-3}, and K_a^{HSO3-}*
8.0×10^{-8} mol dm^{-3}

It is of interest to compare the values obtained for k_2, with those for the corresponding reactions of aniline with formaldehyde[3]. These range from 8.0×10^3 dm^3 mol^{-1} s^{-1} for R = 3-NO_2, to 2.4×10^5 dm^3 mol^{-1} s^{-1} for R = 4-Me. The dependence in the substituent, R, is similar for the two processes, but values are *ca.* 250 times larger for reaction of formaldehyde. This is reasonable in view of the results presented in chapter 2, which show that nucleophilic attack on formaldehyde, is a considerably faster process, than on propanal. This gives confidence that the values calculated in table 4.9 do indeed represent k_2, and that this is the rate-limiting step at pH 4.7 – 5.0.

There is evidence[3, 4] that carbinolamine formation may be subject to weak general acid catalysis. However, at the relatively low buffer concentrations used in this work, acid catalysis of the k_2 step is unlikely to be very important.

The values of $k_r[SO_3^{2-}]_{stoich}$ in table 4.9 will correspond to the reverse term, as shown in equation 4.8.

$$k_r[SO_3^{2-}]_{stoich} = \frac{k_{-2}}{K_3 K_4 K_a^{HSO_3^-}}$$

<div align="right">(4.8)</div>

Nevertheless, since values of K_3 and K_4 are not known, it is not possible to obtain values for k_{-2}. However, the dependence of the reverse term on the nature of the substituents, R, is similar to that observed for the forward rate term. This indicates that values of the equilibrium constant, K_2, will not depend strongly on the nature of R. Similar behaviour was observed in the formation of carbinolamine from anilines and formaldehyde.

The overall conclusion is that the rate-limiting step changes from carbinolamine formation to carbinolamine dehydration, in the pH range 6 – 7. It should be noted that the observed dependence on sulfite concentration, showing that the value of the $k_f[SO_3^{2-}]_{stoich}$ and $k_r[SO_3^{2-}]_{stoich}$ terms are independent of sulfite concentration, is not consistent with the rate determining step, being either dissociation of HPS (the k_1 step), or reaction of the iminium ion with sulfite (the k_4 step).

4.5: References

1) (a) G. L. Kok, S. N. Gitlin and A. L. Lazrus, *J. Geophys. Res.,D*, 1986, **91**, 2801; (b) E. Haydon, A. Treinin and J. Wilf, *J. Am. Chem. Soc.*, 1972, **94**, 47; (c) V. H. Tartar and H. H. Garretson, *ibid.*, 1941, **63**, 808

2) P. W. Atkins, 'Physical Chemistry', Oxford University Press, 4th Ed. p.251

3) J. H. Atherton, K. H. Brown and M. R. Crampton, *J. Chem. Soc. Perkin Trans. 2*, 2000, 941

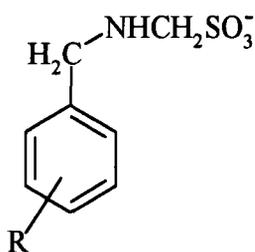4) E. H. Cordes and W. P. Jencks, *J. Am. Chem. Soc.*, 1962, **84**, 4319

Chapter five

5 Reaction of hydroxymethanesulfonate, HMS, with benzylamine and benzylamine derivatives
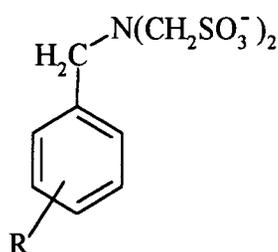
5.1: Introduction

5.1.1: Previous studies

To date, only one study has been reported of the reactions of hydroxymethanesulfonate, HMS, with benzylamine and its derivatives. Brown[1] observed the formation of adducts **5.1**, with 1:1 stoichiometry, and **5.2**, with 1:2 stoichiometry, using ^{1}H NMR spectroscopy.

5.1   **5.2**

Measurements were also made to gauge the effects of electron donation and withdrawal using N-methylbenzylamine and ring substituted benzylamines, (R = OMe, Me, NO$_2$). The formation of the 1:2 adducts, which contrasts with reactions involving aniline where only 1:1 adducts were observed, may be attributed to the greater basicity of benzylamine. Some initial kinetic and equilibrium measurements were made using UV/Vis spectroscopy. Results are summarised in table 5.1. In these measurements no sulfite was added, so that the concentration of free sulfite is uncertain. This means that the values obtained for k_f^* and k_b are of uncertain reliability. They will, as in the case of aniline, be expected to be strongly dependent on the sulfite concentration. Nevertheless, the values obtained for K* should be independent of sulfite concentration and hence should be reliable.

Table 5.1: Rate and equilibium constants[1] for the reaction of HMS with benzylamine and benzylamine derivatives (4-RC$_6$H$_4$CH$_2$NHR') obtained at 25 °C

R	R'	pH	k_f*/ dm^3 mol^{-1} s^{-1}	k_b/ s^{-1}	K $*$/ dm^3 mol^{-1}
H	H	unbuffered	$(8.2 \pm 0.3) \times 10^{-3}$	$(1.0 \pm 0.2) \times 10^{-4}$	80 ± 10
-OCH$_3$	H	7.0	$1.1 \times 10^{-3} \pm 9 \times 10^{-6}$	$1.6 \times 10^{-4} \pm 5 \times 10^{-7}$	6.8 ± 0.1
		8.1	$1.3 \times 10^{-2} \pm 4 \times 10^{-5}$	$(1.5 \pm 0.03) \times 10^{-4}$	86 ± 2
		8.9	$(1.7 \pm 0.01) \times 10^{-2}$	$(2.2 \pm 0.07) \times 10^{-4}$	77 ± 3
		10.1	$(1.7 \pm 0.02) \times 10^{-2}$	$(1.8 \pm 0.09) \times 10^{-4}$	93 ± 5
-CH$_3$	H	7.0	$(5.4 \pm 0.5) \times 10^{-3}$	$(3.8 \pm 3) \times 10^{-5}$	140 ± 120
-NO$_2$	H	7.0	$(9.9 \pm 3) \times 10^{-4}$	$(9.2 \pm 2) \times 10^{-5}$	11 ± 4
H	-CH$_3$	7.0	$(1.2 \pm 0.08) \times 10^{-3}$	$(3.6 \pm 0.5) \times 10^{-5}$	33 ± 3

The values of k_f* and K$*$ in table 5.1 are written in terms of the stoichiometric amine concentration. At the pH values studied the amine will be partially protonated. Since reaction with HMS is likely to involve only the free amine the values will be expected to decrease with increasing acidity. This can be seen in the data for 4-methoxybenzylamine. Values of k_f and K for reaction with the free amine, are related to values of k_f* and K$*$ by equations 5.2 and 5.3.

$$K^* = \frac{k_f^*}{k_b} = \frac{[RC_6H_4CH_2NHCH_2SO_3^-]}{[RC_6H_4CH_2NHR']_{stoich}[CH_2(OH)(SO_3^-)]}$$

(5.1)
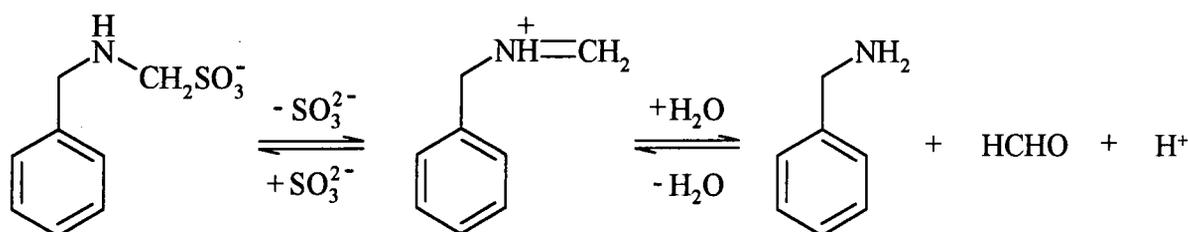
$$K = K^* \frac{K_a + [H^+]}{K_a}$$

(5.2)

$$k_f = k_f^* \frac{K_a + [H^+]}{K_a}$$

(5.3)

Some problems were encountered in these studies, for example, in the reaction of HMS with N-methylbenzylamine, where only a single adduct should be possible, two time dependent processes were observed in the UV/Vis spectra.

Further studies were made by Brown[1] on the decomposition of 1:1 adducts formed by reaction of HMS and benzylamine in equimolar amounts. The first step in the decomposition, scheme 5.1, involves release of sulfite to give an iminium ion. The free sulfite reacts irreversibly with iodine in a reaction which is zero-order with respect to iodine. This led to the evaluation of values for k, the rate constant for release of sulfite.

Scheme 5.1:

The pH dependence of the observed values for k was interesting. Above pH 6, values were independent of acidity. However at lower pH values there was a linear dependence in value of Log k with pH. This was attributed to protonation of the adduct, which inhibits sulfite expulsion. Values of the pK_a were found to be between 5.4 and 5.6 for the ring substituted benzylamines and 4.9 for N-methylbenzylamine. The low value obtained here was attributed to the steric effects of the methyl group resulting in a reduction in solvation of the protonated nitrogen.
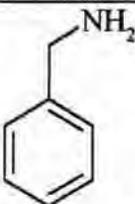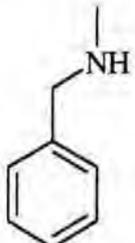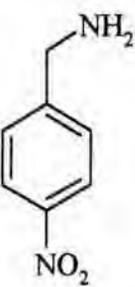
5.1.2: Present studies

1H NMR spectroscopy was used to measure the values of equilibrium constants for the reaction of benzylamine with HMS over a wide pH range. This was possible since separate bands were observed for the parent amine and for the 1:1 and 1:2 adducts. Therefore, using

integral intensities the relative concentrations of reactants and products could be determined. These measurements were thought to be useful to reinforce previous work[1].

The amines studied are shown in table 5.2. Investigations were primarily with benzylamine, which gave both 1:1 and 1:2 adducts; subsequent studies were with N-methylbenzylamine which could only produce the 1:1 adduct. Later studies involved 4-nitrobenzylamine, where, contrary to a previous report, formation of the 1:2 adduct was observed.

Table 5.2: Amines[†] studied in the reactions with HMS

Amine			pK$_a$
Benzylamine		**5.1**	9.33
N-methylbenzylamine		**5.2**	9.59
4-nitrobenzylamine		**5.3**	8.50

[†] *pK$_a$ values correspond to dissociation of the protonated amines, 25 °C, ref 2*

The pH range in which studies were conducted was 5.5 to 10, and, since the pK$_a$ values of benzylamines studied were 8.50 to 9.59, the amines will be extensively protonated. The reactions are most likely to involve the free amine, and therefore, protonation will

substantially reduce the observed reactivity. The adducts formed by the reaction, are expected to have much lower pK_a values and will predominately exist as their unprotonated forms.

The equilibria associated with 1:1 adduct formation are shown in scheme 5.2. $K_{1:1}$ and $K_{1:1}*$ are defined in equations 5.4 and 5.5 and the stoichiometric concentrations of amine and adduct are related to the free concentrations as shown in equations 5.6 and 5.7.

Scheme 5.2:

$$K_{1:1} = \frac{[PhCH_2NHCH_2SO_3^-]}{[PhCH_2NH_2][CH_2(OH)(SO_3^-)]}$$

(5.4)

$$K_{1:1}* = \frac{[PhCH_2NH_2^+CH_2SO_3^-]}{[PhCH_2NH_3^+][CH_2(OH)(SO_3^-)]}$$

(5.5)

$$[PhCH_2NH_2]_{stoich} = [PhCH_2NH_2]\left(\frac{K_a + [H^+]}{K_a}\right)$$

(5.6)

$$[PhCH_2NHCH_2SO_3^-]_{stoich} = [PhCH_2NHCH_2SO_3^-]\left(\frac{K_a^{1:1} + [H^+]}{K_a^{1:1}}\right)$$

(5.7)

A stoichiometric equilibrium constant is defined in scheme 5.4 and equation 5.8. It is shown in equation 5.10 how this is related to the equilibrium constant $K_{1:1}$.

Scheme 5.4:

$$[PhCH_2NH_2]_{stoich} + CH_2(OH)(SO_3^-) \underset{}{\overset{K_{1:1}{}^{stoich}}{\rightleftharpoons}} [PhCH_2NHCH_2SO_3^-]_{stoich}$$

$$K_{1:1}{}^{stoich} = \frac{[PhCH_2NHCH_2SO_3^-]_{stoich}}{[PhCH_2NH_2]_{stoich}[CH_2(OH)(SO_3^-)]}$$

(5.8)

$$K_{1:1}{}^{stoich} = \frac{[PhCH_2NHCH_2SO_3^-]}{[PhCH_2NH_2][CH_2(OH)(SO_3^-)]}\left(\frac{K_a^{1:1} + [H^+]}{K_a^{1:1}}\right)\left(\frac{K_a}{K_a + [H^+]}\right)$$

(5.9)

$$K_{1:1}{}^{stoich} = K_{1:1}\left(\frac{K_a^{1:1} + [H^+]}{K_a^{1:1}}\right)\left(\frac{K_a}{K_a + [H^+]}\right)$$

(5.10)

For most of the pH range studied, $K_a^{1:1}$ is likely to be larger than the proton concentration, and therefore, its bracketed term, becomes unity and hence, can be cancelled. Hence when $[H^+] >$

K_a, i.e. lower than pH 9, equation 5.10 reduces to equation 5.11, indicating an inverse dependence upon acidity.

$$K_{1:1}{}^{stoich} = K_{1:1} \frac{K_a}{[H^+]}$$

(5.11)

However, in alkaline solutions where the proton concentration is smaller than the acid dissociation constant for the amine, the term $K_{1:1}{}^{stoich}$ becomes equal to $K_{1:1}$.

It was necessary to use deuterium oxide, D_2O, for ^1H NMR measurements. All buffers, phosphate or acetate, were made up in the usual way using the concentrations (both equalled 0.2 mol dm^{-3} in the NMR tube) appropriate for solutions in H_2O, and 'pH' values were measured using a conventional glass electrode.

Coetzee and Ritchie[3] have shown that the relationship between the 'operationa pH', measured in the conventional way with a glass electrode and aqueous reference solutions, and pD is,

$$pD = pH + 0.40$$

(5.12)

where pD measures the activity of D^+ ions. Hence pD values are about 0.4 units higher than the measured values.

However it is known[56] that for acidic species $pK_{BD+} > pK_{BH+}$ by about 0.5 units[4].

$$\Delta pK = pK_{aD} - pK_{aH} \sim 0.4 \sim 0.5$$

(5.13)

Hence there is compensation between these two effects, so that if 'operational pH' values are used in uncorrected form, then the values obtained will correspond to pK_{BH+} values.

Now that the relationship for the solvent systems is known, a plot for the theoretical trends that would be observed with formation of both the 1:1 and 1:2 adducts may be drawn.

214

Figure 5.1 shows the theoretical plot of $K_{1:1}^{stoich}$ versus acidity, derived from equation 5.10. The two plots represent the results for the different solvent systems, H_2O and D_2O. The dashed line, representing the deuterated solvent, has the sigmoidal shifted slightly to higher pH/pD values, compared to when observed in water, even though the trend remains.

Figure 5.1: Theoretical plot of $K_{1:1}^{stoich}$ versus pH/pD derived from equation 5.10

The equilibria associated with 1:2 formation are shown in scheme 5.5.

Scheme 5.5:

$$\text{PhCH}_2\text{–NH–CH}_2\text{SO}_3^- + \text{CH}_2(\text{OH})(\text{SO}_3^-) + \text{H}^+ \underset{K_{1:2}}{\rightleftharpoons} \text{PhCH}_2\text{–N}(\text{CH}_2\text{SO}_3^-)_2 + \text{H}^+ + \text{H}_2\text{O}$$

$$K_a^{1:1} \updownarrow \qquad\qquad\qquad\qquad\qquad K_a^{1:2} \updownarrow$$

$$\text{PhCH}_2\text{–}\overset{+}{\text{N}}\text{H}_2\text{–CH}_2\text{SO}_3^- + \text{CH}_2(\text{OH})(\text{SO}_3^-) \underset{K_{1:2}*}{\rightleftharpoons} \text{PhCH}_2\text{–}\overset{+}{\text{N}}\text{H}(\text{CH}_2\text{SO}_3^-)_2 + \text{H}_2\text{O}$$

If neither the 1:1 nor 1:2 adducts are appreciably protonated then the value of $K_{1:2}^{\text{stoich}}$, defined by equation 5.14, should be independent of pH.

$$K_{1:2}^{\text{stoich}} = \frac{[\text{PhCH}_2\text{N}(\text{CH}_2\text{SO}_3^-)_2]_{\text{stoich}}}{[\text{PhCH}_2\text{NHCH}_2\text{SO}_3^-]_{\text{stoich}}[\text{CH}_2(\text{OH})(\text{SO}_3^-)]}$$

$$(5.14)$$

Hence the predicted plot of $K_{1:2}^{\text{stoich}}$ versus pH/pD would show a line parallel to the x-axis with no variation with acidity. As described later the observed behaviour fits this pattern.

5.2: Results and discussion

5.2.1: Initial observations

Initially, it was thought necessary, to observe ${}^1\text{H}$ NMR spectra for all reagents. Spectra of HMS **(5.1)**, benzylamine **(5.2)**, N-methylbenzylamine **(5.3)** and 4-nitrobenzylamine **(5.4)** all

at 0.1 mol dm^{-3} in unbuffered D_2O solutions, were obtained. Figures 5.3 to 5.5 show spectra for the benzylamines, and peak assignment is show for all reagents in tables 5.3 to 5.6. In order to help with spectral assignments in the presence of HMS, a sample of benzylamine-α,α-d$_2$-N,N-d$_2$ was synthesised.

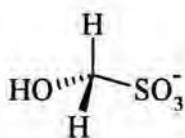### 5.2.1.1: Synthesis of benzylamine-α,α-d$_2$-N,N-d$_2$

Benzylamine-α,α-d$_2$-N,N-d$_2$ was prepared, as previously reported by Hamid[5]; with the procedure closely followed. The method involves reduction of benzonitrile with lithium aluminium deuteride, according to a modified procedure of Nystrom and Brown[6]. To avoid adventitious water the apparatus was set up, so that every opening to the atmosphere was protected with calcium chloride drying tubes. Lithium aluminium deuteride (1g, 0.024mol) was carefully added, as a solution in dry diethyl ether (40cm^3)(dried overnight with Calcium chloride). This was added dropwise over 45 minutes to benzonitrile (2.1g, 0.02mol), and dissolved also in dry diethyl ether (40cm^3), in a 250cm^3 round bottomed flask fitted with a reflux condenser and magnetic stirrer. Addition was maintained, so that the mixture was kept at gentle reflux. After the addition of the lithium aluminium deuteride was complete, reflux was continued for a further 30 minutes. D_2O (5-10ml) was then added dropwise, (exercising great care) with stirring and cooling of the mixture, in an ice-water bath to decompose the excess deuteride. The resultant solution was then filtered, and the precipitate was washed with diethyl ether. The filtrate was then dried with anhydrous sodium sulfate, before further filtration; evaporation of the ether on a rotary evaporator gave the product, a yellow-coloured liquid (2.04g, 96% yield). The ^1H NMR spectrum in D_2O reveals the absence of the benzyl hydrogen atoms, shown below in figure 5.2.

Figure 5.2: ^{1}H NMR spectrum of benzylamine-α,α-d${}_2$-N,N-d${}_2$ in DMSO

Table 5.3: ^{1}H NMR spectrum of benzylamine-α,α-d${}_2$-N,N-d${}_2$ in DMSO; peak assignment

δ / ppm	Multiplicity	Intensity	Assignment
7.3	m	5	Aromatic hydrogens
2.54	-	-	DMSO reference peak

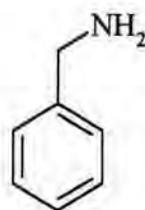### 5.2.1.2: ^{1}H NMR spectra for the reagents studied

Hydroxymethanesulfonate, HMS, **5.1**, produced a very simple spectrum with only peaks present for the methylene group and solvent peak, and thus, only peak assignment is shown.

$$HO^{\prime\prime\prime\prime} \overset{\displaystyle H}{\underset{\displaystyle H}{\diagdown\diagup}} SO_3^-$$

(5.1)

Table 5.4: ^{1}H NMR spectrum of HMS, **5.1**, 0.1 mol dm^{-3} in D$_2$O: peak assignment

δ / ppm	Multiplicity	Intensity	Assignment
4.67	-	-	H$_2$O
4.35	s	2	CH$_2$
3.29	-	-	Residual methanol

$$\underset{\text{(5.2)}}{\bigcirc\!\!\!\!\!\diagup^{NH_2}}$$
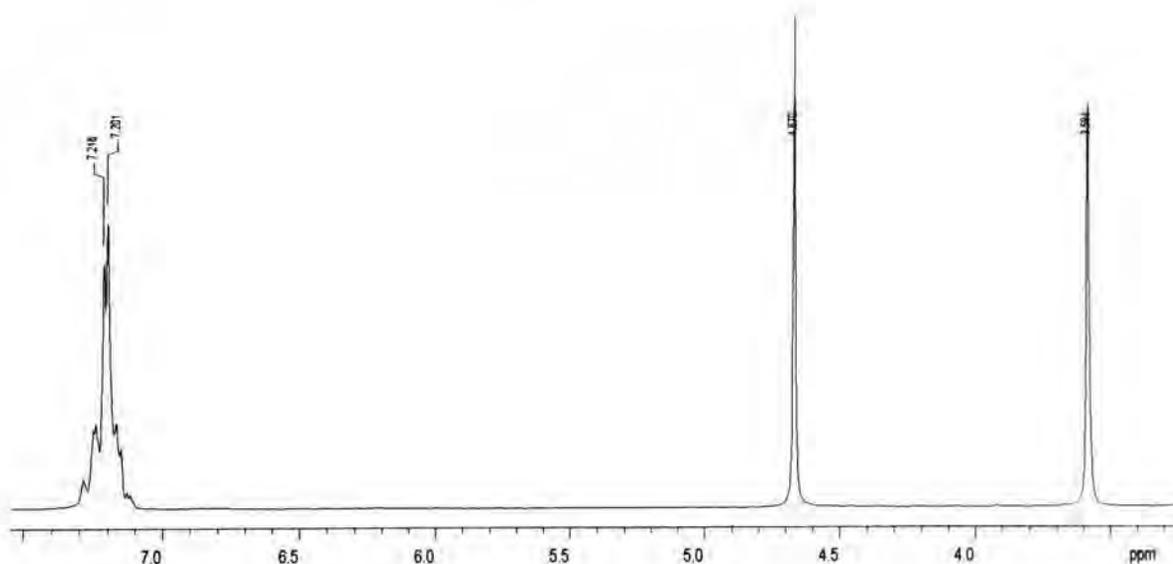
(5.2)

Figure 5.3: ^{1}H NMR spectrum of benzylamine, **5.2**, 0.1 mol dm^{-3} in D$_2$O

219

Table 5.5: ^{1}H NMR spectrum of benzylamine, **5.2**, 0.1 mol dm^{-3} in D$_2$O: peak assignment

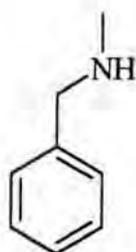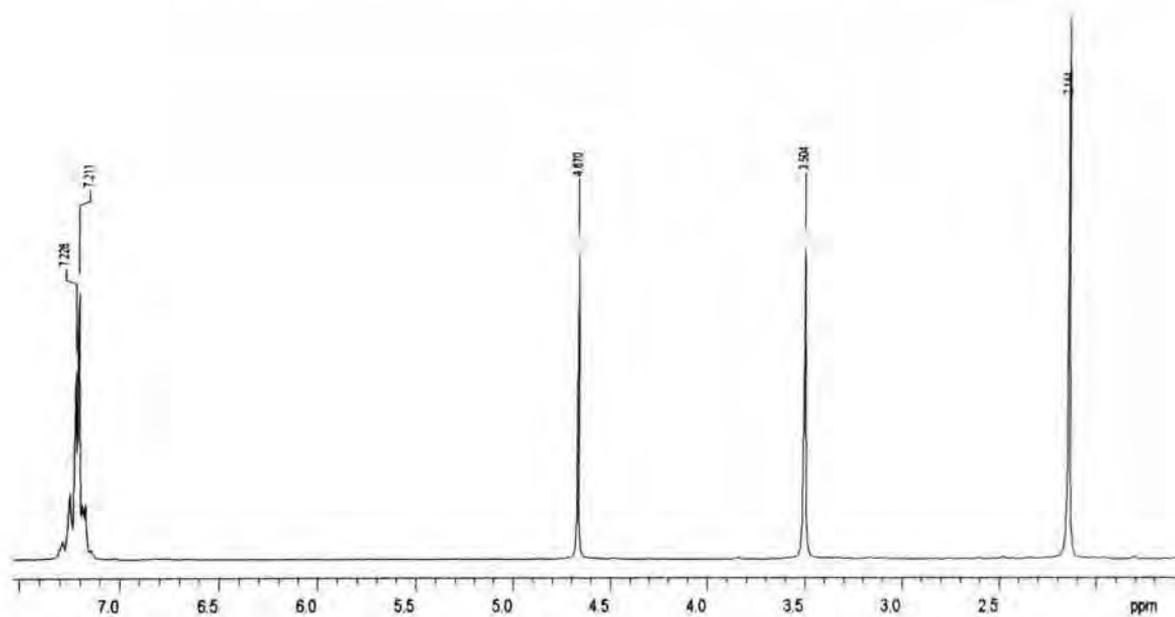| δ / ppm	Multiplicity	Intensity	Assignment
7.20	s	5	Aromatic protons
4.67	-	-	H$_2$O
3.58	s	2	-CH$_2$-NH$_2$

(5.3)

Figure 5.4: ^{1}H NMR spectrum of N-methylbenzylamine, **5.3**, 0.1 mol dm^{-3} in D$_2$O

Table 5.6: ^{1}H NMR spectrum of N-methylbenzylamine, **5.3**, 0.1 mol dm^{-3} in D$_2$O: peak assignment

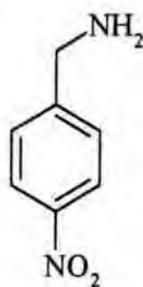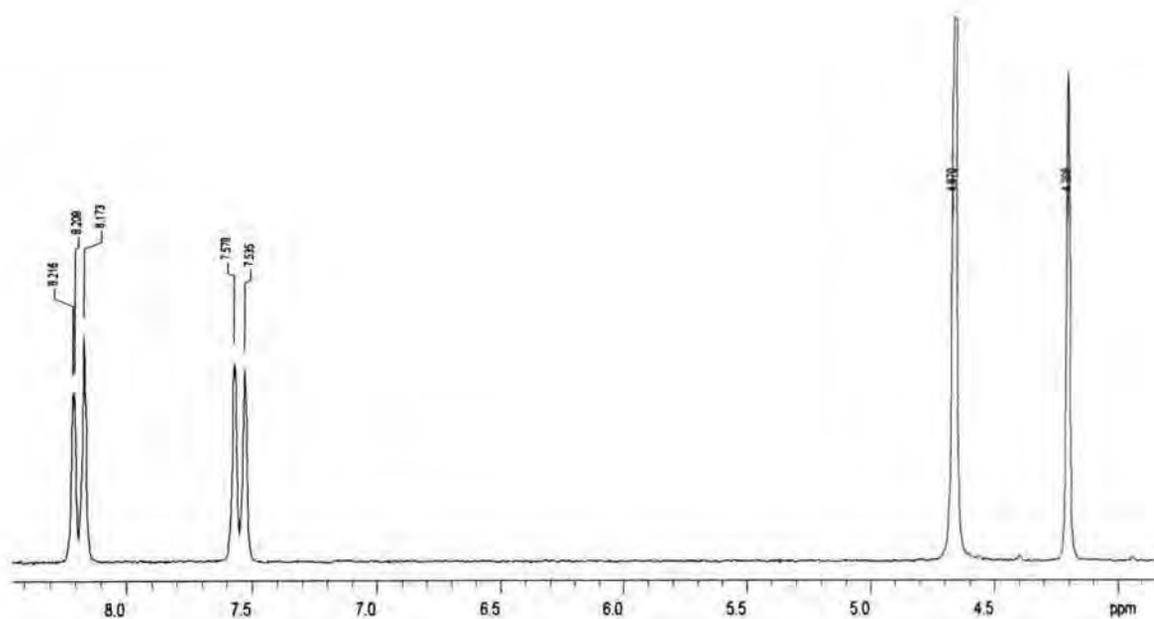| δ / ppm	Multiplicity	Intensity	Assignment
7.21	s	5	Aromatic protons
4.67	-	-	H$_2$O
3.50	s	2	-CH$_2$-N
2.14	s	3	CH$_3$-N

(5.4)

Figure 5.5: ^{1}H NMR spectrum of 4-nitrobenzylamine, **5.4**, 0.1 mol dm^{-3} in D$_2$O

Table 5.7: ^1H NMR spectrum of 4-nitrobenzylamine, **5.4**, 0.1 mol dm^{-3} in D$_2$O: peak assignment

δ / ppm	Multiplicity	J / Hz	Intensity	Assignment
8.19	d	8.5	2	Ar – H$_3$, H$_5$
7.56	d	8.5	2	Ar – H$_2$, H$_6$
4.67	-	-	-	H$_2$O
4.21	s	-	2	-CH$_2$-NH$_2$

5.2.2: Product spectra and equilibrium constants

Reactions observed, using ^1H NMR spectroscopy, were carried out, with HMS always being in at least a tenfold excess to the amine, in an attempt to observe peaks, which could give quantitative information. Spectra were recorded using buffers made up in deuterated solvents, over the pH range 5.8 to 10.2 (pD + 0.4 units greater). Spectra were taken at regular intervals, in order to quantify the processes occurring. Spectra for all reactions after 24 hours were recorded, so that the completed reaction spectrum could be obtained. Figures 5.6 to 5.9, show examples of the reactions of HMS with benzylamine, N-methylbenzylamine and 4-nitrobenzylamine respectively, after 30 minutes of reaction, and the peak assignment is shown in tables 5.8 to 5.10. the two types of CH$_2$ protons in the 1:1 adduct of benzylamine were distinguished using the spectra obtained from deutrated benzylamine.

Figure 5.6: ¹H NMR spectrum for the observed reaction of HMS (0.2 mol dm⁻³) and benzylamine, **5.2**, (2x10⁻² mol dm⁻³) with a pH 7.7 buffer in D_2O, after 30 minutes

Table 5.8: ¹H NMR spectrum for the observed reaction of HMS (0.2 mol dm⁻³) and benzylamine, **5.2**, (2x10⁻² mol dm⁻³) with a pH 7.7 buffer in D_2O, after 30 minutes: peak assignment

δ / ppm	Multiplicity	Intensity	Assignment
7.30	m	8.93	Aromatic hydrogens
4.67	-	-	H_2O
4.27	s	21.8	$CH_2(OH)(SO_3^-)$
4.20	s	1.84	$-CH_2-N(CH_2SO_3^-)_2$ (1:2 adduct)
4.03	s	1.26	$-CH_2-N$
3.99	s	3.67	$-CH_2-N(CH_2SO_3^-)_2$ (1:2 adduct)
3.87	s	1.47	$-CH_2-NHCH_2SO_3^-$ (1:1 adduct)
3.66	s	1.47	$-CH_2-NHCH_2SO_3^-$ (1:1 adduct)

223

Figure 5.7: ^{1}H NMR spectrum for the observed reaction of HMS (0.2 mol dm^{-3}) and N-methylbenzylamine, **5.3**, (1x10^{-2} mol dm^{-3}) with a pH 7.7 buffer in D$_2$O, after 30 minutes
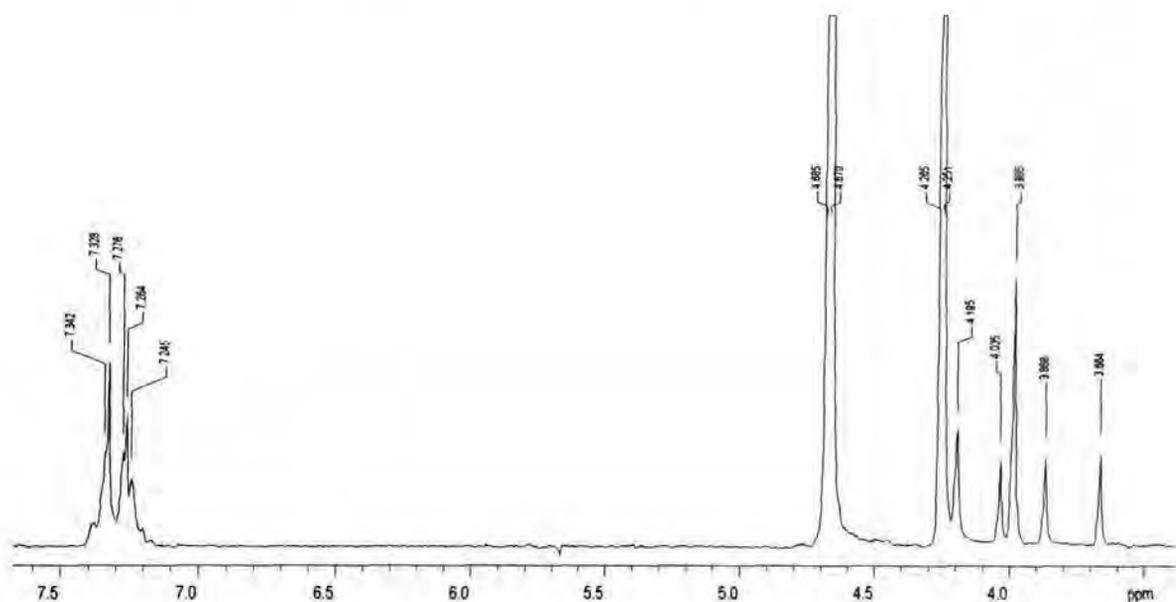

Table 5.9: ^{1}H NMR spectrum for the observed reaction of HMS (0.2 mol dm^{-3}) and N-methylbenzylamine, **5.3**, (1x10^{-2} mol dm^{-3}) with a pH 7.7 buffer in D$_2$O, after 30 minutes: peak assignment

δ / ppm	Multiplicity	Intensity	Assignment
7.34	m	5.61	Aromatic hydrogens
4.67	-	-	H$_2$O
4.25	s	35.59	CH$_2$(OH)(SO$_3^-$)
4.07	s	1.42	-CH$_2$-N
3.78	s	1.32	-CH$_2$N(CH$_3$)CH$_2$SO$_3^-$
3.69	s	1.32	-CH$_2$N(CH$_3$)CH$_2$SO$_3^-$
3.19	-	-	Residual methanol
2.55	s	2.19	CH$_3$-N
2.37	s	2.04	-CH$_2$N(CH$_3$)CH$_2$SO$_3^-$

Figure 5.8: ^{1}H NMR spectrum for the observed reaction of HMS (0.1 mol dm^{-3}) and 4-nitrobenzylamine, **5.4**, (0.05 mol dm^{-3}) with a pH 7.3 buffer in D$_2$O, after 15 minutes

Figure 5.9: ^{1}H NMR spectrum for the observed reaction of HMS (0.5 mol dm^{-3}) and 4-nitrobenzylamine, **5.4**, (0.05 mol dm^{-3}) with a pH 7.3 buffer in D$_2$O, after 1 day
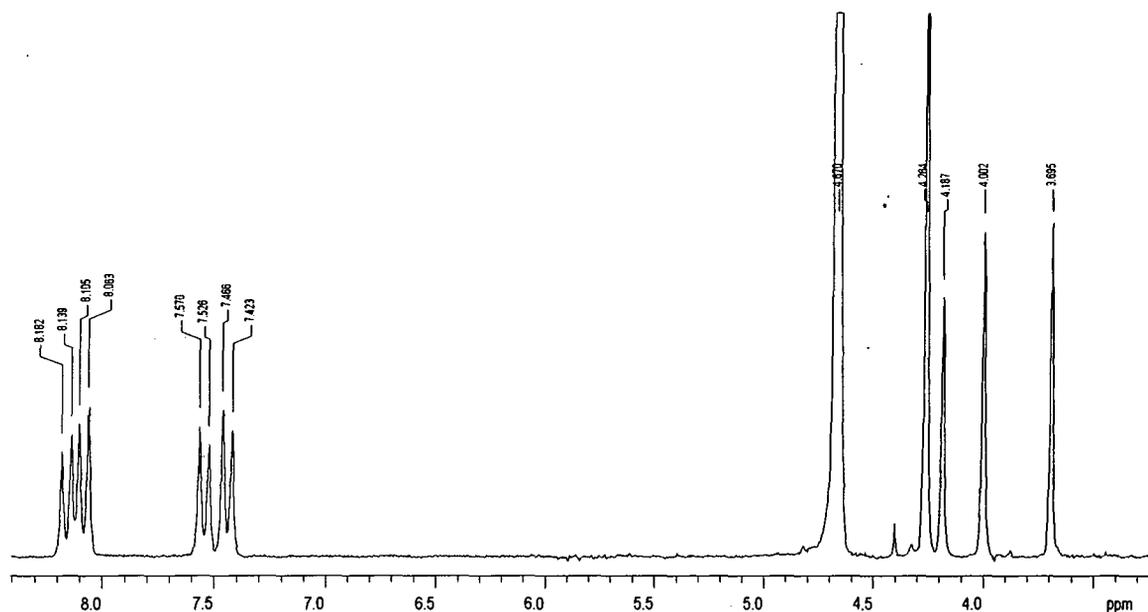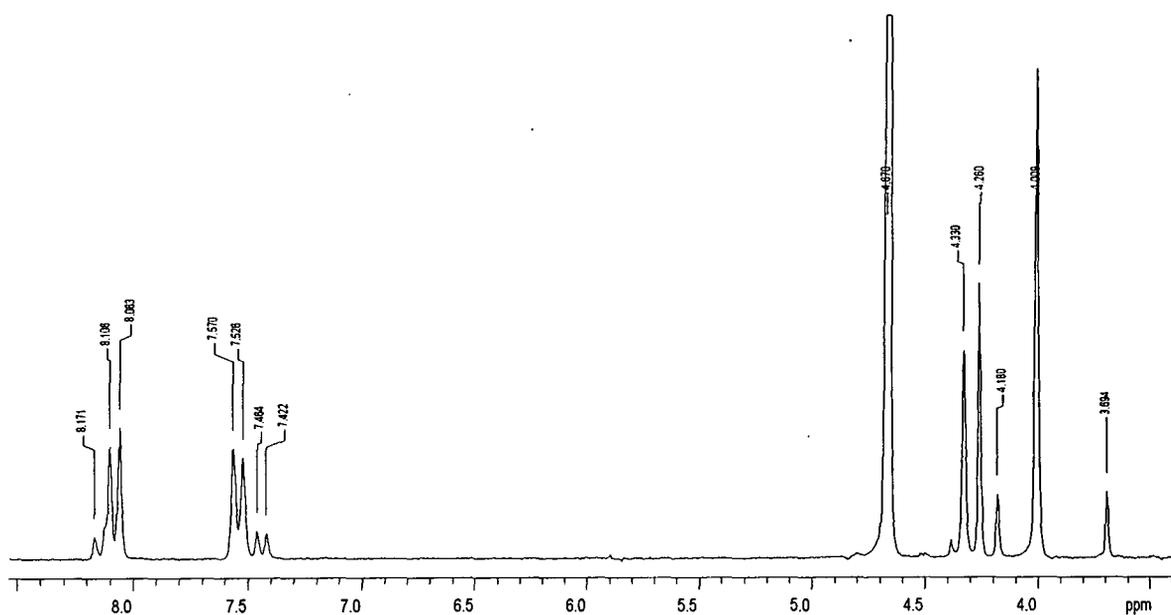
Table 5.10: ^{1}H NMR spectrum for the observed reaction of HMS (0.1 mol dm^{-3}) and 4-nitrobenzylamine, **5.4**, (0.05 mol dm^{-3}) with a pH 7.3 buffer in D$_2$O; peak assignment for time intervals, 15 minutes and 1 day

time	δ / ppm	multip.	J / Hz	Intens.	assignment
15 mins	8.16	d	8.6	2.57	Ar – H$_3$, H$_5$ (parent)
	8.08	d	8.6	3.33	Ar – H$_3$, H$_5$ (1:1 & 1:2)
	7.55	d	8.6	2.89	Ar – H$_2$, H$_6$ (parent & 1:2)
	7.44	d	8.6	3.26	Ar – H$_2$, H$_6$ (1:1)
	4.67	-	-	-	H$_2$O
	4.33	s	-	0.18	-CH$_2$-N- (1:2)
	4.26	s	-	19.41	CH$_2$(OH)(SO$_3^{2-}$)
	4.19	s	-	2.75	-CH$_2$-N- (parent)
	4.00	s	-	3.55	CH$_2$-NHCH$_2$SO$_3^-$ / CH$_2$-N(CH$_2$SO$_3^-$)$_2$
	3.70	s	-	3.25	-CH$_2$-NHCH$_2$SO$_3^-$ (1:1)
24 hrs	8.15	d	8.6	0.97	Ar – H$_3$, H$_5$ (parent)
	8.09	d	8.6	5.79	Ar – H$_3$, H$_5$ (1:1 & 1:2)
	7.55	d	8.6	5.91	Ar – H$_2$, H$_6$ (parent & 1:2)
	7.44	d	8.6	1.28	Ar – H$_2$, H$_6$ (1:1)
	4.67	-	-	-	H$_2$O
	4.33	s	-	4.87	-CH$_2$-N- (1:2)
	4.26	s	-	4.74	CH$_2$(OH)(SO$_3^{2-}$)
	4.19	s	-	1.32	-CH$_2$-N- (parent)
	4.01	s	-	11.00	CH$_2$-NHCH$_2$SO$_3^-$ / CH$_2$-N(CH$_2$SO$_3^-$)$_2$
	3.70	s	-	1.26	-CH$_2$-NHCH$_2$SO$_3^-$ (1:1)

Reaction of HMS with 4-nitrobenzylamine shows formation of the 1:1 adduct instantaneously, and then over time, reaction to yield the 1:2 adduct. The ^{1}H NMR spectrum after 24 hours clearly shows a huge growth of the band, at 4.01 ppm, which is assigned to the combined methylene protons of HMS group, in both adducts. Aromatic shifts are observed through reaction of the parent 4-nitrobenzylamine, to 1:1 and subsequent reaction to form the 1:2 adduct. The first process, shows two new bands for the aromatic protons, both shifting up field by *ca.* ~0.1 ppm, on formation of the 1:1. Further reaction to yield the 1:2 adduct, shows

only the Ar – H_2, H_6 proton band shift back to a position coincident with that of the parent benzylamine.

Due to insufficient quantitative data were collected when observing this reaction the values for $K_{1:1}{}^{stoich}$ and $K_{1:2}{}^{stoich}$ could not be obtained for 4-nitrobenzylamine.

5.2.3: Calculation of $K_{1:1}{}^{stoich}$ and $K_{1:2}{}^{stoich}$ values for the reaction of HMS with benzylamine and N-methylbenzylamine

Calculation of these constants used the relative integral intensities recorded from each spectrum after equilibrium had been reached. In each case the free HMS concentration had first to be calculated. This was achieved by dividing the intensity of the unreacted HMS peaks, by the sum of all the intensities of relevant CH_2 groups incorporated in the HMS adduct, and the value obtained was then multiplied by the known starting concentration for HMS. Using this value, along with the relative intensities for the benzyl CH_2 peaks of the reactants and products gave values for the respective equilibrium constants as shown in equations 5.15 and 5.16 gave values for the respective equilibrium constant.

$$K_{1:1}{}^{stoich} = \frac{[PhCH_2NHCH_2SO_3^-]}{[PhCH_2NH_2][CH_2(OH)(SO_3^-)]_{free}} \qquad (5.15)$$

$$K_{1:2}{}^{stoich} = \frac{[PhCH_2N(CH_2SO_3^-)_2]}{[PhCH_2NHCH_2SO_3^-][CH_2(OH)(SO_3^-)]_{free}} \qquad (5.16)$$

When obtaining the equilibrium constant for the formation of the 1:1 adduct of N-methylbenzylamine, the intensities of the benzyl peaks from reactants and products were used routinely, however, values obtained using the N-methyl peaks were in good agreement.

Values obtained for benzylamine, are shown in table 5.11 at varying pH/pD; a plot of the logarithmic results on acidity, is shown in figure 5.10 and 5.11, for the $K_{1:1}^{stoich}$ and $K_{1:2}^{stoich}$ values respectively.

Table 5.11: Equilibrium constants, $K_{1:1}^{stoich}$ and $K_{1:2}^{stoich}$, calculated for the reaction of benzylamine with HMS using ^1H NMR

pH	pD	$K_{1:1}^{stoich}$ / dm^3 mol^{-1}	$K_{1:2}^{stoich}$ / dm^3 mol^{-1}
5.9	6.3	0.33	120
6.35	6.75	0.51	106
6.8	7.2	0.62	134
7.0	7.4	1.80	115
7.2	7.6	2.98	131
7.3	7.6	2.14	125
7.7	8.1	6.07	141
7.8	8.2	11.0	123
8.3	8.5	15.9	119
8,7	9.1	39.5	135
8.8	9.2	44.25	127
9.4	9.8	75	133
10.0	10.4	94	138
10.2	10.2	99	124

The plot shown for benzylamine in figure 5.10 shows two fits with equation 5.14. In the first, fixed values were used for pK_a (benzylamine) = 9.33, and the $pK_a^{1:1}$ (1:1 adduct) = 5.4[1]. The $pK_a^{1:1}$ is the value obtained from work by Brown and Crampton[1] of the decomposition of the 1:1 adduct by iodine. The value determined for $K_{1:1}$, the value for the reactive form of benzylamine, is 243 mol dm^{-3}. This value is rather higher than that predicted from experimental values at high pH; a rather better fit was obtained (full line) using values for $K_{1:1}$ 160 dm^3 mol^{-1}, pK_a (benzylamine) = 9.2 and $pK_a^{1:1}$ (1:1 adduct) = 5.7.

Figure 5.10: A plot of Log $K_{1:1}^{stoich}$ versus pH for the reaction of benzylamine with HMS, superimposed are fit lines of equation 5.14. (dashed line; $K_{1:1} = 243$ dm^3 mol^{-1}, pK$_a$ = 9.33 and pK$_a^{1:1}$ = 5.4) (full line; $K_{1:1} = 160$ dm^3 mol^{-1}, pK$_a$ = 9.2 and pK$_a^{1:1}$ = 5.7)

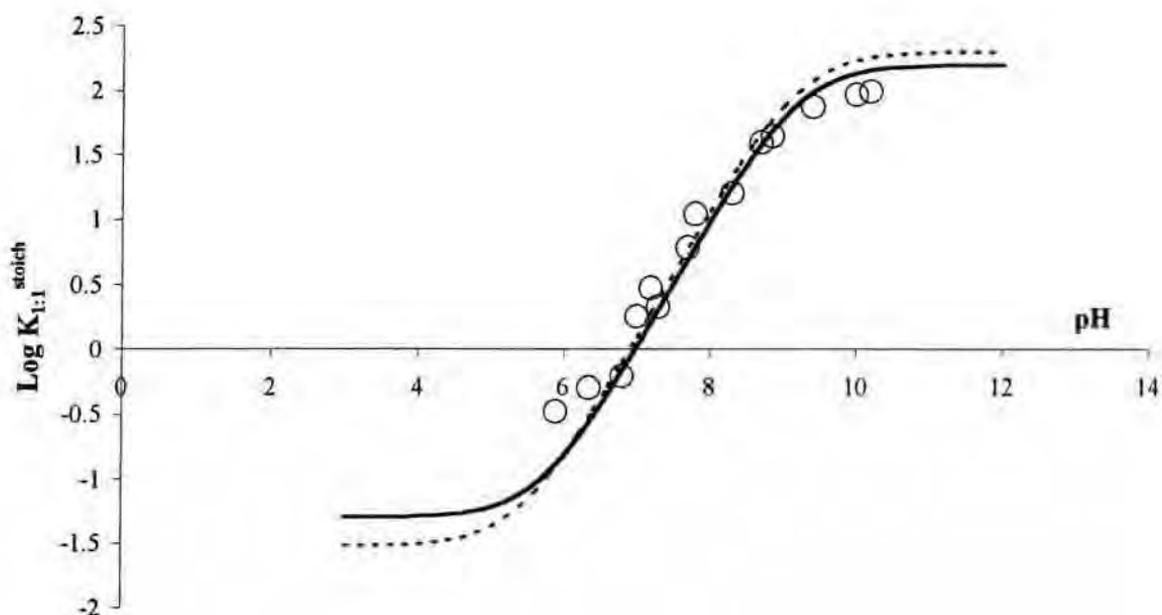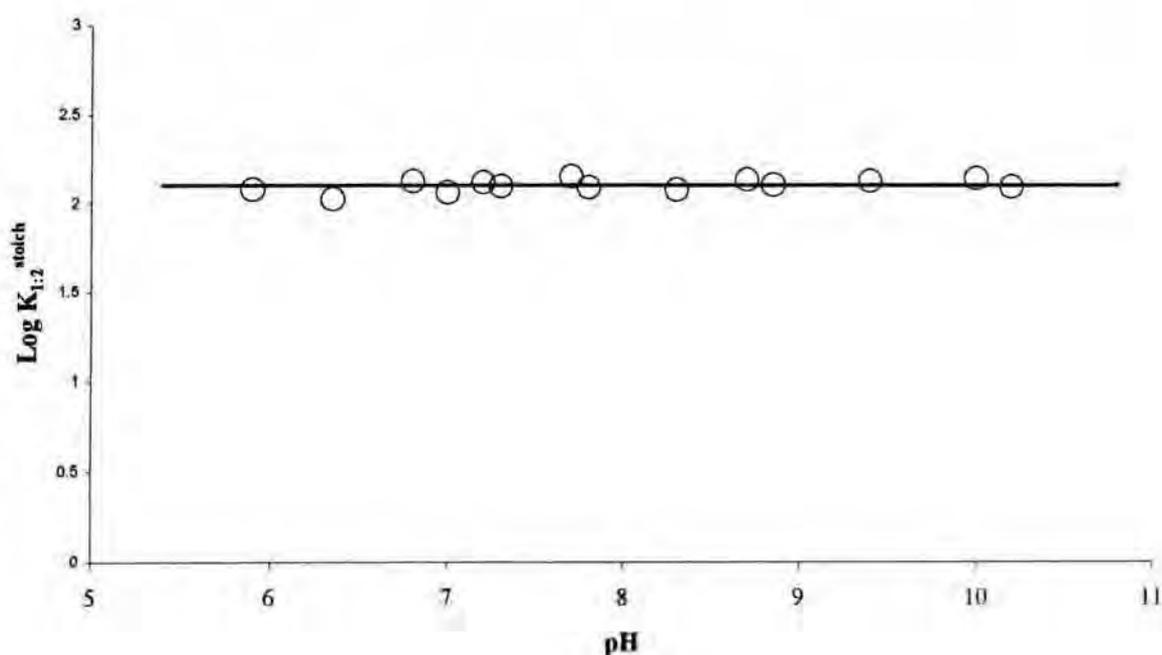**Figure 5.11:** A plot of Log $K_{1:2}^{stoich}$ versus pH for the reaction of benzylamine with HMS showing no dependence on the acidity

As predicted, values obtained for the formation of the 1:2 adduct, were independent of acidity in the pH range studied, given a value for $K_{1:2}$ of 126±10 mol dm^{-3}.
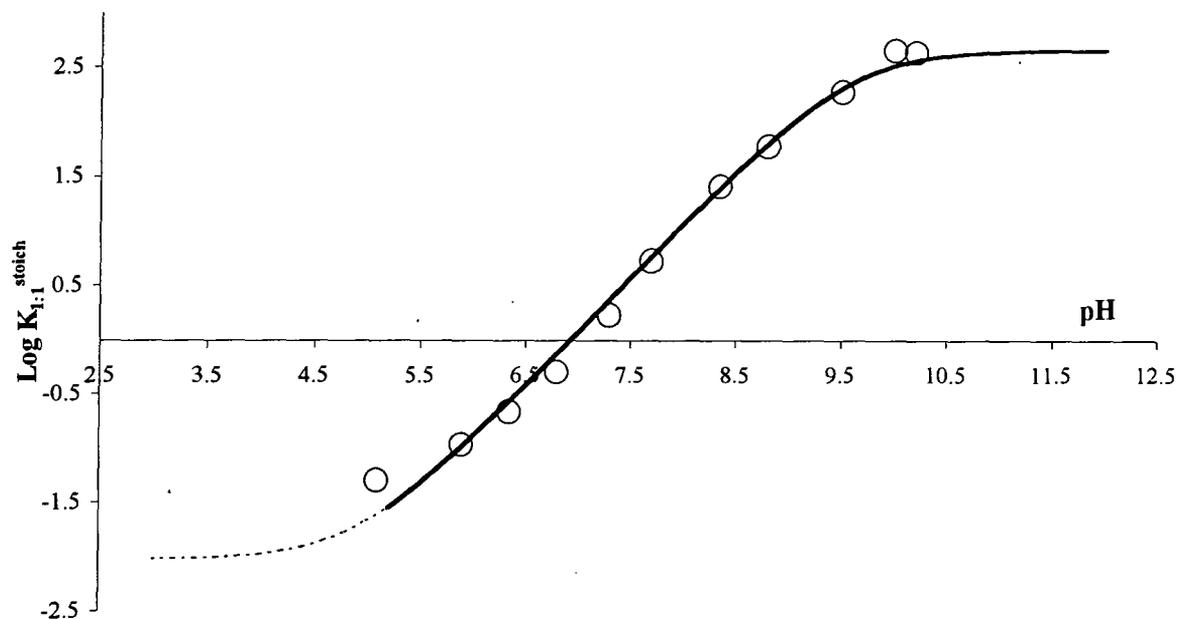
The values of $K_{1:1}{}^{stoich}$, obtained for N-methylbenzylamine, are shown in table 5.12 at various pH/pD values a logarithmic plot of these values against pH is shown in figure 5.12

Figure 5.12, as with benzylamine, shows two superimposed fits, according to equation 5.14. The first, the full line, shows the best fit for the experimental results, using the known pK$_a$ of N-methylbenzylamine. The second, the dashed line included the pK$_a$ for the 1:1 adduct, as calculated by Brown and Crampton[1]. Values used for the plot were; pK$_a$ (N-methylbenzylamine) = 9.59, pK$_a{}^{1:1}$ (for the adduct) = 4.9[1]. The value determined for the true equilibrium constant, for formation for the unprotonated parent, $K_{1:1}$, equalled 460±20 mol dm^{-3}.

Table 5.12: Values for the equilibrium constant, $K_{1:1}{}^{stoich}$ calculated for the reaction of N-methylbenzylamine with HMS using ^{1}H NMR

pH	pD	$K_{1:1}{}^{stoich}$ / dm^3 mol^{-1}
5.1	5.5	0.05
5.9	6.3	0.106
6.35	6.75	0.214
6.8	7.2	0.503
7.3	7.7	1.68
7.7	8.1	5.27
8.35	8.75	25.8
8.8	9.2	59.5
9.5	9.9	189
10.0	10.4	453
10.2	10.6	434

Figure 5.12: A plot of Log $K_{1:1}{}^{stoich}$ versus pH for the reaction of N-methylbenzylamine with HMS, superimposed is a fit line of equation 5.14.

5.3: Conclusions

Formation of both the 1:1 and 1:2 adducts, for both benzylamine and 4-nitrobenzylamine, and formation of the 1:1 adduct for N-methylbenzylamine, were clearly observed with ^{1}H NMR. The results obtained, except for 4-nitrobenzylamine, were used to obtain equilibrium data.

The acidity dependence shown in figure 5.10 and 5.12 clearly shows that values of $K_{1:1}{}^{stoich}$ reach a maximum value at high pH corresponding to deprotonation of the parent benzylamine. The NMR results give some evidence for the presence of a second plateau at pH < 6, but the values of the equilibrium constants were too small here to define precisely a minimum value. Nevertheless using values of $pK_a{}^{1:1}$ previously determined by Brown[1] allowed the complete acidity dependence to be charted.

It is interesting that the values of $pK_a{}^{1:1}$ are at least three orders of magnitude lower than the corresponding values for the parent benzylamine. This may be partially due to the electronic effect of the $CH_2SO_3{}^-$ group, but solvation is likely to be more important. The effect of the

bulky $CH_2SO_3^-$ group will inhibit solvation of the conjugate acids and hence reduce the protonation at nitrogen.

The independence on acidity of the values obtained for $K_{1:2}^{stoich}$ indicate that neither the 1:1 nor 1:2 adducts are extensively protonated in the pH range studied.

Interestingly the value obtained, 460 dm^3 mol^{-1}, for $K_{1:1}$ for N-methylbenzylamine is higher than that, 160 dm^3 mol^{-1}, for benzylamine. This may be attributed to the inductive, electron releasing, effect of the N-methyl group which increases the basicity at nitrogen. The greater size of the methyl group does not apparently inhibit the reaction with HMS.
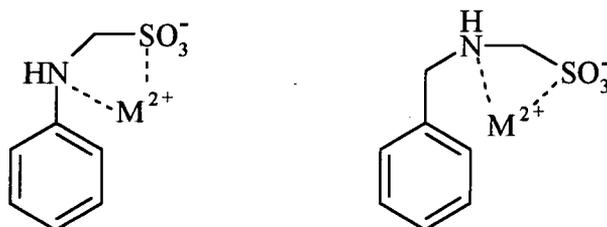
Further evidence that steric effects at nitrogen are not of major importance comes from the observation that for reactions of benzylamine values of $K_{1:1}$, 160 dm^3 mol^{-1}, and $K_{1:2}$, 120 dm^3 mol^{-1}, are similar. The presence of the first $CH_2SO_3^-$ group at nitrogen does not effectively inhibit addition of a second.

5.4: Reaction of HMS and amines in the presence of metal divalent ions

5.4.1: Introduction

It is known that both benzylamine and aniline will react with HMS to produce aminomethanesulfonates. It was thought to be of interest to investigate whether these reactions were affected by the presence of metal cations. In the case of 1:1 adducts it is possible that stabilisation might occur, as shown in scheme 5.5, through interaction of the metal ions with the sulphur or oxygen atoms of the sulfite and with the nitrogen atom to enhance stability.

Metal complexation might have the effects of increasing the values of the rate constants for formation and also the equilibrium constants for formation.

Scheme 5.5:

The reactions of HMS with aniline and benzylamine with added divalent metal cations, were observed independently, using UV/Vis spectroscopy. Reactions were conducted with the amine concentration constant, 1×10^{-4} mol dm^{-3}. However, either the HMS concentration or the metal complex concentration was varied while keeping the other constant. Reactions were conducted in unbuffered solutions; however the pH was recorded; for aniline pH ~ 6.6, and for benzylamine pH ~ 9.0. The divalent metal cations used, were magnesium and barium as the chlorides.

5.4.2: Results and discussion

5.4.2.1: [Amine] and [HMS] constant, [MgCl₂] varied

The UV/Vis absorbance versus time plots at 245nm for the reaction of HMS 0.02 mol dm^{-3} and aniline 1×10^{-4} mol dm^{-3}, fixed, alone (bold line) and with added magnesium chloride, is shown in figure 5.13. The added magnesium chloride increases from 1×10^{-4} to 1×10^{-3} mol dm^{-3} (**1** to **3**) The plots showed first order behaviour, and the observed rate constants, along with absorbance data are in table 5.13. The plots for the reactions when the metal cation is added, vary little, from the plot where no magnesium was added. This is confirmed by the observed rate constants being identical and suggests that the divalent metal cation has no effect on this particular system.

Figure 5.13: UV/Vis absorbance versus time plots for the reaction of aniline 1×10^{-4} mol dm^{-3} with HMS 0.02 mol dm^{-3} alone, as well as with added MgCl$_2$ in varying concentrations (1×10^{-4} to 1×10^{-3} mol dm^{-3}), unbuffered solutions, 25 °C

Table 5.13: Observed rate constant and absorbance data obtained from the 1st order fits of the reaction curves for the reaction of aniline 1×10^{-4} mol dm^{-3} with HMS 0.02 mol dm^{-3} with added magnesium chloride

[MgCl$_2$] / mol dm^{-3}	Initial Abs.	Final Abs.	ΔAbs.	k_{obs} / s^{-1}
-	0.285	1.315	1.03	$(2.6\pm0.1)\times10^{-4}$
1×10^{-4} (1)	0.290	1.340	1.05	$(2.6\pm0.1)\times10^{-4}$
5×10^{-4} (2)	0.281	1.321	1.04	$(2.6\pm0.1)\times10^{-4}$
1×10^{-3} (3)	0.290	1.350	1.06	$(2.6\pm0.1)\times10^{-4}$

The same reaction, where amine and HMS 0.01 mol dm^{-3} were kept constant, was conducted with benzylamine at 1x10^{-3} mol dm^{-3}, also in an unbuffered system. The plot of absorbance versus time, at 245nm, is shown in figure 5.14. The figure shows a absorbance versus time plot of benzylamine 1x10^{-3} mol dm^{-3} and HMS 0.01 mol dm^{-3} without the addition of magnesium chloride (**1**). Plots, which have the added metal cation, increasing from 1x10^{-3} to 0.02 mol dm^{-3} (**2** to **5**) were very similar. The plots unlike, those for observing aniline, show an initial inflection followed by a colour forming process. This latter part was fitted to first order kinetics, yielding observed rate constants and absorbance data for each process (table 5.14). For this reason, the initial absorbance data shown on the plot, is not the true initial absorbance value. Values show that the addition of the magnesium chloride increases the rate of the process, albeit, only very slightly.

Figure 5.14: UV/Vis absorbance versus time plots for the reaction of benzylamine 1x10^{-3} mol dm^{-3} with HMS 0.01 mol dm^{-3} alone, as well as with added MgCl$_2$ in varying concentrations (1x10^{-3} to 0.02 mol dm^{-3}), unbuffered solutions, 25 °C
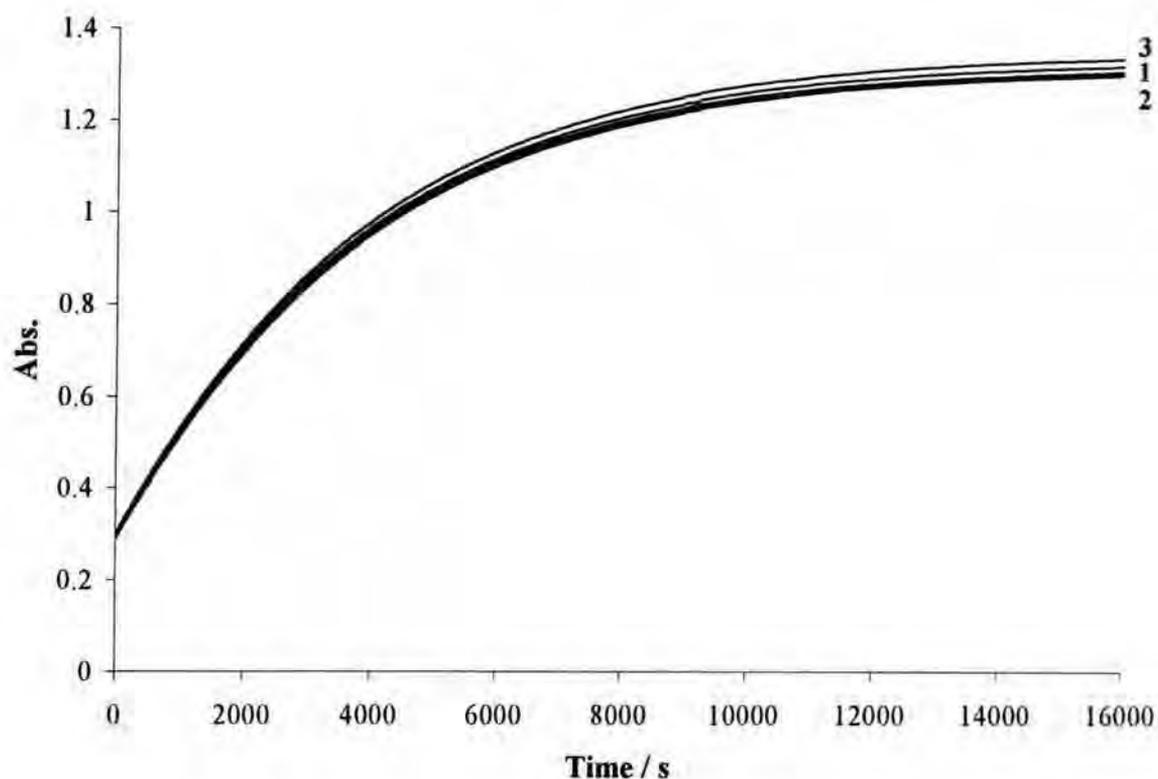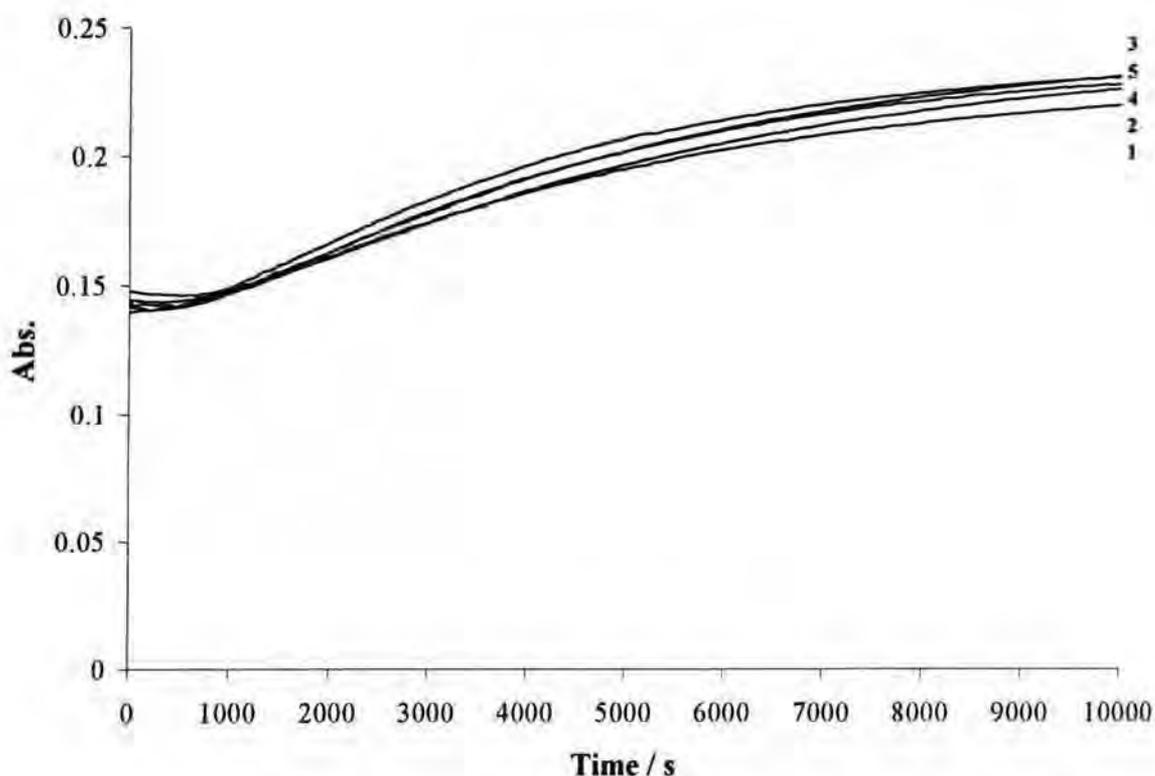
Table 5.14: Observed rate constant and absorbance data obtained from the 1st order fits of the reaction curves for the reaction of benzylamine 1×10^{-3} mol dm^{-3} with HMS 0.01 mol dm^{-3} with added magnesium chloride

[MgCl$_2$] / mol dm^{-3}	Initial Abs.	Final Abs.	ΔAbs.	k_{obs} / s^{-1}
-	0.110	0.248	0.138	$(1.7\pm0.1)\times10^{-4}$
1×10^{-3} (2)	0.120	0.245	0.125	$(1.9\pm0.1)\times10^{-4}$
5×10^{-3} (3)	0.117	0.247	0.130	$(2.1\pm0.1)\times10^{-4}$
0.01 (4)	0.115	0.241	0.126	$(2.4\pm0.1)\times10^{-4}$
0.02 (5)	0.114	0.240	0.126	$(2.7\pm0.1)\times10^{-4}$

5.4.2.2: [Aniline] and [MgCl$_2$] constant, [HMS] varied

The reactions of aniline 1×10^{-4} mol dm^{-3} with varying HMS (2×10^{-4} to 0.05 mol dm^{-3}) and a constant added concentration of magnesium chloride 1×10^{-4} mol dm^{-3} were measured, using UV/Vis spectroscopy. The absorbance versus time plots are shown in figure 5.15. The first order kinetic data, observed rate constants and absorbance data, are shown in table 5.15. The reaction where [HMS] = 0.01 mol dm^{-3}, was conducted and without any magnesium present, in order to observe any effect of the divalent metal cation.

The two plots, where aniline was 1×10^{-4} mol dm^{-3} and HMS was 0.01 mol dm^{-3} were virtually identical, despite one having magnesium chloride present.

Figure 5.15: UV/Vis absorbance versus time plots for the reaction of aniline 1×10^{-4} mol dm^{-3} with varying HMS (2×10^{-4} to 0.05 mol dm^{-3}) with constant added MgCl$_2$ 1×10^{-4} mol dm^{-3}, unbuffered solutions, 25 °C

Table 5.15: Observed rate constant and absorbance data obtained from the 1st order fits of the reaction curves for the reaction of aniline 1×10^{-3} mol dm^{-4} with varying HMS (2×10^{-3} to 0.05 mol dm^{-3}) with a constant added amount of magnesium chloride 1×10^{-4} mol dm^{-3}

[HMS] / mol dm^{-3}	Initial Abs.	Final Abs.	ΔAbs.	k_{obs} / s^{-1}
2×10^{-3} (7)	0.210	0.877	0.676	$(1.97\pm0.1)\times10^{-5}$
5×10^{-3} (6)	0.260	0.906	0.646	$(4.60\pm0.1)\times10^{-5}$
8×10^{-3} (5)	0.287	1.081	0.794	$(6.94\pm0.1)\times10^{-5}$
0.01 (4)	0.308	1.284	0.976	$(9.06\pm0.1)\times10^{-5}$
0.01 no MgCl$_2$ (3)	0.317	1.292	0.975	$(9.23\pm0.1)\times10^{-5}$
0.02 (2)	0.312	1.320	1.008	$(18.0\pm0.1)\times10^{-5}$
0.05 (1)	0.326	1.357	1.031	$(42.0\pm0.1)\times10^{-5}$

The observed rate constants, obtained from first order fits, were plotted against HMS concentration, in order to obtain rate constants, k_f (gradient) and k_r (intercept) and consequently, obtain the equilibrium constant, K, for the process. The values determined are shown in table 5.16, with comparison of rate and equilibrium constants, calculated[1, 8] for the same reaction aniline/HMS, but, without any magnesium chloride present. The sets of results are clearly fit to be compared, which therefore, shows that the divalent metal cation, magnesium, has no effect on the system.

Table 5.16: Rate and equilibrium constants for the reaction of aniline and HMS with/out $MgCl_2$

	Reaction with $MgCl_2$	Reaction without $MgCl_2$ [1, 8]
k_f / dm^3 mol^{-1} s^{-1}	$8.20 \times 10^{-3} \pm 4.1 \times 10^{-5}$	$7.82 \times 10^{-3} \pm 2.0 \times 10^{-5}$
k_r / s^{-1}	$1.06 \times 10^{-5} \pm 1.0 \times 10^{-6}$	$1.01 \times 10^{-5} \pm 8.0 \times 10^{-7}$
K / dm^3 mol^{-1}	770 ± 50	780 ± 60

5.4.2.3: [Amine] and [HMS] constant, [BaCl$_2$] varied

A second metal cation, barium, was used in the same conditions as above, to investigate what effect, a larger, divalent cation may have. Reactions were measured, keeping the amine and HMS concentration constant, while varying the barium chloride concentration.

Firstly, aniline 1×10^{-4} mol dm^{-3} was reacted with HMS 2×10^{-3} mol dm^{-3} and also, with varying BaCl$_2$ concentration (1×10^{-4} to 1×10^{-3} mol dm^{-3}), in unbuffered solutions. The UV/Vis absorbance versus time plots are shown in figure 5.16, with observed rate constants, and absorbance data, obtained from first order fits, are shown in table 5.17.

Figure 5.16: UV/Vis absorbance versus time plots for the reaction of aniline 1×10^{-4} mol dm^{-3} with HMS 2×10^{-3} mol dm^{-3} alone, as well as with extra added BaCl$_2$ in varying concentrations ($1 = 1\times10^{-4}$ mol dm^{-3} $2 = 5\times10^{-4}$ mol dm^{-3} $3 = 1\times10^{-3}$ mol dm^{-3}), unbuffered solutions, 25 °C

Table 5.17: Observed rate constant and absorbance data obtained from the 1st order fits of the reaction curves for the reaction of aniline 1×10^{-4} mol dm^{-3} with HMS 2×10^{-3} mol dm^{-3} with added barium chloride

[BaCl$_2$] / mol dm^{-3}	Initial Abs.	Final Abs.	ΔAbs.	k_{obs} / s^{-1}
1×10^{-4}	0.320	0.992	0.672	$(2.19\pm0.1)\times10^{-5}$
5×10^{-4}	0.317	0.861	0.544	$(2.42\pm0.1)\times10^{-5}$
1×10^{-3}	0.343	1.061	0.718	$(2.15\pm0.1)\times10^{-5}$

Values shown seem to deviate little, suggesting that as with MgCl$_2$, the barium divalent cation has no effect on the aniline/HMS system.

239

The same reaction with benzylamine (1×10^{-3} mol dm^{-3}) and HMS 0.01 mol dm^{-3}, with added barium chloride (varying from 1×10^{-3} to 0.02 mol dm^{-3}), is shown in figure 5.17. The observed rate constants, as well as absorbance data calculated from first order plots, are shown in table 5.18. However, fits were only measured for the second process (after 2000 seconds) of the plots, in order to obtain a value for the rate constant.

Figure 5.17: UV/Vis absorbance versus time plots for the reaction of aniline 1×10^{-4} mol dm^{-3} with HMS 2×10^{-3} mol dm^{-3} alone, as well as with added BaCl$_2$ in varying concentrations (1×10^{-3} to 0.02 mol dm^{-3}), unbuffered solutions, 25 °C

The plots shown above clearly show two processes, as observed previously. However, with added barium, the first process is much more defined. Errors obtained in measuring observed rate constants, by separating the two processes, are likely to be large, regardless that the actual fit, might produce small error.
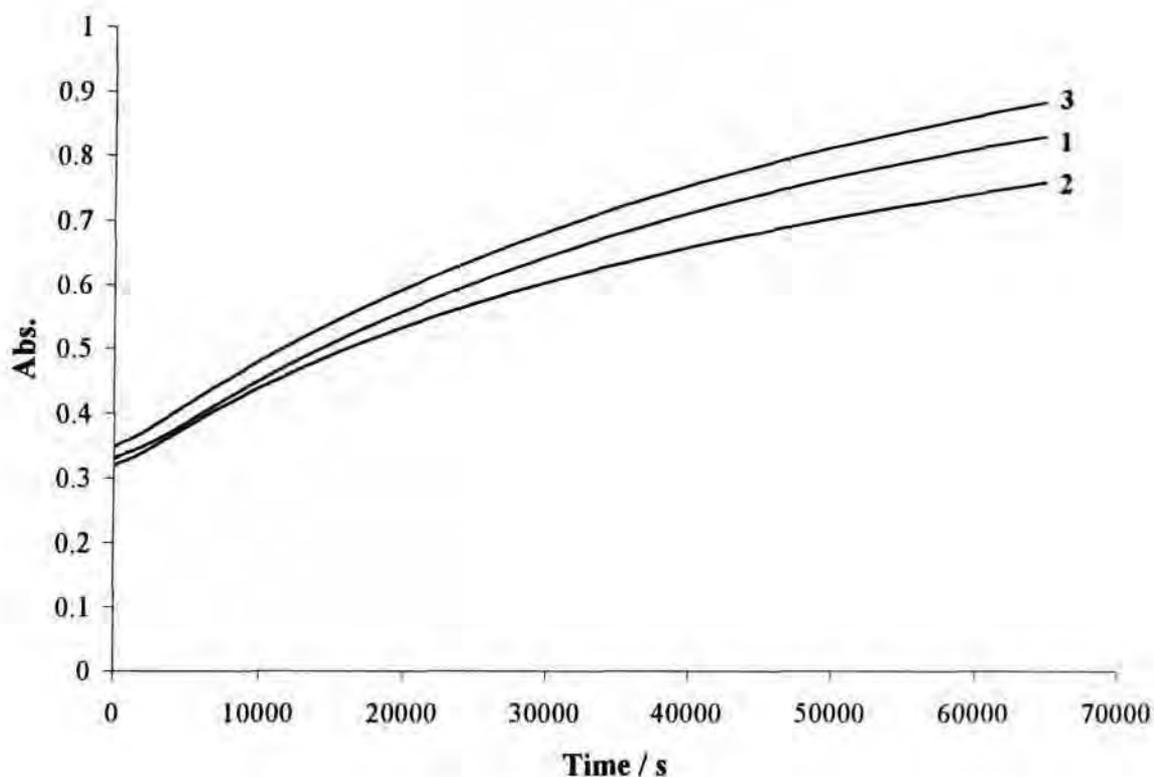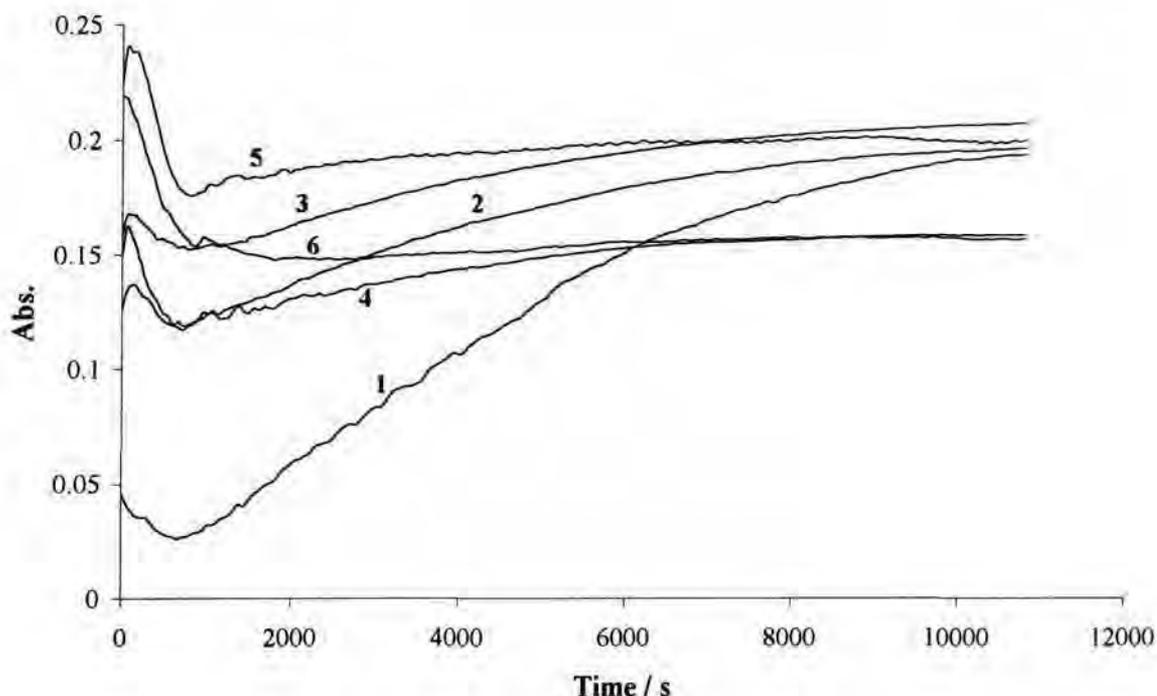
Table 5.18: Observed rate constant and absorbance data, obtained from the first order fits of the reaction curves for the reaction of benzylamine 1×10^{-3} mol dm^{-3} with HMS 0.01 mol dm^{-3} with added magnesium chloride

[MgCl$_2$] / mol dm^{-3}	Initial Abs.	Final Abs.	ΔAbs.	k_{obs} / s^{-1}
1×10^{-3} (1)	0.032	0.231	0.261	$(2.0 \pm 0.1) \times 10^{-4}$
2×10^{-3} (2)	0.094	0.207	0.113	$(2.3 \pm 0.1) \times 10^{-4}$
3×10^{-3} (3)	0.129	0.214	0.085	$(2.5 \pm 0.1) \times 10^{-4}$
5×10^{-3} (4)	0.100	0.161	0.061	$(3.0 \pm 0.1) \times 10^{-4}$
0.01 (5)	0.169	0.250	0.081	$(4.0 \pm 0.1) \times 10^{-4}$
0.02 (6)	0.131	0.158	0.027	$(6.2 \pm 0.1) \times 10^{-4}$

From the data shown, it can be said that at high concentrations, barium has some effect on the benzylamine/HMS system.

5.4.3: Conclusions

Measurements of the reaction of HMS with aniline showed that the effects of the presence of magnesium or barium ions were negligible. However, small effects were observed in the reaction of HMS and benzylamine. Reasons why the reactions might not be affected is due to the possibility of steric hindrance between the large structures involved, i.e. the aromatic ring, the sulfite group and the relatively large divalent metal cation. There is also the possibility of competitive interactions of the metal ions with HMS itself.

5.5: References

1) K. H. Brown, PhD Thesis, University of Durham, 1999

2) D. D. Perrin, 'Dissociation Constants of Organic Bases in Aqueous Solution', Butterworths, London, 1965 and 1972 Supplement

3) J. F. Coetzze and C. D. Ritchie, 'Solute-Solvent Interactions', M. Dekker, New York, 1969

4) P. M. Laughton and R. E. Robertson, *Can. J. Chem.*, 1956, **34**, 1714

5) J. Hamid, PhD Thesis, University of Durham, 1992

6) R. F. Nystrom and W. G. Brown, *J. Am. Chem. Soc.*, 1948, **70**, 3738

Chapter six

6 Synthesis and Reaction of Triazines

6.1: Introduction

A number of authors have shown how the condensation of benzylamine and formaldehyde may yield an imine, which polymerises, to give a 1,3,5-triazine derivatives[1].

Scheme: 6.1:

$$PhCH_2NH_2 \ + \ CH_2O \ \rightleftharpoons \ PhCH_2N=CH_2 \ + \ H_2O$$

$$3 \ PhCH_2N=CH_2 \longrightarrow$$

(6.1)

The triazines are useful, since they can be used as synthetic equivalents of the constituent imine; and reactions with nucleophiles, such as phosphites (Scheme 6.2) and thiols have been reported[2].

Scheme 6.2:

(6.1)

i. (EtO)$_2$POH
ii. HCl

244

In Chapter 5 some studies of the reactions of benzylamine and its derivatives with HMS have been reported. These are likely to involve the intermediacy of imines $PhCH_2=NH_2$, and it was thought to be of interest to examine the reaction of some benzylamine derivatives with formaldehyde in the absence of nucleophiles. The products are found to be a series of previously unreported triazines, which are substituted in the aromatic ring. In the case of N-methylbenzylamine, trimerisation is not possible, but dimer formation is observed.

6.2: Preparation of triazines

6.2.1: (1,3,5)-tribenzyl-(1,3,5)-triazine, 6.1
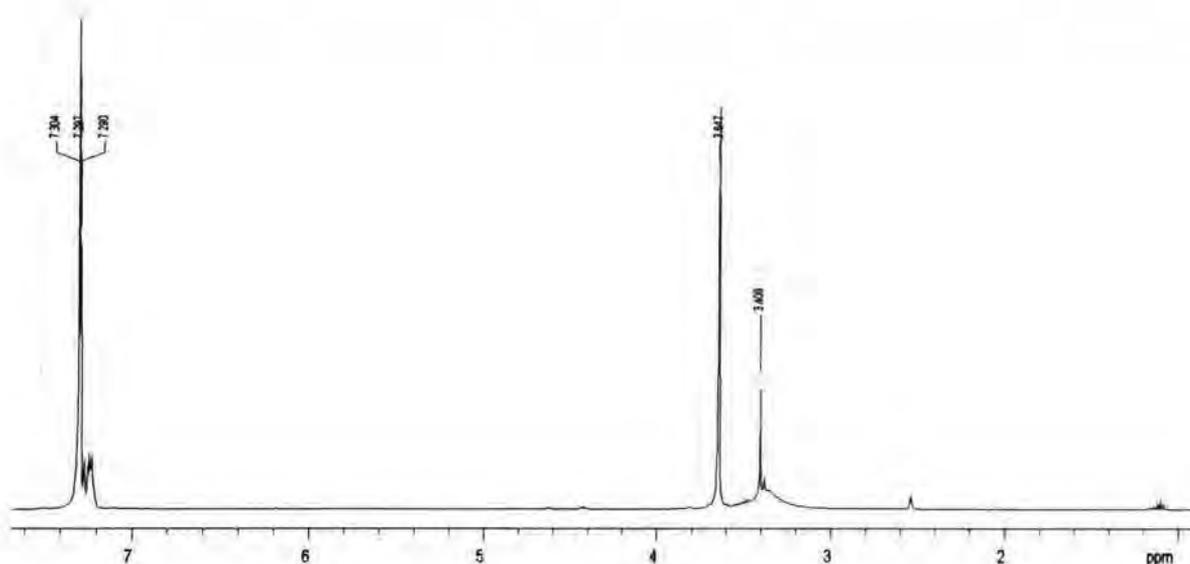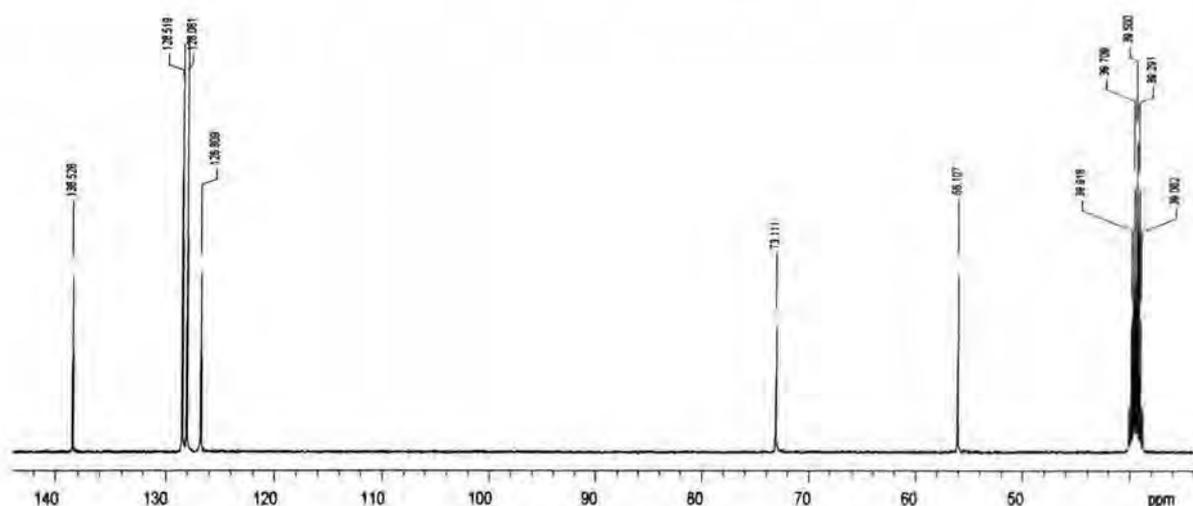
The trimer was synthesised using procedures reported by Lewis and Motherwell[1b]. Benzylamine (20.3g, 0.189mol) was placed in a $250cm^3$ round bottomed flask at 0°C. To this, 37% wt formaldehyde solution (19.4 ml, 0.2mol) was added dropwise, over 45 minutes with continuous stirring, so the temperature did not exceed 10°C. The gummy solution that was formed was left to stand in ice for a further hour, to ensure the reaction was complete. Diethyl ether (50 ml) was added, with stirring, until the gum had been dissolved. The aqueous layer formed was extracted, and washed with diethyl ether (3 x 25 ml). The combined organic layers were washed with brine and then, filtered. The ether was stripped off using the rotary evaporator, to produce the triazine as a colourless viscous liquid. This was then added to ethanol (300 ml) at -10 °C, and by addition of water (20 ml), crystallisation started to occur. After 24hrs standing, the triazine had crystallised to form colourless rods (yield of 69.8%), with a melting point of 48-49°C (literature value 50°C)[1b]. The ^1H and ^{13}C NMR spectra in d-6 dimethylsulphoxide (DMSO) were obtained (Figures 6.1 and 6.2). The chemical shifts, multiplicity and peak assignments are summarised in tables 6.1 and 6.2.

Figure 6.1: ¹H NMR spectrum of 1,3,5-tribenzyl-1,3,5-triazine, **6.1**, in DMSO

Table 6.1: ¹H NMR spectrum of 1,3,5-tribenzyl-1,3,5-triazine, **6.1**, in DMSO: peak assignment

δ / ppm	multplicity	integral ratio	assignment
7.29	m	5	aromatic protons
3.65	s	2	Ph-CH$_2$
3.40	s (broad)	2	N-CH$_2$-N
3.41	-	-	H$_2$O
2.54	-	-	DMSO ref peak

Figure 6.2: ^{13}C NMR spectrum of 1,3,5-tribenzyl,1,3,5-triazine, **6.1**, in DMSO

Table 6.2: ^{13}C NMR spectrum of 1,3,5-tribenzyl,1,3,5-triazine, **6.1**, in DMSO

δ / ppm	assignment
138.53	Ar – C_1
128.52	Ar – C_2 & C_6
128.10	Ar – C_3 & C_5
126.81	Ar – C_4
73.11	N-CH_2-N
56.107	Ph-CH_2-N
39.5 (quintet)	DMSO ref

A mass spectrum was also obtained to confirm that, 1,3,5-tribenzyl-1,3,5-triazine was produced, shown below in figure 6.3. The molecular ion peak (M$^+$) is at m/z 357. Peak assignment for the major peaks is discribed in table 6.3.
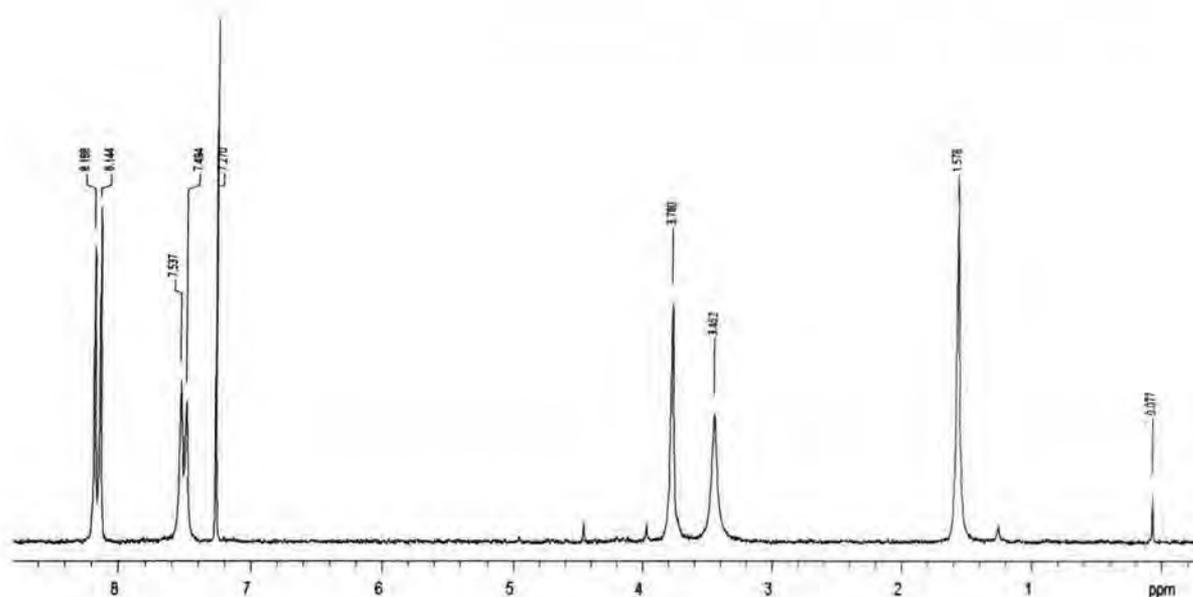
Figure 6.3: Mass spectrum of 1,3,5-tribenzyl-1,3,5-triazine, **6.1**

Table 6.3: Peak assignment for the major peaks of the mass spectrum of 1,3,5-tribenzyl-1,3,5-triazine, **6.1**

mass	assignment
357	(M^{+}) molecular ion, $(PhCH_2NCH_2)_3^{+}$; 1,3,5-tribenzyl-1,3,5-triazine, 6.1
238	M^{+} minus $PhCH_2NCH_2^{+}$
133	M^{+} minus $PhCH_2N\text{-}CH_2\text{-}NCH_2Ph^{+}$
119	M^{+} minus $(PhCH_2NCH_2)_2^{+}$
91	M^{+} minus $(PhCH_2)_2\text{-}(NCH_2)_3^{+}$
77	M^{+} minus all bar Ph^{+}

6.2.2: Preparation of the triazines derived from 4-dimethylaminobenzylamine and 4-nitrobenzylamine

These two compounds were purchased as their hydrochlorides. Therefore, before reaction they were neutralised, using 4M sodium hydroxide. The preparation of the two trimers followed the general method of Lewis and Motherwell[1b]. The only variation was that 4-nitrobenzylamine hydrochloride (1.82g, 96.5mmol) was dissolved in the minimum amount of water, before it was neutralised and then mixed with an equimolar amount of 37% wt

248

formaldehyde. The 4-dimethylaminobenzylamine hydrochloride (0.5g, 2.24×10^{-4} mol dm^{-3}) was dissolved only in the base, and then the formaldehyde was added over 45 minutes.

The yields and melting points of the products were; 1,3,5-tri-(4-nitrobenzyl)-1,3,5-triazine, **6.2**, 51.7% 148°C (decomposed), 1,3,5-tri-(4-dimethylaminobenzyl)-1,3,5-triazine, **6.3**, 61%, 81°C. ^{1}H NMR spectra were obtained, and can be seen in figures (6.4 and 6.5), with peak assignments, chemical shifts and multiplicity in table (6.4 and 6.5)

It is of interest, that the doublet, due to H$_2$ and H$_6$ in the spectrum of the 4-nitro derivative is appreciably broadened. This may indicate some conjugation, resulting in restricted rotation about the C$_1$ and CH$_2$ bond.

(6.2)

Figure 6.4: ^{1}H NMR spectrum of the 4-nitrobenzylamine trimer, **6.2**, in CD$_3$Cl

Table 6.4: ^{1}H NMR spectrum of the 4-nitrobenzylamine trimer, **6.2**, in CD$_3$Cl: peak assignment

δ / ppm	multiplicity	intensity	J / Hz	assignment
8.17	d	2	8.6	Ar – H$_3$ & H$_5$
7.52	d	2	8.6	Ar - H$_2$ & H$_6$
7.27	-	-	-	CDCl$_3$ ref peak
3.78	s	2	-	Ph-CH$_2$
3.45	s	2	-	N-CH$_2$-N
1.58	-	-	-	H$_2$O

The structure of 1,3,5-tri-4-dimethylamino-1,3,5-triazine, **6.3**, can be seen below:

(6.3)

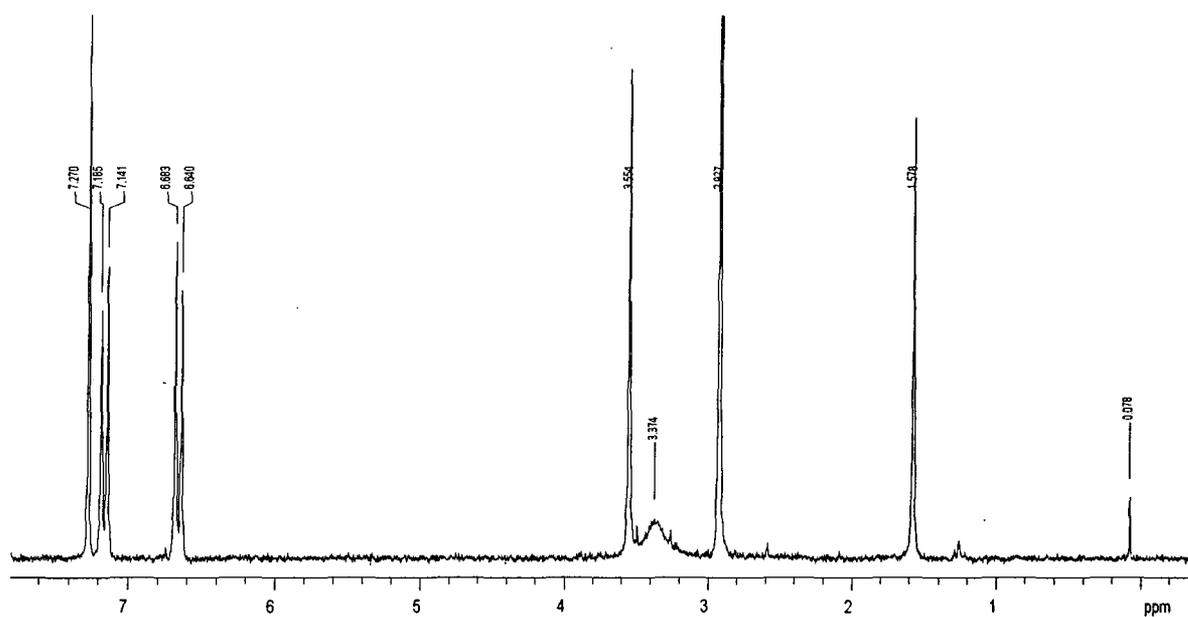**Figure 6.5:** ^{1}H NMR spectrum of 1,3,5-tri-(4-dimethylamino)-1,3,5-triazine, **6.3**, in CD$_3$Cl

Table 6.5: ^{1}H NMR spectrum of the 1,3,5-tri-(4-dimethylamino)-1,3,5-triazine, **6.3**, in CD$_3$Cl: peak assignment

δ / ppm	multiplicity	intensity	J / Hz	assignment
7.27	-	-	-	CDCl$_3$ ref peak
7.16	d	2	8.6	Ar-**H$_3$** & **H$_5$**
6.66	d	2	8.6	Ar-**H$_2$** & **H$_6$**
3.55	s	2	-	Ph-**CH$_2$**
3.37	s (broad)	2	-	N-**CH$_2$**-N
2.93	s	6	-	para-N-(**CH$_3$**)$_2$
1.58	s	9.09	-	**H$_2$O**

6.2.3: Preparation of the dimer derived from N-methylbenzylamine

The procedure of Padwa and Dent[3] was followed for the condensation of formaldehyde with N,N-dimethyl-methylenediamine, **6.4**. A solution of 37% wt formaldehyde (0.314 ml, 3.87×10^{-3} mol) was added dropwise, over 45 minutes to N-methylbenzylamine (1.0g, 8.26×10^{-3} mol), in 1.0M hydrochloric acid (4.13 ml) at 0°C. The reaction was stirred overnight, and then washed with sodium bicarbonate solution. It was then extracted with excess diethyl ether, and dried with magnesium sulfate. The solvent was then evaporated off, using a rotary evaporator to form the product, as a slightly yellow oil. A ^{1}H NMR spectrum was obtained, and can be seen below in figure 6.6. Table 6.6 shows the chemical shifts, multiplicity and peak assignment.

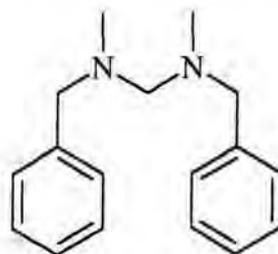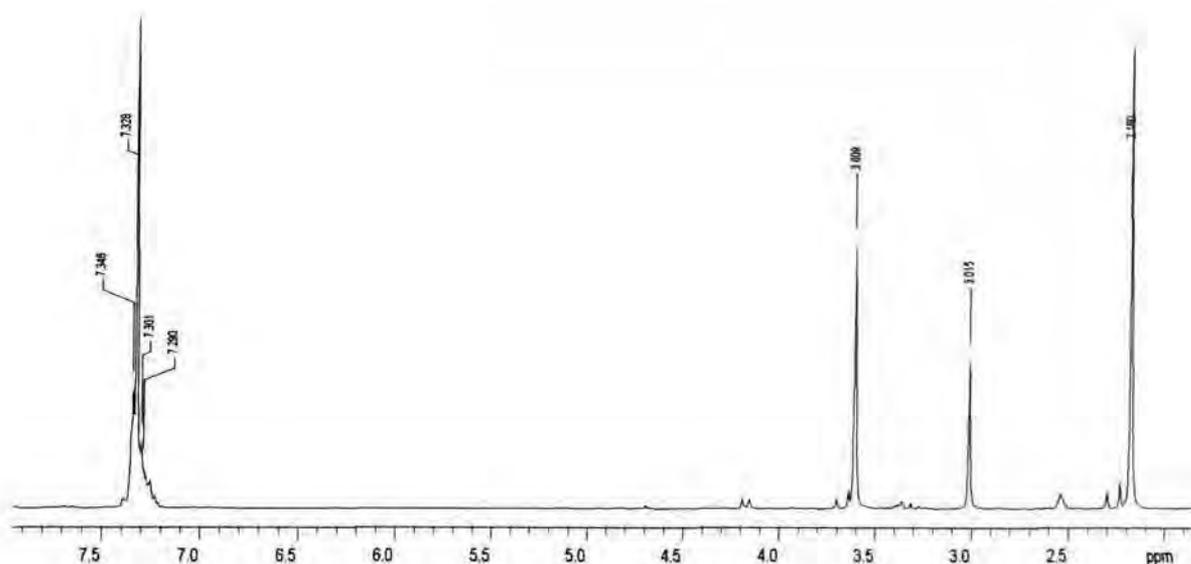The structure of N-N-dimethyl-methylenediamine, **6.4**, is shown below

(6.4)

Figure 6.6: ¹H NMR spectrum of N,N-dimethyl-methylenediamine, **6.4**, in DMSO

Table 6.6: ¹H NMR spectrum of N,N-dimethyl-methylenediamine, **6.4**, in DMSO: peak assignment

δ / ppm	multiplicity	intensity	assignment
7.33	m	10	aromatic protons
3.609	s	4	Ph-CH₂
3.015	s	2	N-CH₂-N
2.54	-	-	DMSO ref peak
2.18	s	6	N-CH₃

A mass spectrum was also obtained, and is shown in figure 6.7, with peak assignment for the major peaks, in table 6.7. The molecular ion peak (M⁺) is at m/z 254.

253

Figure 6.7: Mass spectrum of N,N-dimethyl-methylenediamine, **6.4**

Table 6.7: Peaks assignment for the major peaks from the mass spectrum of N,N-dimethyl-methylenediamine

mass	assignment
254	(M^+), molecular ion; $(PhCH_2N(CH_3))_2$-CH_2
134	M^+ minus $PhCH_2N(CH_3)$
120	M^+ minus $PhCH_2N(CH_3)CH_2$
91	M^+ minus $PhCH_2N(CH_3)$-CH_2-$N(CH_3)$
77	M^+ minus $PhCH_2N(CH_3)$-CH_2-$N(CH_3)CH_2$

6.3: Reaction of 1,3,5-tribenzyl-1,3,5-triazine with diethyl phosphite

It has been reported, that triazines can be broken down by several nucleophiles, and their reaction with phosphates, has been mentioned several times in the literature[4]. The procedure used, was similar to that reported by Oberhauser and Mediuna[1d]. In this particular case, 1,3,5-

tribenzyl-1,3,5-triazine (5g, 0.014mol) was added to a 100cm³ round bottomed flask, and then, dry nitrogen was bled through the system to remove any moisture; a bubbler with silicon oil was used to ensure, that absolutely no moisture was in the system. After 20 minutes, the nitrogen flow was reduced, and 3 equivalents of diethyl phosphite (5.3ml) was added, with heating at 100°C for 18 hours. The reaction was then heated at 50°C, at high vacuum for 8 hours to remove any impurities, using an acetone/cardice bath as the trap. The hard precipitate was then taken up in dry ether (50ml), and heated slightly with intensive stirring, to aid it to dissolve. Hydrogen chloride in ether (5ml) was added, and the solid was filtered, washed with diethyl ether, and dried at high vacuum. A slightly yellow, extremely hydroscopic solid was formed. A ¹H NMR spectrum was obtained yet the peaks proved undecipherable. ¹H NMR spectra for both, un-reacted diethyl phosphite and the wet products can be seen below in figures 6.8 and 6.9.

Figure 6.8: ¹H NMR spectrum of 0.1 mol dm⁻³ diethyl phosphite in DMSO

Table 6.8: ^{1}H NMR spectrum of 0.1 mol dm^{-3} diethyl phosphite in DMSO: peak assignments

δ / ppm	multiplicity	intensity	J / Hz	Assignment
8.572	d	1	692	P-H
5.111				
4.08	quintet	4	6	CH$_2$
2.54	-	-	-	DMSO ref peak
1.291	t	6		CH$_3$

Figure 6.9: ^{1}H NMR spectra for the products of the 1,3,5-tribenzyl-1,3,5-triazine/diethyl phosphite reaction, in DMSO

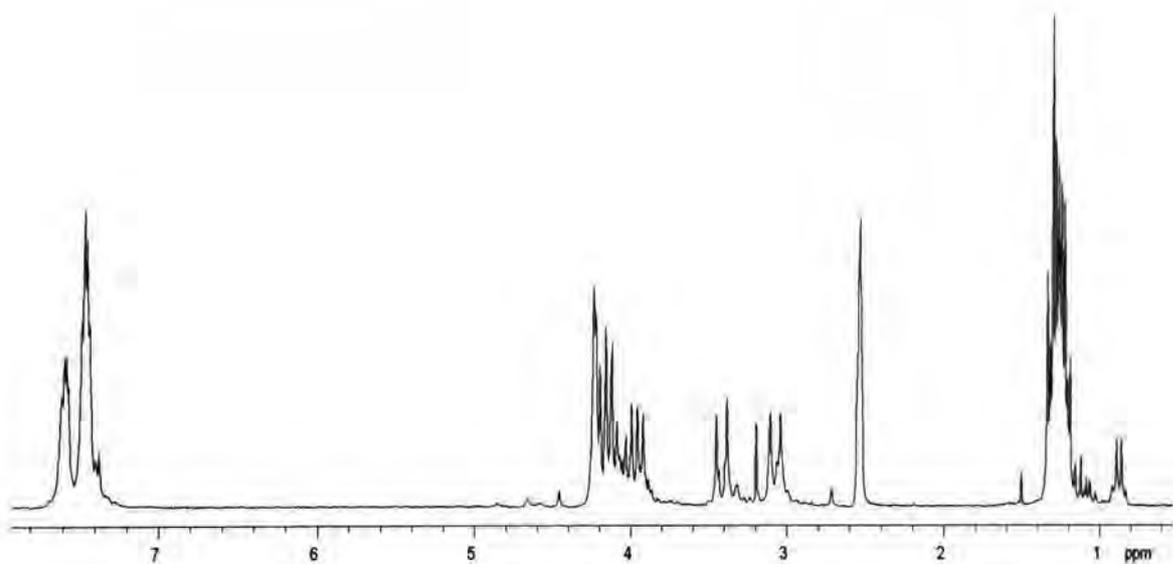**Figure 6.9:** ^{1}H NMR spectra for the products of the 1,3,5-tribenzyl-1,3,5-triazine/diethyl phosphite reaction: peak assignment

δ / ppm	multiplicity	intensity	assignment
7.45	m	24.53	aromatic hydrogens
3.8-4.3	m	24.40	CH_2
3.4	m	4.80	-
3.1	m	5.60	-
2.54	-	-	DMSO ref peak
1.27	m	28.65	CH_3

The reaction of the triazine with diethyl phosphite is inconclusive. Nevertheless a reaction has occurred, since the triazine's spectrum (figure 6.1) has clearly changed. However, this change could not confirm formation of benzylamine and formaldehyde. As these studies were only secondary in relation to other work, they were not pursued further.

6.4: Conclusions

Formation of trimers from the reactions of benzylamine, and benzylamine derivatives with formaldehyde, has been shown to occur, with characterisation for several trimers. Reaction with N-methylbenzylamine yielded a dimer.

Further reaction with nucleophiles proved inconclusive, when diethyl phosphite was used as the nucleophile. However, as the work was not extensive, the reactivity of phosphite could not be truly ascertained.

6.5: References

1) (a) G. S. Smith, *Phosphorus and Sulfur*, 1988, **39**, 91; (b) R. T. Lewis and W. B. Motherwell, *Tetrahedron*, 1992, **48**, 1465; (c) J. C. Duff and V. I. Furness, *J. Chem. Soc.*, 1952, **204**, 1159; (d) T. Oberhauser and V. Meduna, *Tetrahedron*, 1996, **52**, 7691

2) P. M. Laughton and R. E. Robertson, *Can. J. Chem.*, 1956, **34**, 1714

3) A. Padwa and W. Dent, *J. Org. Chem.*, 1987, **52**, 235

4) (a) Ref. 1d; (b) R. W. Ratcliffe and B. G. Christensen, *Tetrahedron*, 1973, **46**, 4645

Chapter seven

7 Experimental

7.1: Materials

i). Kinetic use: all materials used to make aqueous solutions for kinetic experiments were purchased commercially. These substances were used without further purification, using highly purified water, to give solutions of known molarity. Most solid compounds were dissolved with the aid of a Sonomathic ultrasonic bath, to ensure complete dissolution.

ii). Synthetic use: reagents for synthetic use were also purchased commercially, and used without further purification. Substances were used undiluted, except sodium hydroxide and hydrochloric acid solutions that were used, to either neutralize reagents, or make the reaction liquor, acidic or basic. Reaction products were purified by recrystallisation.

General purpose methanol was used for washing all apparatus.

7.2: Experimental measurements

Volumes were generally measured, using glass pipettes for volumes greater than 5 cm^3 and Gilson Pipettman dispensing pipettes, with disposable tips, for smaller volumes. The Gilson Pipettman pipettes were calibrated prior to use, by weighing the volume of water dispensed at a particular setting, assuming a density of water of 1 $g\ cm^{-3}$, and adjusting the volume setting accordingly.

7.3: Buffer solutions

Throughout the work reported in all chapters, buffers with various pH were used. Buffers were made up using CRC Handbook[1], as a guideline. Buffer concentrations, depended on the salt being used. Since all work was in the pH range, 1 to 12, the buffers systems used were;

potassium dihydrogen phosphate/sodium hydroxide, borax/sodium hydroxide or hydrochloric acid, sodium bicarbonate/sodium hydroxide, sodium acetate/acetic acid, and finally, hydrochloric acid, in varying molarities, with potassium chloride to maintain the salt concentration.

The buffer concentration present in the final reaction systems are given in table 7.1. The values given are for the total concentration of buffer present, i.e. they include the sum of the concentrations of acidic and basic forms. The ratio of these concentrations will vary pH. Values of pH were checked using a pH meter and minor adjustments were made by addition of acid or base as appropriate.

Table 7.1: Buffer concentrations, buffer salt and concentration it was in final reaction

buffer salt component	molarity of salt / mol dm^{-3}
potassium dihydrogen phosphate	0.2
borax	0.05
sodium acetate	0.2
sodium bicarbonate	0.1
potassium chloride	0.2

7.4: UV/Vis spectrometry

Most measurements were carried out on conventional UV/Visible spectrophotometers. Repeat scan spectra were measured on a Shimadzu UV-2101PC spectrophotometer. Time course runs were performed on a Perkin Elmer λ12 or λ2 instruments. All spectrophotometric work was at 25°C in stoppered, quartz cuvettes with a 1cm path length. The reference cell contained the appropriate solvent/buffer and the spectrophotometers were zeroed against this, prior to reaction. For spectral scans, a baseline correction was performed, using the reference cell. Absorbance against wavelength plots, were generally recorded, using a scan speed of 480 nm min^{-1}. Spectra were obtained, to determine an appropriate wavelength to follow
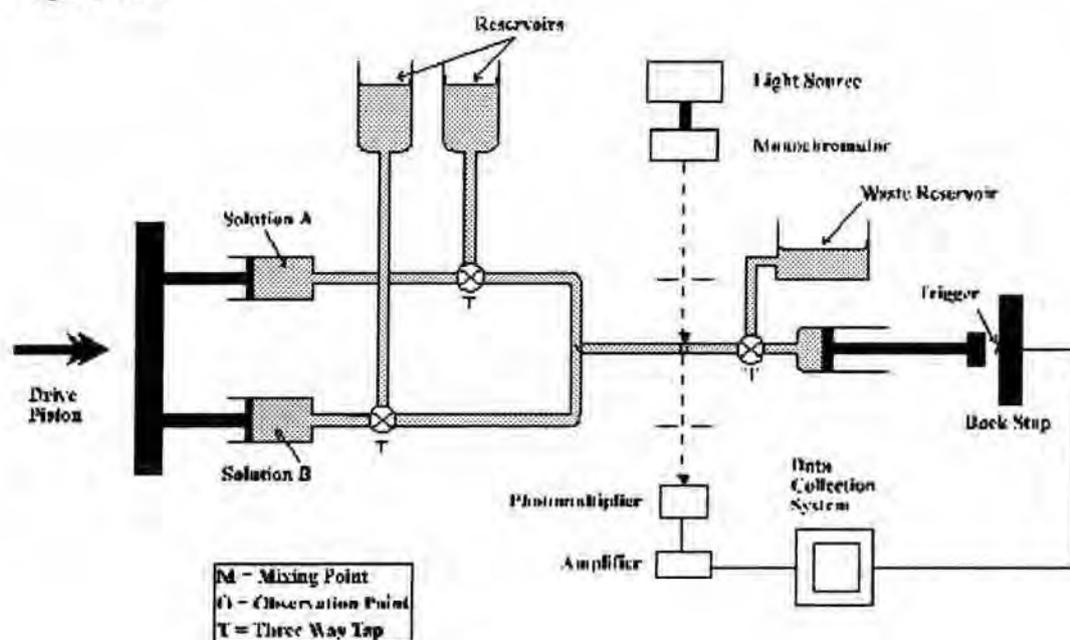
changes in absorbance with time. Reactions were carried out under pseudo first order, or zero order conditions.

Water was generally used as the solvent: mixed solvent systems were used where the compounds were only sparingly soluble in water at the concentration required.

7.5: Stopped-flow spectrophotometry

Reactions that were too fast to be followed by conventional UV/Visible spectrometry were studied using an Applied Photophysics Biosequential DX-17MV stopped-flow spectrophotometer. Reactions were carried out at 24.8 – 25.2 °C. Figure 7.1 shows a schematic of the general stopped-flow apparatus[2].

Figure 7.1:

The reaction solutions were stored in identical syringes, to ensure equal volume delivery. The reaction was initiated using the computer controlled automated drive. This ensured

simultaneous delivery of the reagents through the automated mixing chamber into the observation cell (1 cm path length), within 5 ms. Upon entry to the observation cell, the solution, causes a third syringe to load and trigger the acquisition of the absorbance time data. The drive syringes, delivery tubes and the observation cell, were thermostatted, by the means of a circulating water bath.

A fibre optic cable directs a beam of monochromatic light, of the appropriate wavelength, into the observation cell. The light passes through the reaction solution, into a photomultiplier and the change in voltage/time, is converted to absorbance change/time, by the computer software. The software also allows for the generation of rate constants from the recorded data.

The apparatus was washed through, with distilled water and the appropriate solutions prior to use. To ensure efficient mixing, approximately five short runs were conducted, prior to obtaining the results desired. Water was used as the solvent in all stopped-flow experiments. Reactions were carried out under pseudo first order, or zero order conditions. Runs were often carried out in a random order rather than in increasing/decreasing concentration to minimise errors, due to environmental changes.

7.6: Data fitting and errors in measurement

For experiments, using conventional spectroscopic methods, all rate constants were obtained using the Scientist® computer program[3]. Data manipulation, prior to and proceeding the discovery of rate constants, was carried out by Microsoft Excel®. Stopped-flow spectroscopy experiments were fitted using the single exponential fit function. The zero order plots were fitted, using linear regression on the !SX.17MV program, installed on the spectrometer.

The calculations of all first order rate constants, obtained under pseudo first order conditions, were based upon the following derivation.

For the reaction of type A $\rightarrow$ B, the rate of formation of B, or the rate of decomposition of A, can be expressed in terms of equation 7.1.

$$\frac{d[B]}{dt} = -\frac{d[A]}{dt} = k_{obs}[A]$$

(7.1)

Integration of equation 7.1, generates equation 7.2 and hence, 7.3, where $[A]_0$ and $[A]_t$ are the concentrations of A, at times equalling zero and t, respectively

$$\ln[A]_t - \ln[A]_0 = -k_{obs}t$$

(7.2)

$$k_{obs} = -\frac{1}{t}\ln\frac{[A]_t}{[A]_0}$$

(7.3)

The absorbance, at times equalling 0 and t, can be expressed using the Beer-Lambert law (A = εcl, where A is the absorbance, ε is the molar extinction coefficient, c is the concentration and l is the path length, 1 cm), equations 7.4 and 7.5.

$$A_0 = \varepsilon_A[A]_0$$

(7.4)

$$A_t = \varepsilon_A[A]_t + \varepsilon_B[B]_t$$

(7.5)

$$\text{Since} \quad [B]_t = [A]_0 - [A]_t$$

(7.6)

$$A_t = \varepsilon_A[A]_t + \varepsilon_B[A]_0 - \varepsilon_B[A]_t$$

(7.7)

At the end of the reaction t = ∞ and $[B]_\infty = [A]_0$, therefore;

$$A_\infty = \varepsilon_B[A]_0$$

(7.8)

Substitution of equation 7.8 into equation 7.7 and rearrangement produces equation 7.9.

$$[A]_t = \frac{(A_t - A_\infty)}{(\varepsilon_A - \varepsilon_B)}$$

<div align="right">(7.9)</div>

Similarly, when time equals zero, equation 7.10 is true.

$$A_0 = \varepsilon_A [A]_0$$

<div align="right">(7.10)</div>

Therefore;

$$[A]_0 = \frac{(A_0 - A_\infty)}{(\varepsilon_A - \varepsilon_B)}$$

<div align="right">(7.11)</div>

Substituting equations 7.9 and 7.11 into equation 7.3, equation 7.12 can be derived.

$$k_{obs} = \frac{1}{t} \ln \frac{(A_0 - A_\infty)}{(A_t - A_\infty)}$$

<div align="right">(7.12)</div>

Upon rearrangement, a linear equation is obtained, equation 7.13

$$\ln(A_t - A_\infty) = -k_{obs} t + \ln(A_0 - A_\infty)$$

<div align="right">(7.13)</div>

Therefore, plotting $\ln(A_t - A_\infty)$ versus time, t, should give a linear plot, with a gradient equal to $-k_{obs}$. Infinity values, A_∞, were determined, over at least ten half lives, and the data fitted over approximately 80 % of the reaction.
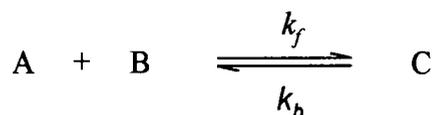
Two techniques were used to fit trend lines to the experimental results obtained. The approach was dependent on the correlation being investigated.

Linear regression fitting was used to obtain the gradient and intercept, from linear plots. This was performed using the data analysis function built into Microsoft Excel®, which also calculated error values present, in the gradient and intercept. Correlation coefficients were also generated by the package, and used to judge the accuracy of the trendline fitted to data points, although visual inspection, was the most valued guideline.

Non-linear least squares fitting were used, to fit trendlines to non-linear relationships, such as first order reaction profiles. This was performed by the Scientist®3 program, which fits experimental data to non-linear equations, plots trendlines, and calculates statistics for the fit.

For a reaction at equilibrium such as that posed in scheme 7.1, where one reactant is excess to the other, the reaction becomes pseudo first order and the rate can be defined by equation 7.14.

Scheme 7.1:

$$A \; + \; B \; \underset{k_b}{\overset{k_f}{\rightleftharpoons}} \; C$$

$$-\frac{d[A]}{dt} \; = \; k_f'[A] - k_b[C] \qquad \text{where} \quad k_f' = k_f[B]$$

$$\tag{7.14}$$

If $[A]_e$ and $[C]_e$ donate the respective concentration of species at equilibrium and x is the distance of the concentrations from equilibrium, then equations 7.15 to 7.17 show their relationship.

$$x \; = \; [A] - [A]_e \; = \; [C]_e - [C] \tag{7.15}$$

$$\text{Therefore} \quad [A] \; = \; [A]_e \; + \; x \tag{7.16}$$

$$\text{and} \quad [C] \; = \; [C]_e \; - \; x \tag{7.17}$$

Substituting equations 7.16 and 7.17 into equation 7.14, gives equation 7.18.

$$-\frac{dx}{dt} = (k_f' + k_b)x + (k_f'[A]_e - k_b[C]_e)$$

(7.18)

Since the reaction is at equilibrium the rates of the forward and reverse reactions are equal, $k_f'[A]_e = k_b[C]_e$, hence, equation 7.18 reduces to equation 7.19.

$$-\frac{dx}{dt} = (k_f' + k_b)x$$

(7.19)

Therefore, the observed pseudo first order rate constant, k_{obs}, is given by the following equations.

$$k_{obs} = k_f' + k_b$$

(7.20)

Therefore $$k_{obs} = k_f'[B] + k_b$$

(7.21)

## 7.7: Determination of extinction coefficient for aqueous iodine

The extinction coefficient, ε, of aqueous iodine is required to calculate rate constants for reactions that are zero order with respect to aqueous iodine solution.

However, firstly, it was relevant to standardise the sodium thiosulfate solutions made to 0.01 mol dm^{-3} with the standardised 0.5 mol dm^{-3} iodine solution. Titration of 0.01 mol dm^{-3} sodium thiosulfate against a known volume of 0.01 mol dm^{-3} iodine solution proved that the concentration was 0.01 mol dm^{-3} within experimental error.

The absorbance of aqueous iodine was found to increase considerably in the presence of potassium iodide, KI. Addition of KI has the effect of pushing the equilibrium over to the

triiodide species, I₃⁻, shown in scheme 7.2. KI addition increases the absorbance suggesting that I₃⁻, is the main absorbing species, rather that I₂.

Scheme 7.2:

$$ I_2 \quad + \quad I^- \quad \rightleftharpoons \quad I_3^- $$
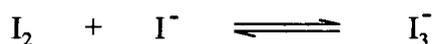
Experiments to obtain extinction coefficient was required to be studied at two different fixed KI concentrations since experiments were conducted with concentrations of 1×10^{-3} mol dm⁻³ when observing propanal reactions and with 5×10^{-3} mol dm⁻³ when observing propanone and chloropropanone reactions.

However, with each fixed KI concentration, the aqueous iodine solution concentration ranging from 1.5×10^{-5} to 1.2×10^{-4} mol dm⁻³, was used to obtain absorbance against wavelength spectra. Spectra were recorded using a UV-2101 PC Shimadzu Corporation spectrometer at 25 °C, with 1 cm stoppered quartz cuvettes, using a scan speed of 480 nm min⁻¹.

Two peaks were observed with λ_{max} values of 287nm and 350nm. Using the Beer-Lambert relationship $A = \varepsilon cl$, where c is the concentration and l is the pathlength, ε may be determined by plotting A against the aqueous iodine solution concentration. The value of ε, is equal to the gradient of the line. For the reactions of propanal where the concentration of KI = 1×10^{-3} mol dm⁻³ extinction coefficient values were determined for both peaks, 287 and 350nm (Figure 7.2), the value at 350nm was used in determining rate constants. However, for the reactions involving propanone, and chloropropanone, a higher KI concentration was used and it was found preferable, in terms of observing the reactions of iodine and the carbonyl compounds, to use a higher wavelength, 385nm. Therefore, for the reaction using the concentration of KI as 5×10^{-3} mol dm⁻³, extinction coefficients were calculated for three wavelengths, 287, 350 and 385nm (Figure 7.3).

Figure 7.2: Plot to determine the extinction coefficient of the aqueous iodine solution with added KI (1×10^{-3} mol dm^{-3})
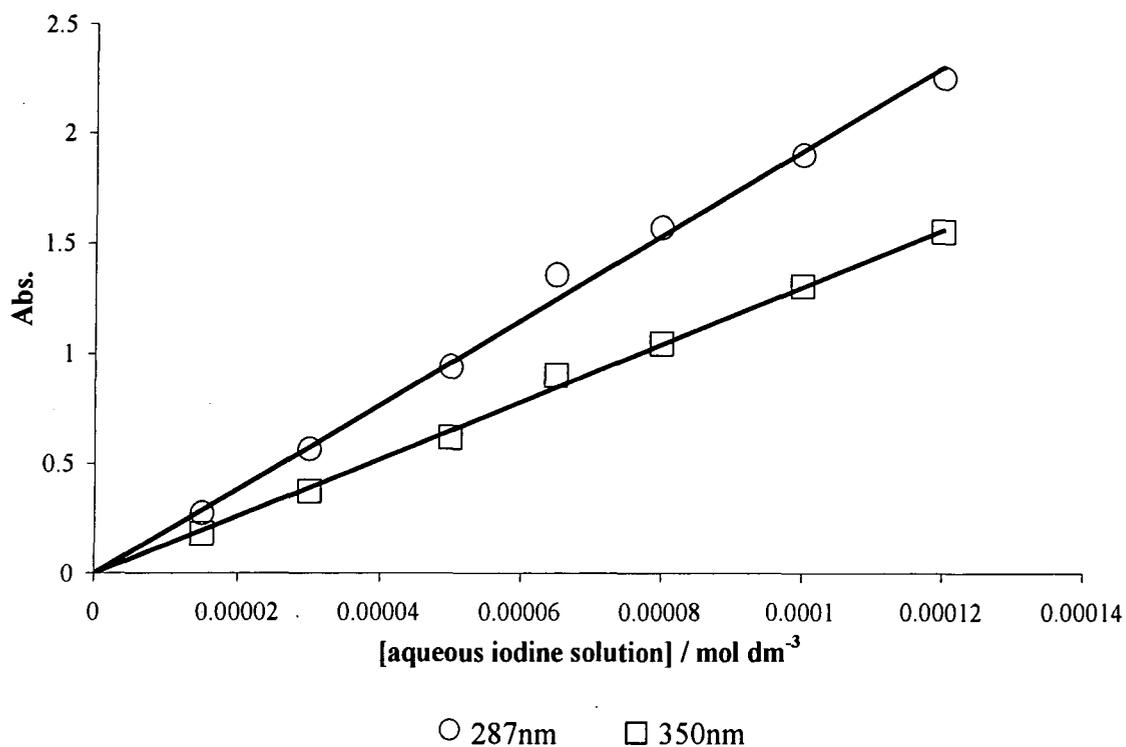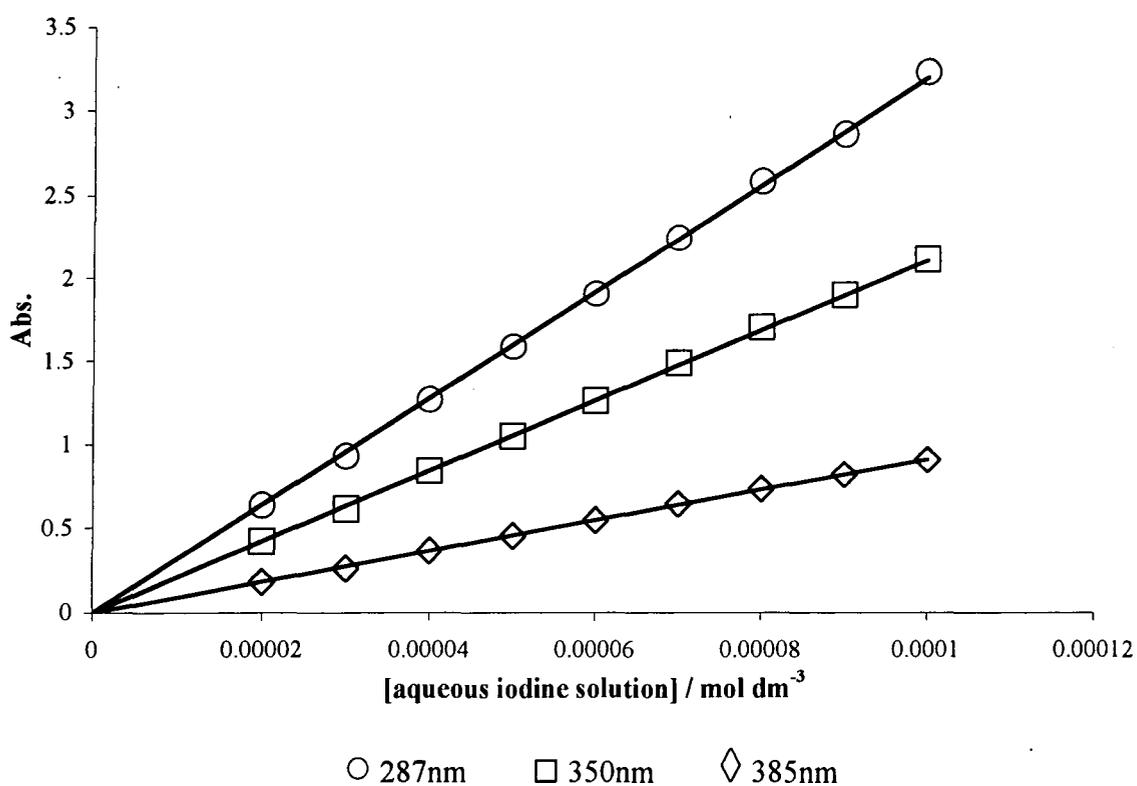

O 287nm   □ 350nm

Figure 7.3: Plot to determine the extinction coefficient of the aqueous iodine solution with added KI (5×10^{-3} mol dm^{-3})

O 287nm   □ 350nm   ◊ 385nm

When the concentration of KI was 1×10^{-3} mol dm^{-3} the values of ε equalled, 19000 ± 600 dm^3 mol^{-1} cm^{-1} and 13200 ± 300 dm^3 mol^{-1} cm^{-1} for 287 and 350 nm respectively. When the concentration of KI was 5×10^{-3} mol dm^{-3} the values of ε equalled, 32500 ± 600 dm^3 mol^{-1} cm^{-1}, 21400 ± 400 dm^3 mol^{-1} cm^{-1} and 9115 ± 100 dm^3 mol^{-1} cm^{-1} for 287, 350 and 385 nm respectively. Linear correlation coefficients between 0.995 and 0.999 were obtained for the plots.

To ensure that the presence of the absorbing species, I$_3^-$, KI was always in great excess to the aqueous iodine solution, with concentrations constant at either 1×10^{-3} or 5×10^{-3} mol dm^{-3}.

7.8: ^{1}H NMR spectroscopy

^{1}H, and ^{13}C NMR spectra were recorded using a 200 MHz Varian 200, or a 400 MHz Varian 400, or a 500 MHz Varian 500 spectrometer. For locking purposes, when running a sample, in mixed solvents, the solvent in the highest proportion was used with its peak being used as the reference. Mixed solvents were used, when the compound was known, not to be soluble in D$_2$O, at the required concentration.

Spectra were generally recorded immediately after the solutions were made. Reactions, being observed via ^{1}H NMR, were recorded immediately after the solutions had been mixed and again, over time, until no further changes occurred. All reagents were made up, prior to reaction in suitable deuterated solvents, and mostly, D$_2$O. These solutions were diluted to the required concentration in a final volume in the NMR tube of 1 cm^3. The start of the reaction was recorded, when the final reagent was added to the NMR tube. The time of each spectrum was taken as the time, when the spectrometer started to acquire the spectrum.

7.9: Mass spectrometry

Mass spectra were recorded by the electron ionisation method (EIMS), on a Micromass Autospec instrument. Chemical ionisation (CIMS) or gas chromatography (GCMS), were also employed.

7.10: pH measurements

The pH values of solutions, were determined using a Jenway 3020 pH meter, calibrated using pH 7 and pH 10 (for alkaline solutions) or pH 4 (for acidic solutions) buffers at 25 °C. The sample was thermostatted at 25 °C, prior to taking a pH measurement, which was achieved by placing the clean pH probe into the sample.

7.11: References

1) 'CRC Handbook of Chemistry and Physics', R. C. Weast, CRC Press, Florida, 63rd Ed., 1982-1983

2) B. G. Cox, 'Modern Liquid Phase Kinetics', Oxford Chemistry Primers, 1996

3) Micromath® Scientist® for Windows®, Version 2.02

Appendix

Appendix 1: Conferences Attended

01.09.2001   8th European Symposium on Organic Reactivity (ESOR), Cavtat
to   (Dubrovnik), Croatia
06.09.2001   Poster presentation entitled 'Condensation Reactions of Formaldehyde and Amines in the Presence of Sulfite'

28.09.2001   Royal Society of Chemistry Organic Reaction Mechanisms Group, Unilever, Port Sunlight
Poster presentation entitled 'Condensation Reactions of Aldehydes and Amines in the Presence of Sulfite'

06.01.2002   11th International Winter School on Organic Reactivity,Bressanone, Italy
to   Sponsored by EU
13.01.2002   Poster presentation entitled 'Condensation Reactions of Aldehydes and Amines in the Presence of Sulfite'

08.04.2002   North East Perkin Symposium, York
Poster presentation entitled 'Condensation Reactions of Aldehydes and Amines in the Presence of Sulfite'

20.09.2002   Royal Society of Chemistry Organic Reaction Mechanisms Group, East Midlands Airport
Oral presentation entitled 'A Mechanistic Study into the Reactions of Aldehydes and Aniline in the Presence of Sulfite'

25.06.2003   University of Durham Graduate Symposium, University of Durham
Oral presentation entitled 'A Mechanistic Study into the Reactions of Aldehydes and Aniline in the Presence of Sulfite'

19.09.2003   Royal Society of Chemistry Organic Reaction Mechanisms Group, Avecia, Huddersfield

Poster presentation entitled 'A Mechanistic Study into the reactions of Aldehydes and Aniline in the presence of Sulfite'